1996

An experimental study of the drag force on a water-supported conveyer belt.

Rick. Anema
University of Windsor

AN EXPERIMENTAL STUDY OF THE DRAG FORCE ON A WATER SUPPORTED CONVEYOR BELT

By

Rick Anema, B.Eng

A Thesis submitted to the
Faculty of Graduate Studies and Research
through the Department of Civil and Environmental Engineering
in Partial Fulfilment of the Requirements for the
Degree of Master of Applied Science
at the University of Windsor

Windsor, Ontario, Canada
April, 1996

ADC 6569

ABSTRACT

Belt conveyor systems have been used to transport materials since the early 1900's. In an effort to reduce the conveying costs, variations of the traditional belt conveyor systems have become common place.

An investigation into an alternate method of supporting the conveyor belt and material was the objective of this research. The method investigated uses water, in lieu of flights of idlers, to support the belt and material. Water flowing in an open channel provides the buoyancy for the support of the conveyor belt and material.

The specific objective of this research was to determine the drag coefficient of a representative section of a water bed conveyor. This involved the investigation of the drag on a flexible membrane form in a confined open channel. Dimensional analysis was used as a basis for the design of the physical model of the water bed conveyor. The physical model was designed, constructed and installed within a flume. Testing of the physical model consisted of measuring the drag force on the Test Section and velocity distribution within the boundary layer developing along the Test Section. The measurements were undertaken while the Test Section was loaded with various quantities of different material types. The Test Section was fixed in the direction of flow by one load cell, while water was pumped through the flume at 25 l/s, 38 l/s and

63 l/s. A power-law velocity distribution within the boundary layer was assumed. The power-law exponents for the three material type set-ups were similar in magnitude and found to be independent of Reynolds Number in the test range. The average exponent, over the length of the Test Section, for the material set-ups of water, rocks and sand were 6.7, 5.5 and 6.5 respectively. However, the exponents at specific locations along the Test Section ranged from 3 to 11.7.

Momentum principle and the velocity data were used to calculate the drag force on the Test Section; this was then compared with the drag force recorded directly. The drag recorded and calculated showed a good correlation and confirmed that momentum principle was suitable for calculating the drag force in the nonuniform flow region of a water bed type conveyor (WBC) system.

The drag coefficient was calculated and comparisons were made to establish whether the tension in the membrane and/or the material type set-ups affected the drag coefficient. The relationship among the drag coefficient, Reynolds Number and Froude Number were investigated. The results indicated that the drag coefficient was independent of Reynolds Number (based on the hydraulic radius of the Test Section) greater than 10000. The effects of Froude number were found to be minimal under the test conditions selected.

ACKNOWLEDGEMENTS

I would like to extend a special thank you to my advisor, Dr. J.A. McCorquodale, for his support, advice and patience throughout the degree. Additional thanks are extended to my committee members, Dr. K. Shridar and Dr. N. Biswas for their availability and constructive criticism; Mr W.T. Pramono for his motivation, encouragement and friendship; Central Workshop staff and fellow graduate students for their practical and technical assistance.

TABLE OF CONTENTS

LIST OF TABLES

LIST OF FIGURES

1.0 INTRODUCTION

Conveyors are one of many devices used by industries to transport commodities. The types of conveyors currently in use span the alphabet from apron conveyors to zero pressure accumulation conveyors. The type of conveyor used is a function of industry demands. The demands of the mining industry are of particular interest to the author. The mining industry has been the greatest proponent of belt conveyor technology, and since transportation costs are an integral part of the economics of the industry it warrants further investigation.

Belt conveyors have been used to transport materials such as coal since the mid-nineteenth century. The principle of operation has not changed significantly to date; however, the components (e.g. belt, idlers) of the conveying system have developed proportionately to the respective component industries. The assimilation of the "new and approved" components have in turn decreased the $/kg of material conveyed, making overland conveying economically viable. However, further reductions in $/kg of material conveyed can be realised if the conveyor system is analyzed as a complete system rather than as an assembly of components. A review of the principle of operation of the traditional conveyor is in order, and further more, will help explain the fundamental limitation of the traditional system in achieving lower $/kg

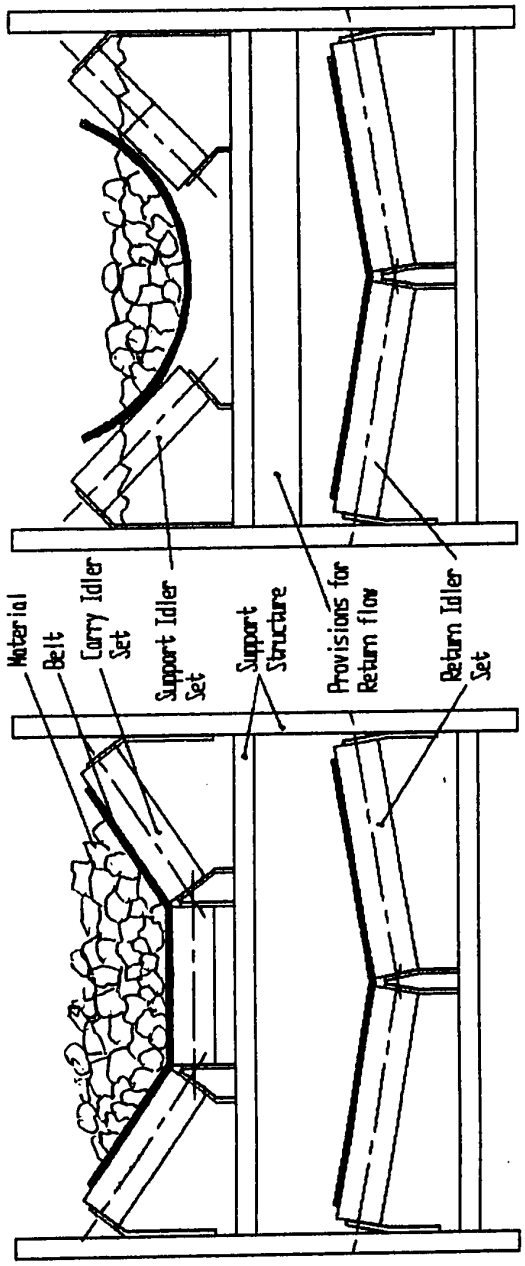

Figure 1.1 Traditional Belt Conveyor

Figure 1.2 Water Bed Conveyor

of material conveyed.

1.1 Traditional Belt Conveyor Systems

In its simplest form traditional belt conveyors comprise at least a head and tail pulley, flights of idlers and a drive train. The raw material is fed onto the conveyor belt at the tail end of the conveyor. The belt and raw material are then dragged over a flight of idlers (Figure 1.1) by the action of the head pulley which is driven by the drive train.

The types of idlers employed in the conveyor system are often broadly categorised as either carry or return idlers. The carry idlers are responsible for providing support to the material being conveyed and are generally assembled in sets of 2,3 or 5. The return idlers provide the support for the returning belt and are assembled in sets of 2 or as a single stand alone idler. The spacing and number of idlers in each set is dependant on the required load carrying capacity of the conveyor system.

The belt provides the medium for the tension required to overcome motional resistances, and is often categorised according to the tension member, i.e., carcass. Three types of carcasses are currently in use : solid woven, plied fabric and steel cord. The carcass is protected from wear and tear by a top and bottom belt cover. The belt covers are generally manufactured from a rubber compound.

It is the interaction of the idlers, belt and material that ultimately lead to the friction that must be overcome by the installed drive train. This friction, which is further quantified in Chapter 2, is the primary limitation of the traditional conveyor system in achieving lower $/kg of material conveyed. The capital and operating costs associated with the installation, operation and maintenance of the traditional belt conveyor system further contribute to the $/kg of material conveyed. These limitations are the reasons why the author sought to investigate a conveying method that is distinctly different in how the belt and material are supported.

1.2 Water Bed Conveyor System

The operating principle of the proposed water bed conveyor (WBC) is inherently the same as the traditional belt conveyor system (Figure 1.2). However, the carry idlers by in large are replaced by water. Water flowing in an open channel forms the support for the belt and the material being conveyed much like water does for a boat. The belt and raw material are thus continuously buoyant in the channel and are pulled by the action of the head pulley and drive train. The water is not pumped and does not drag the belt and material, but instead provides the support for the belt and material. The velocity of the belt in fact drags the water which is continuously recirculated through the

recirculating pipe.

The pressure distribution on the belt and the tension within the belt, may not be sufficient to maintain the troughing form of the belt and material over the length of the conveyor. To ensure a stable troughing form, additional support idlers placed intermittently along the length of the conveyor may be required.

The return side of the WBC system will be similar to the traditional system. The inadequate troughing characteristic of an empty belt supported by water will not permit the same set up as the carry side of the WBC system. The WBC system, like the traditional system, will still require idlers at the feed point and transition sections.

1.3 Advantages and Disadvantages of the WBC system

1.3.1 Advantages

The coefficient of friction, associated with the traditional conveyor system, is replaced by a friction factor between the water and belt (Refer to Chapter 2). This factor is believed to be lower than the coefficient of friction. This results in a reduction in primary resistance and inertia (fewer rotating parts) of the conveyor system. An overall decrease in motional resistance leads to the selection of a belt with a lower tension rating. Furthermore, with greatly reduced belt idler interaction,

mechanical wear is reduced which permits a thinner belt cover. The net result is a lower belt to material weight ratio which further decreases the motional resistance and lift of the conveyor system.

Power requirements are based on the motional resistance of the conveyor system. Lower motional resistance leads to the installation of smaller power packs. Operating costs are thus lower.

Installation of the idlers in the traditional system involves intense labour due to the precision required in locating the idler sets relative to the adjacent set. Precision of up to 2 mm over 3000 mm spans is not uncommon and this leads to installation costs that are significant when compared with the WBC system. The savings become more evident in overland conveyors. Fewer idlers leads to a decrease in maintenance costs as the need for bearing failure detection and consequent idler replacement is reduced.

The operational, installation and maintenance costs are the major contributors to the overall $/kg of material conveyed. The proposed alternative WBC should provide reductions in these costs.

1.3.2 Disadvantages

The nature of the medium used for the support of the belt and material, i.e., the basis of the concept of the

proposed conveyor system, may be the major limitation of the WBC system. The inclination of the channel is, to a large extent, dictated by open prismatic channel flow restraints. Although the water may be dragged by the belt, the inclination of the WBC system is limited by maintaining the equilibrium of the major forces : shear forces of the belt, channel walls and gravitational force. A scheme that may overcome this disadvantage is a scheme that divides the channel into sections. Each section being vertically staggered and containing a separate recirculating pipe. The layout of this proposed scheme would be analogous to a loch system used in the shipping industry.

The choice of material for the construction of the channel and the necessary supports are all unknowns and therefore required specialised attention which may influence design costs. An investigation into the troughing form (Section 1.2) of the WBC system may also be required, and may further increase the design costs.

The installation of the system is obviously limited to areas where water is abundant.

1.4 Objective

The objective of this research was to determine the drag coefficient on a representative section of a water bed conveyor. This involved the investigation of the drag on a flexible membrane form in a confined open channel.

1.5 Scope of Work

The scope of this research included the following:

i) Design of a typical traditional conveyor system to be used as basis for the design of a physical model of a WBC system.

ii) Application of dimensional analysis to the traditional conveyor design for the determination of an appropriate physical model scale factor.

iii) Design, construction and installation of the physical model and required measurement system.

iv) Recording of drag force on the flexible membrane under various drafts and flow rates.

v) Recording of velocity profiles in the developing boundary layer on the flexible membrane.

vi) Developing generalised friction parameters for estimation of the friction drag on the water belt conveyor system.

2.0 BACKGROUND AND LITERATURE REVIEW

2.1 Introduction

A review of the current literature pertaining to water bed type conveyors has proven the uniqueness of the WBC concept. With the exception of work performed by Nagy (1983), no further references to the WBC concept were found. Nagy performed work, at the Central Institute for Mining Development in Hungary, on a conveying system that operated on a similar principle as the proposed water bed type conveyor (WBC) system. Unlike the WBC system, water was introduced and removed at various point along the conveyor. Nagy found that power requirements for the WBC system were 80% lower than for a similar traditional horizontal conveyor operating at 2.5 m/s with a capacity of 990 t/h. The underlining reason for this remarkable power reduction is the objective of this review. The background and literature review will therefore be limited to explaining the sources of the mechanical friction associated with traditional conveyors and the hydraulic skin friction associated with the WBC systems.

2.2 Mechanical Friction

Frictional resistances associated with conveyor systems are generally divided into two groups namely primary and secondary. Primary frictional resistance is often further

categorised into the following:

a) Idler rotational resistance,

b) Belt indentation resistance,

c) Flexure resistance of belt,

d) Flexure resistance of bulk material.

In determining the required power of the conveyor system, primary frictional resistance calculations dominate, nevertheless, secondary frictional resistance is worth mentioning. The secondary frictional resistance is the sum of the resistances associated with the removal of overburden from the belt (using belt scrapers) and the acceleration of the bulk material at the feeding point. The secondary frictional resistance is often calculated as a fraction of the total primary frictional resistance. The following discussions will thus be limited to issues pertaining to the primary frictional resistance.

2.2.1 Idler Rotational Resistance

Greune (1990) highlighted that bearing and seal friction are the cause of this type of resistance. It is often a measure of the force, at the circumference of the idler, required to overcome the frictional moment due to the presence of the bearing and seal. Increases in belt velocity, bearing diameter, bearing load and lubricant viscosity are believed to increase the idler rotational resistance. Furthermore manufacturing tolerances and general

maintenance practices impact on the average rim drag resistances.

2.2.2 Belt Indentation Resistance

Jonkers (1980) commented that hysteresis is the primary reason for this type of resistance. As the conveyor belt moves over the idler the belt is subjected to a deformation and, since the belt is not free of hysteresis, a transfer of energy to the idlers occurs. Spaans (1991) used a linearised approximation to the hysteresis loop of the belt which simplified the determination of this resistance. Spaans (1991) also mentions that the visco-elastic properties of the belt covers, loading and unloading of the belt as it passes over the idlers leads to a time delay in recovering the deformation of the belt. This time delay gives rise to a horizontal force component which is another source of belt indentation resistance. Naturally with fewer idlers in the WBC system, this source of friction, as well as the idler rotational resistance, becomes negligible in comparison.

2.2.3 Flexure Resistance of belt

The bending moment induced in the belt due to the idlers is the main factor contributing to flexure resistance of the belt. The bending moment experienced by the belt when approaching the idler is larger than when leaving the idler due to the presence of hysteresis, and this difference in

bending moment is what leads to an energy transfer (Spaans 1991).

2.2.4 Flexure Resistance of Bulk Material

The catenary shape of the belt between idler sets is one of two factors that contribute to the flexure resistance of the material. The bulk material is subjected to a sequential (cyclic) loading as it passes over the idler sets. The second factor contributing to this resistance is the affect of a continuous change in cross-section of the bulk material as the material approaches and leaves the idler sets. This deformation of the material volume leads to a passive stress state (closing of the material volume) and active stress state (opening of the material volume) as it flows. Since the internal friction of the bulk material is not negligible there is a net transfer of energy, Spaans (1991). In the WBC system both the belt and material flexure resistance is minimal as the cross-sectional area of the belt and material remain essentially constant over the length of the conveyor.

2.3 Hydraulic Skin Friction

The boundary layer theory associated with a flat plate will be discussed to demonstrate how the drag force and skin friction can be determined. Discussions regarding drag forces over a flexible membranes will follow.

2.3.1 Boundary Layer Theory

Boundary layer growth along a flat plate under zero pressure gradient will be the focus of this section. Steady turbulent uniform flow in an unconfined space is assumed, as well as a power - law velocity distribution within the boundary layer. The assumption of a power - law velocity distribution in a pipe was confirmed experimentally by Nikuradse (Schlicting 1968) for Reynolds number between 4 x 10^3 and 3 x 10^6. Since the theory of boundary layer growth along a flat plate has been based on experimental work on boundary layer development in pipes, the power - law assumption followed.

The drag force, F_D acting on a fluid/boundary interface is a function of the momentum of the fluid particles in the boundary layer. The momentum integral equation (Equation 2.1)

$$\tau_0 / \rho = x\, d(U_\infty^2 \delta_2(x))/dx + [d(U_\infty)/dx]\, U_\infty \delta_1 \qquad \ldots 2.1$$

provides a means for determining the drag force acting on the boundary. This equation is based on the application of the momentum equation (Equation 2.2) to a boundary layer.

$$\Sigma F = d(mv) / dt \qquad \ldots 2.2$$

The derivation of the momentum integral equation is covered in most fluid mechanics text books (e.g. Massey (1984)) and will

not be derived here. Equation 2.1 is a function of the change in momentum thickness, δ_2 and displacement thickness, δ_1 with distance; and since a zero pressure gradient was assumed, the displacement term is neglected and Equation 2.2 reduces to Equation 2.3.

$$\tau_0 / \rho = x \, d(U_\infty^2 \delta_2(x))/dx \qquad \ldots 2.3$$

The calculation of the drag force therefore reduces to solving an expression that relates the momentum thickness with distance. This expression can be derived using experimental data collected over the years by various researchers. Schlicting (1968) showed that, for a power - law velocity distribution within a boundary layer, the relationship between momentum thickness and boundary layer thickness, δ is dependent on the power - law exponent, n only (Equation 2.4).

$$\delta_2 = \delta / (n+1)(n+2) \qquad \ldots 2.4$$

The derivation of the boundary layer growth equation (Equation 2.5) was based on Blasius's formula (Equation 2.6) for hydraulically smooth pipes, momentum integral equation (Equation 2.3) and Reynolds Number (Equation 2.7).

$$\delta(x) = C_\delta \, x \, / Re_x^{-0.2} \qquad \ldots 2.5$$

$$\tau_0 / (\rho U_\infty^2) = 0.0225 \, (\nu / U_\infty \delta)^{0.25} \qquad \ldots 2.6$$

$$Re_x = v \, x \, / \nu \qquad \ldots 2.7$$

The drag force can be determined using the simplified momentum integral equation and an equation relating the power-law exponent and the momentum thickness, Equation 2.8. Note C_δ and $C_{\delta 2}$ are constants of integration ($C_\delta = 0.37$, $C_{\delta 1} = 0.0463$). These two equations may be simplified to Equation 2.9.

$$\delta_2 = xC_\delta/((n+1)(n+2))Re_x^{0.2}) \quad \ldots 2.8$$

$$F_D = C_{\delta 2}\rho U_\infty^2 A_w Re_x^{-0.2} \quad \ldots 2.9$$

The average skin friction, Equation 2.10, can be reduced to Equation 2.11 using Equations 2.10 and 2.8. The coefficient of Equation 2.11 was modified from 0.072 to 0.074 as Schlicting (1968) suggests that this leads to a better agreement with experimental data.

$$C_f = F_D \; / \; 0.5\rho U_\infty^2 \; A_w \quad \ldots 2.10$$

$$C_f = 0.074Re_x^{-0.2} \quad \ldots 2.11$$

2.3.2 Flexible membrane

A concise historical review of research conducted on drag forces on flexible membranes was undertaken by Sharekh (1994). The first studies on flexible membranes were performed by Gray in 1936. The agility of dolphins was investigated by Gray to explain the reason behind their speed and manoeuvrability. Gray implied that dolphins have a unique ability to delay the

onset of turbulence. The first laboratory experiments, according to Sharekh (1994), on flexible surfaces were conducted by Kramer during the late 1950's and early 1960's. Kramer claimed a 60% reduction in drag force. Carpenter and Garrard (1985) provide an overview of Kramer's work and that of other earlier researchers. As the theoretical knowledge base of the subject increased in the 1980's, Kramer's work became quite topical and perhaps even controversial. Kramer's observations and conclusions have been disputed based on today's understanding of the phenomenon. Nevertheless his observations of a reduction in drag force (compared to a rigid body) have been verified on numerous occasions by various researchers including Sharekh (1994).

Sharekh (1994) attempted to characterize the turbulent boundary layer development, through experimentation and numerical modelling, over three flexible surfaces and one rigid body. The flexible surfaces comprised a rubber membrane covering a foam base (of various configurations) supported by a rigid flat plate. The rubber membrane was not under tension. Sharekh (1994) recorded drag reductions in the range of 8 - 20% when compared with the rigid surface. The reduction depended on the dampening characteristics of the flexible membrane.

The desirable characteristic of flexible membranes has been investigated both numerically (via suitable turbulence computer models) and experimentally. The general consensus is

that flexible membranes have a stabilizing effect on the boundary layer by reducing the amplification rate of the disturbance waves in the flow near the boundary (Carpenter and Garrad 1985,1986; Babenko and Kozlov 1973) as cited by Sharekh (1994). This results in an increase in the critical Reynolds number and a delay in the transition to turbulence.

3.0 DIMENSIONAL ANALYSIS

3.1 Introduction

Dimensional analysis was used as a basis for determining the configuration of the physical model and the testing programme. To quantify the selection, an analysis of the lay-out and the components comprising the full scale traditional conveyor system was necessary. Tables 3.1 provides a summary of the overall design parameters associated with the traditional conveyor that was used as a bench mark for the physical model. In brief a 1.2 m wide conveyor belt carrying aggregate at a mass flow rate of 1000 t/h (0.6 m/s) over 500 m was selected. An operating tension ranging from 59 kN (slack side of drive pulley) to 100 kN (tight side of drive pulley) was calculated, which required 24.7 kW to overcome the total motional resistance. The design of the traditional conveyor was based on the design practices recommended in the design manual provided by Contitech. The design was confirmed, by comparison, with an example from the design manual provided by Bridgestone and the example cited by Brouwers (1986).

3.2 Dimensional Variables

The drag force of the WBC system was selected as the dependent variable. The following groups of dimensions were considered appropriate.

Table 3.1 Design Summary of Traditional Conveyor

Principal data:

Design tonnage, t/h	1000
Conveying length, m	500
Elevation, m	0
Belt width, mm	1200
Belt speed, m/sec	0.6
Acceleration - loaded, m/sec^2	0.09
Decceleration - loaded, m/sec^2	NA

Material Specification:

Type	Aggregate
Lump size, mm	40
Bulk density, kg/m^3	2500
Angle of repose, deg	18

Belt Specification :

Belt manufacturer	NA
Type, EP	200/3
Width, mm	1200
Carcass thickness, mm	3.1
Cover thickness - top, mm	6
- bottom, mm	4
Weight, kg/m	17.5
Maximum sag, %	1

Idler Specification:

Manufacturer	NA
Carry - troughing angle, deg	35
- diameter, mm	108
- rotating weight, kg/m	17
- spacing, mm	1000
Return - troughing angle, deg	10
- diameter, mm	108
- rotating weight, kg/m	6
- spacing, mm	2500

Table 3.1 Design Summary of Traditional Conveyor - Continued

Factors and Coefficents:

Primary resistance coefficient	0.0135
Secondary resistance coefficient	1.2
Friction - pulleys and belt	0.3
Motor efficiency,%	85
Starting factor	1.5
Breakaway factor	1.3
Belt Safety factor - start	5.88
- operating	7.22
Angle of wrap - head pulley,deg	180

Resistance forces:

Primary resistance - top run, kN	32.81
- bottom run, kN	1.46
- total, kN	34.26
Secondary resistance, kN	6.84
Gradient resistance - top run, kN	0.0
- bottom run, kN	0.0
- total, kN	0.00
Special resistance, kN	0.0
Total resistance, kN	41.10

Power:

Required - loaded, kW	24.7
- unloaded, kW	NA
Installed, kW	30.0
Peripheral and inertia forces:	
Peripheral force:	
Normal operation, kN	41.10
Start operation, kN	63.75
Inertia force:	
Start operation - top run, kN	21.71
- bottom run, kN	0.94

Belt Tensions:

Normal Operation	
Belt tension - T1, kN	99.8
Belt tension - T2, kN	58.7
Belt tension - T3, kN	60.1
Belt tension - T4, kN	60.1
Belt tension - T5, kN	67.0
Start Operation:	
Belt tension - T1, kN	122.4
Belt tension - T2, kN	58.7
Belt tension - T3, kN	61.1
Belt tension - T4, kN	61.1
Belt tension - T5, kN	67.9

Belting:

- w - width of conveyor belting [L]
- t - thickness of conveyor belting [L]
- m_l - mass of belt per unit length [M/L]
- ρ_b - average density of belt material [M/L^3]
- G_c - modulus of rigidity of the cover [M/LT^2]
- G_{wa} - modulus of rigidity of the carcass - warp [$M/(LT^2)$]
- G_{we} - modulus of rigidity of the carcass - weft [$M/(LT^2)$]
- T - tension in the belt [ML/T^2]
- k - roughness of cover material [L]
- A - cross-sectional area of belt perpendicular to flow [L^2]

Bulk Material:

- m_m - mass of bulk material per unit length of belt [M/L]

Water :

- v - average velocity of water in flume [L/T]
- ρ_w - average density of water [M/L^3]
- ν - kinematic viscosity of water [L^2/T]
- R - hydraulic radius of Test Section [L]
- F_D - drag force per metre length of belt [M/T^2]
- g - acceleration due to gravity [L/T^2]
- d - water depth [L]
- g_p - gap between Transition and Test Section bulkheads [L]
- σ - surface tension [M/T^2]

3.3 Dimensionless Groups

Given the above twenty dimensional variables, seventeen dimensional groups were determined using the Indicial Method. The groups have been divided according to the type of physical similarity

$$F_D = \rho_w v^2 w F\{ \pi_2, \pi_4, \ldots\ldots \pi_{17} \} \qquad \ldots\ldots 3.1$$

$$\pi_1 = F_D/\rho_w v^2 w \quad ; \quad \pi_2 = v d /\nu \quad ; \quad \pi_3 = v/(dg)^{0.5};$$
$$\pi_4 = \rho_w g_p v^2/\sigma \quad ; \quad \pi_5 = T / \rho_w v^2 A \quad ;$$

$$\pi_6 = m_m/m_1 \quad ; \quad \pi_7 = m_m v^2/T \quad ; \quad \pi_8 = \rho_w v^2/G_c \quad ;$$
$$\pi_9 = \rho_m v^2/G_c \quad ;$$

$$\pi_{10} = AG_c/T \quad ; \quad \pi_{11} = w / d \quad ; \quad \pi_{12} = k / R \quad ;$$
$$\pi_{13} = R / d \quad ; \quad \pi_{14} = dG_c^{0.5}/T^{0.5} \quad ; \quad \pi_{15} = G_{wa}/G_c;$$
$$\pi_{16} = G_{we}/G_c \quad ; \quad \pi_{17} = w / t$$

3.4 Laws of Similarity

As discussed in Section 1.2 the principle of operation of the WBC is that water provides the support for the belt and material. The water is therefore confined to flowing in an open prismatic channel. The forces associated with open channel flow were therefore considered appropriate for dynamic similarity. These forces are : inertia, gravity, viscous and surface tension. The surface tensions (π_4) between the

bulkheads of the transition sections and the bulkheads of the Test Section were assumed to be in equilibrium. The validity of this assumption was based on the condition that the gap between the bulkheads remained constant (refer to Figure 4.2). Satisfying dynamic similarity of the remaining forces is practically impossible and inertia and gravity force were considered more important than viscous forces. Dynamic similarity was thus based on Froude Law (π_3) but the effect of Reynolds number (π_2) was investigated by varying the velocity through the flume.

The tension in the membrane was kept constant which prevented investigation into the effects of tension on load carrying capacity of the Test Section. However, if future studies were conducted with tension as a variable, dimensionless groups π_7, π_{10}, π_{14} and π_{17} may provide insight into the effect of the tension on the load carrying capacity of the conveyor system (Appendix A: Bench Top Model Test). The dimensionless groups; π_{15}, π_{16} and π_{17}, were categorised under structural properties of the membrane and were kept constant. A prototype to model length ratio of 4:1 was determined based on laboratory constraints. This led to Froude Law kinematic ratio of 2:1 and dynamic ratio of 64:1. The design of the physical model was based on these ratios and led to the following relationship between the dimensions listed in Table 3.1 and the dimensions of the physical model:

$(w)_{model} = (w)_p / 4 \quad ; \quad (w)_{model} = 1200 \text{ mm} / 4 = 300 \text{ mm}$

$(v)_{model} = (v)_p / 2 \quad ; \quad (v)_{model} = 0.6 \text{ m/s} / 2 = 0.30 \text{ m/s}$

$(T)_{model} = (T)_p / 4^3 \quad ; \quad (T)_{model} = 67.9 \text{ kN} / 64 = 1.06 \text{ kN}$

The width of the belt actually selected for the model was 400 mm since this was a standard size available by the vendor. The velocity through the flume varied between 0.18 m/s and 0.38 m/s. The tension in the membrane was 1.0 kN based on the tension T5 in Table 3.1. Tension, T5 represents the belt tension between the head and tail pulley.

4.0 DESIGN, FABRICATION, INSTALLATION AND MATERIALS

4.1 Physical Model

A physical model was designed, fabricated and installed in an existing Flume, hereafter referred to as Outer Flume, depicted in Figure 4.1. The Outer Flume was 1.22 m wide by 11.7 m long. The flow rate capacity of the Outer Flume was 100 l/s (1600 Gpm). The design, fabrication and installation of the physical model, encompassed all work associated with the Inner Flume, Test Section, Transition Sections and the Measurement Systems (Figure 4.2).

The model was designed to simulate a water bed conveyor (WBC) system under normal operating tension. Water flowing through the Inner Flume (Item 1 in Figure 4.2) provides the support for the Test Section (Item 2) and the Transition Sections (Item 3). Tension is applied to the belt, hereafter referred to as the flexible membrane (or membrane), via a Tensioning Device (Item 4). The operation of this Device is analogous to a turnbuckle, whereby the Outer Section of the Tensioning Device is rotated, resulting in the displacement of the Inner Sections of the Tensioning Device. This displacement, which is consistent with twice the pitch of the Tensioning Device, exerts an equivalent displacement to the membrane (Item 5) via the Rods (Item 6), Rod Supports (Item 7), End Plates (Item 8) and Bulkheads (Item 9).

The components of the model were fabricated from either

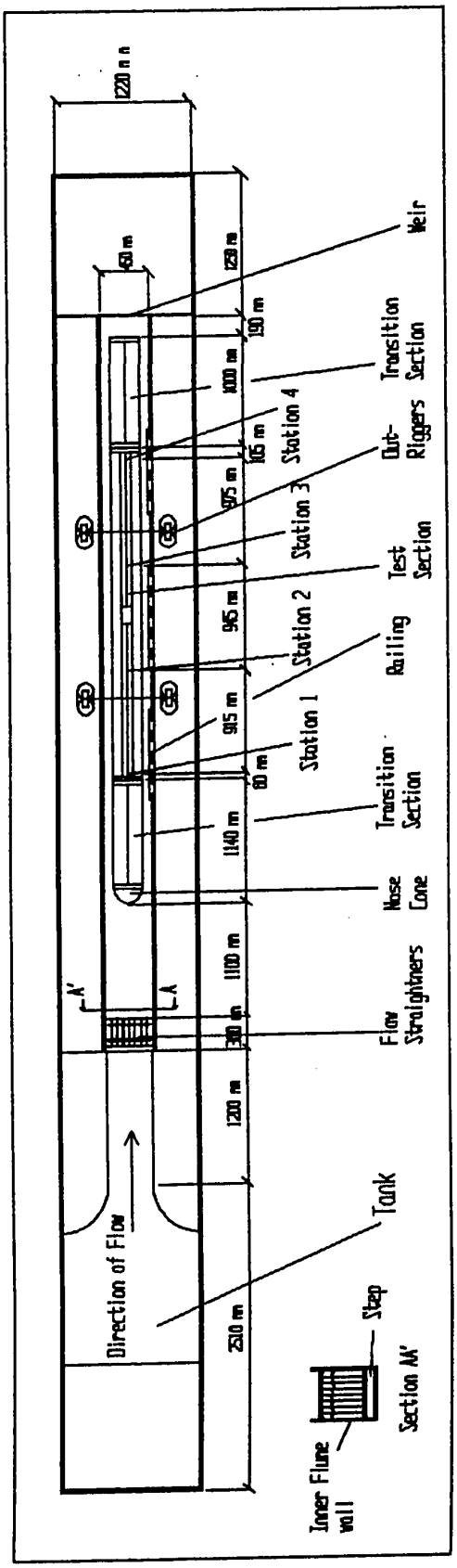

Figure 4.1 Plan View of Flume and Physical Model

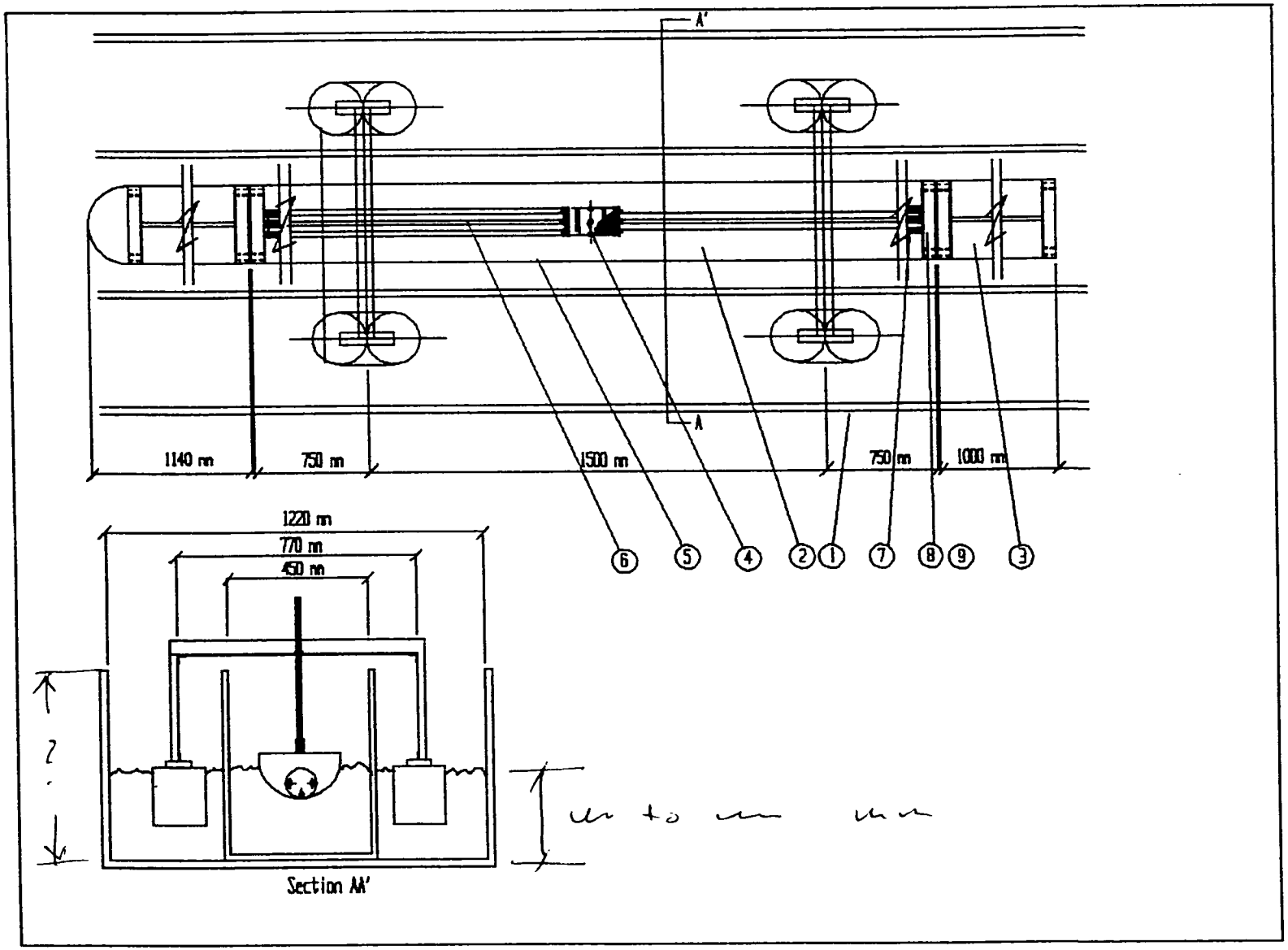

Figure 4.2 Plan and Cross-sectional view of Physical Model

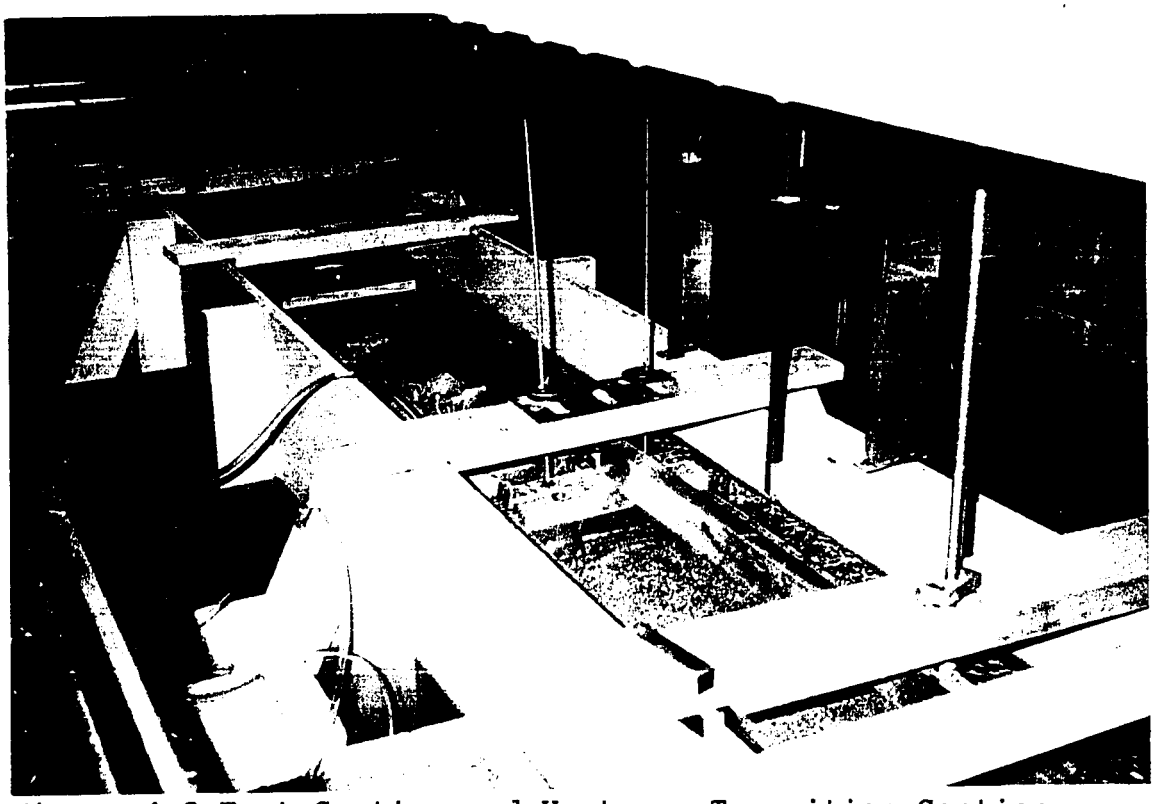

Figure 4.3 Test Section and Upstream Transition Section

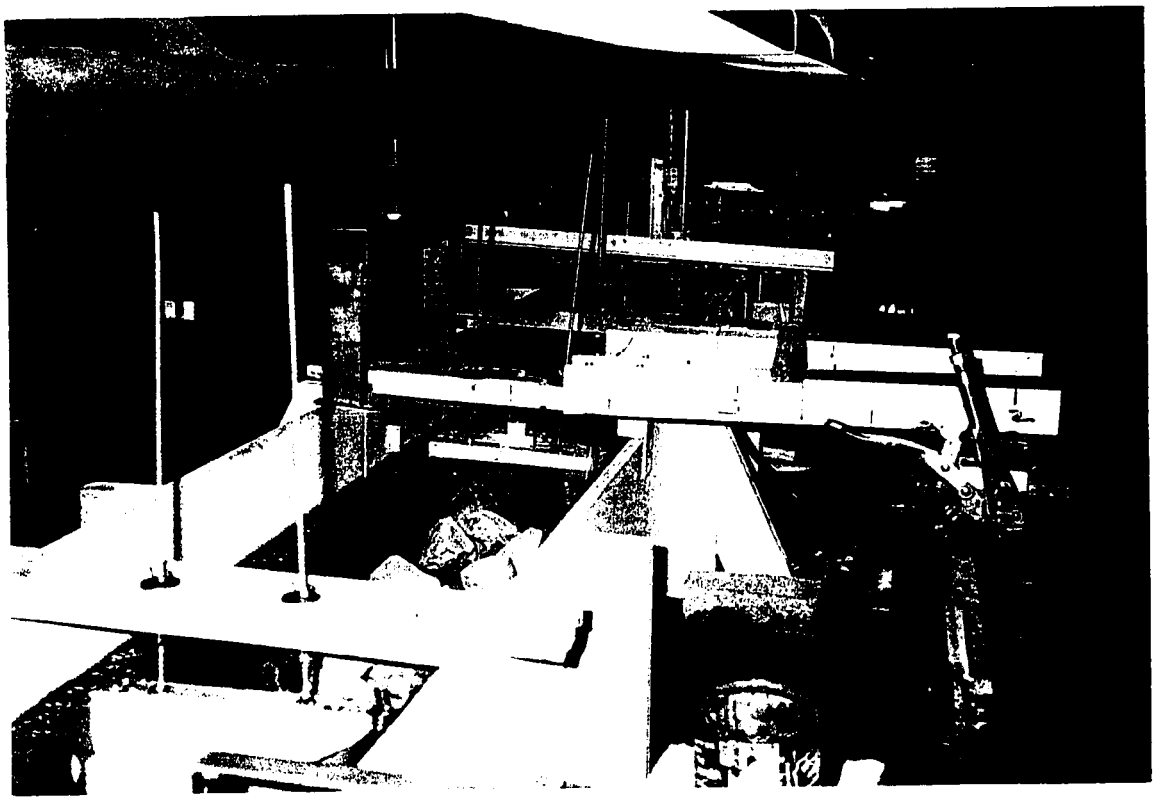

Figure 4.4 Upstream Transition Section

stainless Steel (Type 304), aluminium or plywood using standard workshop machinery. The components were then assembled, tensioned and position in the Inner Flume (Figure 4.2 and 4.3).

4.2 Inner Flume

Modifications to the Outer Flume were performed to ensure that the desired velocities were attainable. These modifications included the construction and installation of the Inner Flume (450 mm wide) within the Outer Flume, Figure 4.2.

The side walls, floor and floor supports were constructed from 19-mm and 12.5-mm GIS plywood; and the wall supports from 100-mm x 50-mm sprucewood. The wall supports were located at 610-mm spacing, and the floor supports at 200-mm spacing (Figure 4.5 and 4.6). Prior to construction, two coats of marine varnish were applied to the wood to prevent swelling.

The walls were constructed and installed in 2400-mm section lengths, and joined at specific wall support locations. Floor supports were then located and the floor installed in 1200-mm section lengths. All joint were sealed (see Section 4.3.5 for exception) and a finishing coat of a latex paint was applied. Two pressure taps were installed in the Inner Flume, and located adjacent to Station 1 and 4.

The centre line of the Outer Flume was determined. Wedges were used to position the centre-line of the Inner Flume to

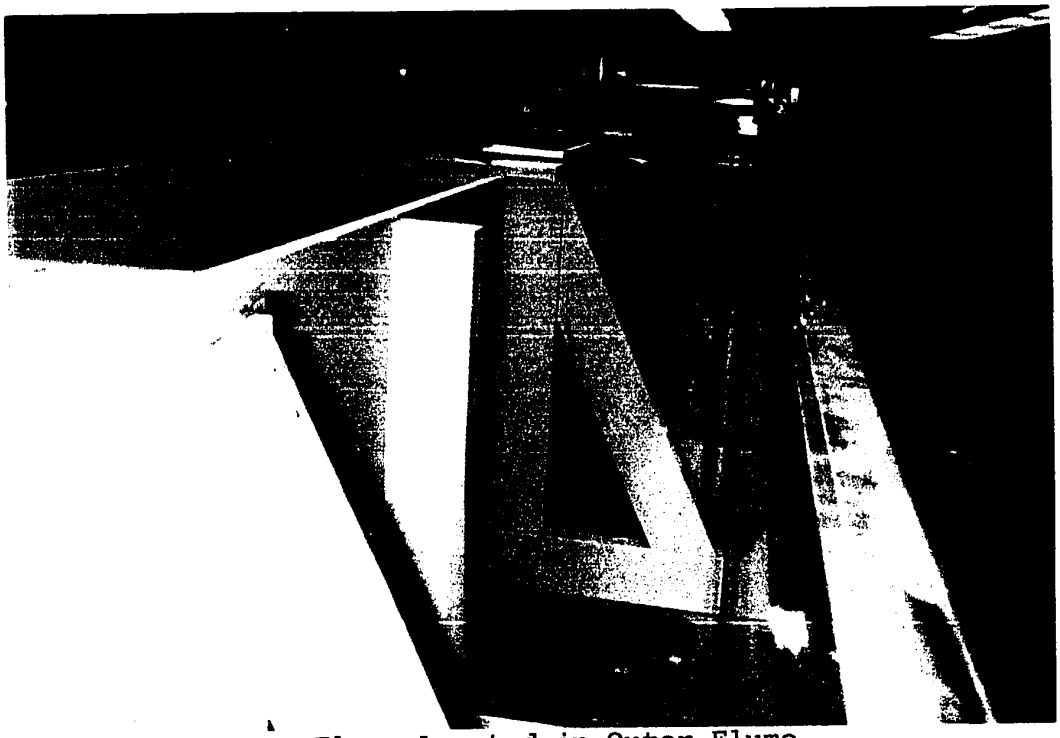

Figure 4.5 Inner Flume Located in Outer Flume

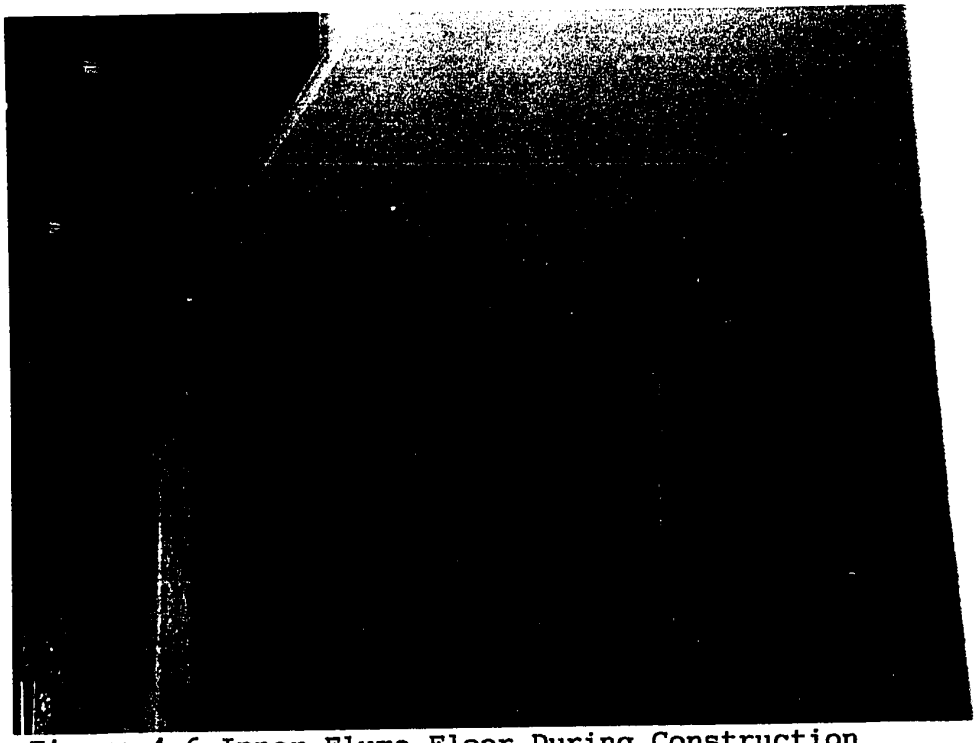

Figure 4.6 Inner Flume Floor During Construction

within 1.5 mm of the Outer Flume centre-line.

Flow straighteners were fabricated from 3-mm plexiglass and 19-mm plywood and located at the start of the Inner Flume. A weir was installed across the Outer Flume (Figure 4.1). This provided a means of controlling the water level in the Inner Flume. The height of the weir was 280 mm.

4.3 Test Section

The components associated with the Test Section (Figure 4.2 and 4.7) include the flexible membrane; Inner and Outer Sections of the Tensioning Device; Tensioning Rods and Rod Supports; Bulkheads and Endplates; and the Outriggers. See Figure 4.8 and 4.9.

4.3.1 Flexible Membrane

The Flexible Membrane is, in essence, standard conveyor belting used in the manufacturing and service industries. Although it is believed to be unsuitable for the mining industry, it sufficed for this application. The characteristics of the membrane are listed below :

Carcass : warp - polyester
weft - polyester
Cover : top - PVC
Bottom - PVC
Thickness : 1.6 mm (total)

Figure 4.7 Test Section

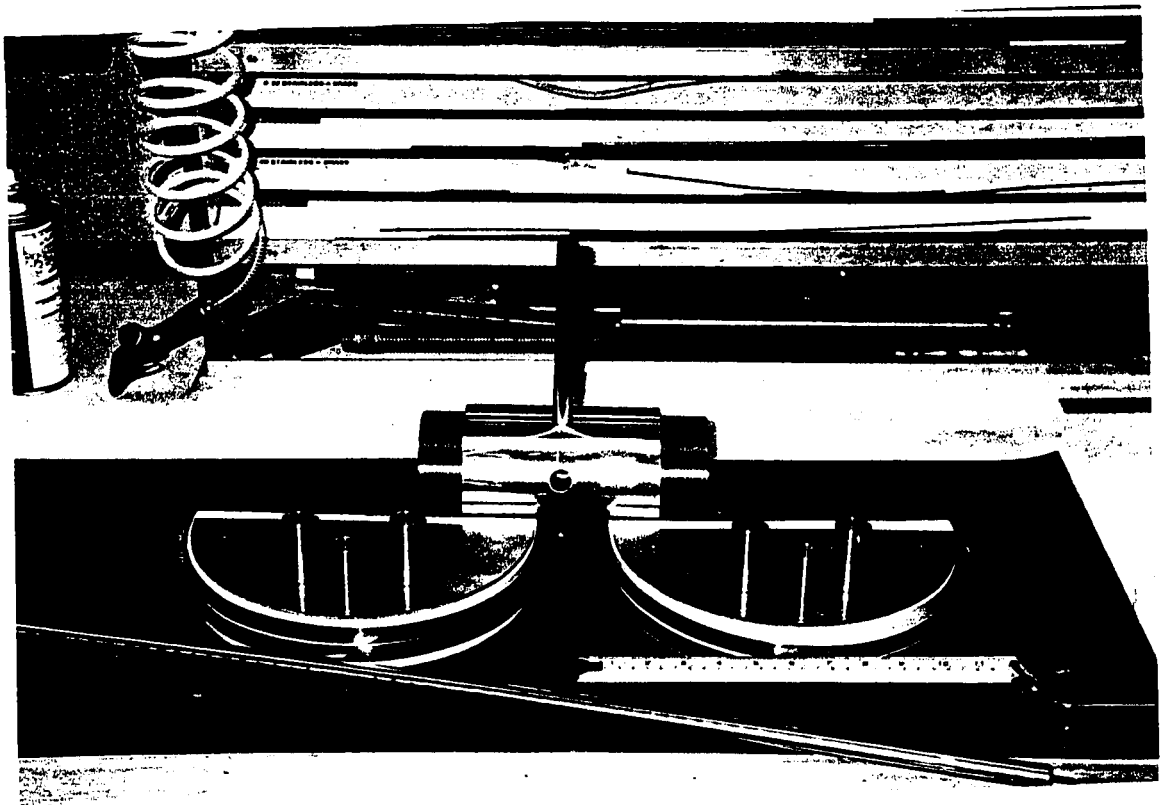

Figure 4.8 Test Section Components

Length : 3000 mm

Siegling Catalogue No. : E4/1 V5/V5 - Green

The tension in the belt was selected at 1.0 kN. This was calculated based on the stress/strain relationship (Section 6.1) and cross-sectional area of the membrane.

4.3.2 Tensioning Device

The Tensioning Device comprised the Inner and Outer Sections. It was designed to transmit a maximum tension (to the belt) of 1500 N. The diameter and pitch of the thread was 3 5/8 - 10 T.P.I; and 75% of full depth of thread was selected. The choice of pitch was based on the decision to minimise the number of turns of the Outer Sections while providing an accuracy of approximately 5 mm per rotation of the Outer Section. Alternatively, 17% of the maximum elongation of 30 mm is realised per each rotation of the Outer Section. The torque required to exert 1500 N in the belt was in the range of 7 - 20 Nm depending on, amongst other factors, the coefficient of friction of the lubricant used. The resulting screw efficiency thus ranges from 6 - 18%. The maximum combined shear stress in the thread was calculated to be approximately 0.1 MPa, well within the design limits of the materials.

The Outer and Inner Sections were fabricated from solid bars of aluminium and stainless steel respectively. Boring,

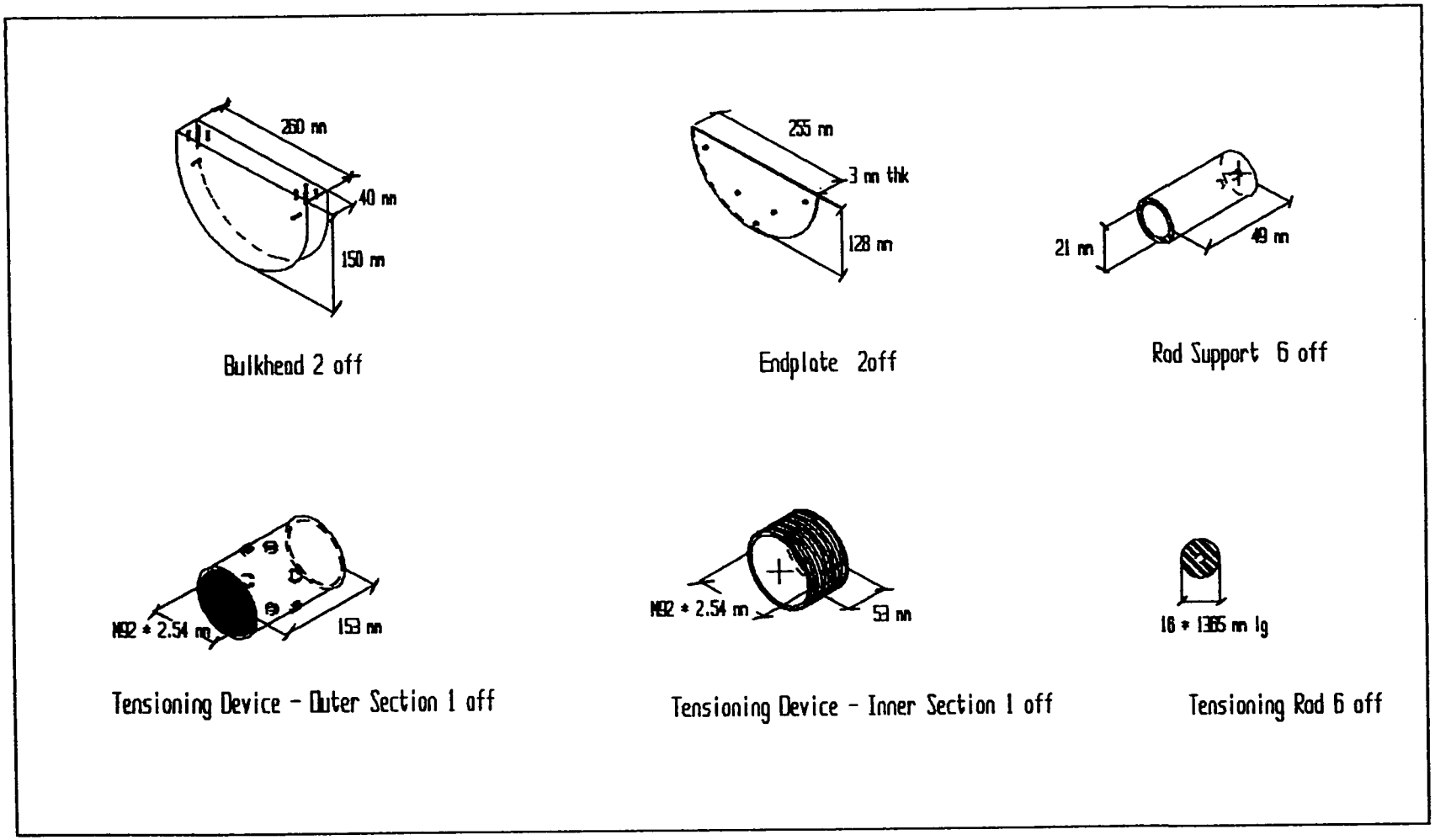

Figure 4.9 Test Section Components (Sketch)

turning, tapping and cutting of a left and right hand thread on the bars were performed on a lathe in the Central Research Shop. The choice of material was based on: a) availability of material at time of fabrication and b) the specific need for dissimilar materials to prevent possible seizure.

4.3.3 Belt Tensioning Rods and Rod Supports

The Belt Tensioning Rods were each designed to carry a compressive load. Design for buckling was the basis for material selection and cross-section. The diameter of the Belt Tensioning Rods was 15.9 mm enabling a total of 1500 N to be applied to the belt with a safety factor of 1.35 against buckling. Stainless steel was selected over standard low-carbon steel since protection against corrosion was required. Although low-carbon steel may have sufficed over the test period, possible further experimentation (at a later date by others) warranted the selection of stainless steel.

The purpose of the Rod Supports was twofold: firstly and primarily to locate the Rods near the centroid of the Bulkhead, and secondly to support the rods. The locations of the Rod Supports were based on the need to minimise the bending moment on the Bulkheads. This was achieved by locating the Rod Supports as close as possible to the centroid of the line representing the contour of the flexible membrane. The choice of material was again based on the operating environment.

4.3.4 Bulkheads and End Plates

The shape of the Bulkheads and consequently the End Plates were based on the maximum carrying capacity of the Test Section of 50 kg. The width of the bulkhead was selected based on the need for sufficient surface area for attaching the modified hose clamps. Four 250-mm hose clamps were modified and attached to either end of the Bulkheads. The hose clamps provided the clamping force required to prevent "pulling out" of the flexible membrane once under tension. The hose clamps required a width greater than 25 mm. To attain this width two pieces of standard 19-mm GIS plywood were bonded together and coated with latex paint and marine varnish to protected against swelling.

The End Plates were fabricated from stainless steel and functioned as distributors of the applied load over the face of the Bulkheads, as well as base plates for the Rod Supports.

4.3.5 Outriggers

The purpose of the Outriggers was to offset the dead load of the Test Section and thus permit measurements to be based on the live loads only. The dead load of the Test Section was offset by permitting water to enter the space between the Outer Flume and Inner Flume (Figure 4.2). The method in which the water entered this space was discovered by accident rather than by design; however the method proved effective and was not modified. The Inner Flume walls and floor joints would

ordinarily have been sealed to prevent leakage; however by not sealing the joints at selected points along the first 500 mm of the Inner Flume, water flowed into the space in question. The water level in the space would rise until the hydrostatic head was balanced by the water level in the Inner Flume. The flow rate in the space was monitored and recorded as approximately 0.5 l/s. The water in this space provided the buoyancy to the Outriggers and thus the Test Section via the Outrigger arms.

The Outriggers were fabricated from 25-mm x 25-mm aluminium angles, 50-mm x 50-mm T-section and plywood. The plywood was used as a base for attaching the Outrigger arms to eight "paint" cans. These cans each had a 3.8 l displacement. The total mass of the Test Section including the Outriggers was 29 kg.

4.4 Transition Sections

Transition Sections were located upstream and downstream of the Test Section. The upstream Transition Section was 1160 mm in length and the downstream Transition Section 1000 mm (Figure 4.1). A nose cone was attached to the front of the Bulkhead of the upstream Transition Section and is the reason for the difference in lengths. The purpose of the cone was to minimise possible flow separation at the bulkhead and ensure smooth boundary layer development before the Test Section. The position of the nose cone relative to the Outer Flume is

depicted in Figure 4.1. The Transition Sections were constructed in a similar manner as the Test Section; however, the tension mechanism was far simpler. Instead of a turnbuckle arrangement, a single stainless steel rod was end drilled and tapped, and placed in the centre of the Transition Section. Tension was imparted to the membrane via a torque applied to the bolt located in the end of the rod.

Pressure taps were located in the Bulkheads. They were positioned such that they were below the draft of the no load case, and such that "edge effects" on the pressure readings were minimal.

4.5 Measurement Systems

The three measurement systems used were : force measurement, pressure measurement and profile measurement.

4.5.1 Force Measurement Rig

The force measurement rig (Figure 4.10 and 4.11) consisted of a load cell positioned within a loop system. The loop system consisted of a force measurement device developed by Pramono (1995), hereafter referred to as Wasidevice (Item 4 Figure 4.11), one load cell (Item 1), four pulleys (Item 2), two turnbuckles (Item 3), and piano wire (Item 5).

The pulleys and load cell were mounted onto vertical supports that contained slots that facilitated precise positioning of both load cell and pulleys. The Wasidevice was

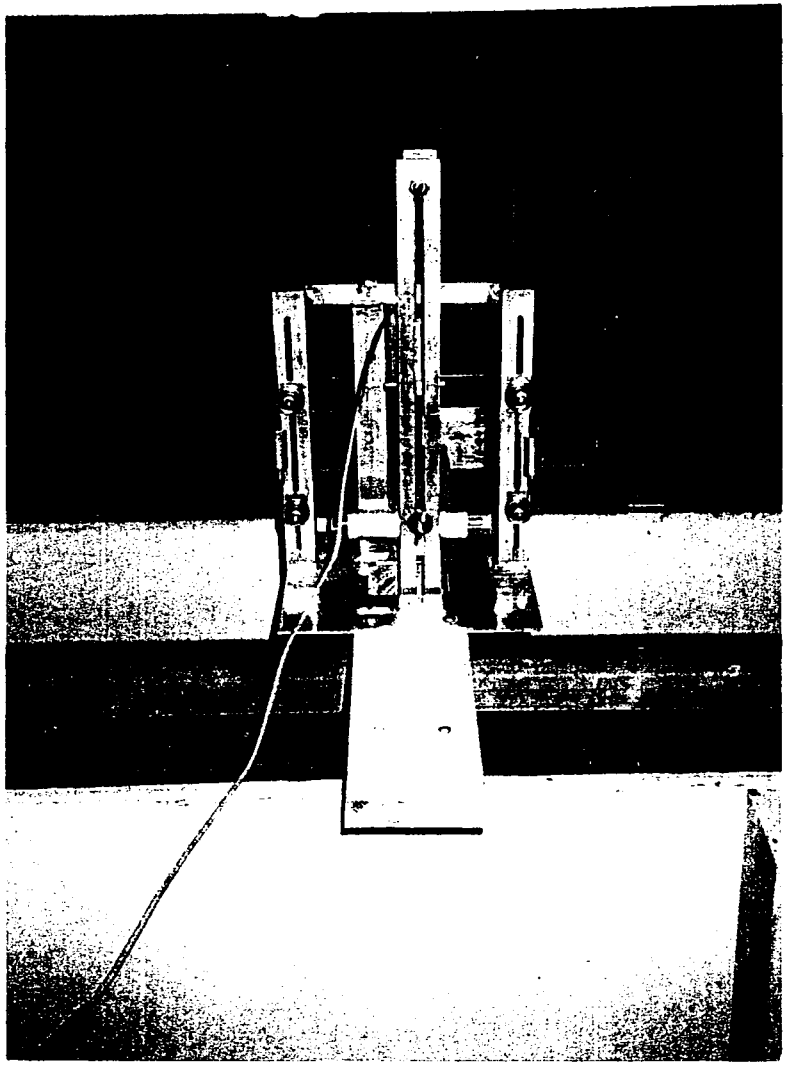

Figure 4.10 Force Measurement Rig

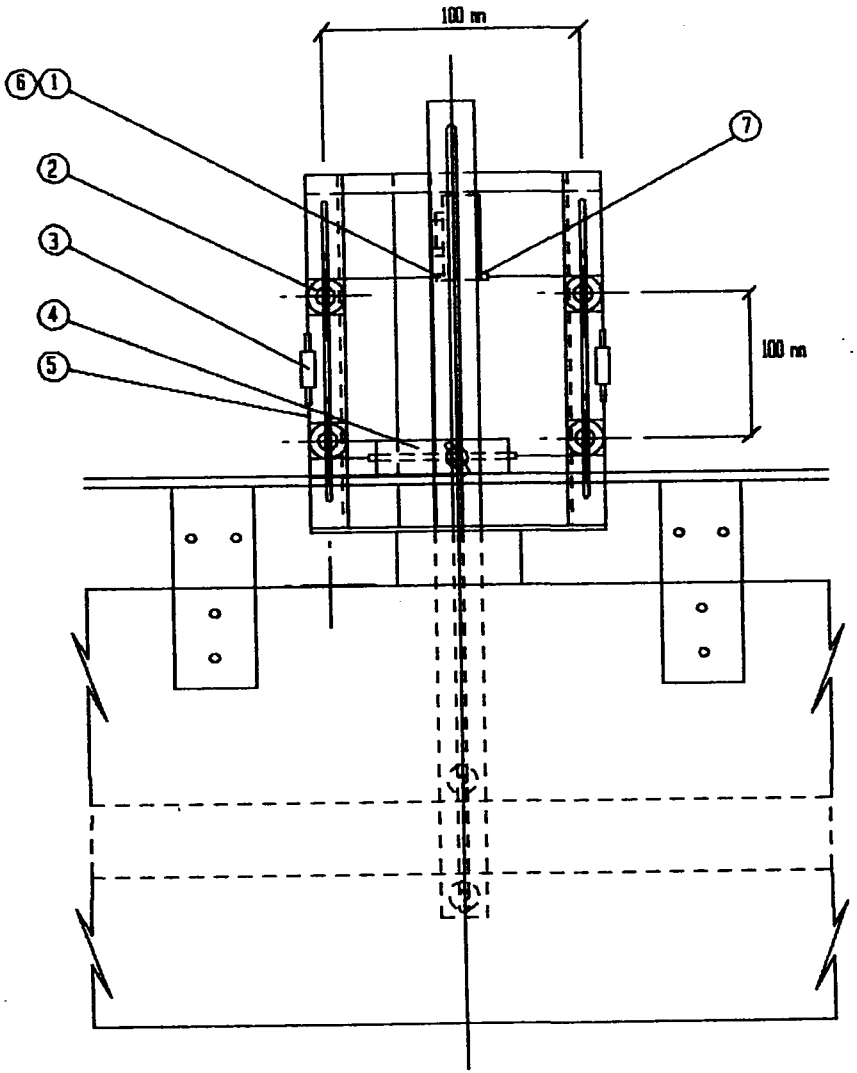

Figure 4.11 Force Measurement Rig (Sketch)

a unique design and consists of a restricted ball and socket type of arrangement located within a cylindrical aluminium tube. This design has three degrees of freedom permitting horizontal, vertical forces to be measured. The Wasidevice was attached to the Test Section via the slotted supports. Piano wire was used to transmit the desired drag force applied to the Test Section to the load cell. The tension within the loop system was selected to ensure transmission of the drag force. This selection was based on minimising the effects of friction within the loop system.

4.5.2 Pressure Measurement Rig

The pressure measurement rig consisted of a pitot static tube attached to a vernier calliper that traversed the Inner Flume on a rail, see Figures 4.1 and 4.12 to 4.14. The pitot static tube was an "in house design" as space requirements within the Inner Flume prevented the use of a standard pitot tube. The dimensions of the pitot static tube were selected according to a manufacturers recommendations. The pitot tube was manufactured from stainless steel.

The mechanism used to attach the pitot static tube to the vernier calliper consisted of a simple bracket with set screws. This design permitted quick and easy adjustment during commissioning of the pressure measurement rig, see Figure 4.11. Quick release clamps were used to attach the vernier calliper to the railing.

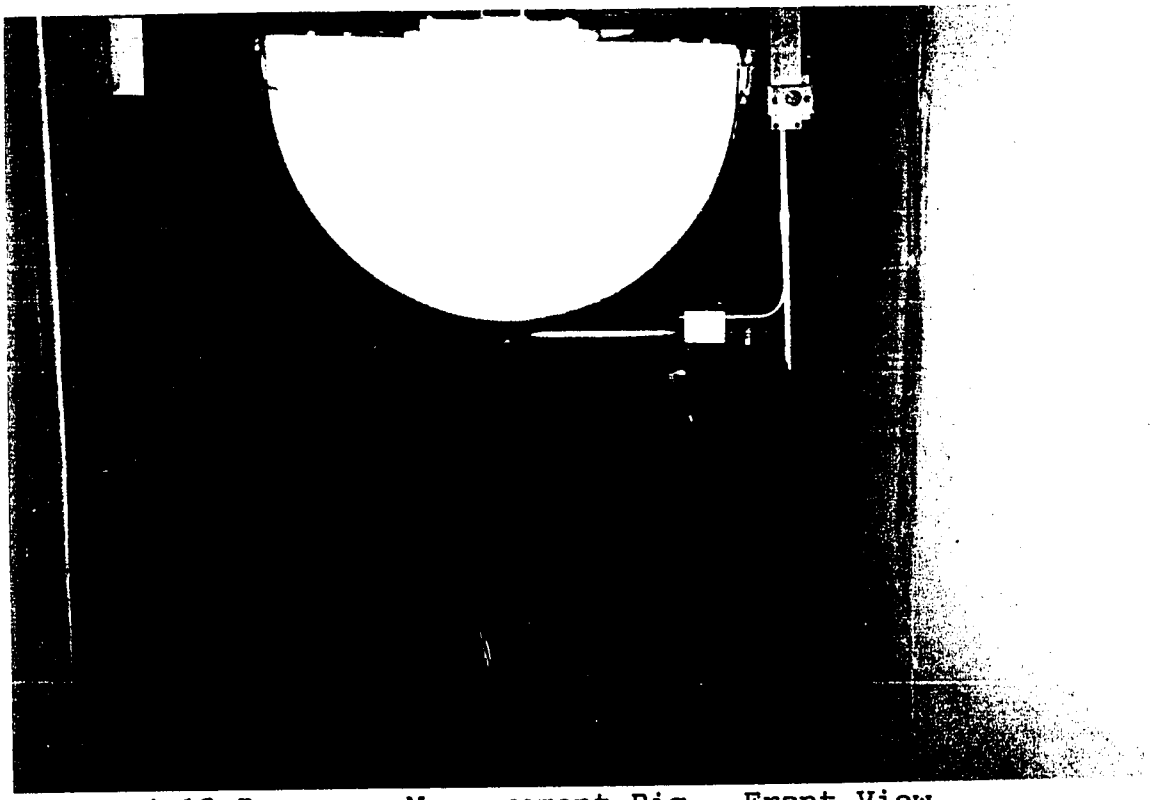

Figure 4.12 Pressure Measurement Rig - Front View

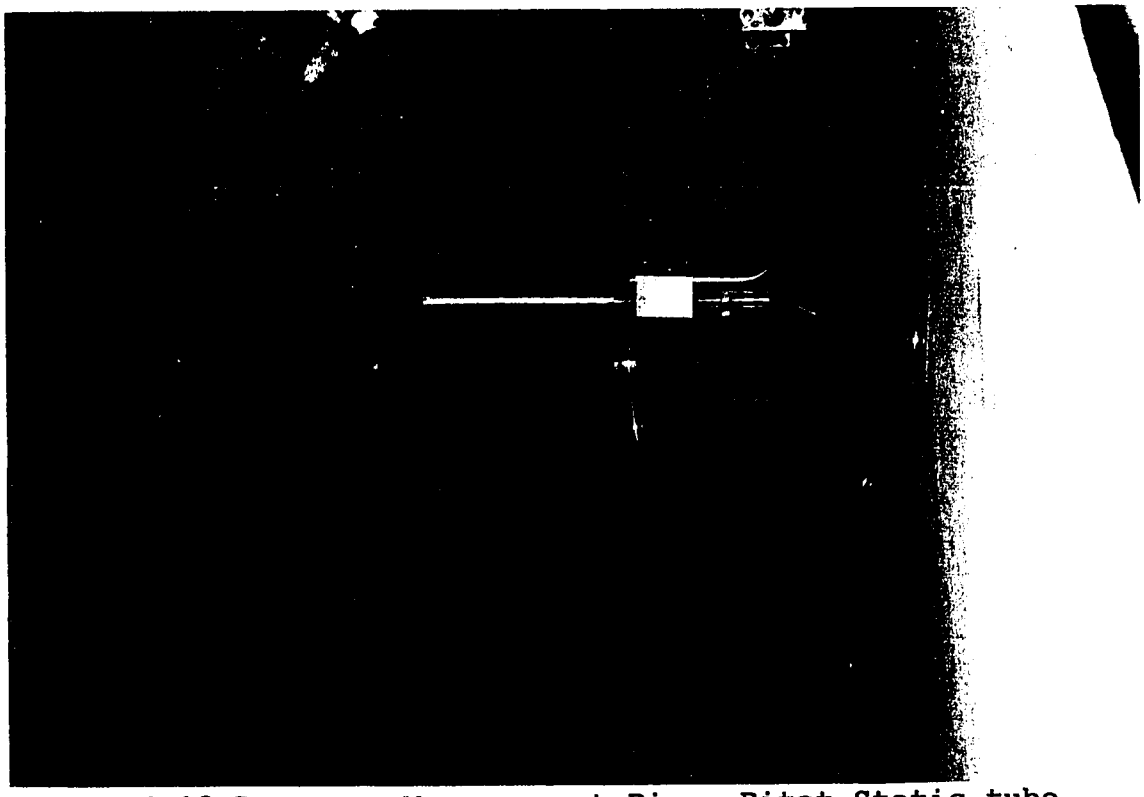

Figure 4.13 Pressure Measurement Rig - Pitot-Static tube

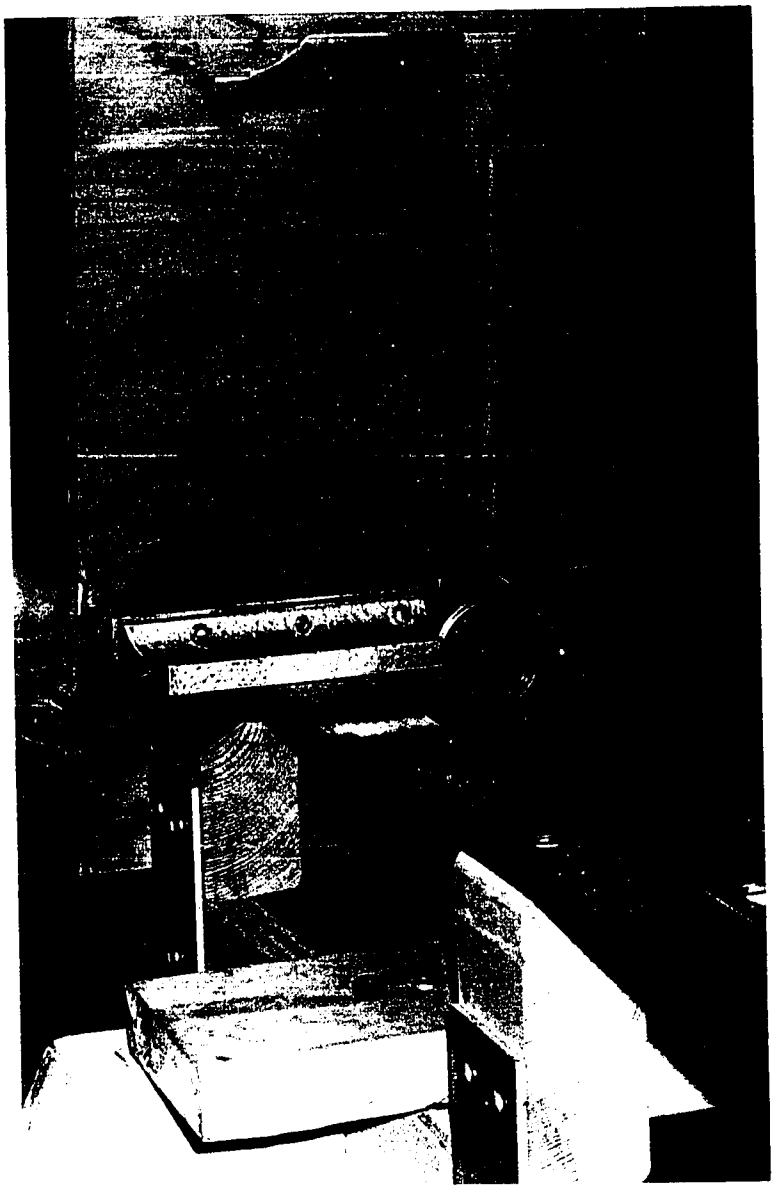

Figure 4.14 Pressure Measurement Rig - Vernier Calliper

4.5.3 Profile rig

The profile rig shown in Figure 4.15 was used to record the profile of the membrane while under load. It was constructed from aluminium and formed to a radius of 180 mm using a bending machine. Ten adjustable knobs were positioned at 30 mm intervals.

4.6 Materials

The materials used, include the materials of construction listed above and the materials associated with the tests. The three material types used were water, sand and rocks.

The type of sand used was masonry. The test results of a sieve analysis of the sand are included in Appendix B: Material Types. In brief approximately 40% of the sand was in the 300 μm - 600 μm range.

The mass and volume of the rocks used are listed in Appendix B: Material Types. In brief the average mass and volume of the rocks were 0.569 kg and 0.233 ml respectively.

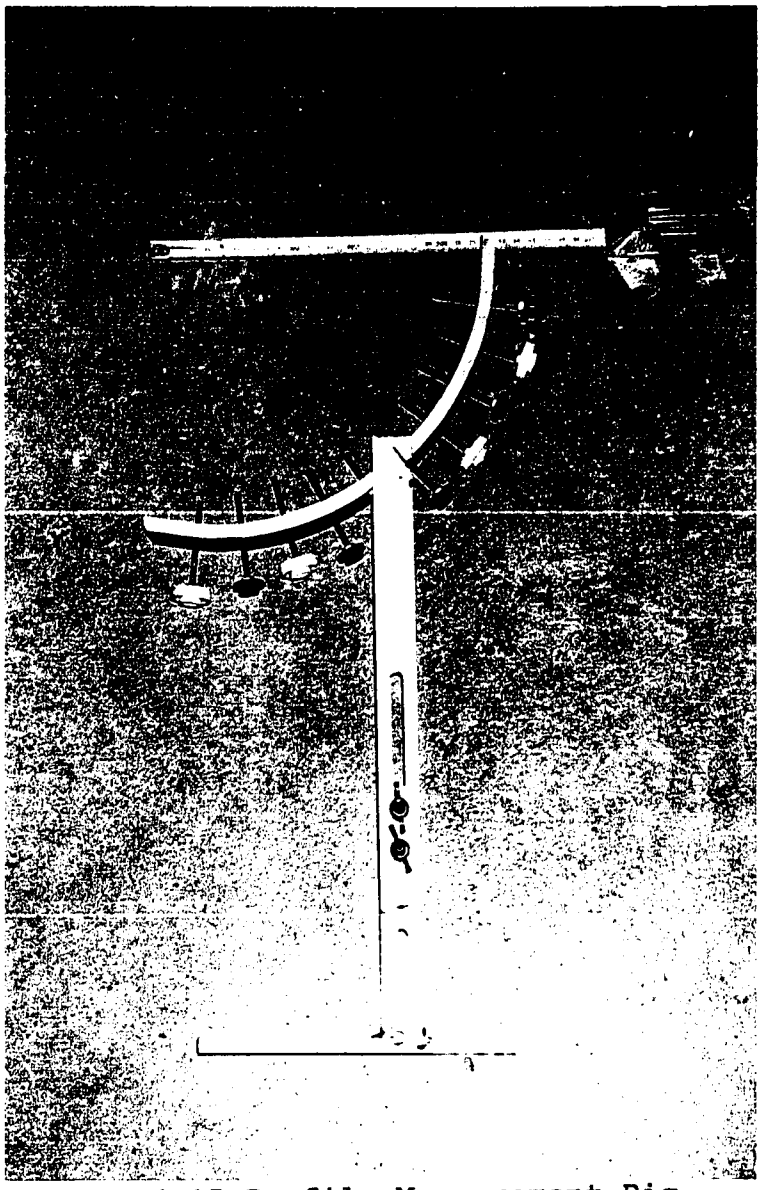

Figure 4.15 Profile Measurement Rig

5.0 INSTRUMENTATION AND METHODS

The instrumentation used in recording, calibrating and testing of the physical model are shown in Table 5.1.

5.1 Methods

The force and pressure measurements were conducted in two stages. The first stage referred, to as Phase 1.0, consisted of recording the force acting on the Test Section. The next stage, referred to as Phase 2.0, consisted of recording the velocity in the developing boundary layer. The profile measurements were conducted after the force and pressure measurement.

5.2 Phase 1.0 Force Measurement Methodology

The force recorded by the load cell includes the differential pressure force acting on the bulkheads. The pressure drop between the upstream and downstream was thus recorded as part of this phase. The test procedure was as follows;

1) The pump was started and the gate valve, connecting the pump to the Inner and Outer Flumes, opened to produce the desired flow rate.
2) Ten minutes were allowed to establish steady state conditions in the Inner Flume, and to ensure that the

Table 5.1 Instrumentation

Name	Description	Purpose	Manufacturer
Megadac Data Aquisition System	Model No. 3008AC	Excite and record signals from load cell and pressure transducer.	Optim Electronics
Minibeam Load Cell	Model No. mb - 5 - 89 Capacity: 5 lb	Record the force acting on the Test Section.	Interface Inc
Wet Differential Pressure Transducers	Series P - 3061. Capacity: 2" & 5"	Record pressure at the following locations: a) Boundary layer, b) Bulkheads and flume walls.	Lucas Schaewitz
Propeller Flow Meter	Model FP 5301	Record flow rate through flume.	Omega Engineering
Portable Water Current Meter	Model # 201D Range 0 - 20 feet/s	Record average velocity in inner flume.	Marsh McBirney
Pitot-Static Tube	Outer dia: 6.35 mm	Convey water pressure to pressure tranducer.	In house fabrication
Vernier Callipers	Range 0 - 13"	Accurately position the pito-static tube.	Helios
Force Gauge	Model DFG - 10 0 - 10 lb Range.	Used to calibrate the load cell and force rig.	Omega Engineering
Instron Tensile Testing Machine	Model No. 8500	Record the strain rate in a sample of membrane.	Instron

water level in the Outer Flume was constant.

3) Next the Test Section was freed from the backup supports. This permitted the Test Section to float in the Inner Flume. Note that the backup supports functioned as protection against possible overloading of the load cell. Overloading may result from a loss in water level in the Inner or Outer Flume. Pump failure may lead to a loss in water level.

4) The Test Section was then loaded with the desired material.

5) The material was then evenly distributed within the Test Section. To ensure an even distribution, the elevations relative to two bench marks, were recorded. The difference in elevation was less than 1 mm in all tests. Note that the two bench marks were surveyed.

6) The nuts, located in the centre of the Outrigger system, were adjusted such that less then 2% of the height of the paint cans was above the water level (Figure 4.2). Note that the height of the Outrigger system was a direct indication of the displaced dead weight.

7) The Transition Sections were next loaded with rocks. The Transition Sections were positioned such that the distances between the bulkheads of the Transition Sections and the Bulkheads of the Test Section were less than 2 mm. Note that rocks were used in the Transition Sections for all experiments as it was found to be the

most convenient type of material to transport and position.

8) The Test Section and the load cell were next attached to the loop system via the turnbuckles (Item 3 : Figure 4.11).

9) Stopcock 1,7,2 and 9 (Figure 5.1) were closed for Bulkhead pressure measurements.

10) The load cell and pressure transducer were next balanced. In the case of the load cell this was achieved by loosening nut No.2 (Item 6: Figure 4.11). This deactivated the load cell and allowed the Test Section to move freely. The load cell thus experienced no load and is balanced. The Test Section was next moved upstream manually and nut No.1 (Item 7) tightened. The force measurement now recorded is the profile drag force on the Test Section. Refer to the Pressure Measurement Methodology described in Section 5.3 for balancing of pressure transducer.

11) Load cell and Pressure measurements were next recorded for 60 seconds using the data acquisition system.

12) Steps 9, 10 and 11 were repeated for Inner Flume wall pressure measurements, except in step 9 stopcock 1,6,2 and 8 were closed.

13) Next the load cell and pressure transducer were deactivated and steps 1 to 13 repeated for the next load type or flow rate.

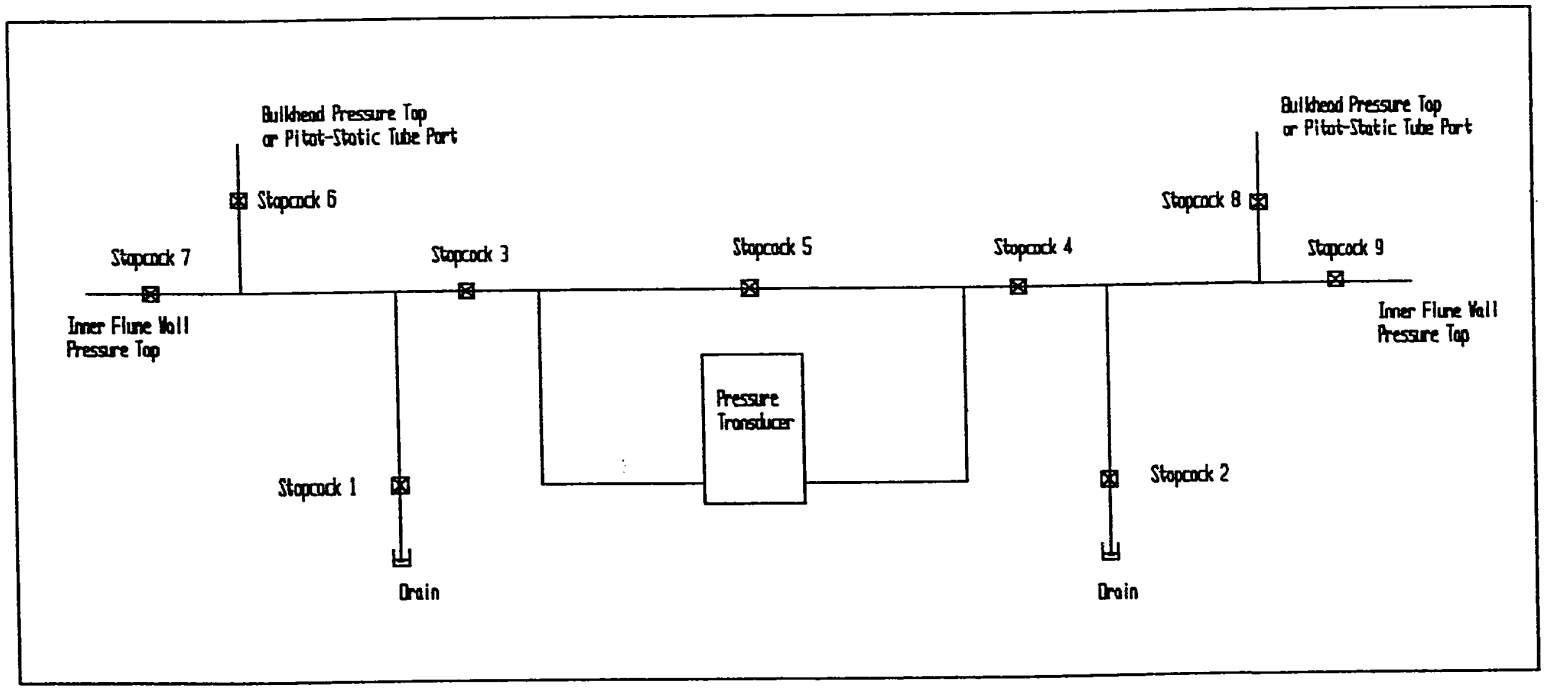

Figure 5.1 Pressure Measurement Set-up - Pressure Transducer

5.3 Phase 2.0 Pressure Measurement Methodology

The methodology associated with this phase consisted of recording the differential pressure:

- within the boundary layer using a pitot-static tube;
- between the Bulkheads of the upstream and downstream Transition Sections using pressure taps;
- over the Test Section length using the pressure taps installed in the Inner Flume wall.

The reason for repeating the Bulkhead and Inner Flume wall tests was because different pressure transducers were used in Phases 1 and 2.

Phases 1 and 2 were conducted over different periods, consistent model set-up was thus imperative. The methodology of Phase 1 was therefore repeated in Phase 2, except; the original load cell was replaced with a dummy load cell and the pressure transducers changed. The following test procedure was conducted.

1) The pitot-static tube was positioned at the respective Station (Figure 4.1) and adjusted such that it contacted the underside of the flexible membrane.
2) Air was next removed from the tubing that linked the pitot-static tube with the pressure transducer.
3) The data acquisition system was activated and the pressure transducer balanced.
4) The test commenced and data was collected over a 60

second period.

5) Next the pitot-static tube was moved to the subsequent position within the boundary layer and steps 3 to 5 repeated.

6) After completing all the measurements at Station 1, the pressure transducer was isolated, by closing stopcock 2 and 3 (Figure 5.1), and the pressure measurement rig moved to Station 2.

   Note the following:

   - the pressure transducer was isolated to prevent possible overloading;
   - the pitot-static tube was moved manually and maintained below the water level to prevent air from entering the tubing.

7) Steps 3 to 6 were repeated for the remaining Stations.

8) Next the Bulkhead pressure drops were recorded. This was achieved by disconnecting the tubing connecting the pitot-static tube with the transducer and connecting it to the Bulkhead pressure taps.

9) The pressure transducer was balanced and the differential pressure recorded.

10) Steps 8 and 9 were repeated for the Inner Flume wall differential pressure measurements.

11) Steps 1 to 10 were repeated for the next material type and/or flow rate.

5.4 Profile Measurement Methodology

After completing all force and pressure measurements, profile measurement rig was manually positioned in the Inner Flume and the knobs adjusted until contact between the knob and membrane was evident. The rig was then removed and the position of the individual knobs recorded.

6.0 RESULTS AND DATA REDUCTION

6.1 Preliminary Tests

Two preliminary tests were conducted. The first test consisted of determining the properties of the flexible membrane used. The second test consisted of two parts: construction of a 1/8th scaled bench top model of the Test Section; and an investigation into the relationship between the depth of submergence of the bench top model, tension in the membrane and the inward side curvature of the membrane.

6.1.1 Flexible Membrane Sample Test

The results of the experiments on the samples of flexible membrane are depicted in Figure 6.1. Figure 6.1 indicates a linear relationship between the stress and strain and thus verifying that the samples obeyed Hook's law in the range of the strain tested. The modulus of elasticity of each specimen was calculated; and the average of the four specimens was found to be approximately 73 MPa (see Appendix C: Tensile Test).

6.1.2 Bench Top Model Test

The results of the tests conducted confirmed the prediction that the inward side curvature of the bench model was a function of the tension in the membrane. An increase in

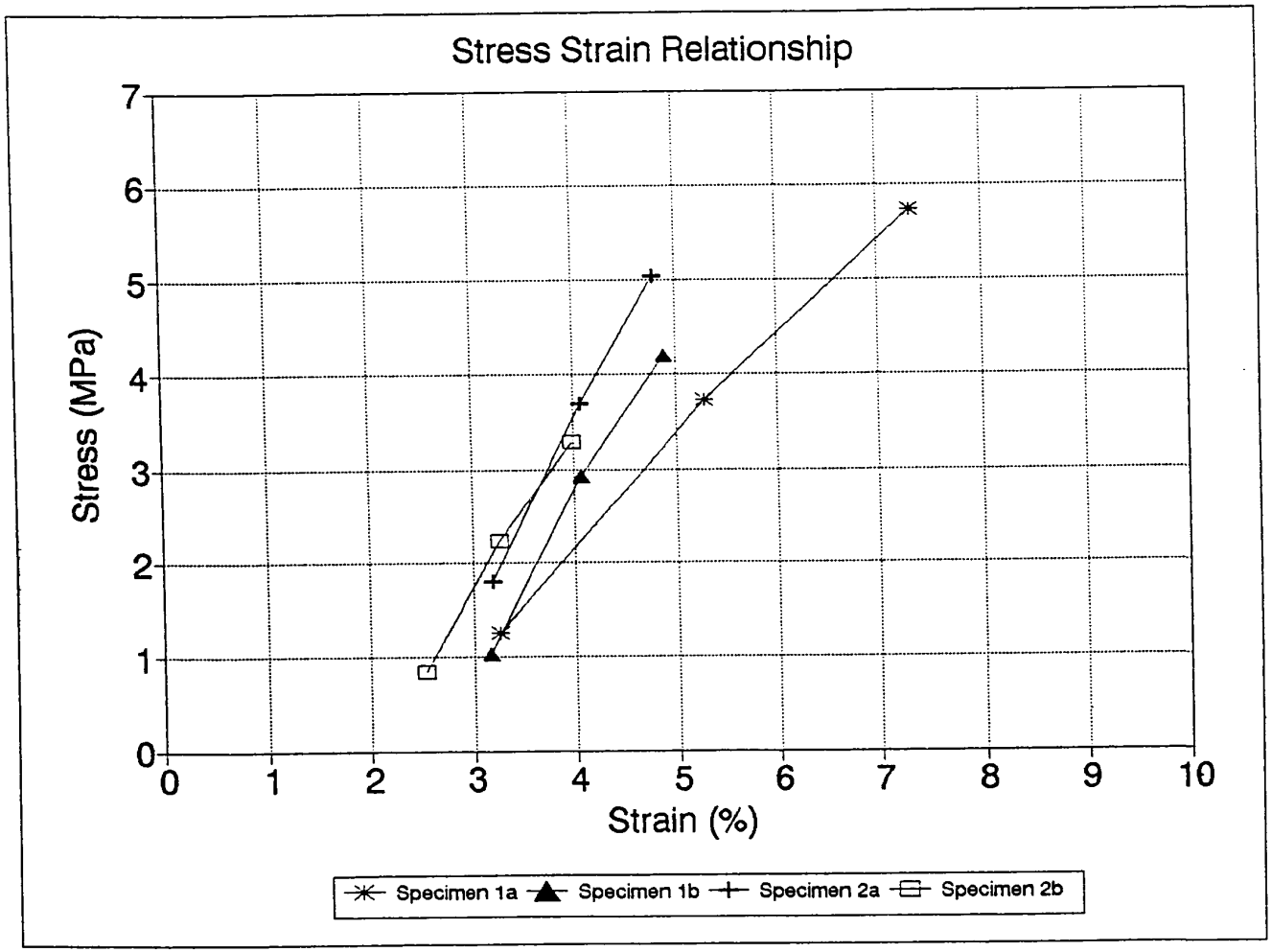

Figure 6.1 Stress Strain Relationship of Samples of Flexible Membrane

membrane tension produces both a reduction in side curvature; and an increase in load carrying capacity of the model (see Appendix A: Bench Top Model Test). The inward side curvature was caused by the hydrostatic pressure distribution on the sides of the model.

6.2 Physical Model Tests

The tests performed are summarised in Tables 6.1 and 6.2. In essence Phase 1.0 consisted of recording the drag force acting on the Test Section while under tension and subjected to various material loads and flow rates. The drag force was recorded simultaneously with the Bulkhead differential pressure and then simultaneously with the Inner Flume wall differential pressure. Each test was thus conducted twice (see Section 5.2). The tests conducted in Phase 2.0 consisted of recording the pitot-static tube differential pressure at ten points in the boundary layer and at four different positions along the Test Section. Each test thus consisted of recording the differential pressure at forty points, and the Bulkhead and Inner Flume wall differential pressure. The tension in the membrane was 1.0 kN (see Section 4.3.1).

6.2.1 Calibration of the Force Measurement Rig

To determine the relationship between the actual load applied and the load recorded by the load cell, a calibration curve for the system was required. Figure 6.2 and 6.3 show the

Table 6.1 Summary of Phase 1.0 Tests

Test No.	Material Type	Flow rate l/s	Load kg
1.1	na	25	0
1.2	Water	25	12.5
1.3	Water	25	25
1.4	Water	25	50
1.5	Water	38	12.5
1.6	Water	38	25
1.7	Water	38	50
1.8	Water	63	50
1.9	Sand	25	12.5
1.10	Sand	25	25
1.11	Sand	25	50
1.12	Sand	38	12.5
1.13	Sand	38	25
1.14	Sand	38	50
1.15	Sand	63	50
1.16	Rocks	25	12.5
1.17	Rocks	25	25
1.18	Rocks	25	50
1.19	Rocks	38	12.5
1.20	Rocks	38	25
1.21	Rocks	38	50
1.22	Rocks	63	50

na - not applicable

Table 6.2 Summary of Phase 2.0 Tests

Test No.	Material Type	Flow rate l/s	Load kg
2.1	Water	25	50
2.2	Water	38	50
2.3	Water	63	50
2.4	Sand	25	50
2.5	Sand	38	50
2.6	Sand	63	50
2.7	Rocks	25	50
2.8	Rocks	38	50
2.9	Rocks	63	50

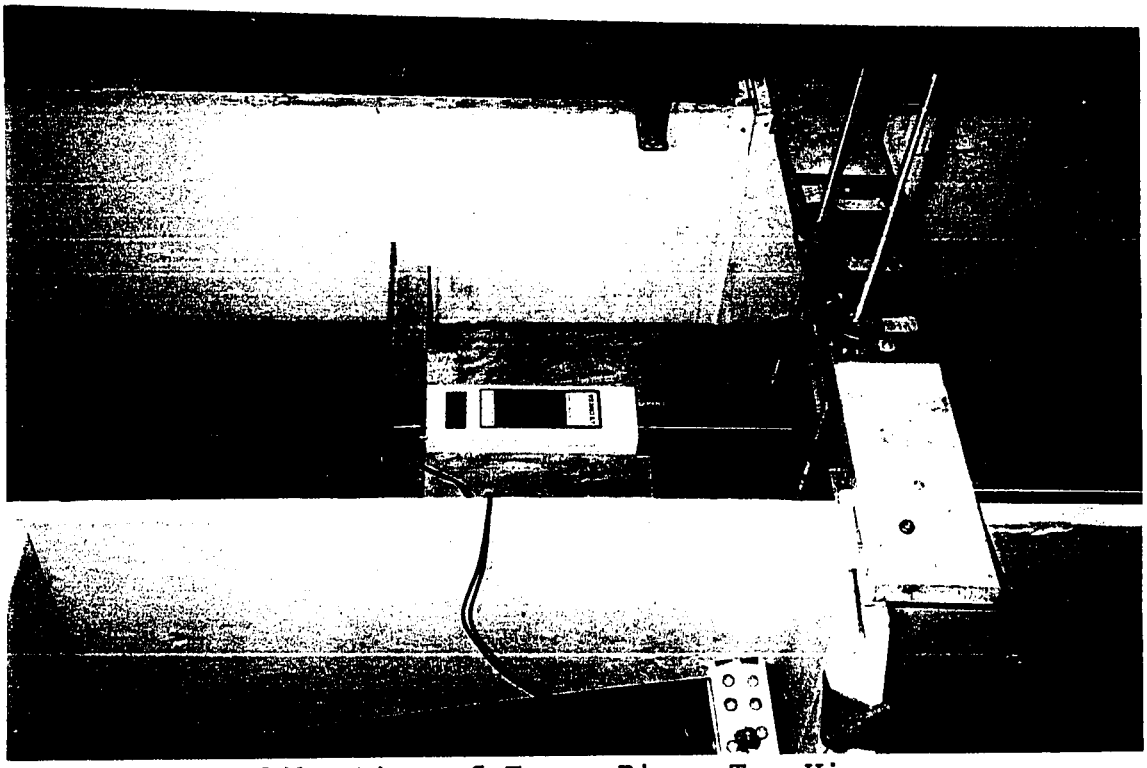

Figure 6.2 Calibration of Force Rig - Top View

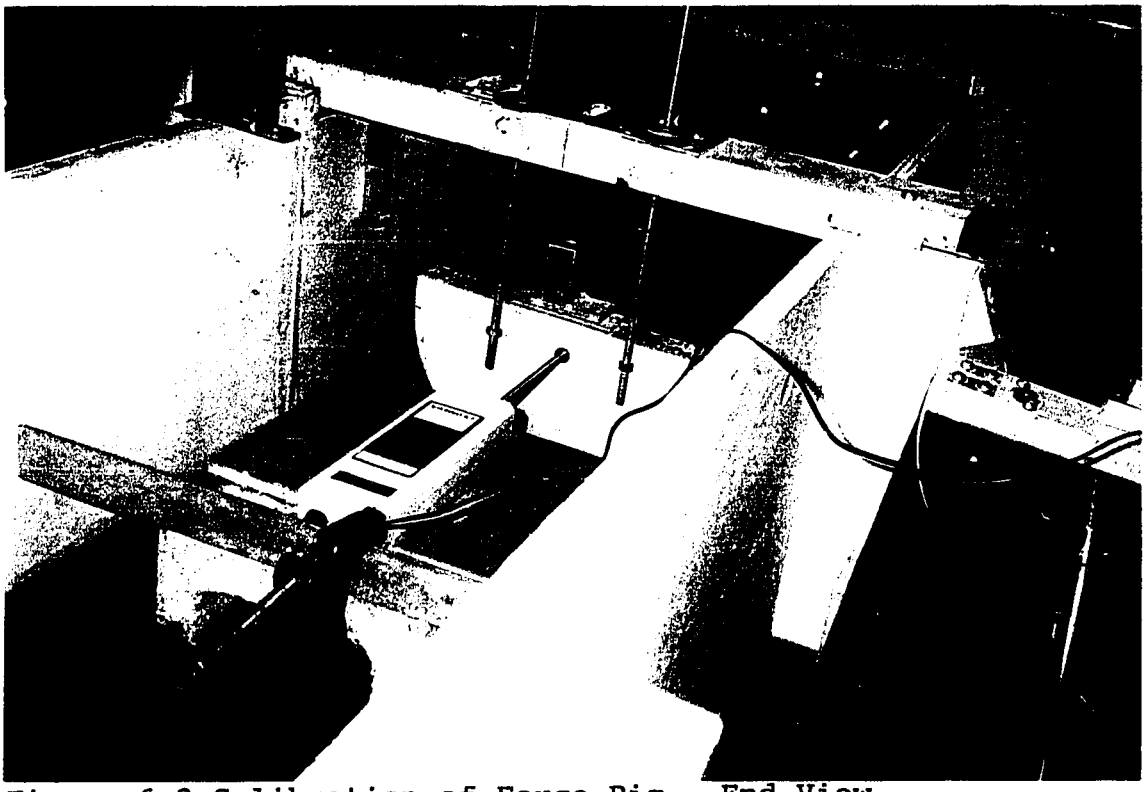

Figure 6.3 Calibration of Force Rig - End View

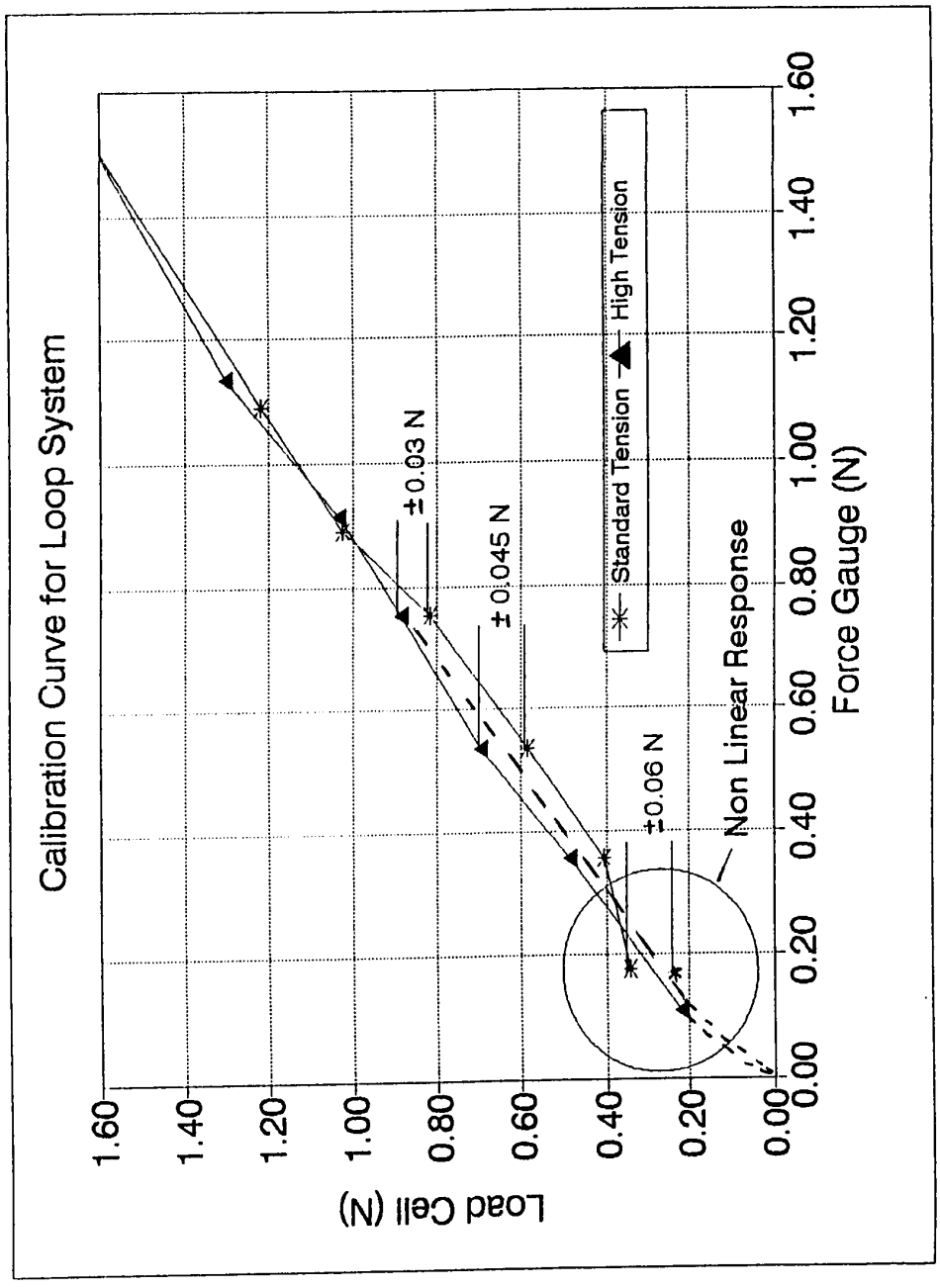

Figure 6.4 Calibration Curves for Loop System

set-up and Figure 6.4 depict the trends under different loop tensions. The plots indicate a lack of linearity in the lower range of load cell readings. This non linearity is more evident in the standard tension case, and an error band of ±0.06N in the low range and ±0.03N in the high range was found. This error band was deduced by placing a line of best fit through the high and standard tension data points, and comparing a point on this line with the actual data point recorded.

6.2.2 Raw Data

The test conditions for the raw data collected are summarised in Table 6.3 for Phase 1.0, and Table 6.4 for Phase 2.0. The raw data collected by the data acquisition system are described in Sections 6.2.2a and 6.2.2b.

6.2.2a Force Measurements

Figures 6.5 to 6.14 indicated the typical data trends associated with the load cell measurements. A test length of 60 seconds, and a sampling rate of 5 data/second was selected for all load cell measurements. Each experiment was repeated for every test conducted. Each experiment recorded simultaneously the force acting on the Test Section and either the Bulkhead or Inner Flume wall differential pressure. Table 6.5 provides a summary of the load cell measurements.

6.2.2b Pressure Measurements

Figures 6.15 to 6.26 indicate the typical data trends associated with the recording of the differential pressure, within the boundary layer, by the pressure transducer. A test length of 60 seconds, and a sampling rate of 20 data/second was selected for all pressure transducer measurements. Tables 6.6 to 6.8 provide a summary of the pressure transducer measurements. The differential pressure recorded is the velocity head from which the local mean velocity was calculated. This was then plotted against the perpendicular distance from the flexible membrane. The data trends are shown in Figures 6.27 to 6.35.

6.2.3 Calculated Velocities

The local mean (time averaged) free stream velocity was calculated and indicated in Table 6.9. This velocity represents the velocity of the free stream at the respective stations. The average free stream velocities are displayed in Table 6.10 and represents the average of the local mean free stream velocities indicated in Table 6.9.

6.2.4 Boundary Layer Thickness

The pressure measurements collected were converted into velocity and plotted against the normal distance (y) on a log/log scale. The plot was then extrapolated to the 99% mainstream velocity line to determine the boundary layer

thickness. Samples of this procedure are shown in Figures 6.36 to 6.39. The local boundary layer thickness was then plotted against $x/Re^{0.2}$ to determine the growth of the boundary layer along the Test Section. The results are plotted and tabulated in Figures 6.40 to 6.48 and Table 6.11. Linear regression was used to determine the line of best fit and the corresponding boundary layer thicknesses are included in Table 6.11.

6.2.5 Power-law Exponents

The local power-law exponents are summarised in Table 6.12. These exponents were determined by plotting log (u/U) against log(y/$\tilde{U}$), Figures 6.49 to 6.57, and calculating the slope. Linear regression was used to calculate the slopes.

6.2.6 Drag force

The measured and calculated drag forces associated with a full load case are shown in Table 6.13. The force recorded by the load cell represents an average of two forces recorded during each test (see Section 6.2.2a). The range indicated includes the non-linearity associated with the loop system. Table 6.14 highlights the drag force recorded under various live loads, i.e., different drafts or displacements. The local drag force between stations is highlighted in Table 6.15.

6.2.7 Skin Friction

The local skin friction coefficients are listed in Table

6.16. The average skin friction coefficient for Phase 1.0 and Phase 2.0 are listed in Table 6.12.

6.3 Profile data

The profiles associated with the water, sand and rock set-ups are shown in Figure 6.58, 6.59, 6.60 respectively.

Table 6.3 Raw Data: Phase 1.0

Test No.	Material Type	Q l/s	Load kg	WL[1] mm	HT mm	Draft mm	P[2] mm	R[3] mm	Area mm^2	v m/s	T[4] deg C	Re[5] Rv/ν	Re[6] Dv/ν
1.1	na	25	0	381	43	25	163	16	168987	0.148	22.6	2.27E+03	3.82E+04
1.2	Water	25	12.5	381	68	49	236	30	164378	0.152	22.6	4.46E+03	3.92E+04
1.3	Water	25	25	381	88	70	285	41	159872	0.156	22.6	6.22E+03	4.04E+04
1.4	Water	25	50	381	123	104	358	56	151359	0.165	22.6	9.07E+03	4.26E+04
1.5	Water	38	12.5	408	47	56	252	33	175369	0.217	22.6	7.09E+03	5.59E+04
1.6	Water	38	25	408	61	70	285	41	172232	0.221	22.6	8.77E+03	5.69E+04
1.7	Water	38	50	408	98	107	363	57	163076	0.233	22.6	1.30E+04	6.01E+04
1.8	Water	63	50	454	49	103	356	56	184446	0.342	22.6	1.86E+04	8.81E+04
1.9	Sand	25	12.5	381	70	51	241	31	163964	0.152	22.6	4.64E+03	3.93E+04
1.10	Sand	25	25	381	92	73	293	42	159052	0.157	22.6	6.52E+03	4.06E+04
1.11	Sand	25	50	381	127	108	367	58	150325	0.166	22.6	9.39E+03	4.29E+04
1.12	Sand	38	12.5	410	44	54	247	32	176311	0.216	22.6	6.86E+03	5.56E+04
1.13	Sand	38	25	410	65	75	296	43	171565	0.221	22.6	9.36E+03	5.72E+04
1.14	Sand	38	50	410	103	113	376	59	162020	0.235	22.6	1.36E+04	6.05E+04
1.15	Sand	63	50	455	57	112	375	59	182570	0.345	22.6	2.00E+04	8.90E+04
1.16	Rocks	25	12.5	381	78	60	261	35	162307	0.154	22.6	5.35E+03	3.97E+04
1.17	Rocks	25	25	381	88	70	284	40	160043	0.156	22.6	6.20E+03	4.03E+04
1.18	Rocks	25	50	381	118	100	349	54	152690	0.164	22.6	8.68E+03	4.22E+04
1.19	Rocks	38	12.5	409	44	54	247	32	176250	0.216	22.6	6.84E+03	5.56E+04
1.20	Rocks	38	25	409	59	69	282	40	172917	0.220	22.6	8.63E+03	5.67E+04
1.21	Rocks	38	50	409	90	100	349	54	165328	0.230	22.6	1.22E+04	5.93E+04
1.22	Rocks	63	50	455	59	114	379	60	182049	0.346	22.6	2.03E+04	8.93E+04

1 - Water level in Inner Flume ; 2 - Wetted perimeter ; 3 - Hydraulic radius ; 4 - Average temperature from Phase 2.0

5 - Reynolds Number based on hydraulic radius ; 6 - Reynolds Number based on diameter of Bulkheads.

Table 6.4 Raw Data: Phase 2.0

Test No.	Material Type	Q l/s	Load kg	WL[1] mm	HT mm	Draft mm	P[2] mm	R[3] mm	Area mm^2	v m/s	T deg F	Re[4] Rv/ν	Re[5] Dv/ν
2.1	Water	25	50	381	120	101	352	55	152129	0.164	76 - na	8.83E+03	4.24E+04
2.2	Water	38	50	408	92	100	351	54	164570	0.231	72	1.23E+04	5.96E+04
2.3	Water	63	50	454	50	105	359	56	184287	0.342	72 - 72	1.88E+04	8.82E+04
2.4	Sand	25	50	381	129	110	371	58	149807	0.167	70 - 70	9.54E+03	4.31E+04
2.5	Sand	38	50	408	103	111	373	59	161774	0.235	70 - 70	1.35E+04	6.06E+04
2.6	Sand	63	50	454	59	114	378	60	181953	0.346	70	2.02E+04	8.93E+04
2.7	Rocks	25	50	381	124	105	360	56	151101	0.165	72 - 76	9.15E+03	4.27E+04
2.8	Rocks	38	50	408	102	110	371	58	161991	0.235	70 - na	1.34E+04	6.05E+04
2.9	Rocks	63	50	454	59	114	378	60	181953	0.346	74 - 76	2.02E+04	8.93E+04

1 - Water level in Inner Flume ; 2 - Wetted perimeter ; 3 - Hydraulic radius ; na - Not available

4 - Reynolds Number based on hydraulic radius ; 5 - Reynolds Number based on diameter of Bulkheads.

Table 6.5 Raw Data: Phase 1.0 - Load Cell Measurements

Test Number	Bulkhead or Flume wall	Average Force (N)	Standard Deviation	Degrees of Freedom	Frequency	Std/Freq
1.1	Bulkhead	0.1918	NA	NA	NA	NA
	Flume wall	0.1859	NA	NA	NA	NA
1.2	Bulkhead	0.1606	0.0124	155	2.58	0.0048
	Flume wall	0.1628	0.0127	156	2.60	0.0049
1.3	Bulkhead	0.1630	0.0228	148	2.47	0.0092
	Flume wall	0.1124	0.0323	107	1.78	0.0181
1.4	Bulkhead	0.1755	0.0294	153	2.55	0.0115
	Flume wall	0.1877	0.0210	145	2.42	0.0087
1.5	Bulkhead	0.2404	0.0207	150	2.50	0.0083
	Flume wall	0.1951	0.0184	163	2.72	0.0068
1.6	Bulkhead	0.2472	0.0696	150	2.50	0.0279
	Flume wall	0.2225	0.0257	150	2.50	0.0103
1.7	Bulkhead	0.2253	0.0354	154	2.57	0.0138
	Flume wall	0.2150	0.0404	153	2.55	0.0158
1.8	Bulkhead	0.6380	0.1453	150	2.50	0.0581
	Flume wall	0.7482	0.1398	146	2.43	0.0575
1.9	Bulkhead	0.2551	0.0147	160	2.67	0.0055
	Flume wall	0.2645	0.0160	151	2.52	0.0064
1.10	Bulkhead	0.1889	0.0287	151	2.52	0.0114
	Flume wall	0.1923	0.0213	154	2.57	0.0083
1.11	Bulkhead	0.2531	0.0352	149	2.48	0.0142
	Flume wall	0.2623	0.0305	156	2.60	0.0117
1.2	Bulkhead	0.2032	0.0405	156	2.60	0.0156
	Flume wall	0.3142	0.0515	157	2.62	0.0197
1.13	Bulkhead	0.2512	0.0590	157	2.62	0.0226
	Flume wall	0.2272	0.0594	161	2.68	0.0221
1.14	Bulkhead	0.2969	0.0590	144	2.40	0.0246
	Flume wall	0.2813	0.0521	164	2.73	0.0191
1.15	Bulkhead	0.7510	0.2832	146	2.43	0.1164
	Flume wall	0.7793	0.3185	151	2.52	0.1266
1.16	Bulkhead	0.1613	0.0180	169	2.82	0.0064
	Flume wall	0.1702	0.0175	162	2.70	0.0065
1.17	Bulkhead	0.1779	0.0182	152	2.53	0.0072
	Flume wall	0.1762	0.0194	154	2.57	0.0076
1.18	Bulkhead	0.2688	0.0251	166	2.77	0.0091
	Flume wall	0.3381	0.0271	160	2.67	0.0102
1.19	Bulkhead	0.2832	0.0503	150	2.50	0.0201
	Flume wall	0.2412	0.0444	150	2.50	0.0178
1.20	Bulkhead	0.3227	0.0474	143	2.38	0.0199
	Flume wall	0.2814	0.0494	148	2.47	0.0200
1.21	Bulkhead	0.3072	0.0704	144	2.40	0.0293
	Flume wall	0.3638	0.0631	154	2.57	0.0246
1.22	Bulkhead	0.7589	0.2691	151	2.52	0.1069
	Flume wall	0.7757	0.2314	147	2.45	0.0944

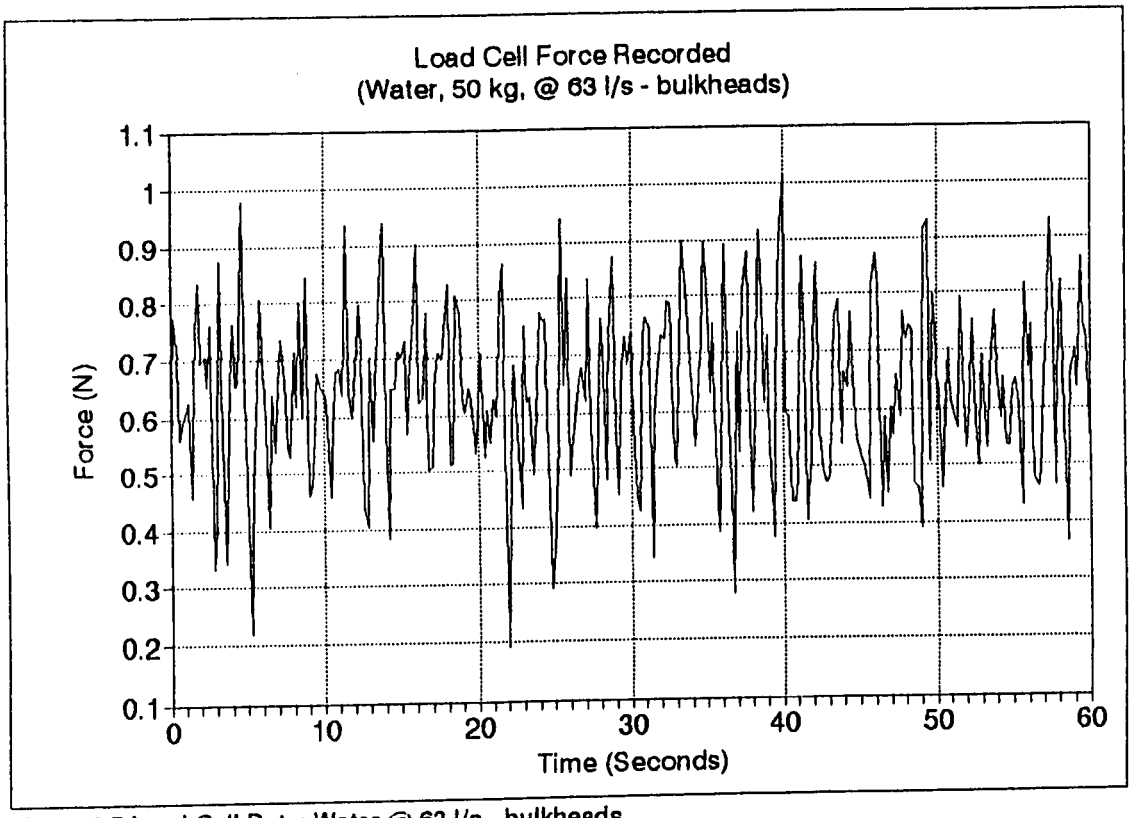

Figure 6.5 Load Cell Data: Water @ 63 l/s - bulkheads

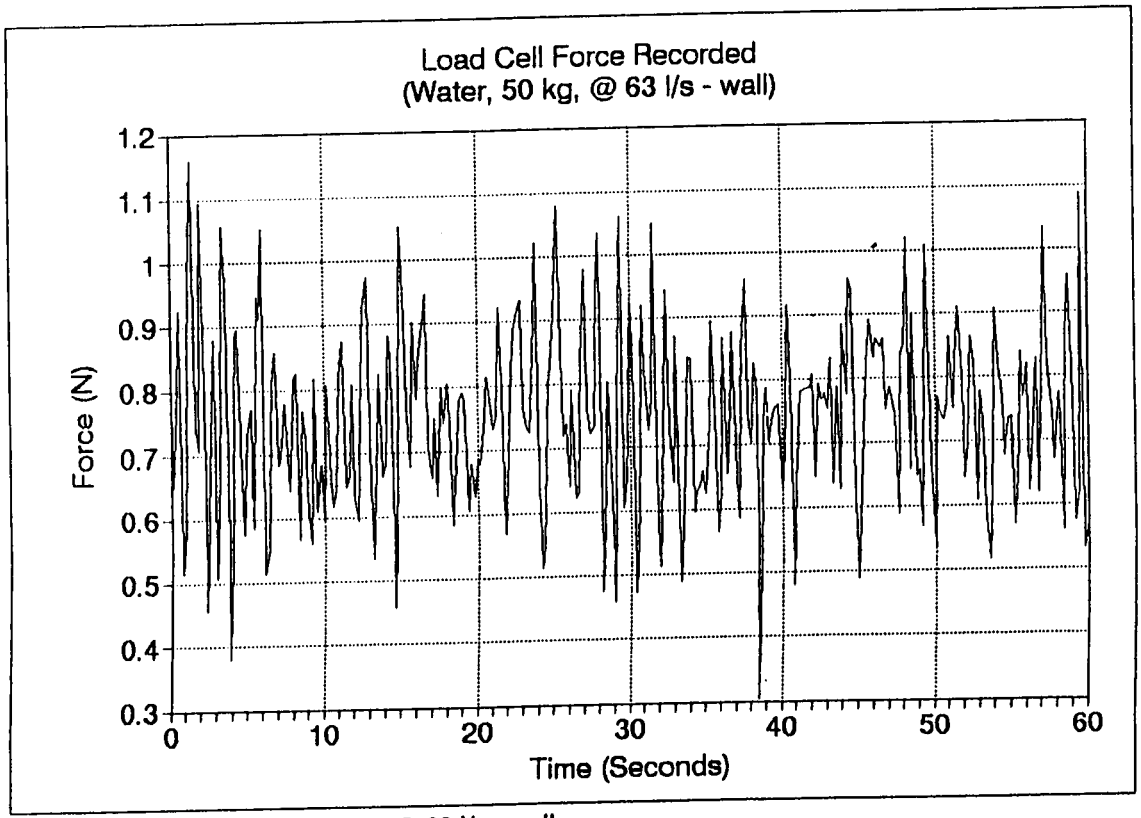

Figure 6.6 Load Cell Data: Water @ 63 l/s - wall

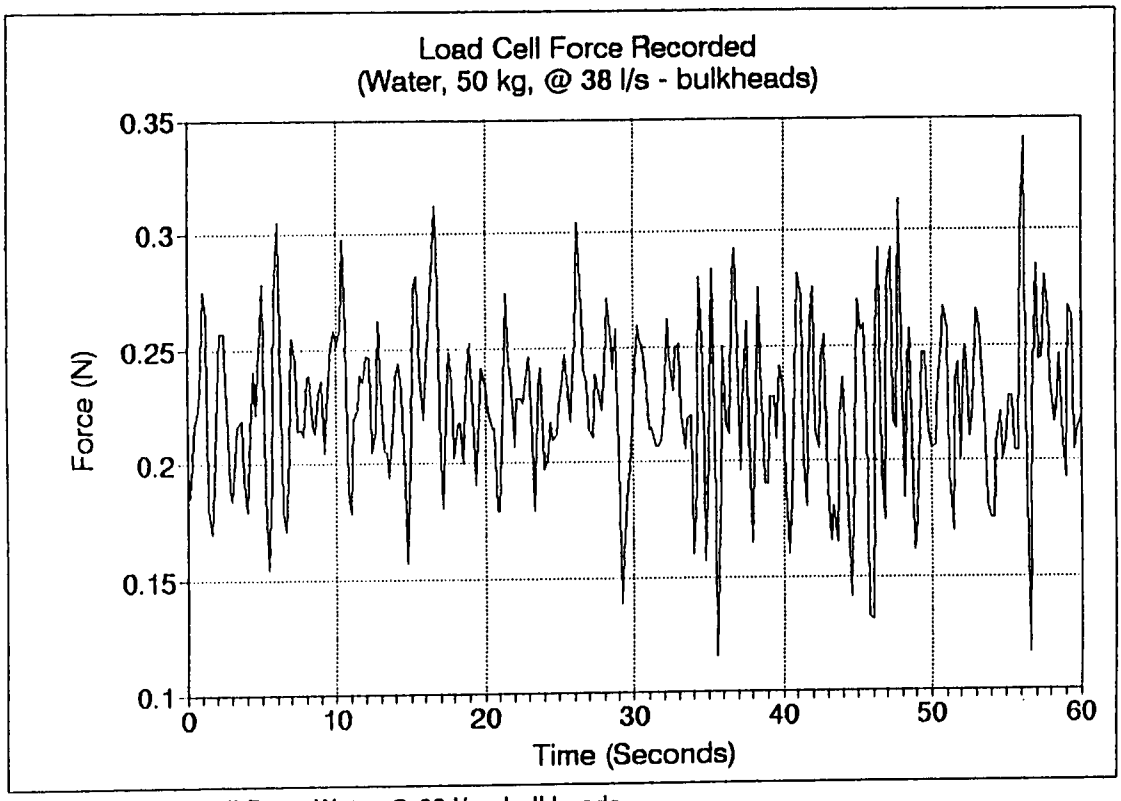

Figure 6.7 Load Cell Data: Water @ 38 l/s - bulkheads

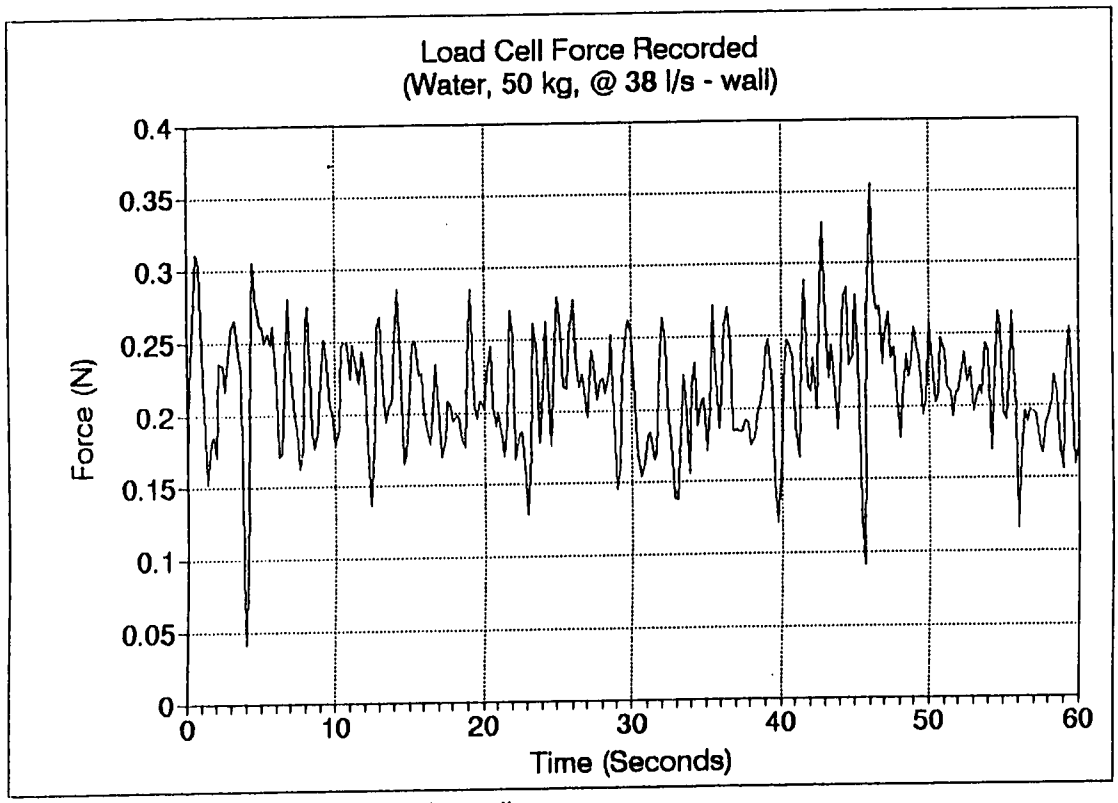

Figure 6.8 Load Cell Data: Water 38 l/s - wall

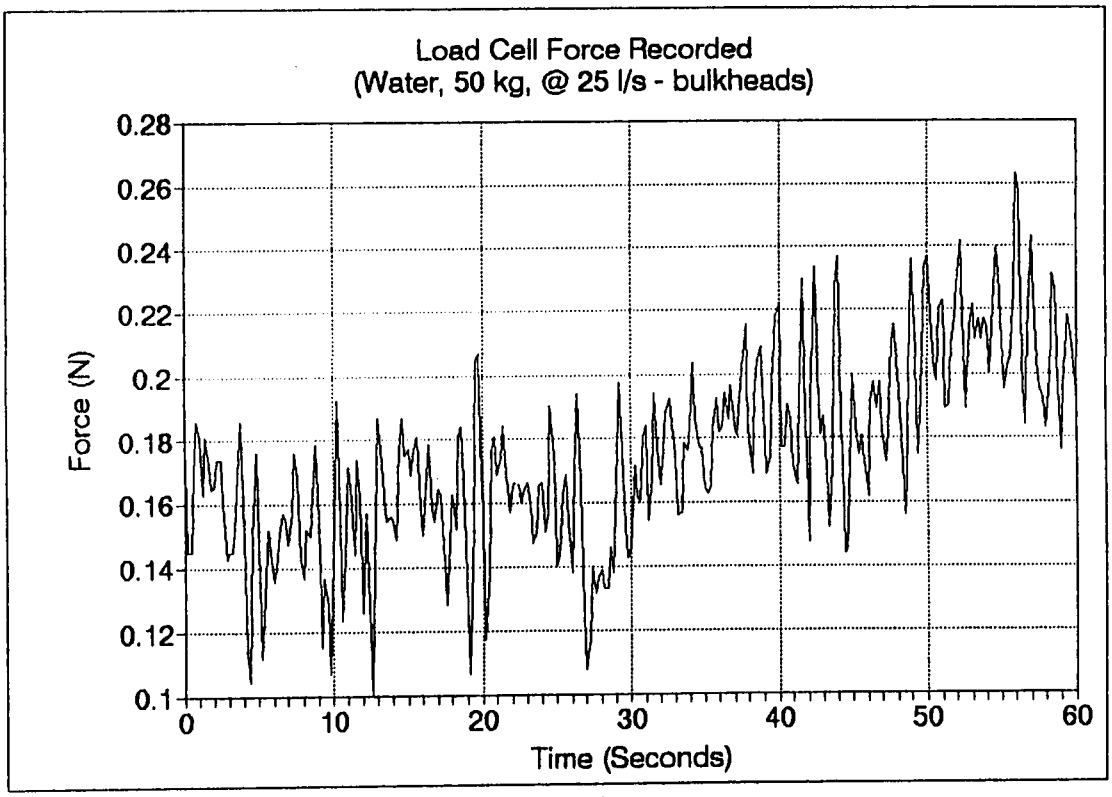

Figure 6.9 Load Cell Data: Water @ 25 l/s - bulkheads

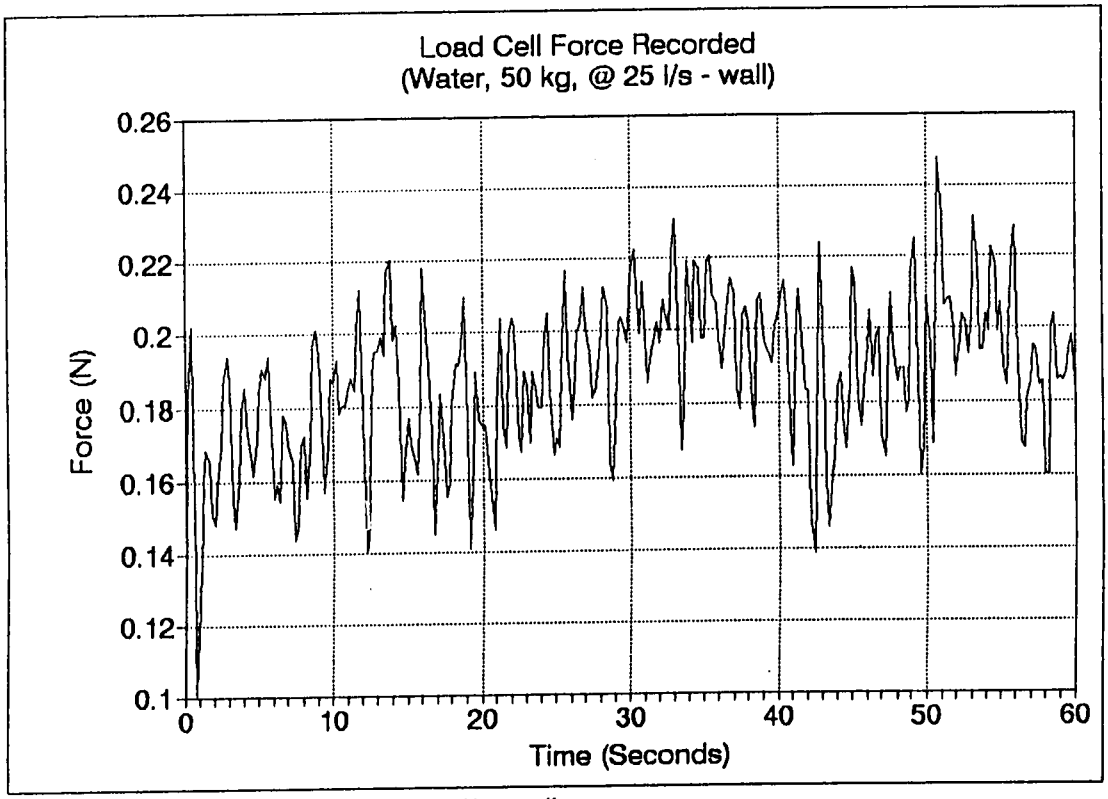

Figure 6.10 Load Cell Data: Water @ 25 l/s - wall

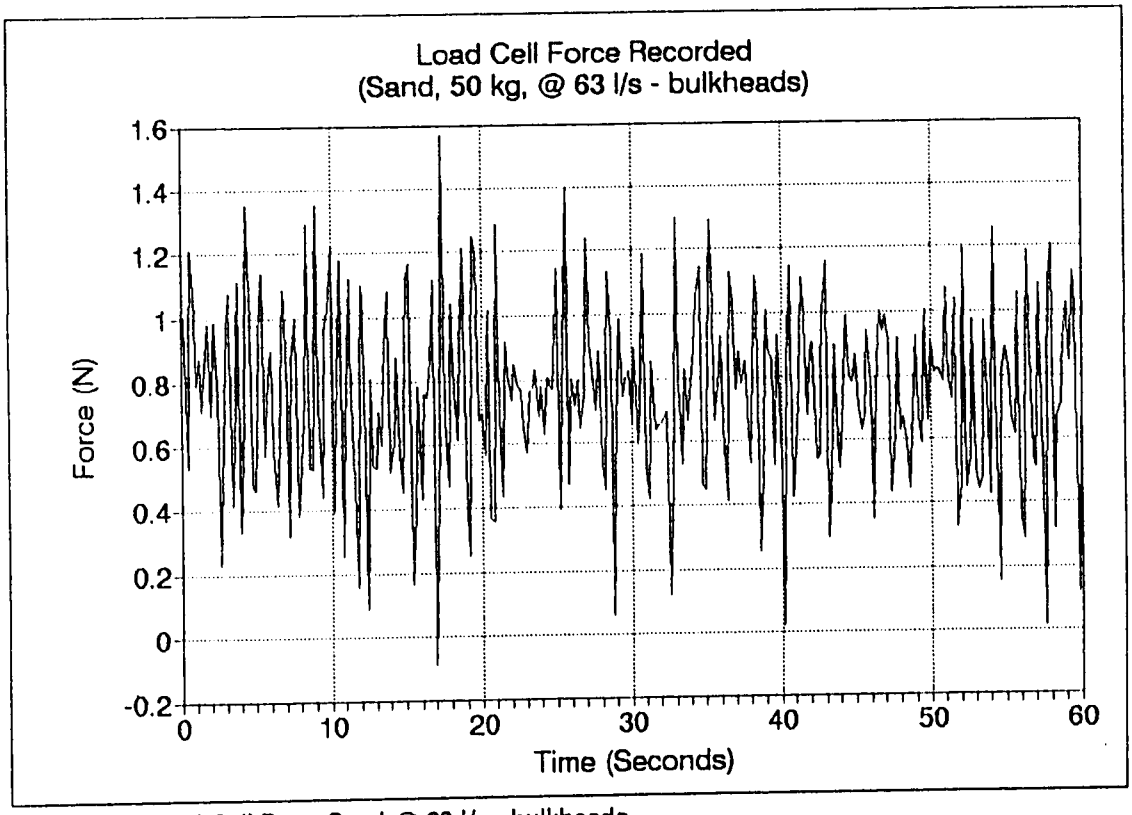

Figure 6.11 Load Cell Data: Sand @ 63 l/s - bulkheads

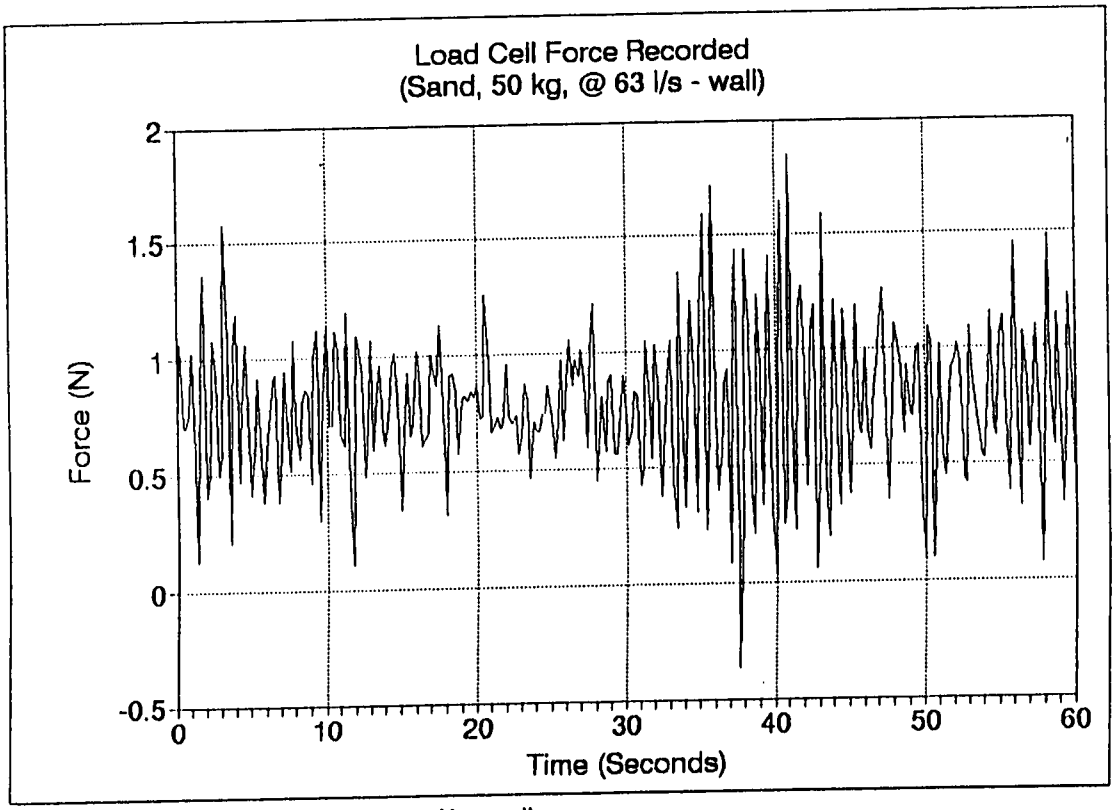

Figure 12 Load Cell Data: Sand @ 63 l/s - wall

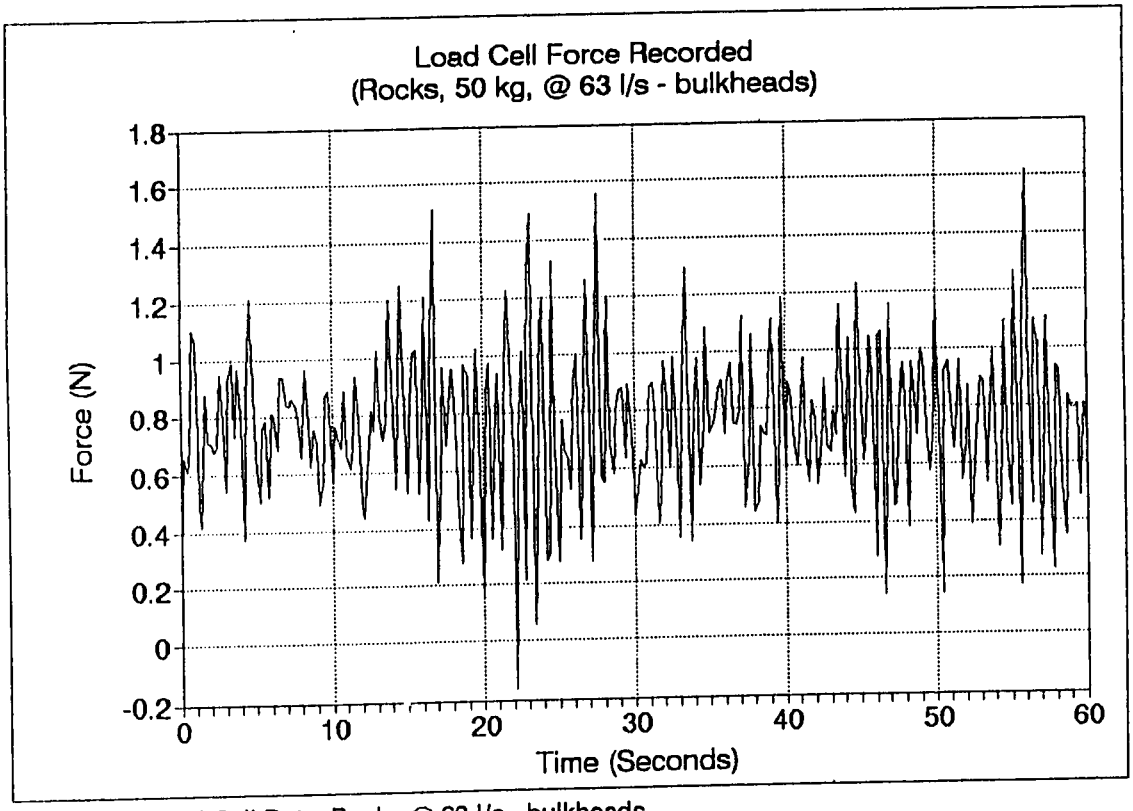

Figure 6.13 Load Cell Data: Rocks @ 63 l/s - bulkheads

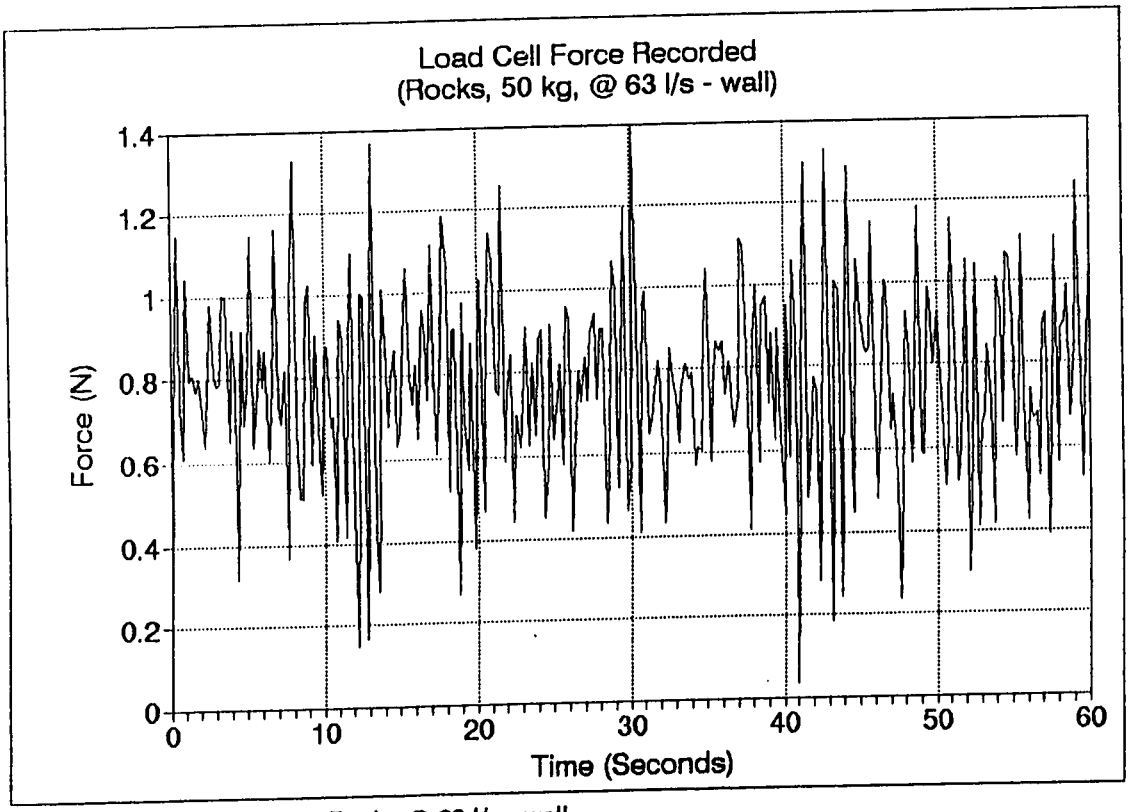

Figure 6.14 Load Cell Data: Rocks @ 63 l/s - wall

Table 6.6 Raw Data: Phase 2.0 - Pressure Transducer
Boundary Layer Measurements - Water @ 63 l/s

Station	Normal Distance (mm)[1]	Average Pressure (mm)	Standard Deviation	Degrees of Freedom	Frequency	Std/Freq
1	3.175	2.9579	0.1680	619	10.32	0.0163
	5	3.3522	0.2396	644	10.73	0.0223
	7.5	3.9879	0.2049	623	10.38	0.0197
	10	4.7794	0.3992	526	8.77	0.0455
	15	5.3670	0.1625	690	11.50	0.0141
	20	5.7492	0.3851	725	12.08	0.0319
	25	6.2636	0.1999	499	8.32	0.0240
	30	6.0164	0.2915	503	8.38	0.0348
	50	6.3112	0.1754	540	9.00	0.0195
	93	6.1406	0.1932	501	8.35	0.0231
2	3.175	2.4614	0.1131	600	10.00	0.0113
	5	2.8110	0.0811	587	9.78	0.0083
	7.5	3.4561	0.2641	533	8.88	0.0297
	10	3.6370	0.1905	554	9.23	0.0206
	15	4.4543	0.3132	608	10.13	0.0309
	20	5.0212	0.1902	497	8.28	0.0230
	25	5.0646	0.3428	641	10.68	0.0321
	30	5.3557	0.3681	687	11.45	0.0321
	50	6.0576	0.2640	505	8.42	0.0314
	90	6.4350	0.2061	409	6.82	0.0302
3	3.175	1.8973	0.0400	700	11.67	0.0034
	5	2.3143	0.1125	466	7.77	0.0145
	7.5	2.8465	0.2633	732	12.20	0.0216
	10	2.9906	0.1255	629	10.48	0.0120
	15	3.5338	0.2066	664	11.07	0.0187
	20	3.9982	0.2021	668	11.13	0.0182
	25	4.4287	0.1584	763	12.72	0.0125
	30	4.5014	0.2505	653	10.88	0.0230
	50	5.2202	0.1018	555	9.25	0.0110
	90	6.0372	0.1518	431	7.18	0.0211
4	3.175	2.2740	0.1022	645	10.75	0.0095
	5	2.6759	0.1315	752	12.53	0.0105
	7.5	2.9439	0.0822	614	10.23	0.0080
	10	3.4841	0.1811	558	9.30	0.0195
	15	3.7953	0.2078	560	9.33	0.0223
	20	4.2139	0.2319	570	9.50	0.0244
	25	4.3725	0.1451	554	9.23	0.0157
	30	4.6373	0.2174	557	9.28	0.0234
	50	5.2685	0.1972	692	11.53	0.0171
	90	6.0733	0.2001	657	10.95	0.0183

1 - Distance normal to flexible membrane

Table 6.7 Raw Data: Phase 2.0 - Pressure Transducer
Boundary Layer Measurements - Sand @ 63 l/s

Station	Normal Distance (mm)[1]	Average Pressure (mm)	Standard Deviation	Degrees of Freedom	Frequency	Std/Freq
1	3.175	4.4293	0.2508	588	9.80	0.0256
	5	4.6950	0.2817	633	10.55	0.0267
	7.5	5.5044	0.4307	364	6.07	0.0710
	10	5.7337	0.2014	623	10.38	0.0194
	15	6.3358	0.2932	668	11.13	0.0263
	20	6.6734	0.3399	552	9.20	0.0369
	25	6.7475	0.3157	541	9.02	0.0350
	30	7.1271	0.1106	625	10.42	0.0106
	50	7.1959	0.3577	648	10.80	0.0331
	90	6.9818	0.2399	616	10.27	0.0234
2	3.175	2.2005	0.1627	407	6.78	0.0240
	5	2.6807	0.1174	647	10.78	0.0109
	7.5	3.2936	0.2787	551	9.18	0.0303
	10	3.5808	0.2578	538	8.97	0.0288
	15	4.3125	0.2240	554	9.23	0.0243
	20	4.8155	0.3107	604	10.07	0.0309
	25	5.3353	0.3610	664	11.07	0.0326
	30	5.4233	0.1701	662	11.03	0.0154
	50	5.9293	0.2664	551	9.18	0.0290
	90	6.4585	0.1628	485	8.08	0.0201
3	3.175	2.5519	0.1603	581	9.68	0.0166
	5	2.7901	0.1883	502	8.37	0.0225
	7.5	3.0690	0.2333	564	9.40	0.0248
	10	3.8148	0.3923	723	12.05	0.0326
	15	4.0500	0.2752	546	9.10	0.0302
	20	4.8416	0.2190	618	10.30	0.0213
	25	4.5724	0.2953	653	10.88	0.0271
	30	5.2436	0.4083	611	10.18	0.0401
	50	5.7990	0.2915	657	10.95	0.0266
	90	6.4222	0.1965	738	12.30	0.0160
4	3.175	2.0236	0.0806	469	7.82	0.0103
	5	2.4695	0.1016	740	12.33	0.0082
	7.5	2.8853	0.1739	582	9.70	0.0179
	10	3.0432	0.1853	699	11.65	0.0159
	15	3.4981	0.1721	702	11.70	0.0147
	20	3.8191	0.2614	765	12.75	0.0205
	25	4.2772	0.2273	579	9.65	0.0236
	30	4.4534	0.2249	552	9.20	0.0245
	50	5.2283	0.2345	678	11.30	0.0208
	90	6.2251	0.2363	616	10.27	0.0230

1 - Distance normal to flexible membrane

Table 6.8 Raw Data: Phase 2.0 - Pressure Transducer
Boundary Layer Measurements - Rocks @ 63 l/s

Station	Normal Distance (mm)	Average Pressure (mm)[1]	Standard Deviation	Degrees of Freedom	Frequency	Std/Freq
1	3.175	3.3807	0.2914	550	9.17	0.0318
	5	3.3757	0.3828	652	10.87	0.0352
	7.5	4.1719	0.3246	574	9.57	0.0339
	10	4.4498	0.3362	684	11.40	0.0295
	15	4.9829	0.4193	741	12.35	0.0340
	20	5.5945	0.4384	608	10.13	0.0433
	25	6.0567	0.3335	599	9.98	0.0334
	30	6.6631	0.3650	624	10.40	0.0351
	50	6.6660	0.4275	700	11.67	0.0366
	90	6.2967	0.3483	587	9.78	0.0356
2	3.175	1.9574	0.1940	723	12.05	0.0161
	5	2.0653	0.2112	624	10.40	0.0203
	7.5	2.0976	0.2020	693	11.55	0.0175
	10	2.1199	0.2111	599	9.98	0.0211
	15	2.6742	0.3040	597	9.95	0.0306
	20	3.6668	0.2968	628	10.47	0.0284
	25	3.8878	0.4603	579	9.65	0.0477
	30	4.0780	0.3404	569	9.48	0.0359
	50	5.4249	0.3962	582	9.70	0.0408
	90	6.3803	0.3835	617	10.28	0.0373
3	3.175	2.2894	0.2110	622	10.37	0.0204
	5	2.1208	0.2090	575	9.58	0.0218
	7.5	2.0494	0.2595	672	11.20	0.0232
	10	2.3792	0.1892	646	10.77	0.0176
	15	3.3201	0.5498	684	11.40	0.0482
	20	3.9382	0.2934	550	9.17	0.0320
	25	4.1799	0.3703	527	8.78	0.0422
	30	4.6835	0.5347	651	10.85	0.0493
	50	5.4321	0.4761	689	11.48	0.0415
	90	6.2391	0.2231	683	11.38	0.0196
4	3.175	2.2568	0.1828	679	11.32	0.0162
	5	2.5152	0.1920	646	10.77	0.0178
	7.5	3.0780	0.2975	570	9.50	0.0313
	10	3.2428	0.1880	664	11.07	0.0170
	15	3.8497	0.2207	720	12.00	0.0184
	20	4.1191	0.3667	666	11.10	0.0330
	25	4.5503	0.2719	598	9.97	0.0273
	30	4.6061	0.2685	579	9.65	0.0278
	50	5.6909	0.3598	632	10.53	0.0342
	90	6.5293	0.3522	645	10.75	0.0328

1 - Distance normal to flexible membrane

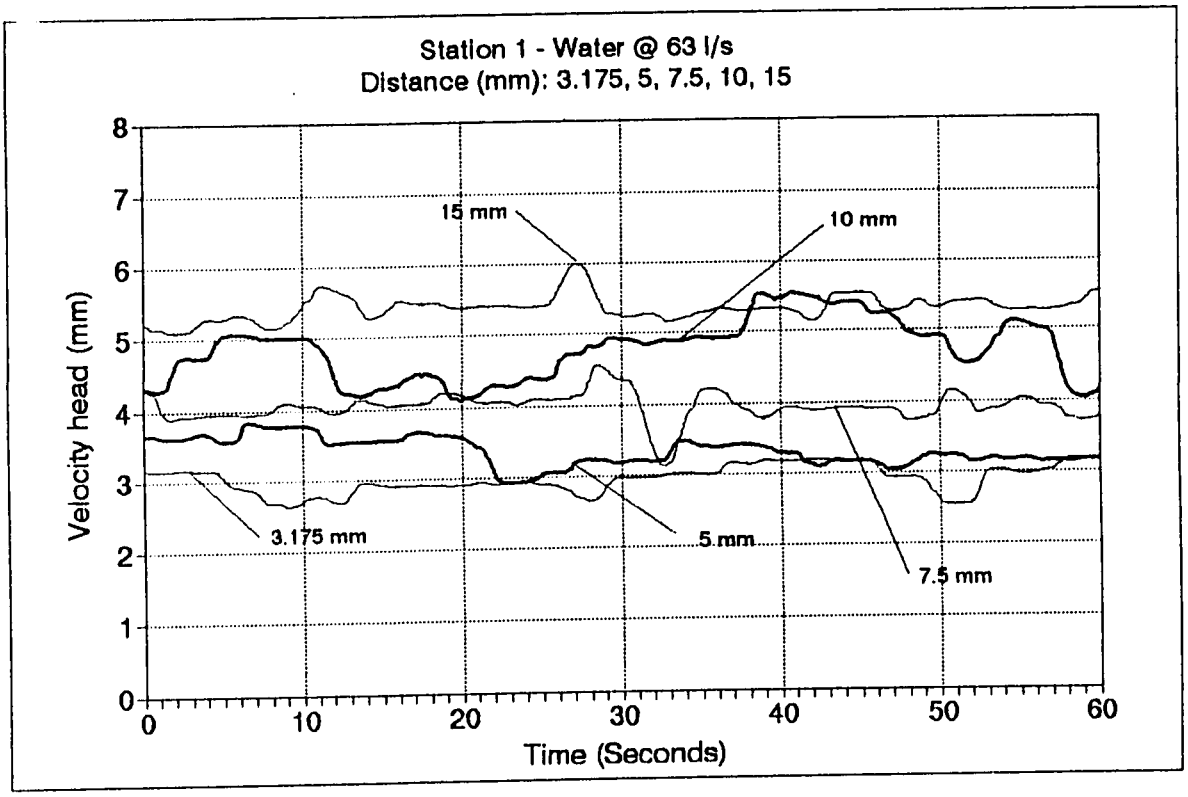

Figure 6.15 Pressure Transducer Data: Water @ 63 l/s - Station 1

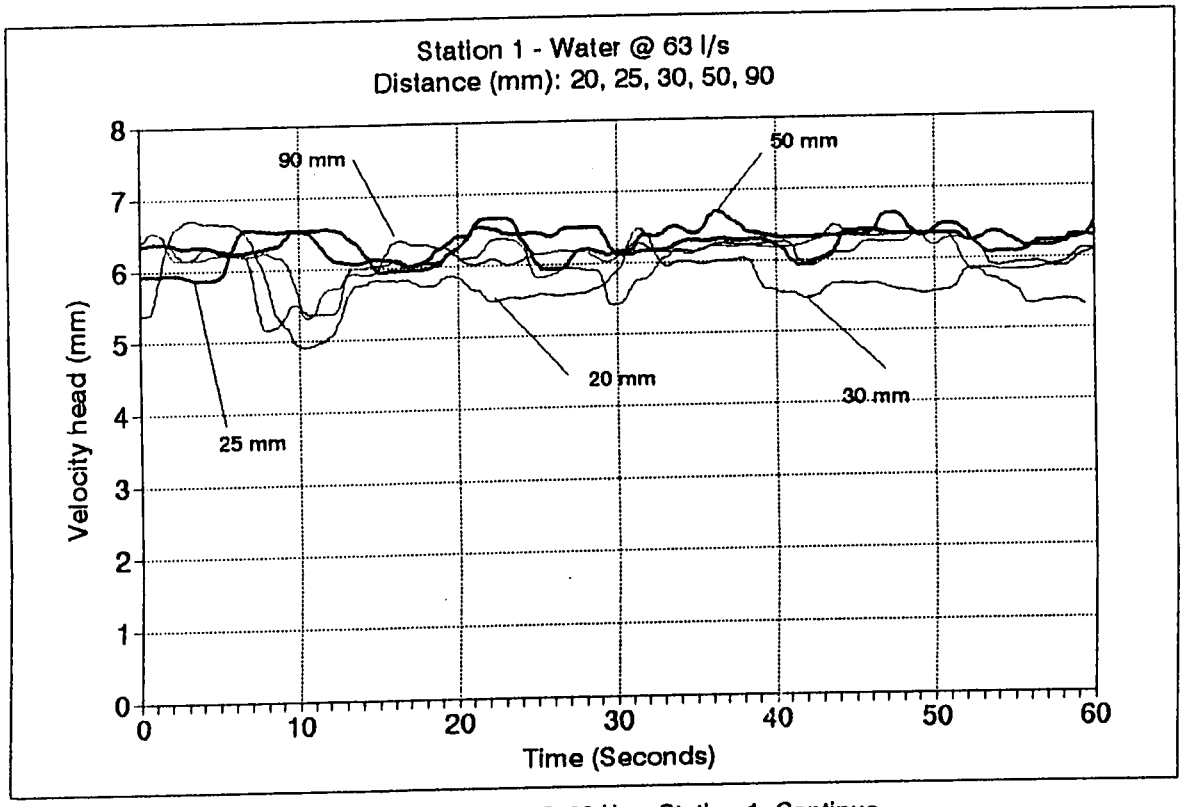

Figure 6.15 Pressure Transducer Data: Water @ 63 l/s - Station 1- Continue

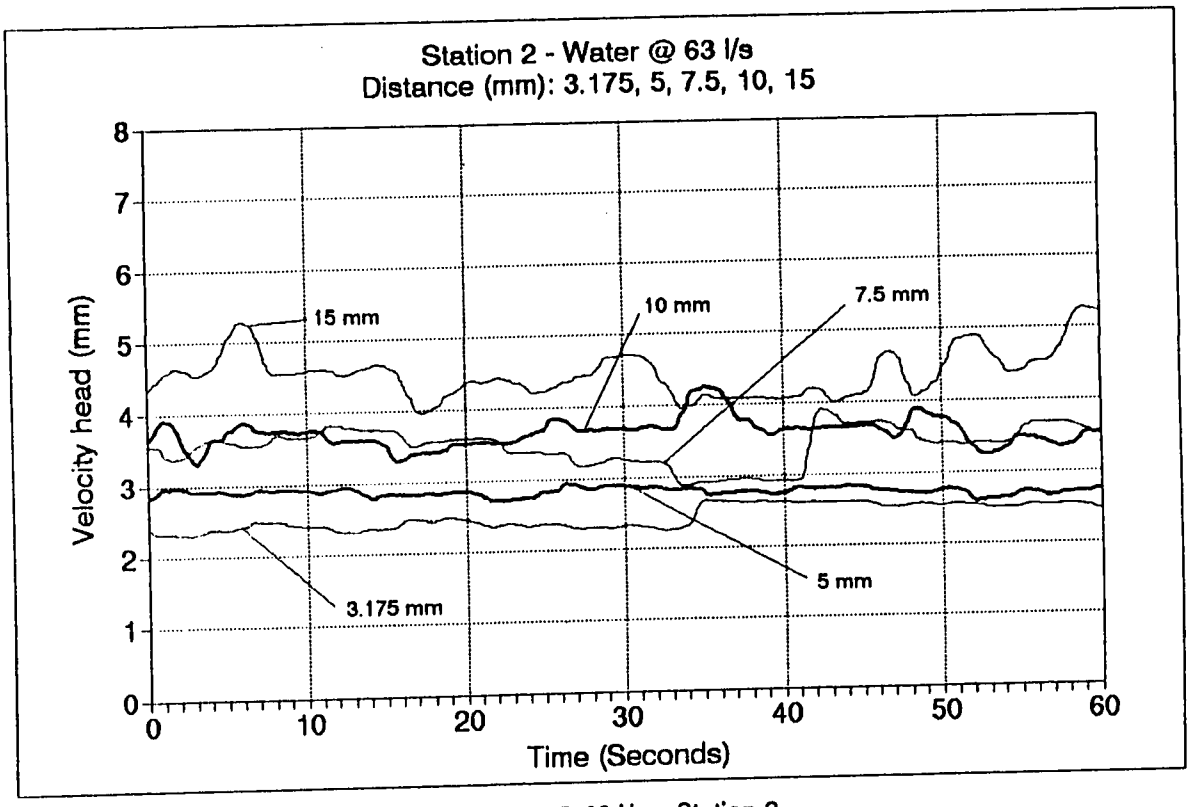

Figure 6.16 Pressure Transducer Data: Water @ 63 l/s - Station 2

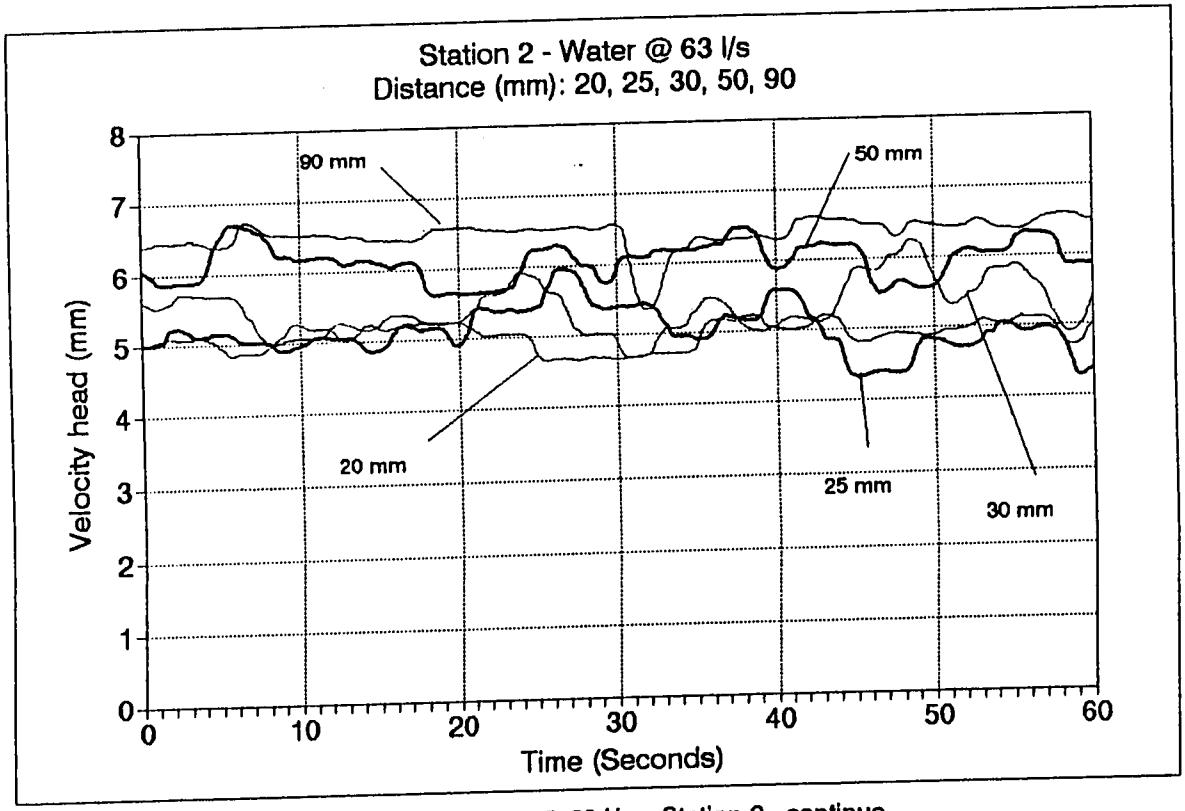

Figure 6.16 Pressure Transducer Data: Water @ 63 l/s - Station 2 - continue

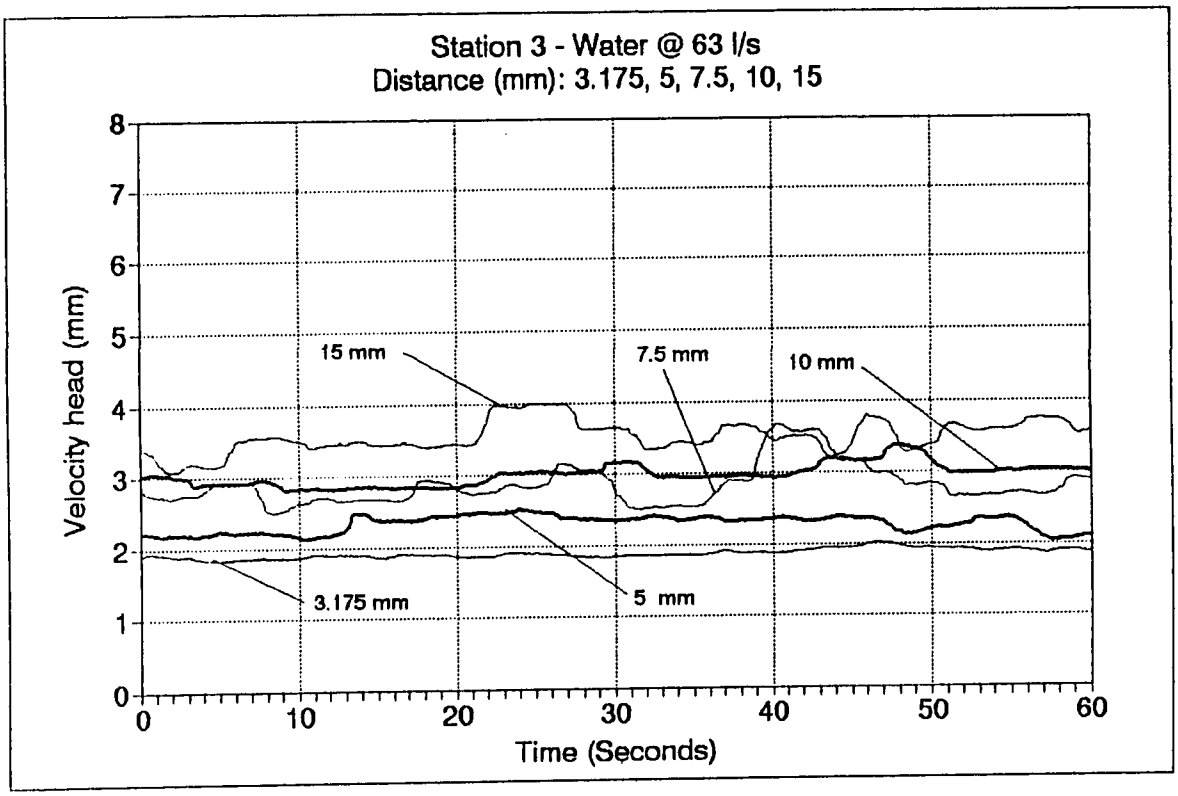

Figure 6.17 Pressure Transducer Data: Water @ 63 l/s - Station 3

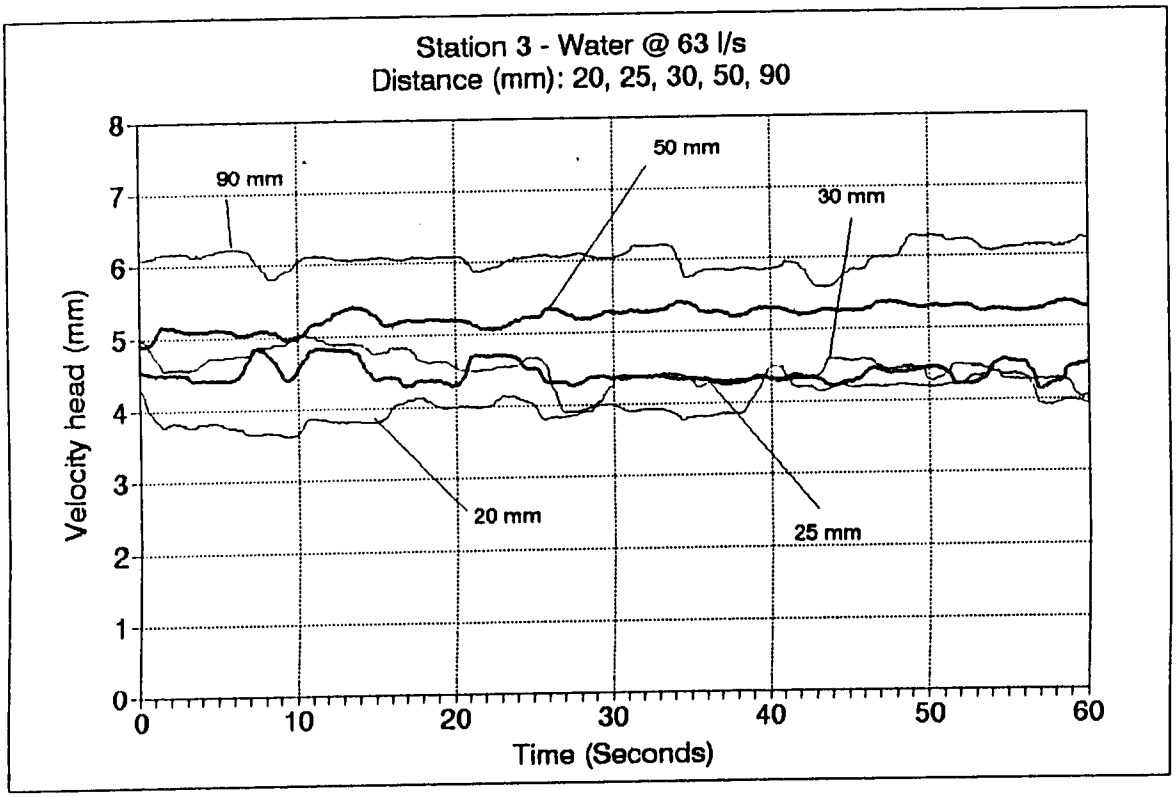

Figure 6.17 Pressure Transducer Data: Water @ 63 l/s - Station 3 - continue

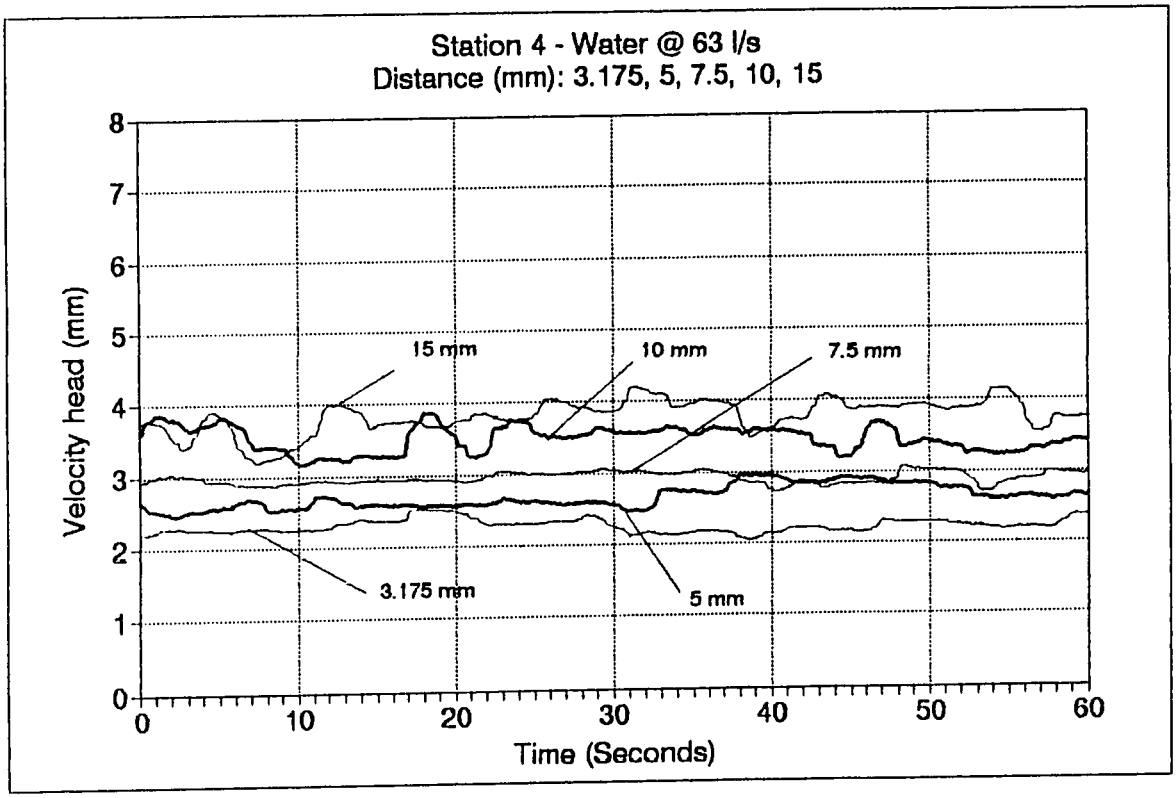

Figure 6.18 Pressure Transducer Data: Water @ 63 l/s - Station 4

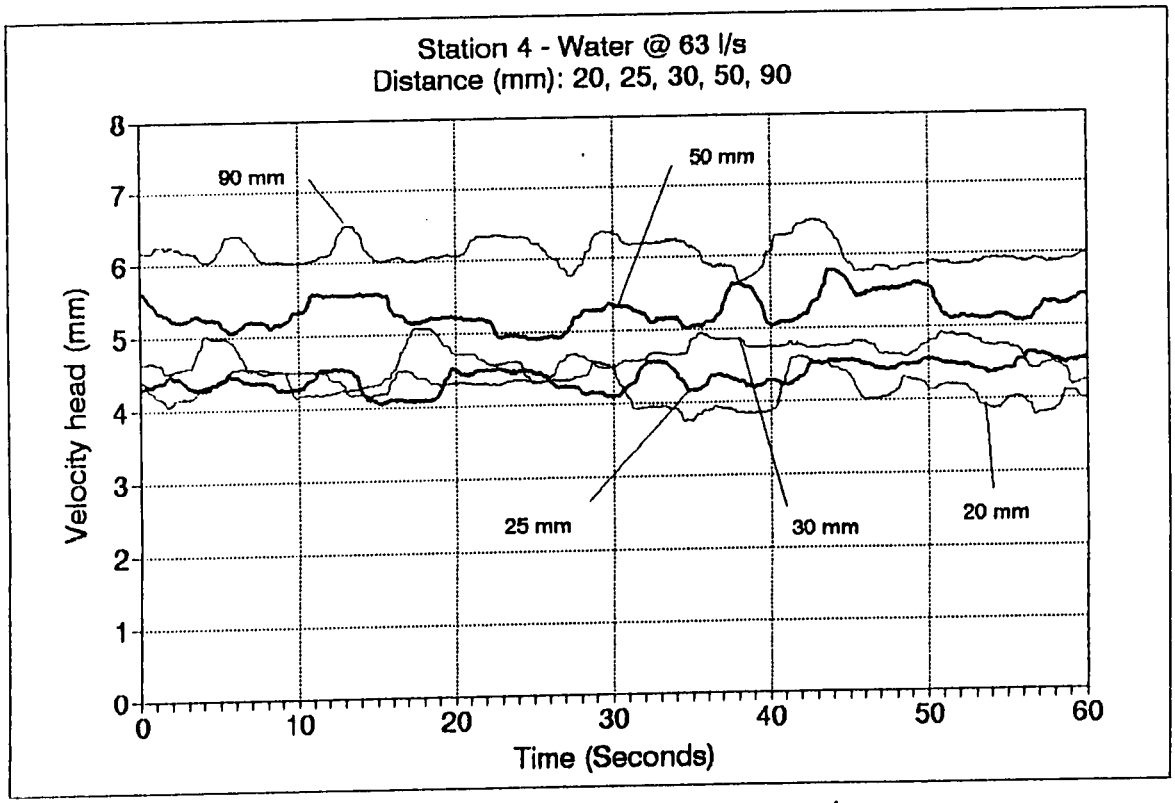

Figure 6.18 Pressure Transducer Data: Water @ 63 l/s - Station 4 - continue

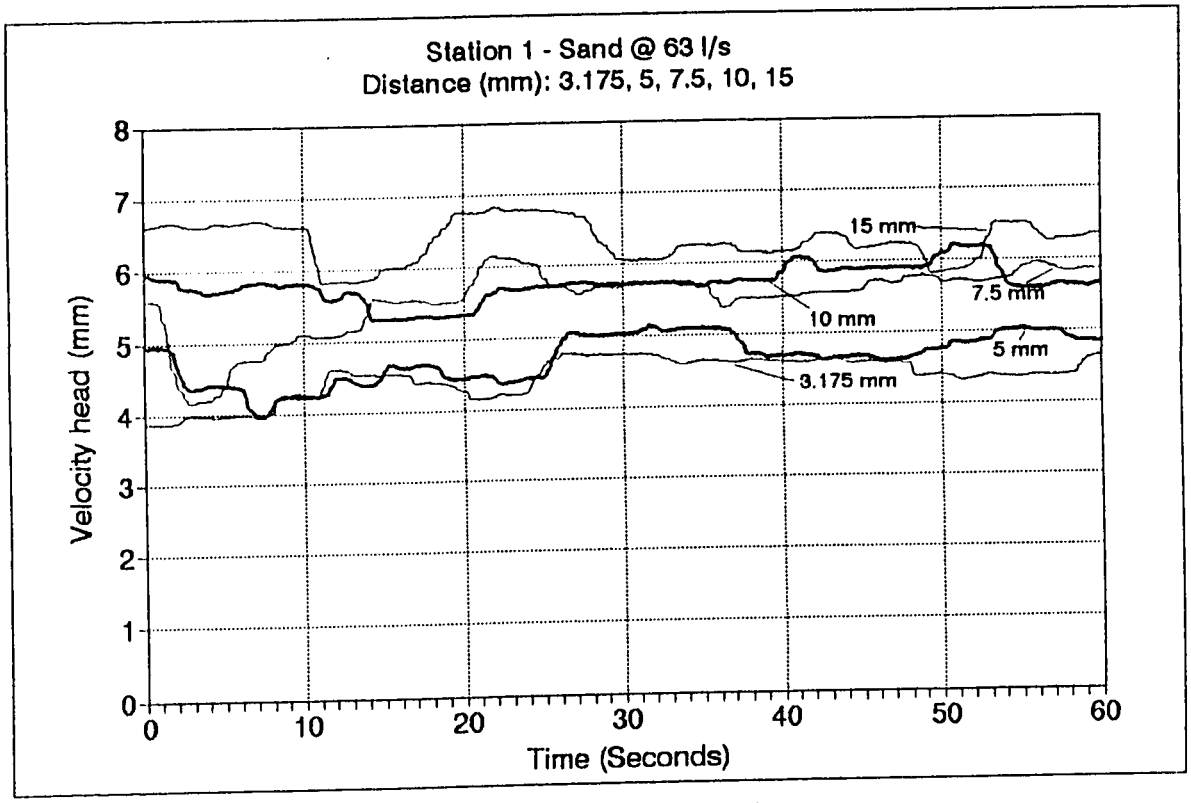

Figure 6.19 Pressure Transducer Data: Sand @ 63 l/s - Station 1

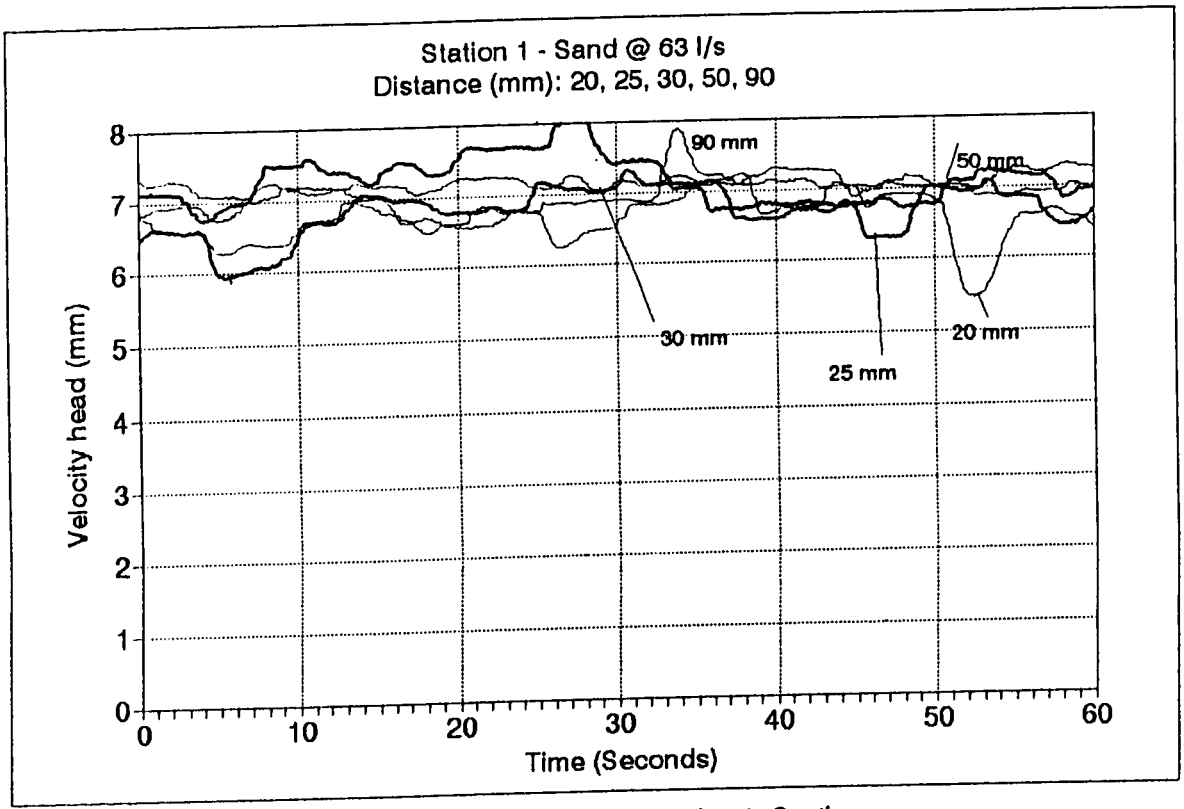

Figure 6.19 Pressure Transducer Data: Sand @ 63 l/s - Station 1- Continue

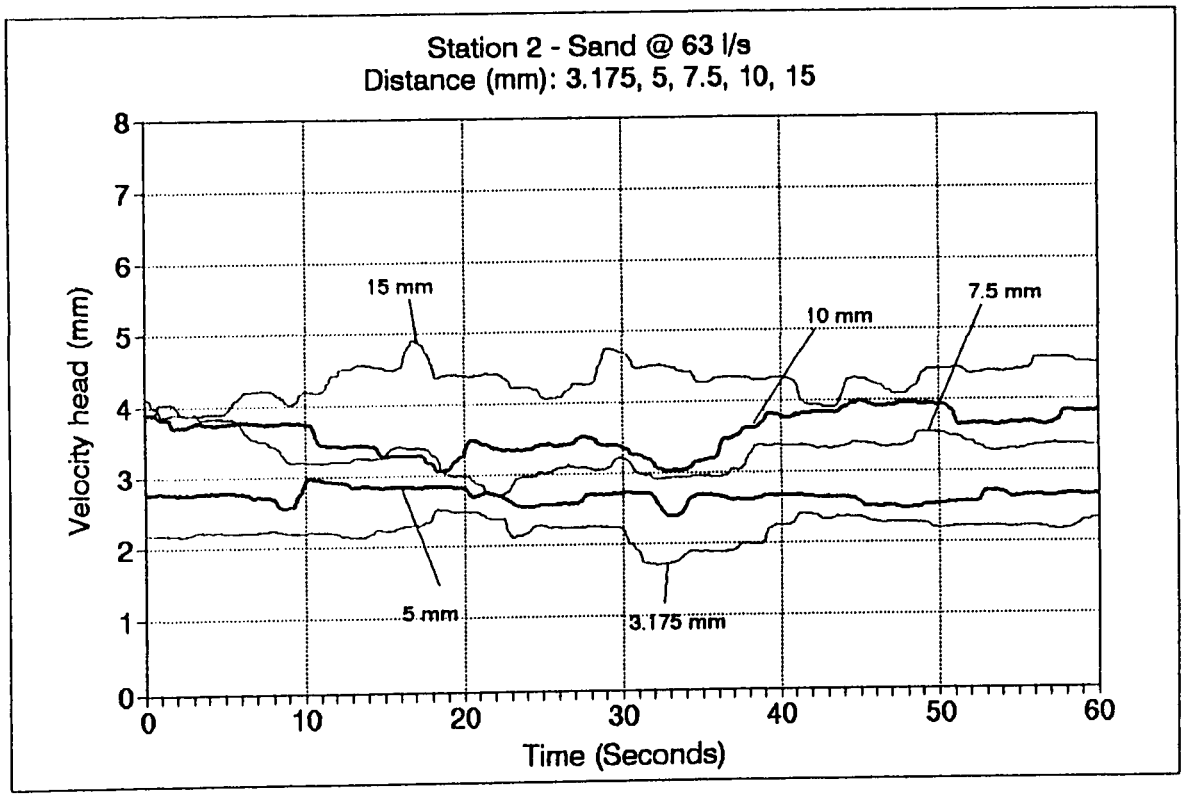

Figure 6.20 Pressure Transducer Data: Sand @ 63 l/s - Station 2

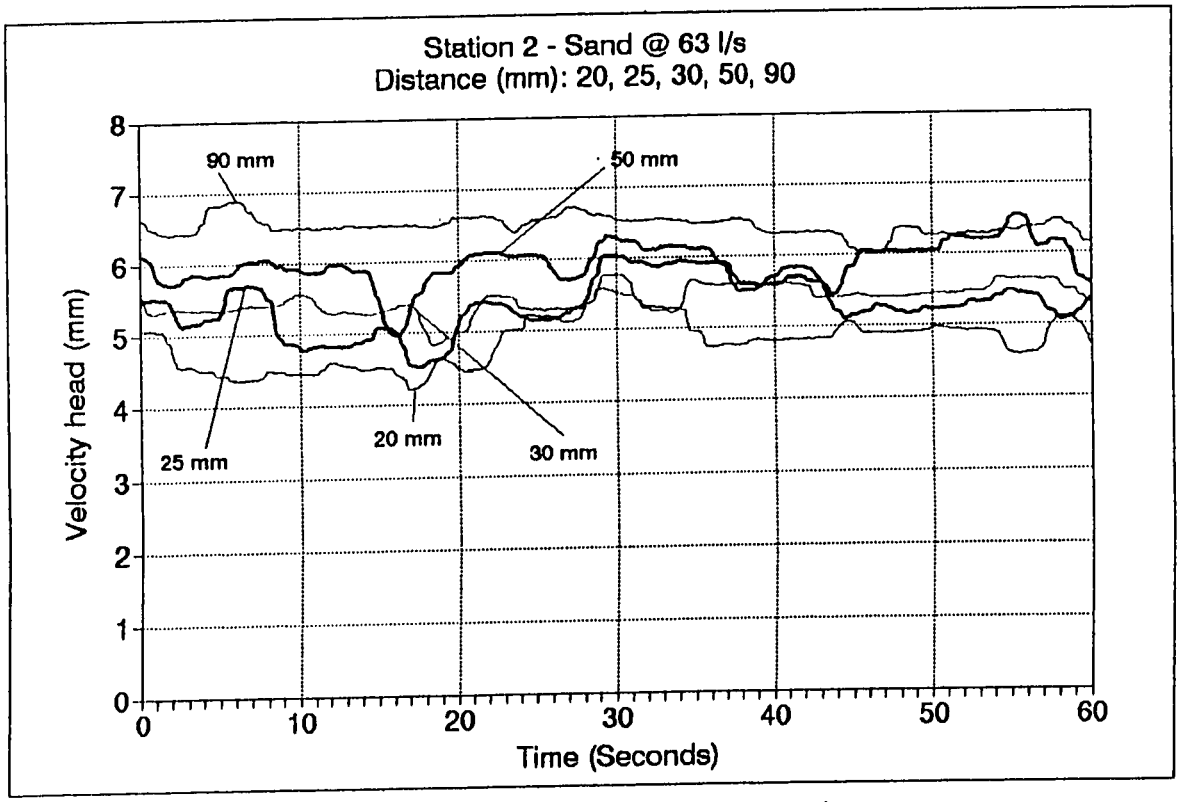

Figure 6.20 Pressure Transducer Data: Sand @ 63 l/s - Station 2 - continue

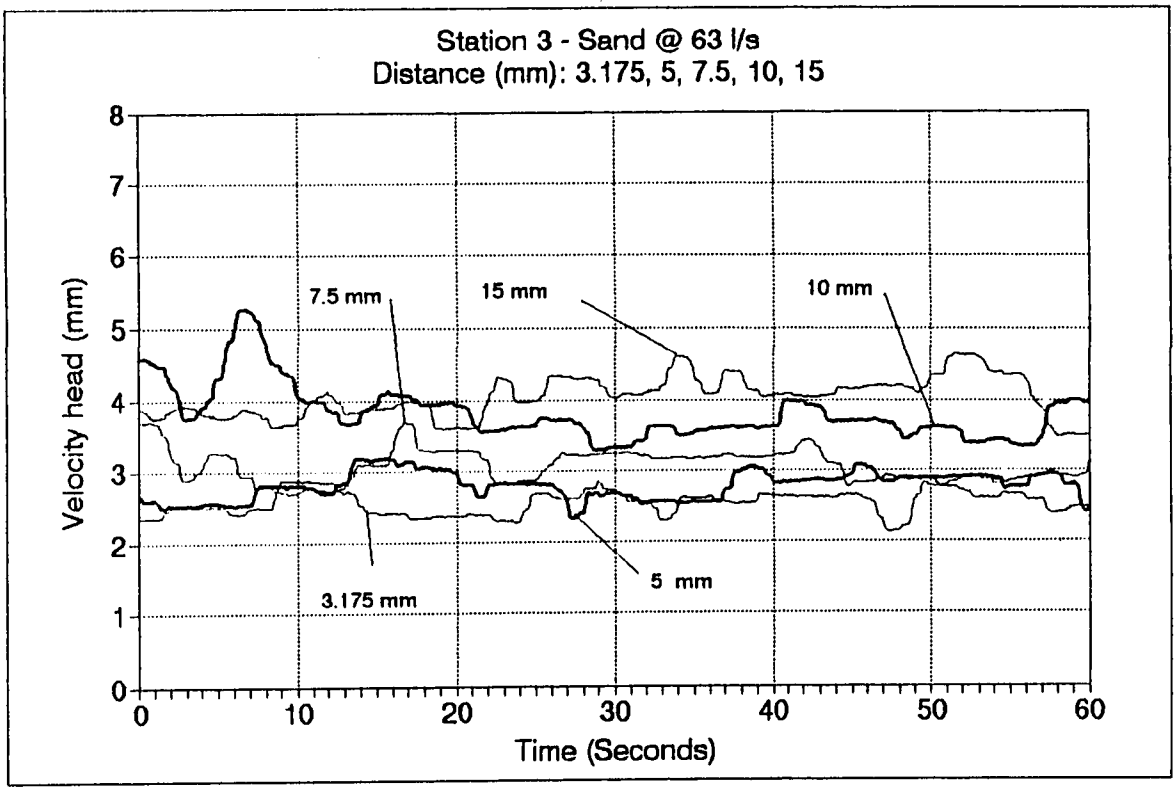

Figure 6.21 Pressure Transducer Data: Sand @ 63 l/s - Station 3

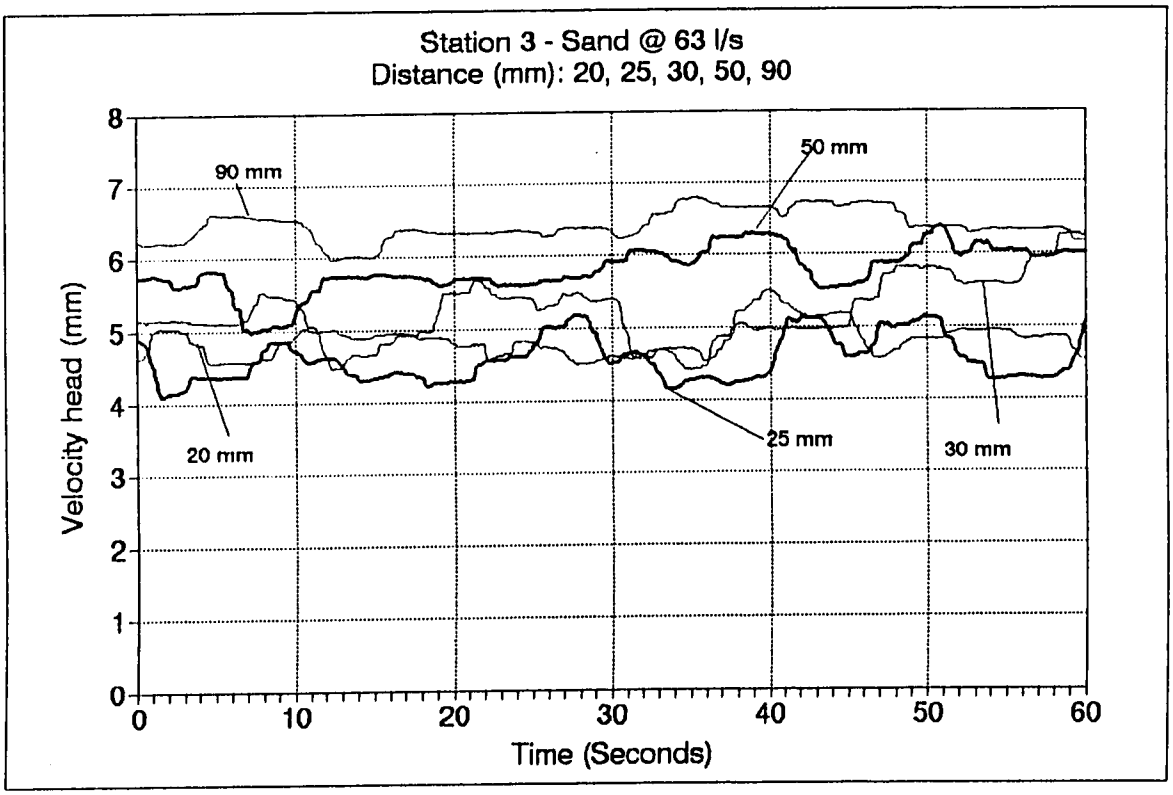

Figure 6.21 Pressure Transducer Data: Sand @ 63 l/s - Station 3 - continue

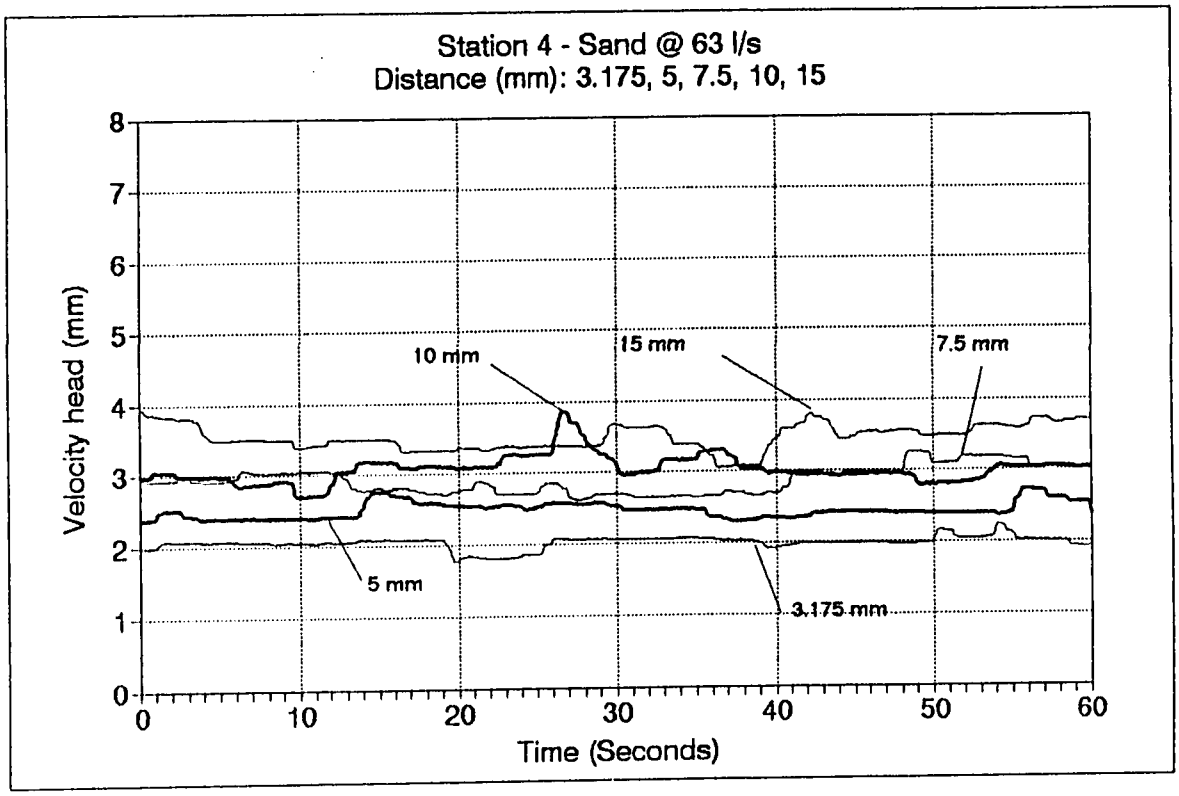

Figure 6.22 Pressure Transducer Data: Sand @ 63 l/s - Station 4

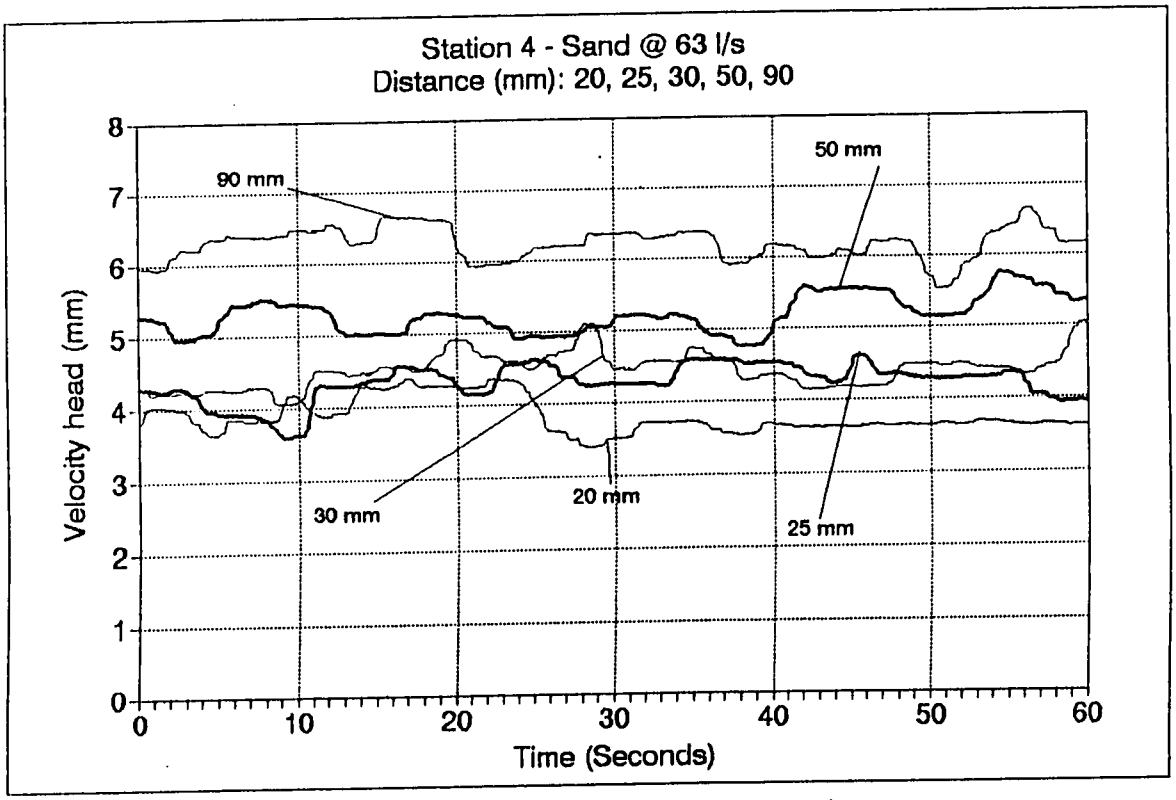

Figure 6.22 Pressure Transducer Data: Sand @ 63 l/s - Station 4 - continue

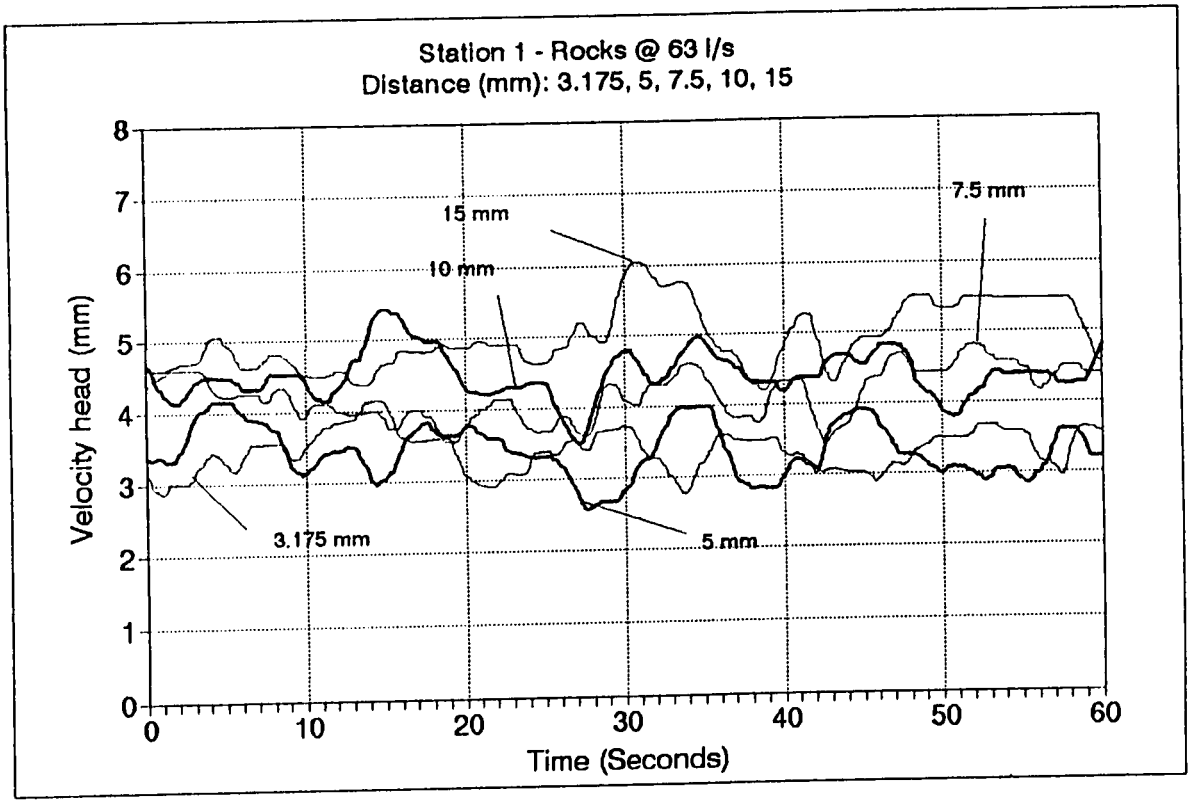

Figure 6.23 Pressure Transducer Data: Rocks @ 63 l/s - Station 1

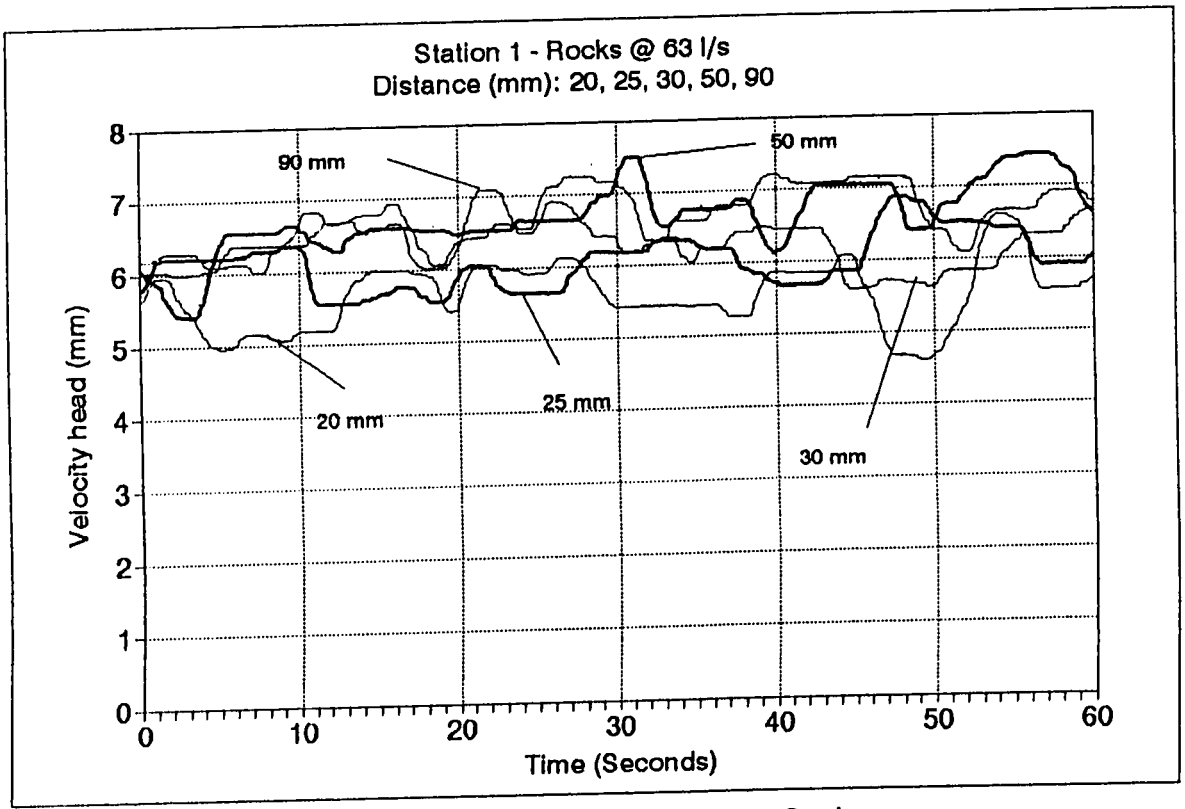

Figure 6.23 Pressure Transducer Data: Rocks @ 63 l/s - Station 1- Continue

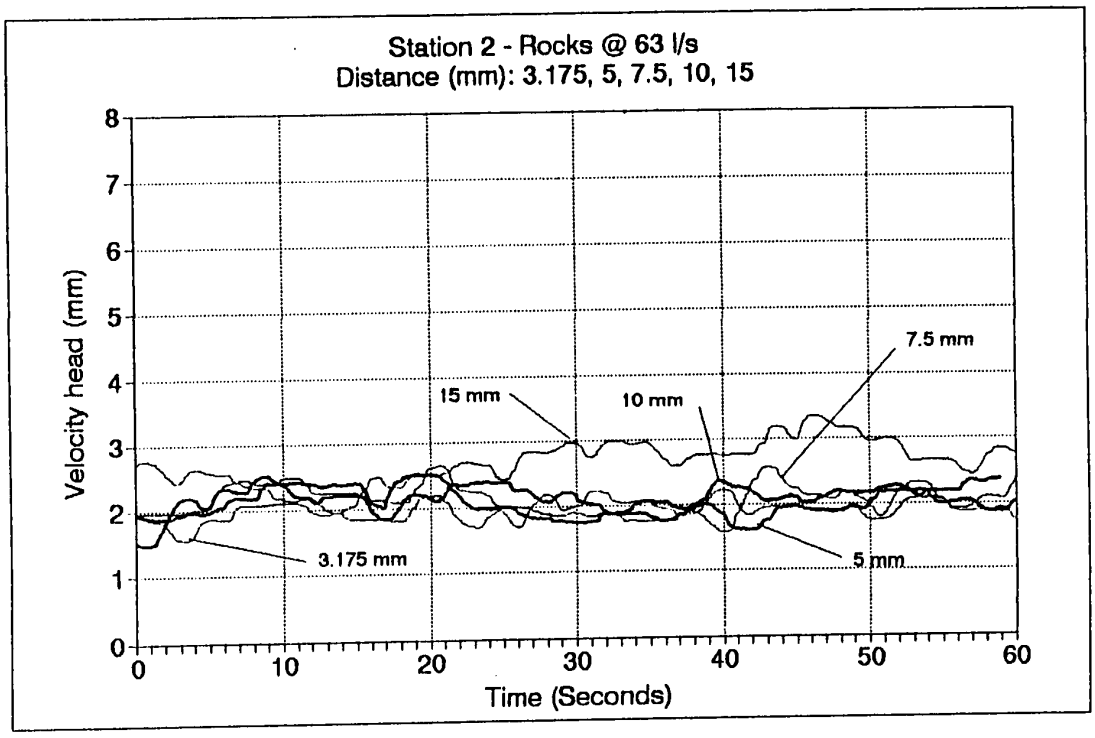

Figure 6.24 Pressure Transducer Data: Rocks @ 63 l/s - Station 2

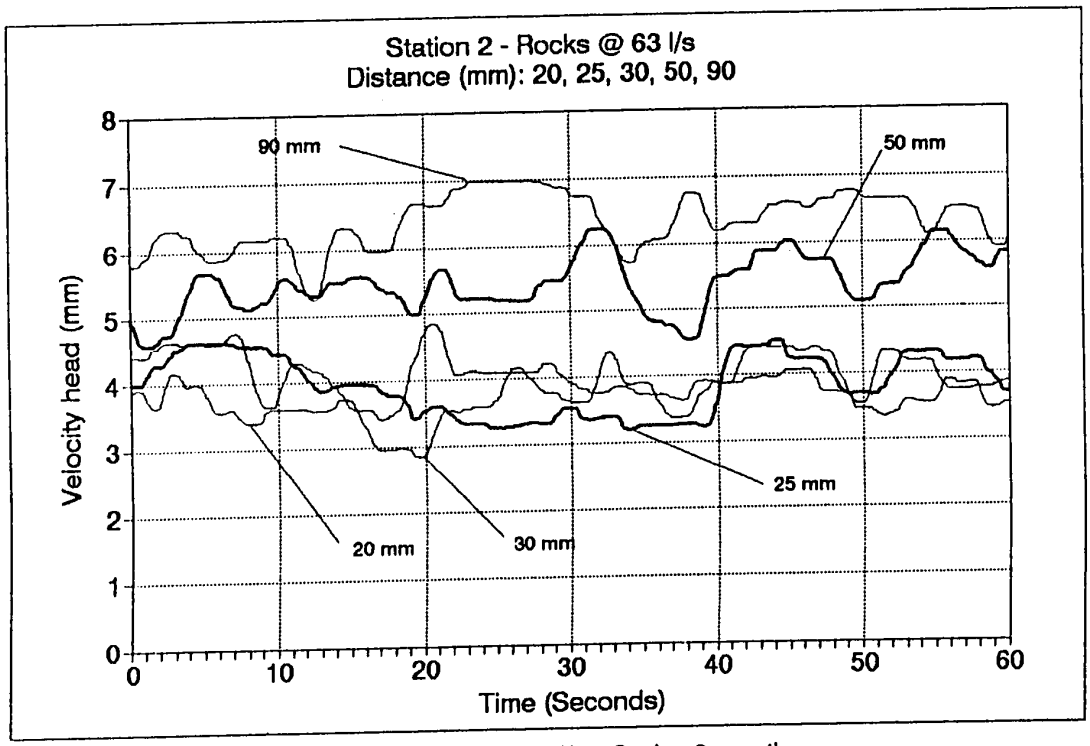

Figure 6.24 Pressure Transducer Data: Rocks @ 63 l/s - Station 2 - continue

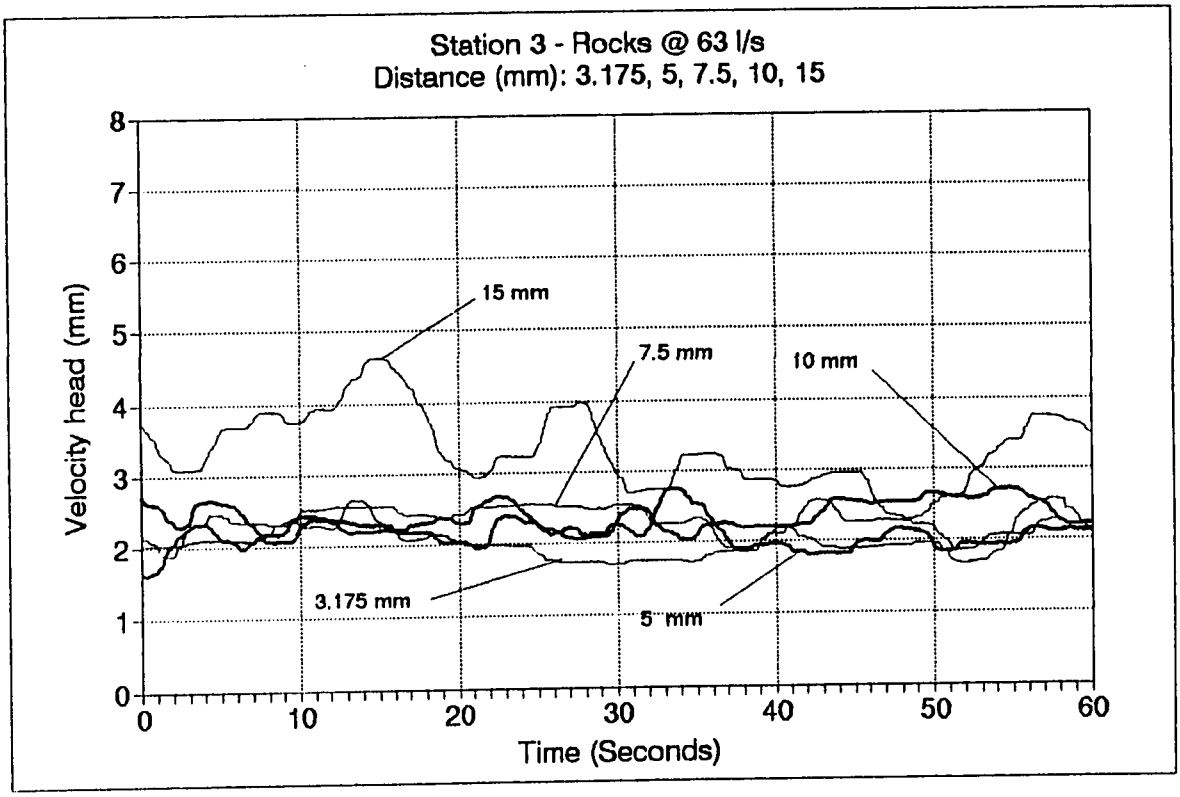

Figure 6.25 Pressure Transducer Data: Rocks @ 63 l/s - Station 3

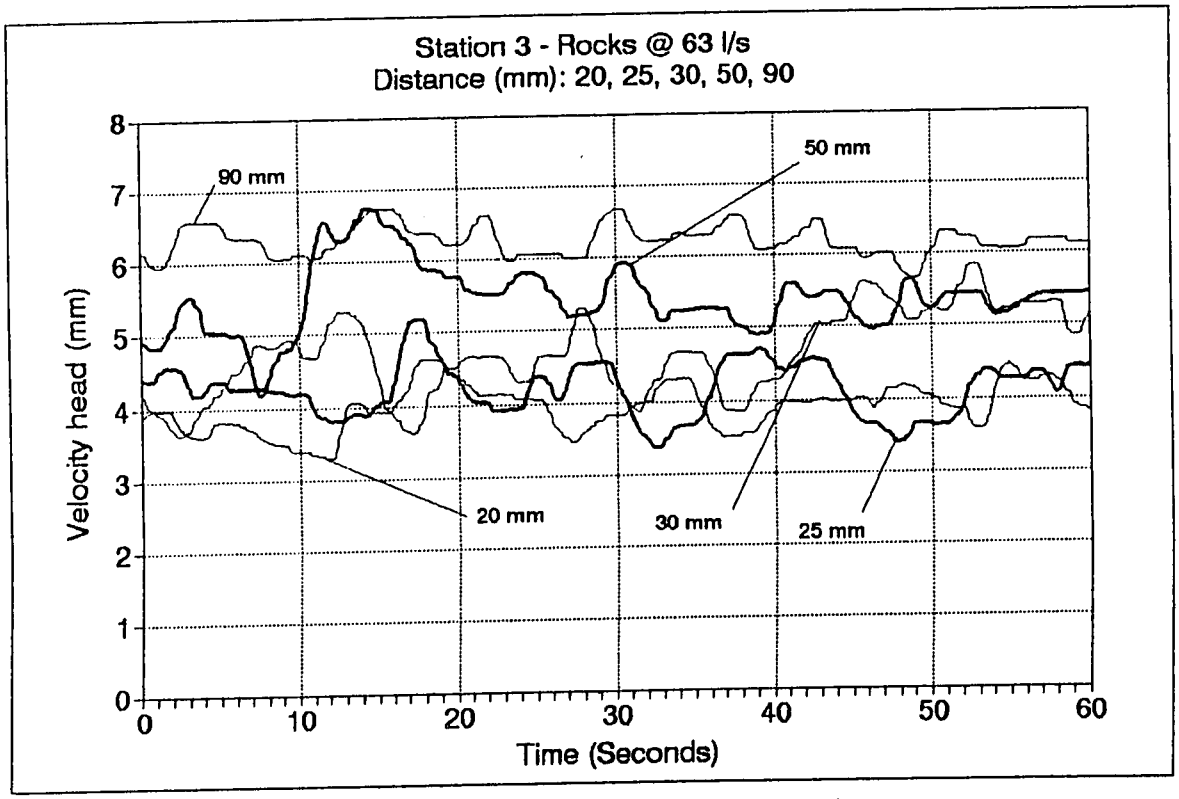

Figure 6.25 Pressure Transducer Data: Rocks @ 63 l/s - Station 3 - continue

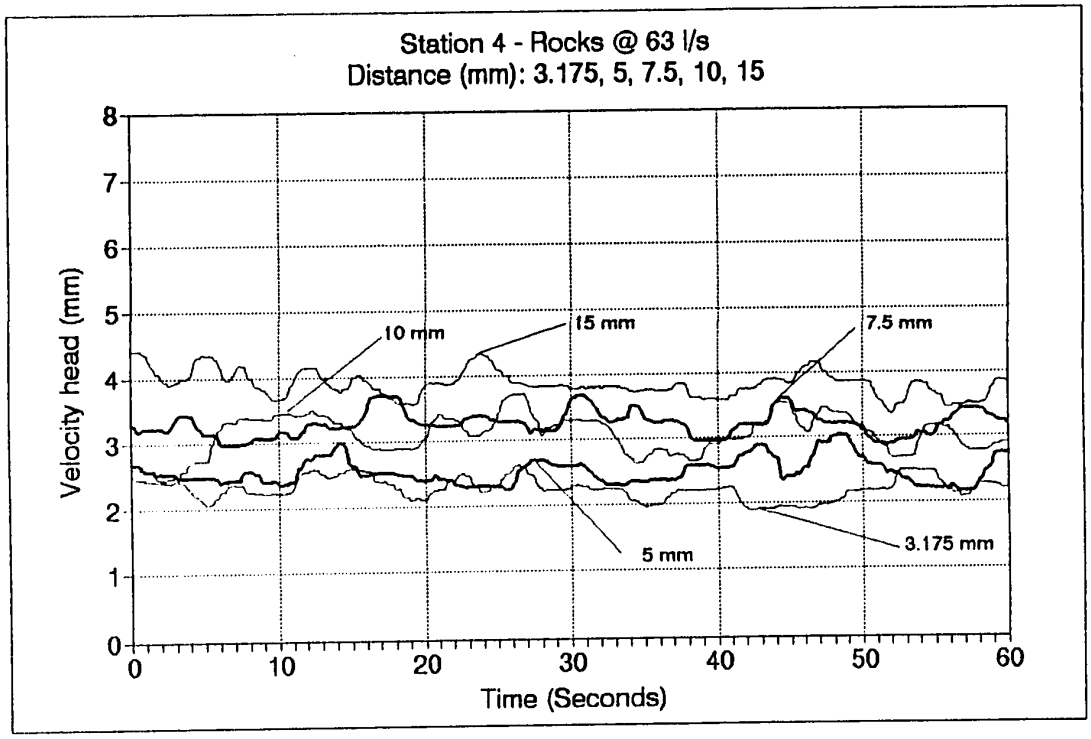

Figure 6.26 Pressure Transducer Data: Rocks @ 63 l/s - Station 4

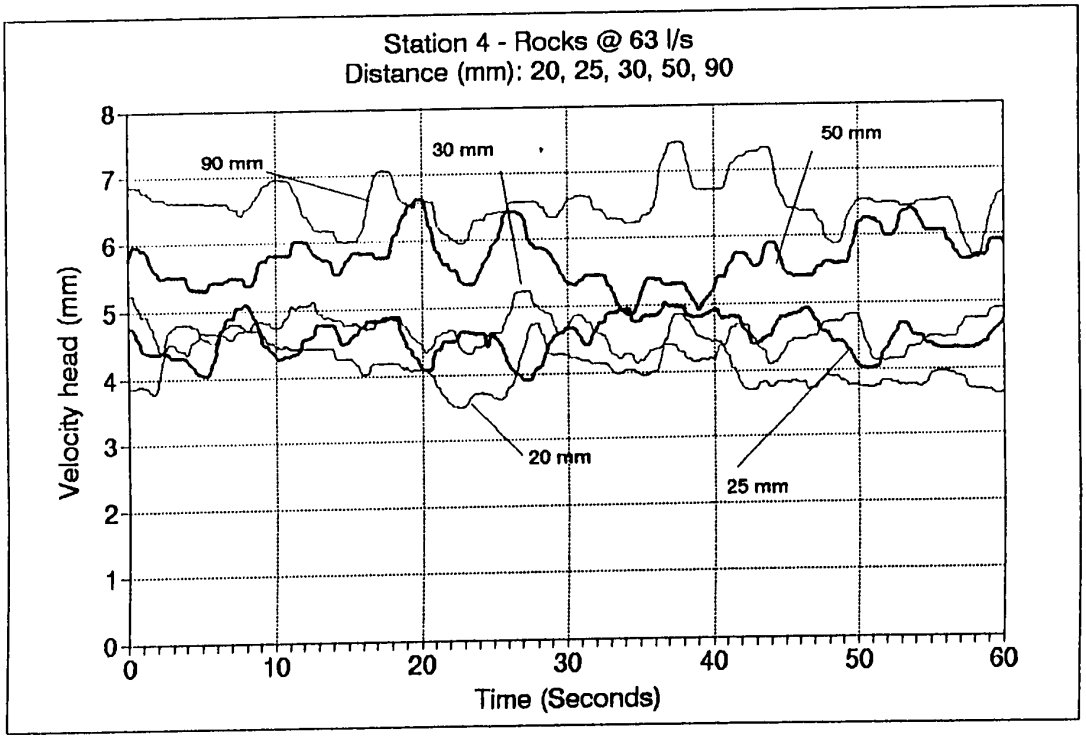

Figure 6.26 Pressure Transducer Data: Rocks @ 63 l/s - Station 4 - continue

Table 6.9 Calculated Local Mean Free Stream Velocities for Phase 2.0

Material	Q (l/s)	Velocity (m/s)			
		Station 1	Station 2	Station 3	Station 4
Water	25	0.177	0.181	0.169	0.173
	38	0.244	0.249	0.254	0.245
	63	0.361	0.367	0.374	0.380
Sand	25	0.180	0.168	0.172	0.176
	38	0.263	0.254	0.259	0.265
	63	0.366	0.373	0.379	0.386
Rocks	25	0.179	0.183	0.187	0.191
	38	0.248	0.254	0.259	0.264
	63	0.366	0.373	0.379	0.386

1 - Flow rates lower by approximately 3 l/s; 2 - Flow rate higher by approximately 3 l/s

Table 6.10 Calculated Average Free Stream Velocities

Material	Q (l/s)	Phase 1.0 (m/s) NL (0 kg)	QL (12.5 kg)	HL (25 kg)	FL (50 kg)	Phase 2.0 (m/s) FL (50 kg)
Water	25 l/s	0.163	0.168	0.173	0.185	0.183
	38 l/s	NA	0.234	0.239	0.254	0.252
	63 l/s	NA	NA	NA	0.370	0.371
Sand	25 l/s	0.163	0.168	0.174	0.186	0.170
	38 l/s	NA	0.233	0.240	0.256	0.257
	63 l/s	NA	NA	NA	0.375	0.376
Rocks	25 l/s	0.163	0.170	0.173	0.183	0.185
	38 l/s	NA	0.233	0.238	0.250	0.256
	63 l/s	NA	NA	NA	0.376	0.376

Note: NL - No Load ; QL - Quarter Load ; HL - Half Load; FL - Full Load; NA - Not Applicable

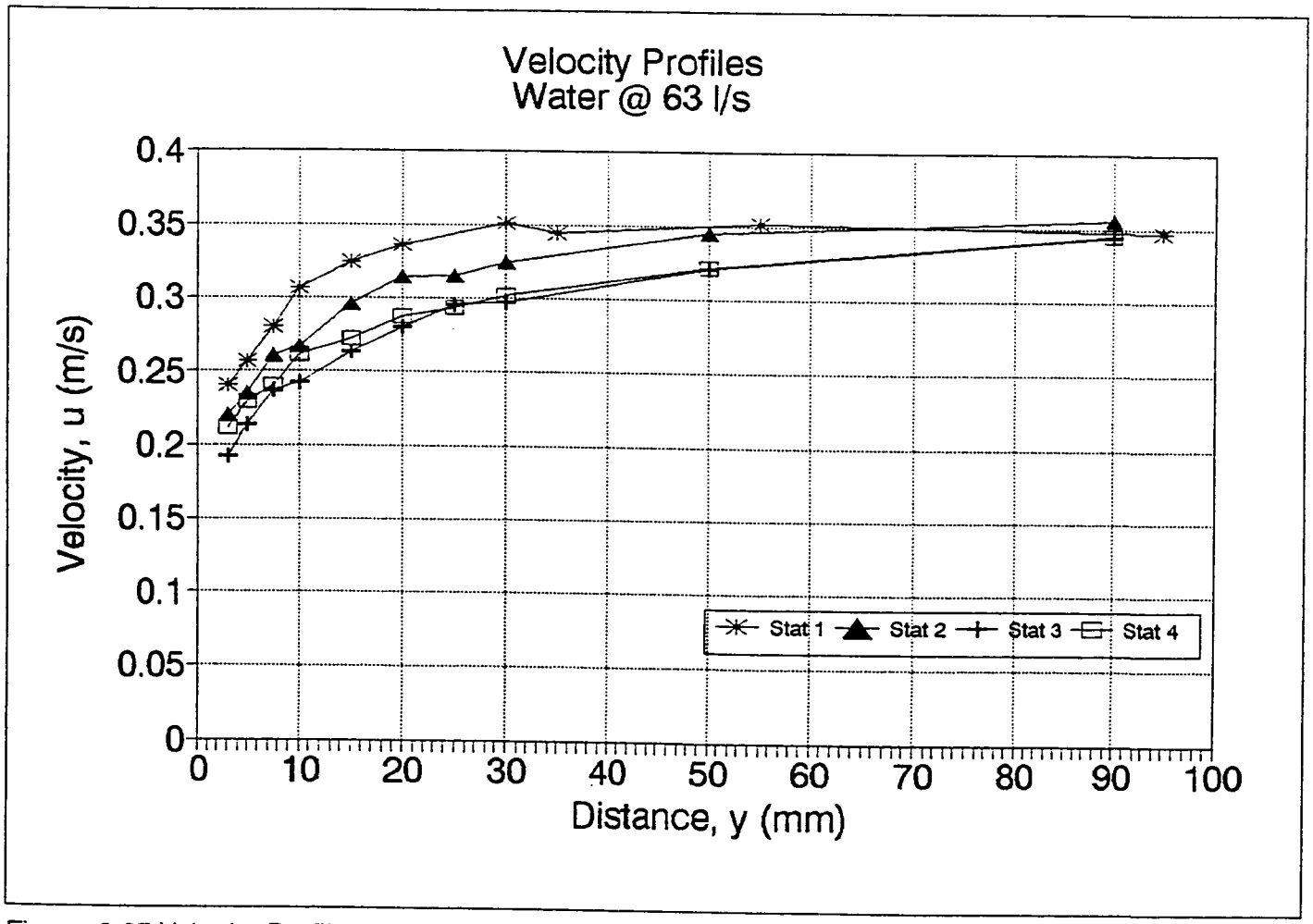

Figure 6.27 Velocity Profiles - Water @ 63 l/s

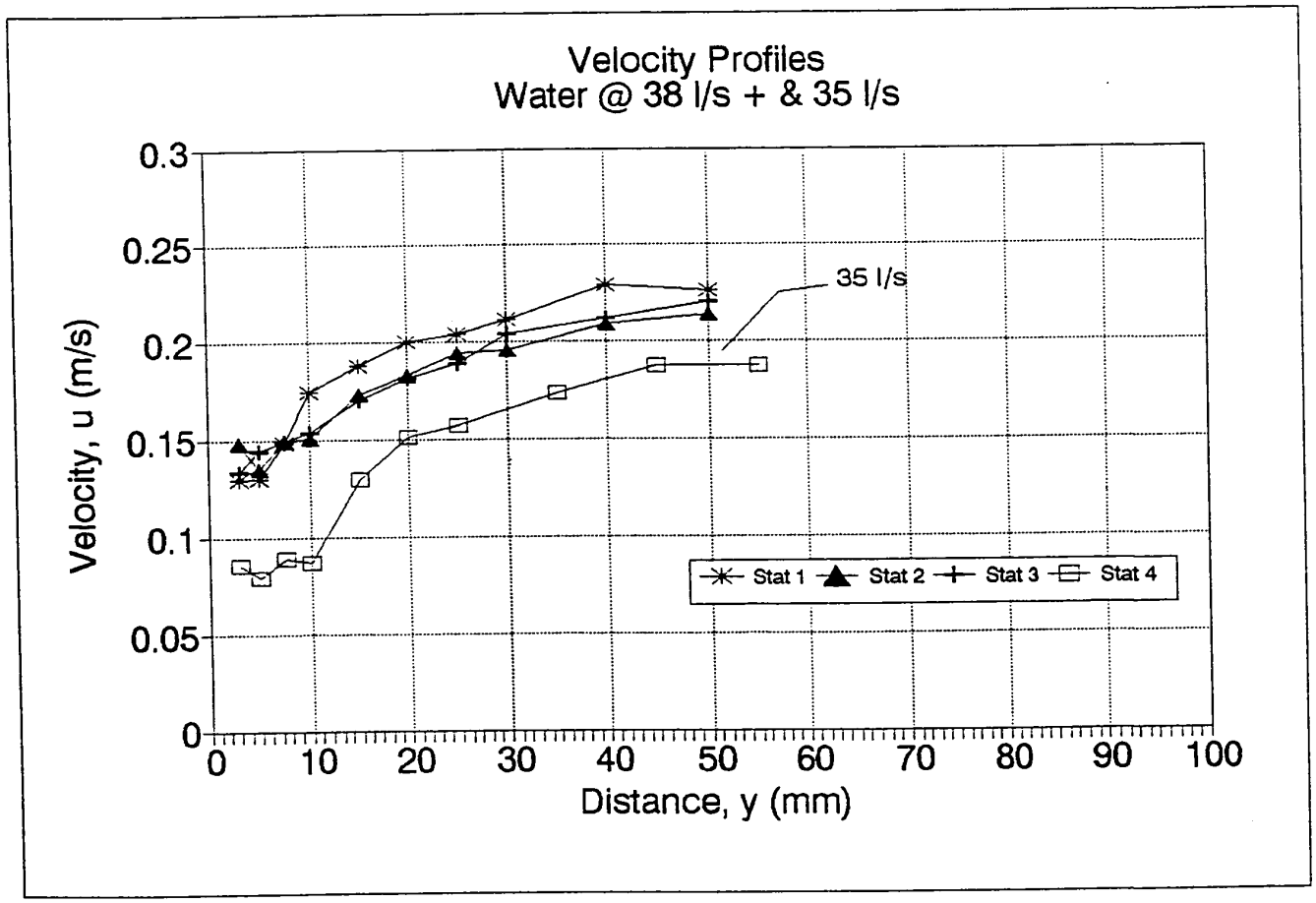

Figure 6.28 Velocity Profiles - Water @ 38 l/s & 35 l/s

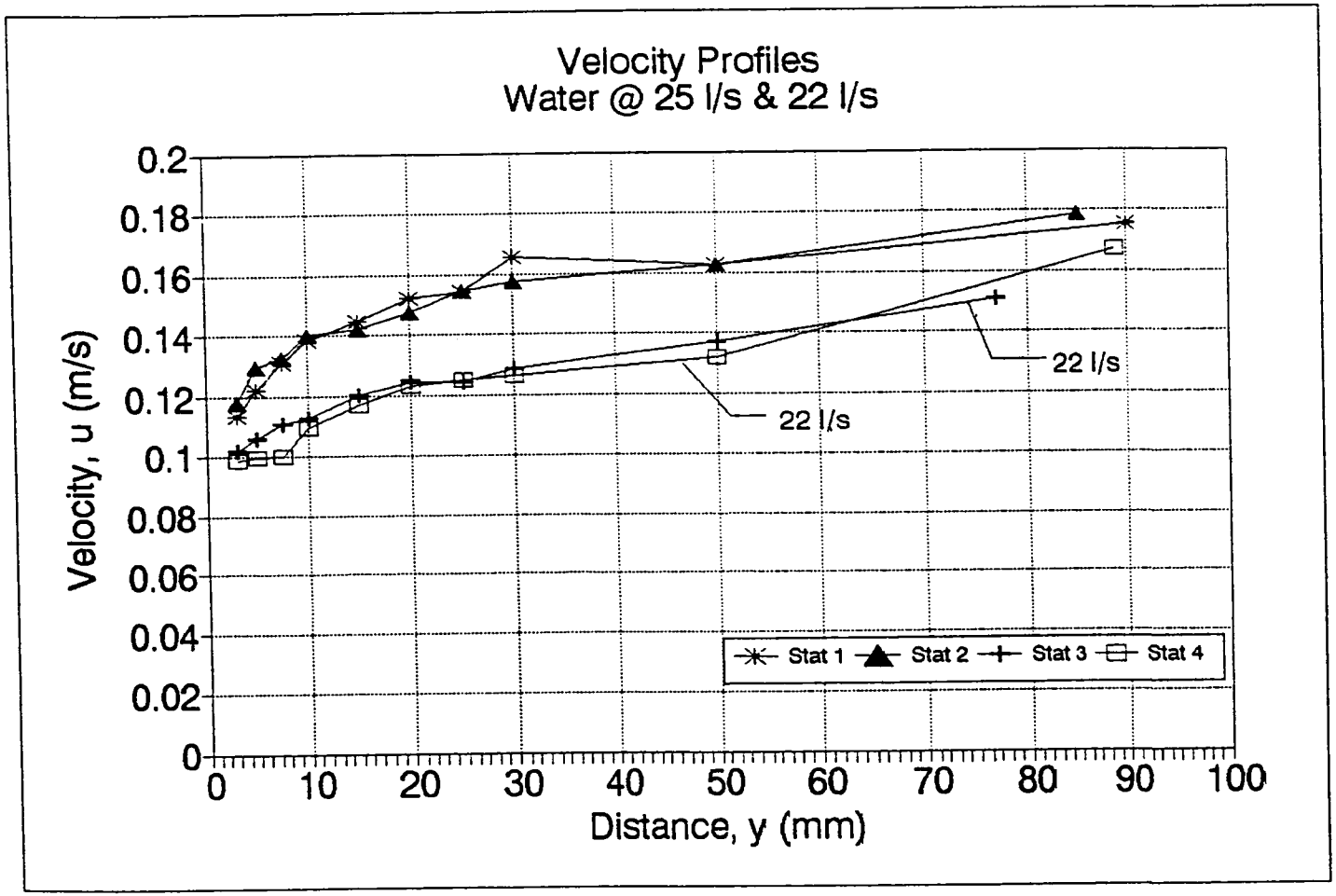

Figure 6.29 Velocity Profiles - Water @ 25 l/s & 22 l/s

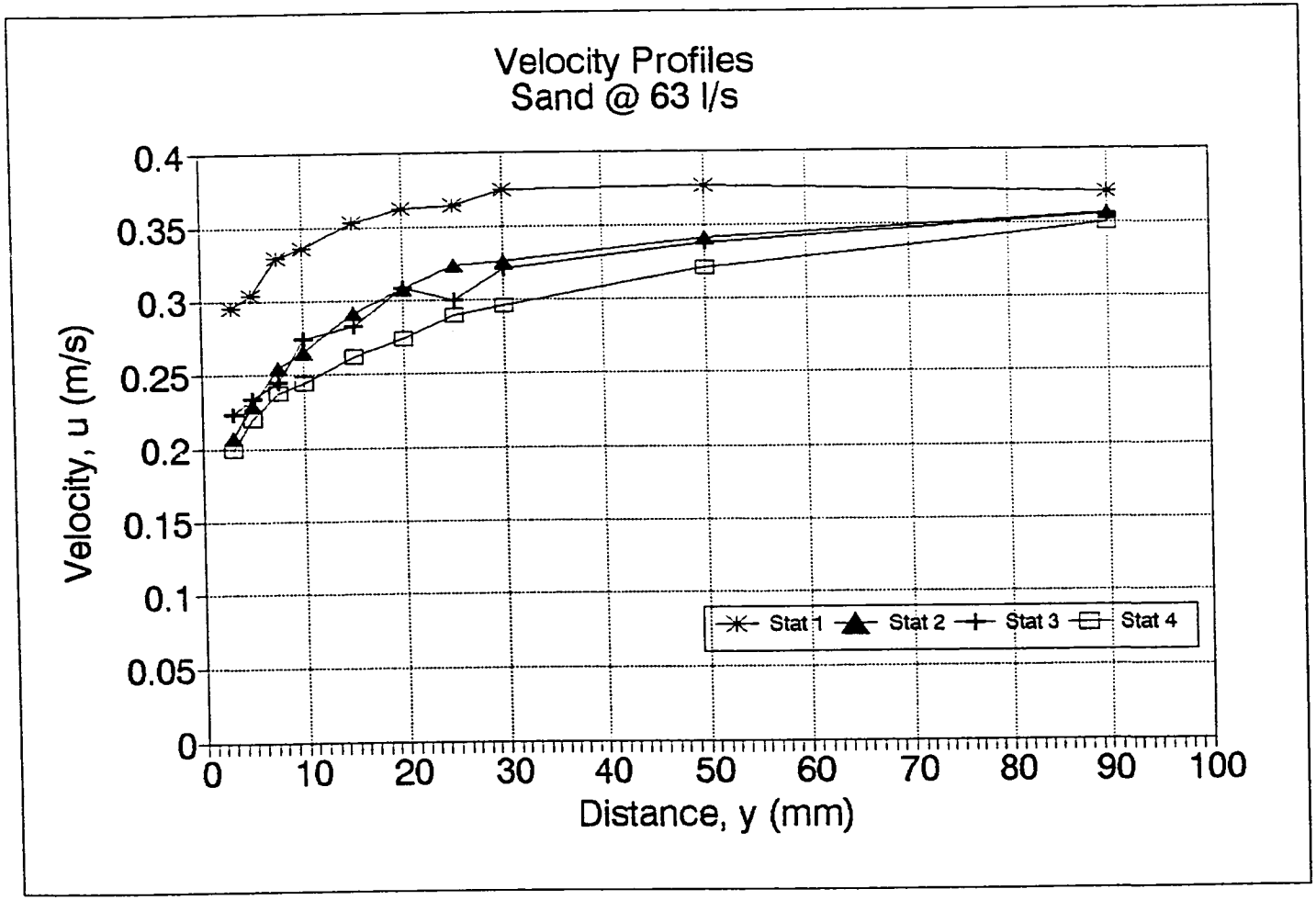

Figure 6.30 Velocity Profiles - Sand @ 63 l/s

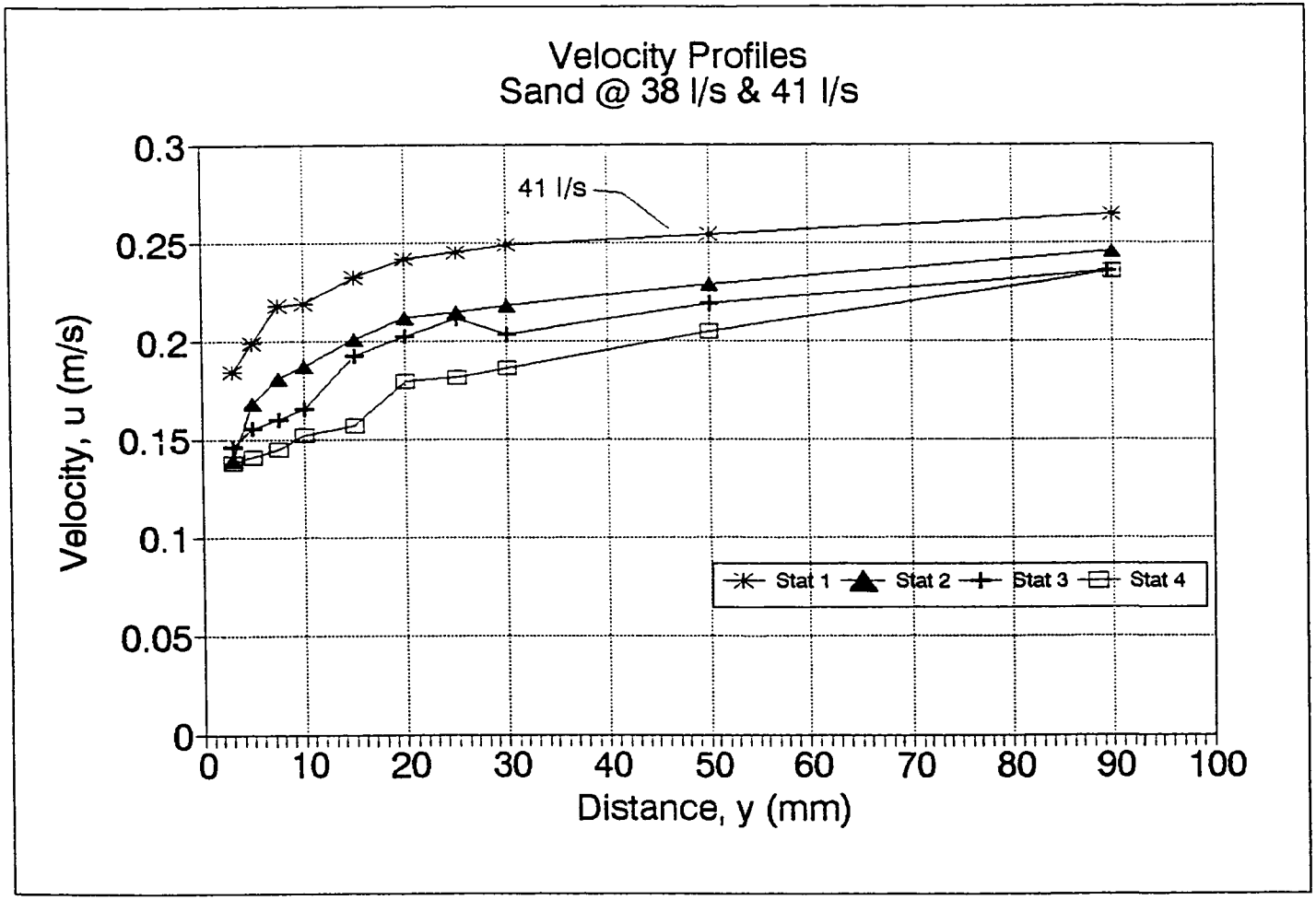

Figure 6.31 Velocity Profiles - Sand @ 38 l/s & 41 l/s

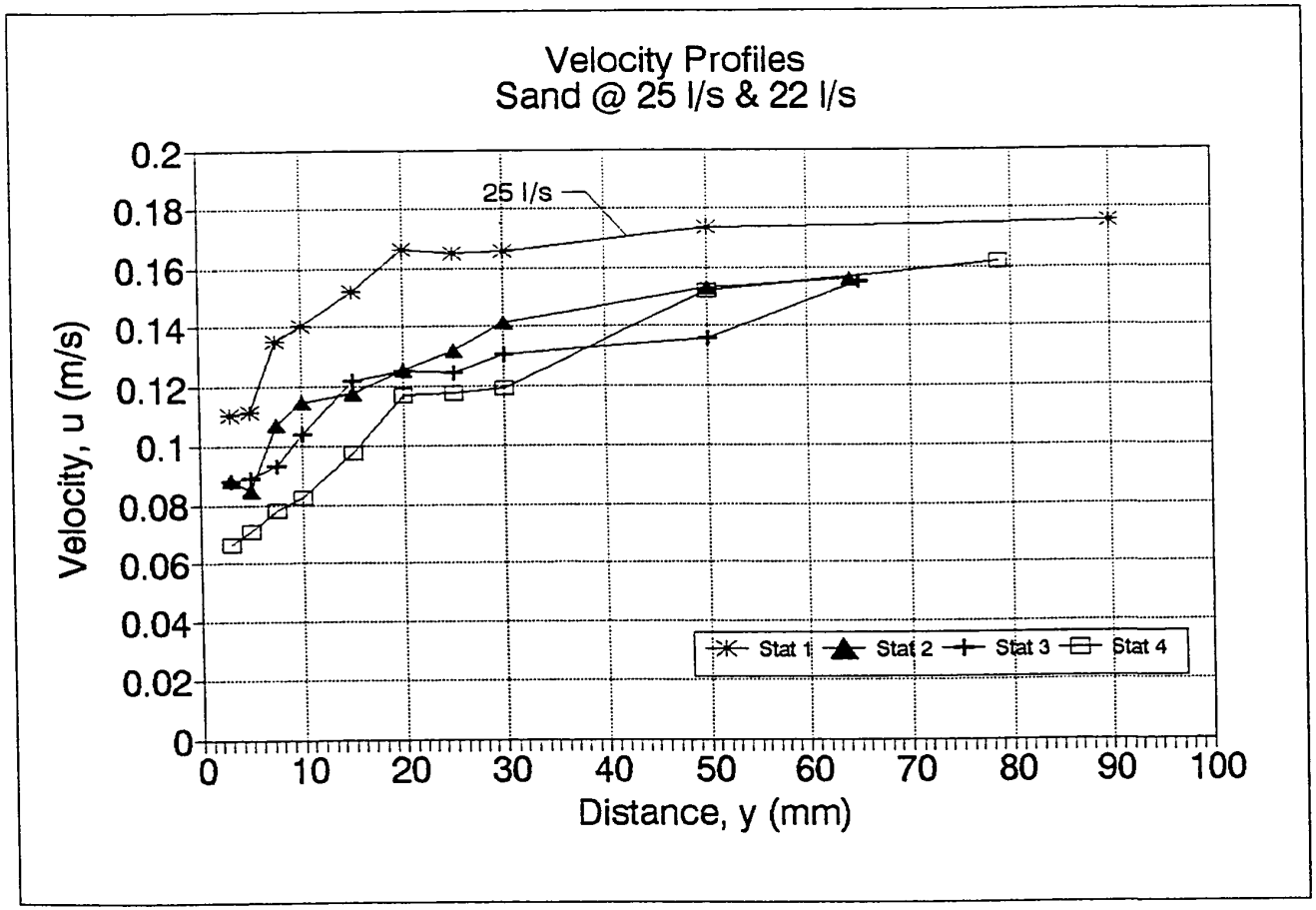

Figure 6.32 Velocity Profiles - Sand 25 l/s & 22 l/s

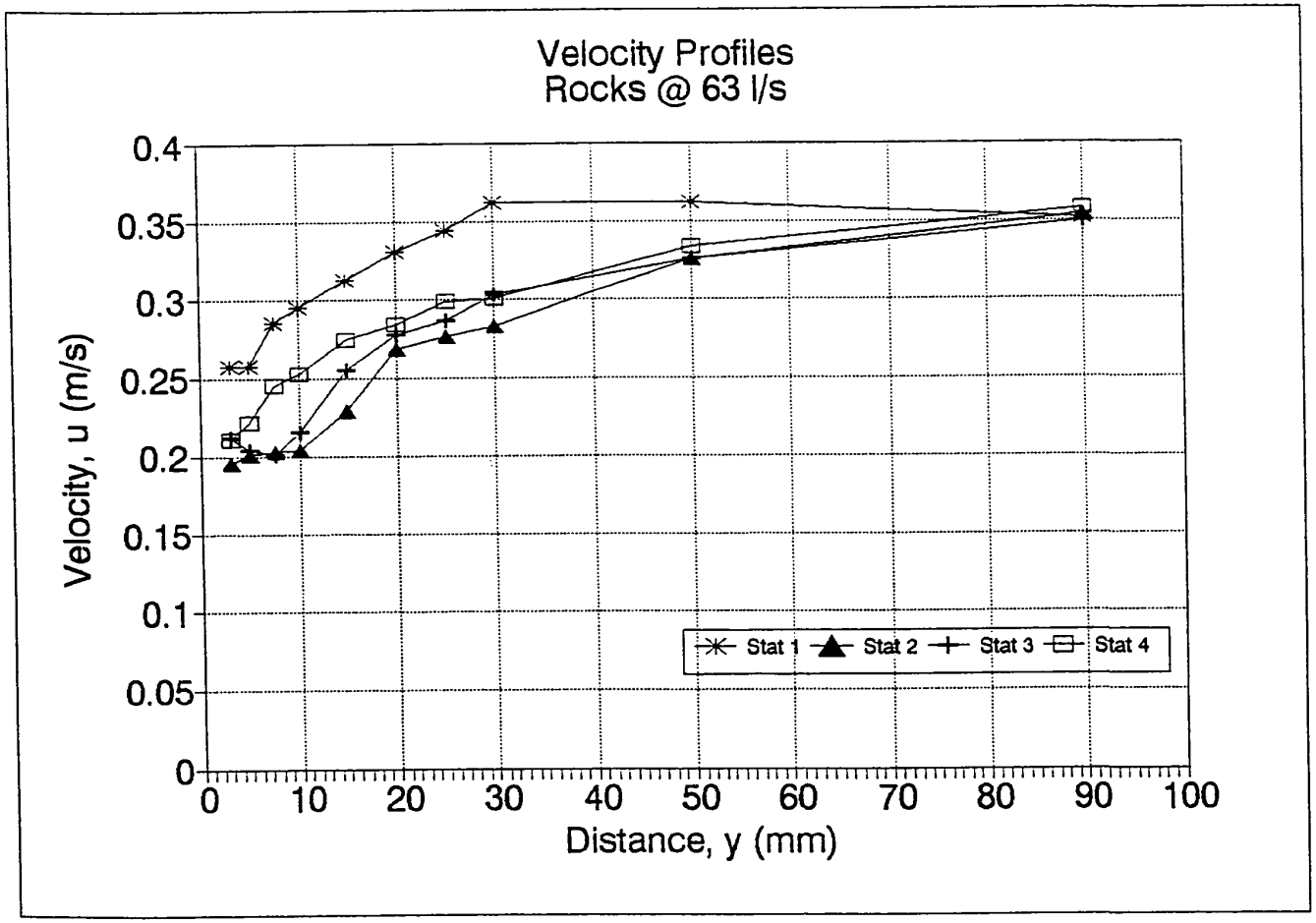

Figure 6.33 Velocity Profiles - Rocks @ 63 l/s

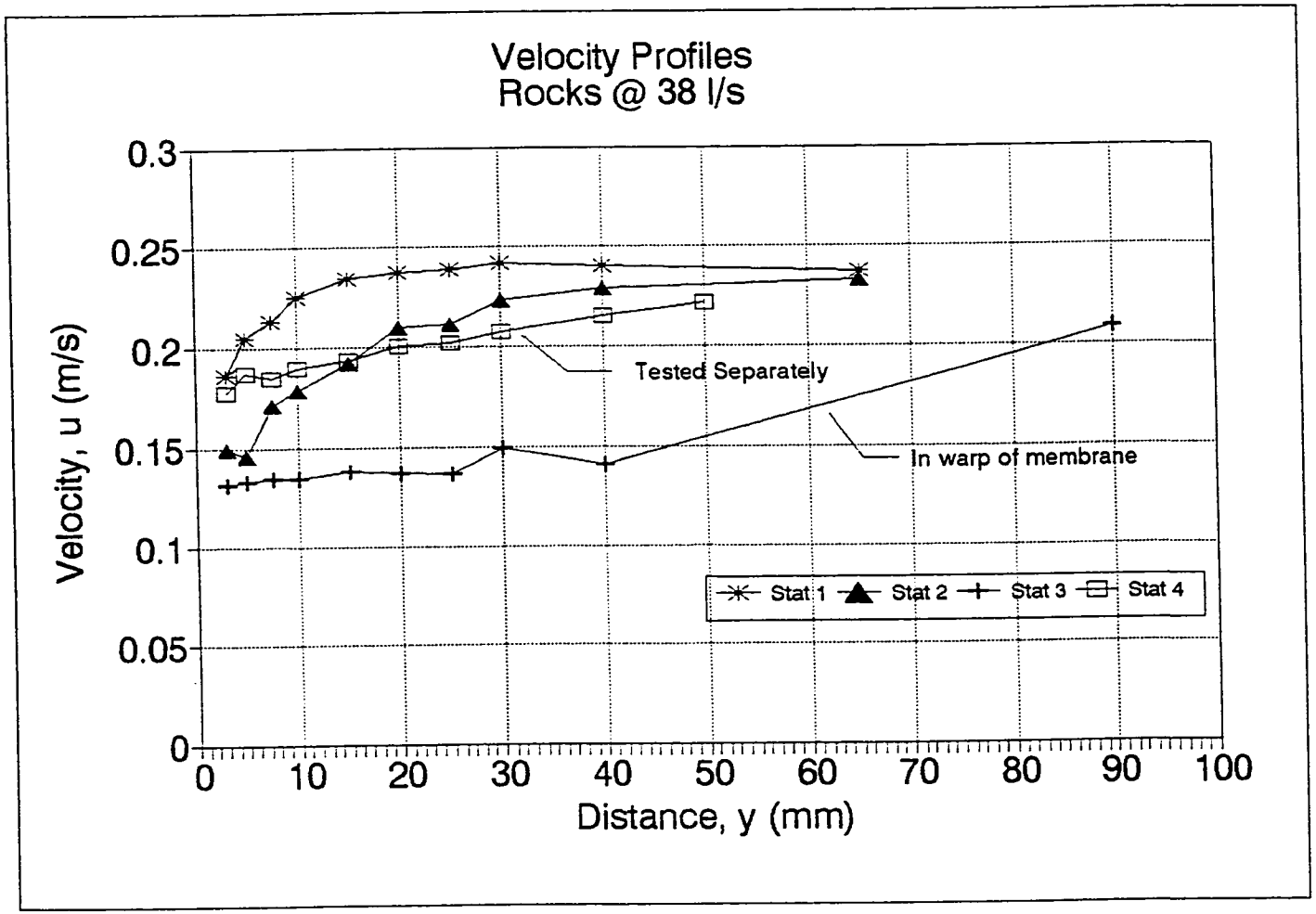

Figure 6.34 Velocity Profiles - Rocks @ 38 l/s

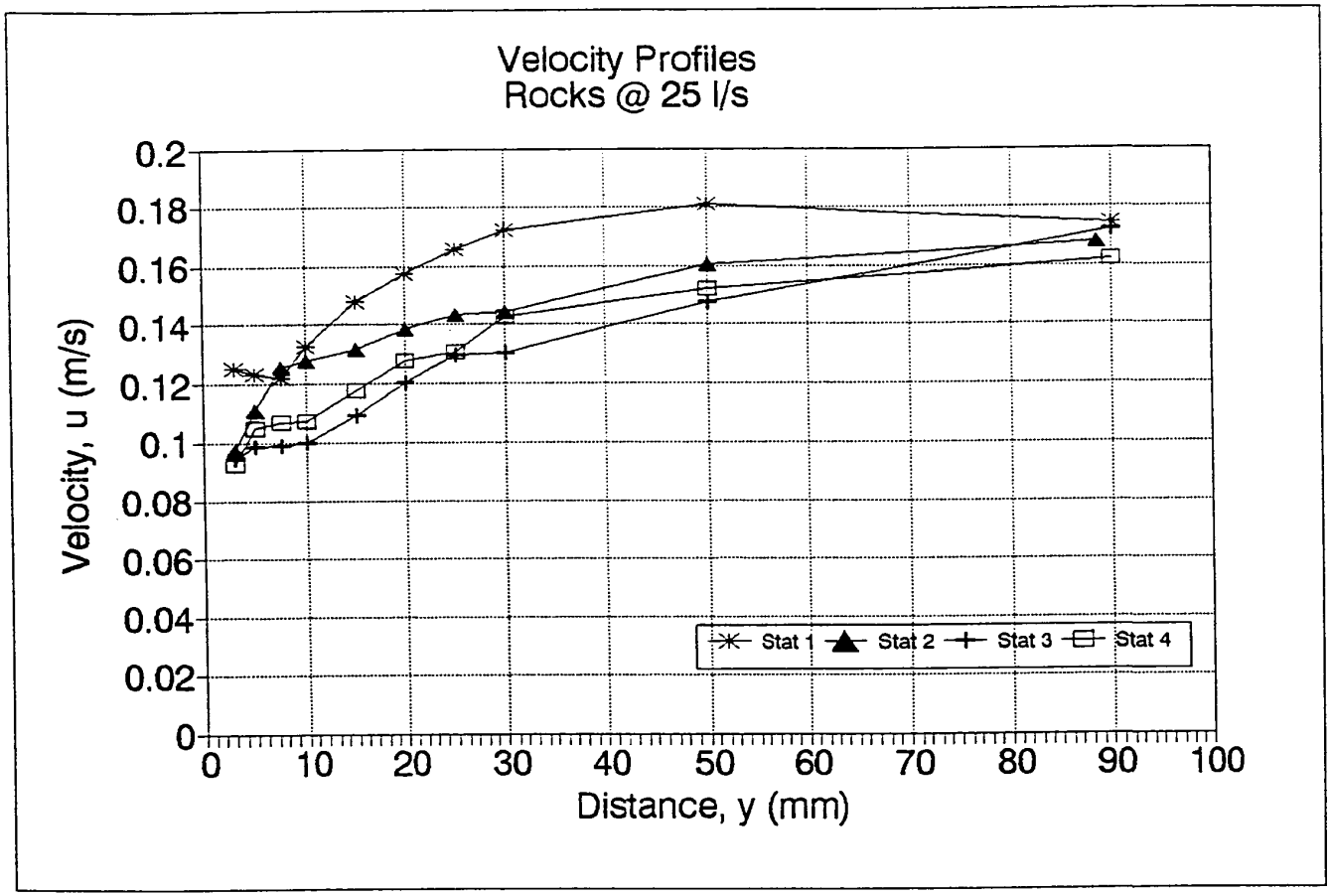

Figure 6.35 Velocity Profiles - Rocks @ 25 l/s

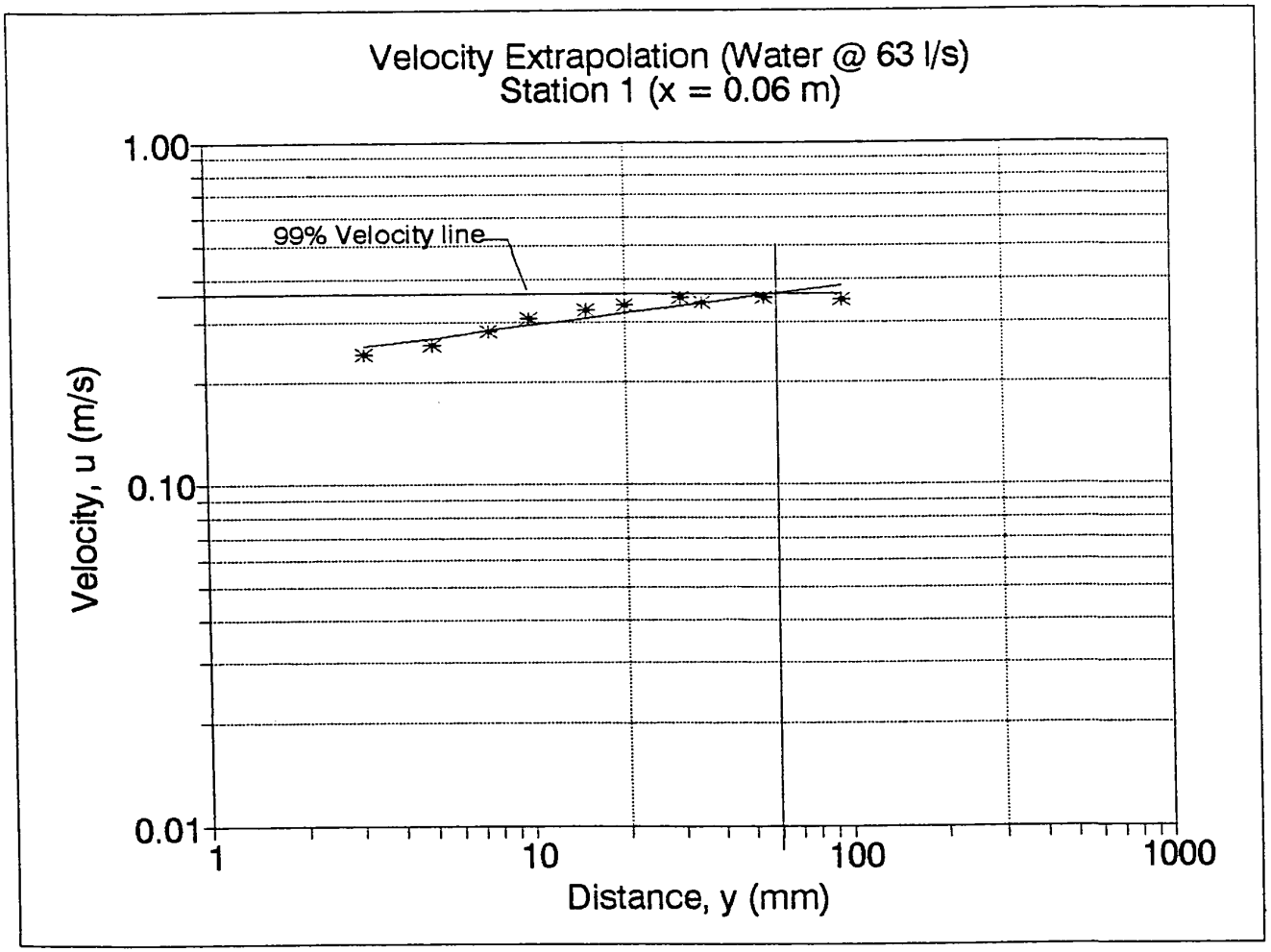

Figure 6.36 Extrapolation of Velocity: Water @ 63 l/s - Station 1

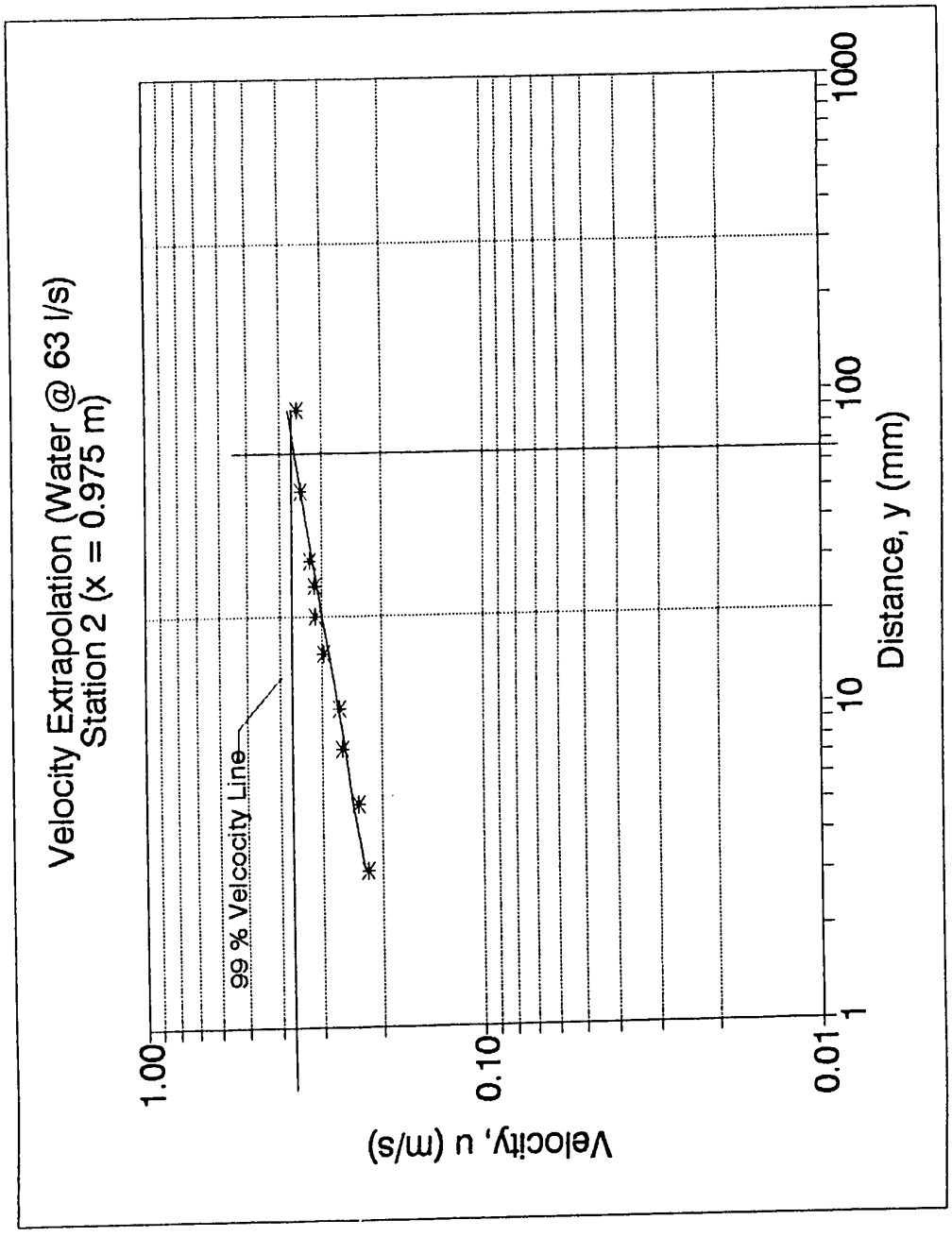

Figure 6.37 Extrapolation of Velocity: Water @ 63 l/s - Station 2

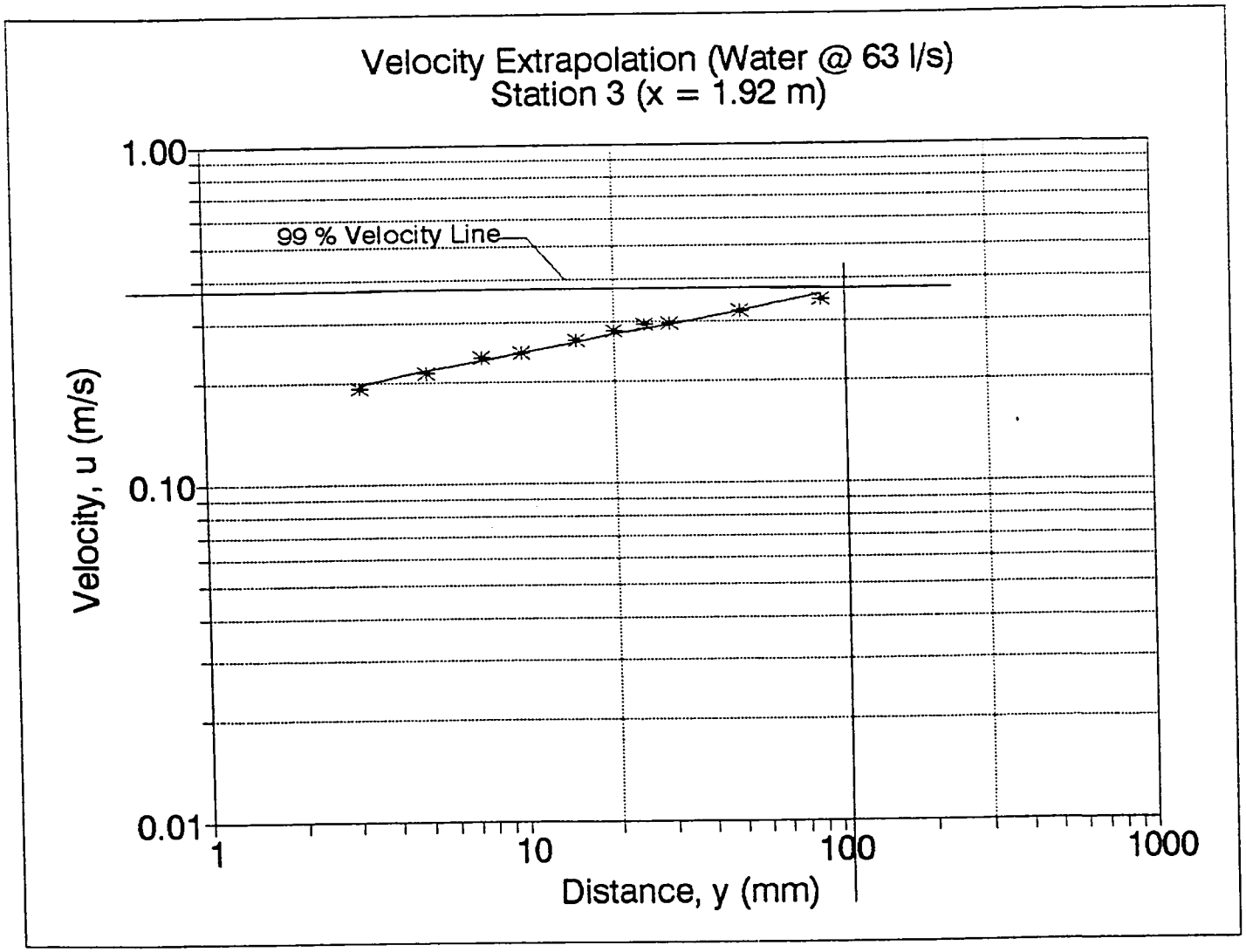

Figure 6.38 Extrapolation of Velocity: Water @ 63 l/s - Station 3

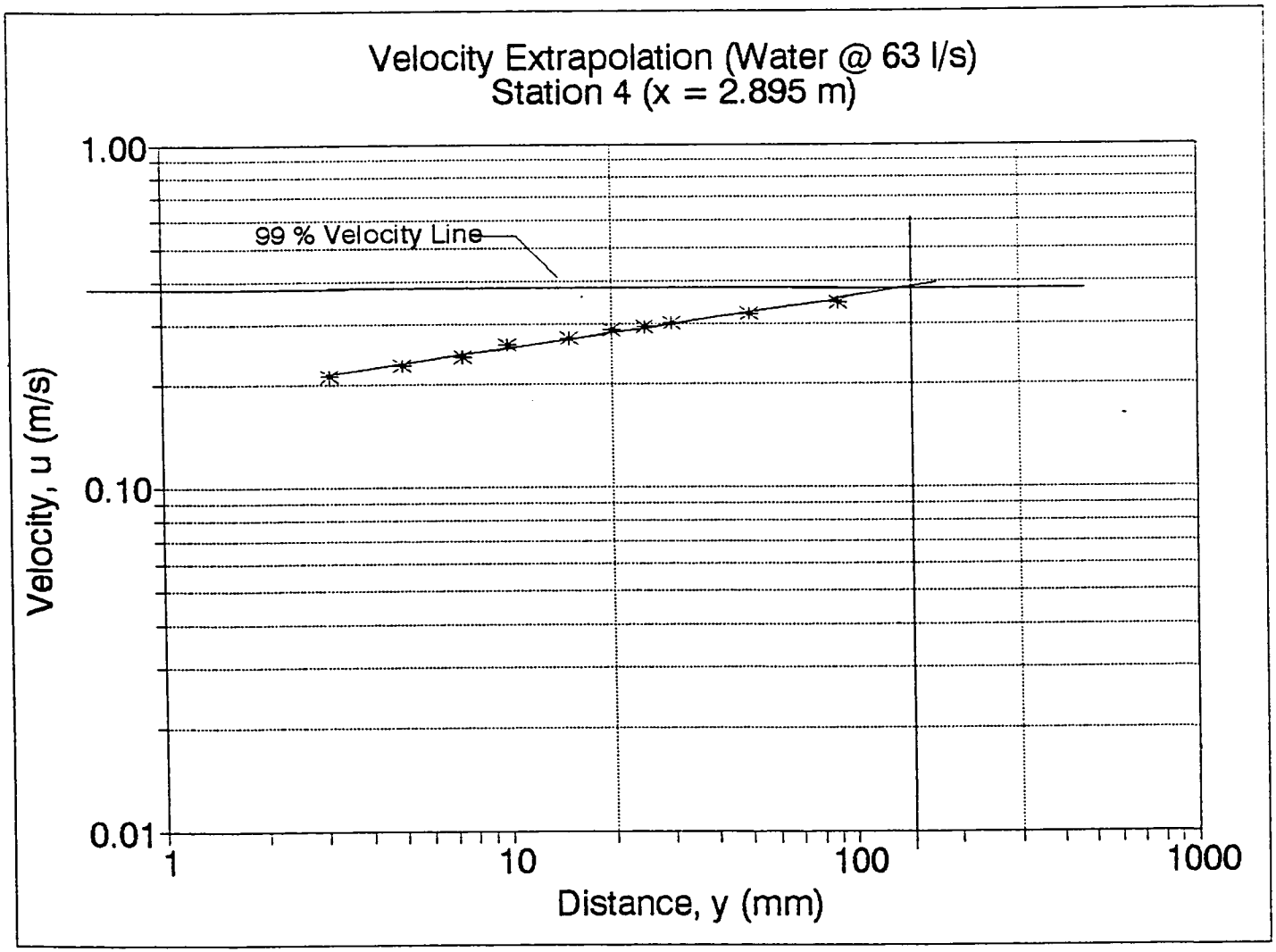

Figure 6.39 Extrapolation of Velocity: Water @ 63 l/s - Station 4

Table 6.11 Boundary Layer Thickness - Phase 2.0

Material	Q (l/s)	Boundary Layer Thickness (mm)							
		Station 1		Station 2		Station 3		Station 4	
		Raw	Fit[1]	Raw	Fit[1]	Raw	Fit[1]	Raw	Fit[1]
Water	25	76	76	107	107	273[2]	136	147[2]	164
	38	47	51	93	85	113	117	104[2]	148
	63	60	53	76	86	117	118	151	148
Sand	25	44	74	74[2]	87	127[2]	99	97[2]	111
	38	59[3]	59	101	99	135	137	174	173
	63	35	34	78	76	112	116	155	153
Rocks	25	39	55	127	99	135	141	175	181
	38	31	31	71	71	na	109	na	145
	63	34	43	93	75	97	104	131	132

1 - Line of best fit (See Figure 6.40 to 6.48); 2 - Flow rates lower by approximately 3 l/s; 3 - Flow rate higher by approximately 3 l/s.

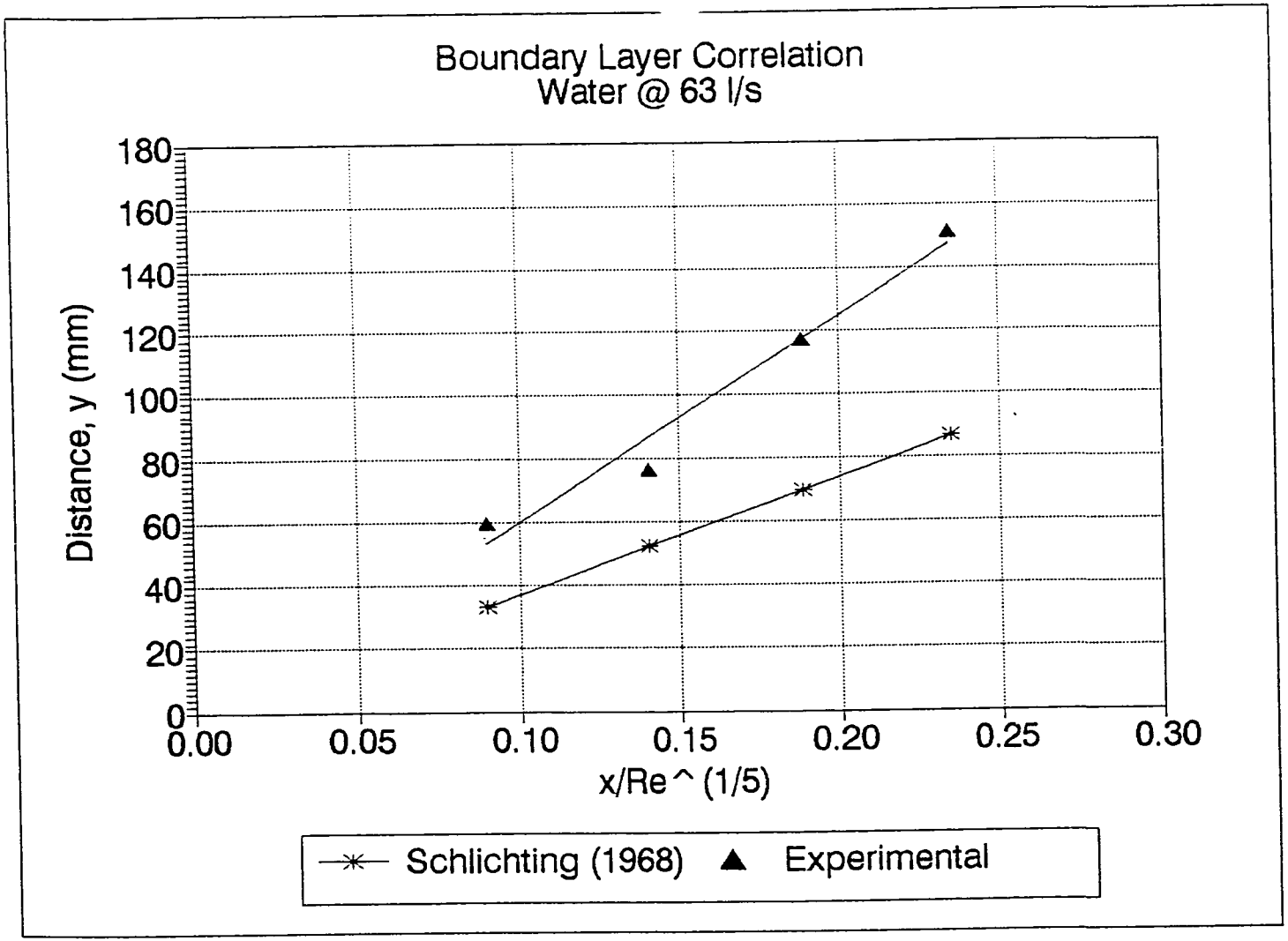

Figure 6.40 Boundary Layer Development: Water @ 63 l/s

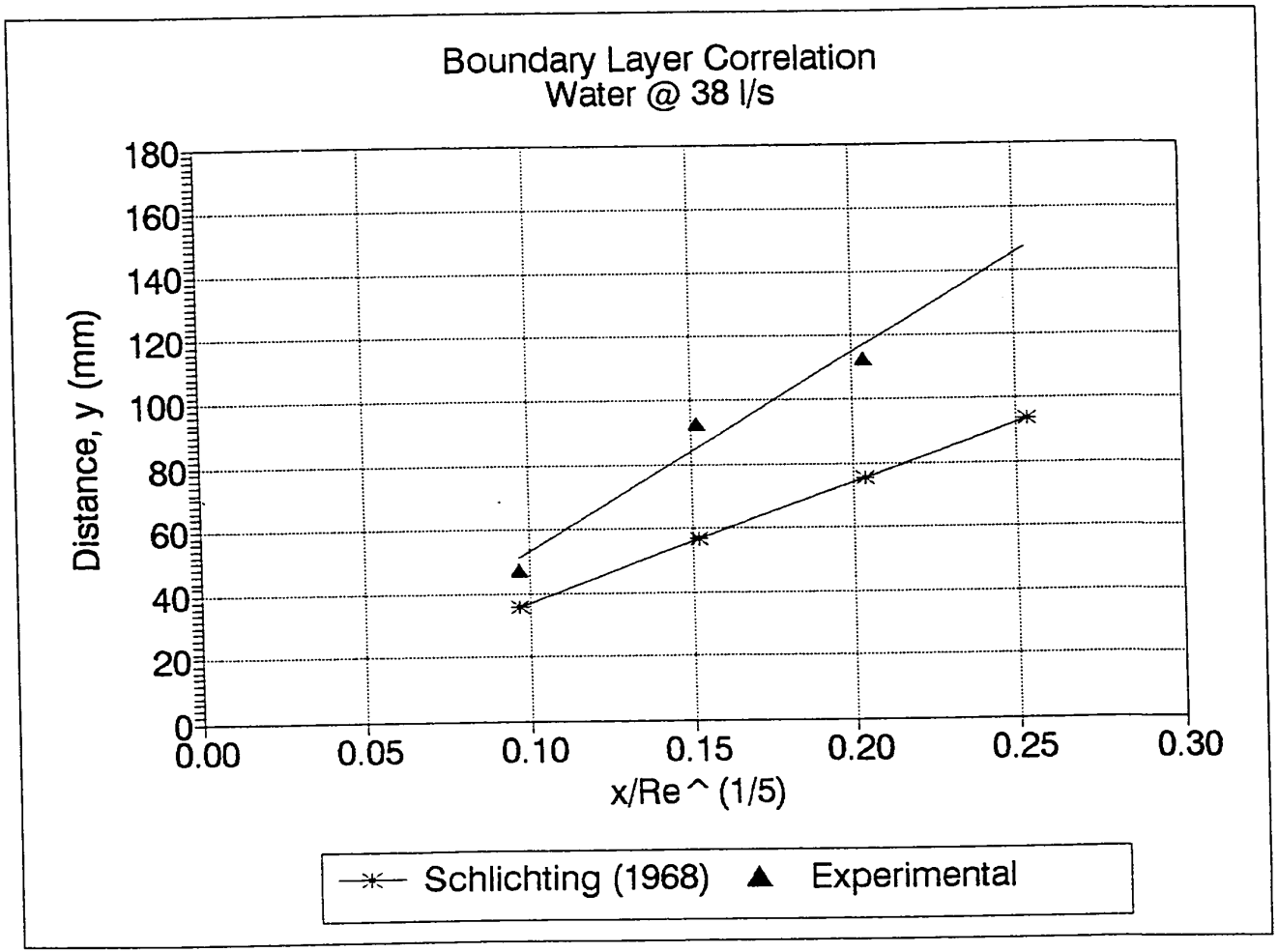

Figure 6.41 Boundary Layer Development: Water @ 38 l/s

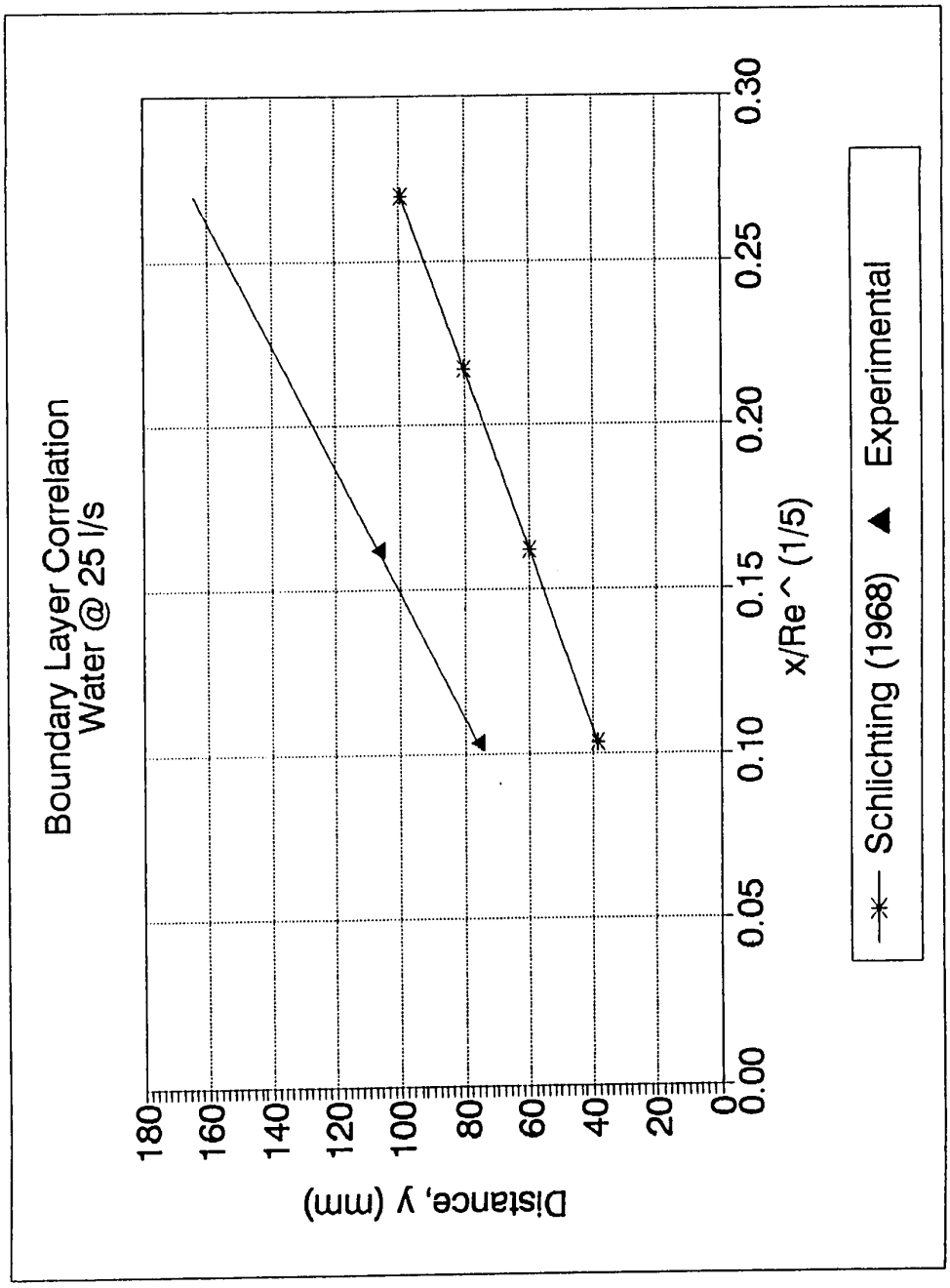

Figure 6.42 Boundary Layer Development: Water @ 25 l/s

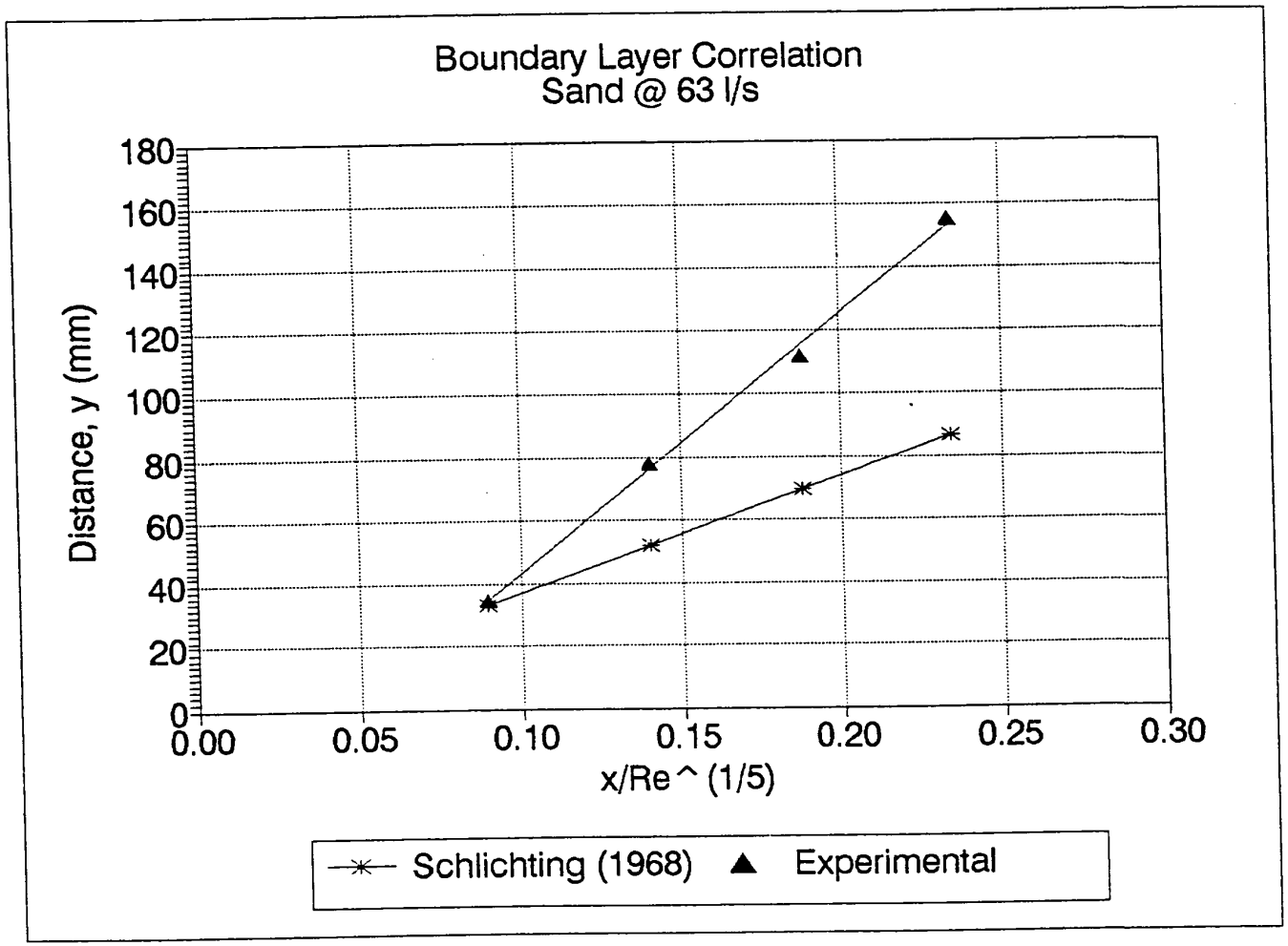

Figure 6.43 Boundary Layer Development: Sand @ 63 l/s

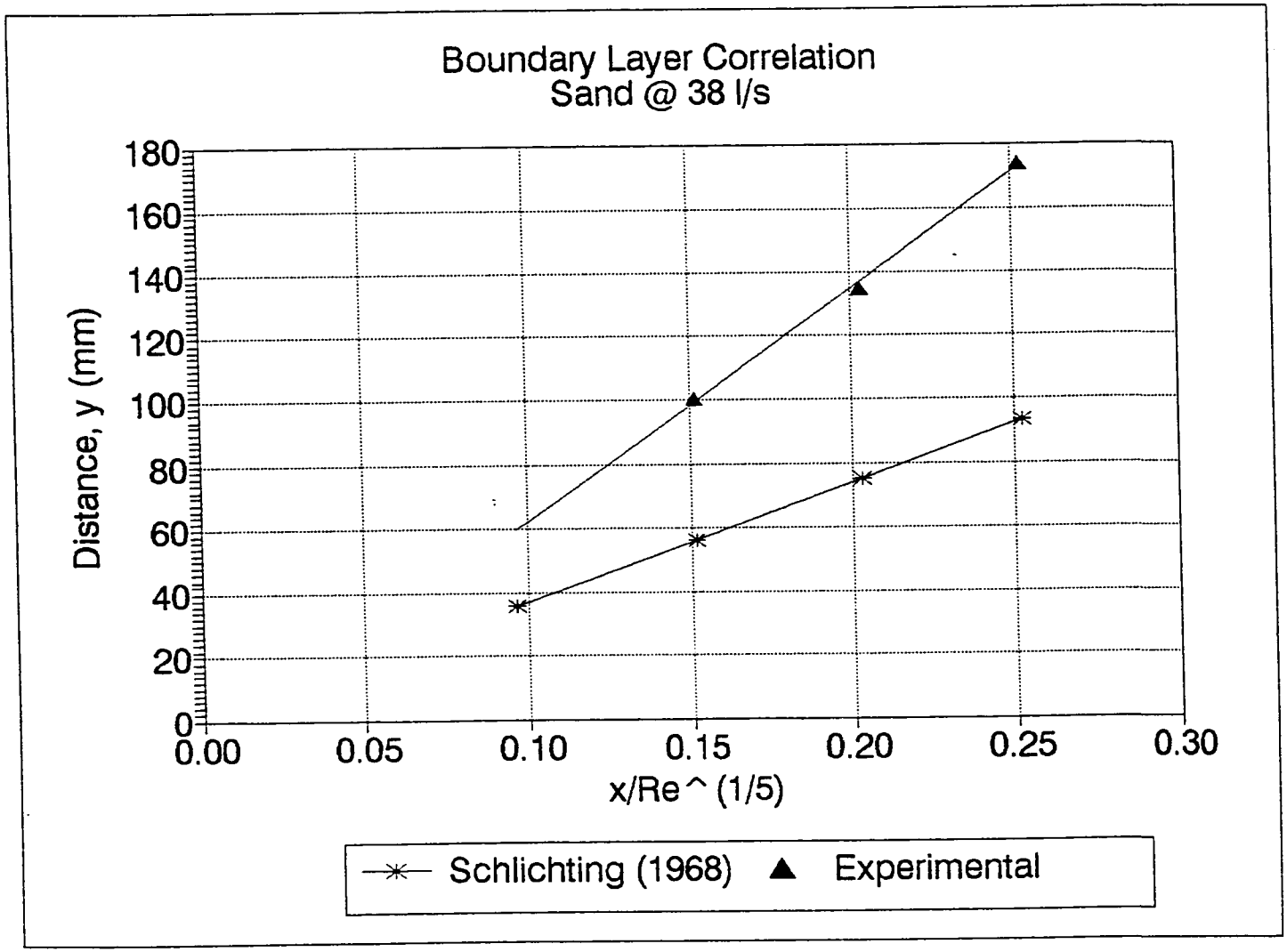

Figure 6.44 Boundary Layer Development: Sand @ 38 l/s

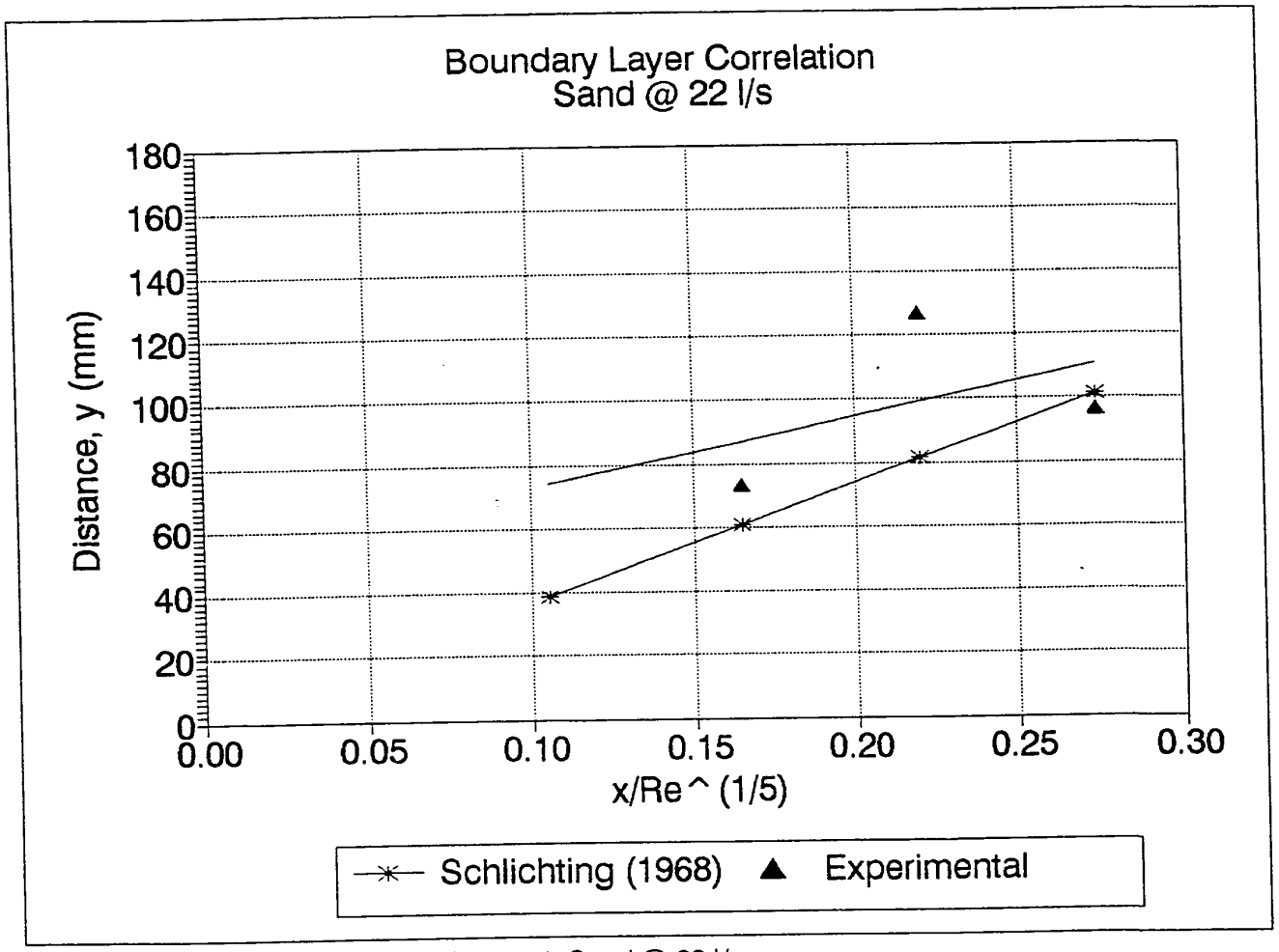

Figure 6.45 Boundary Layer Development: Sand @ 22 l/s

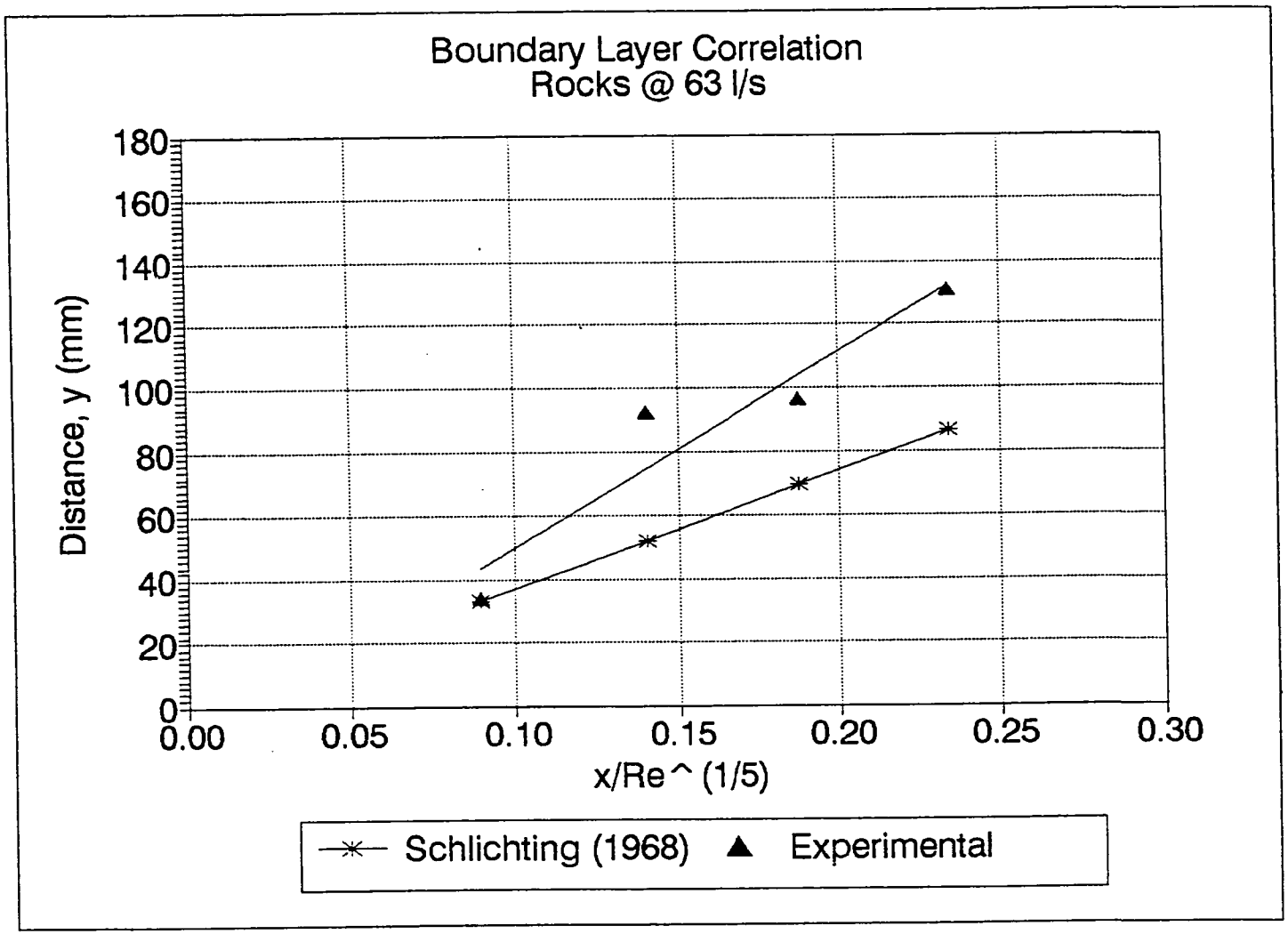

Figure 6.46 Boundary Layer Development: Rocks @ 63 l/s

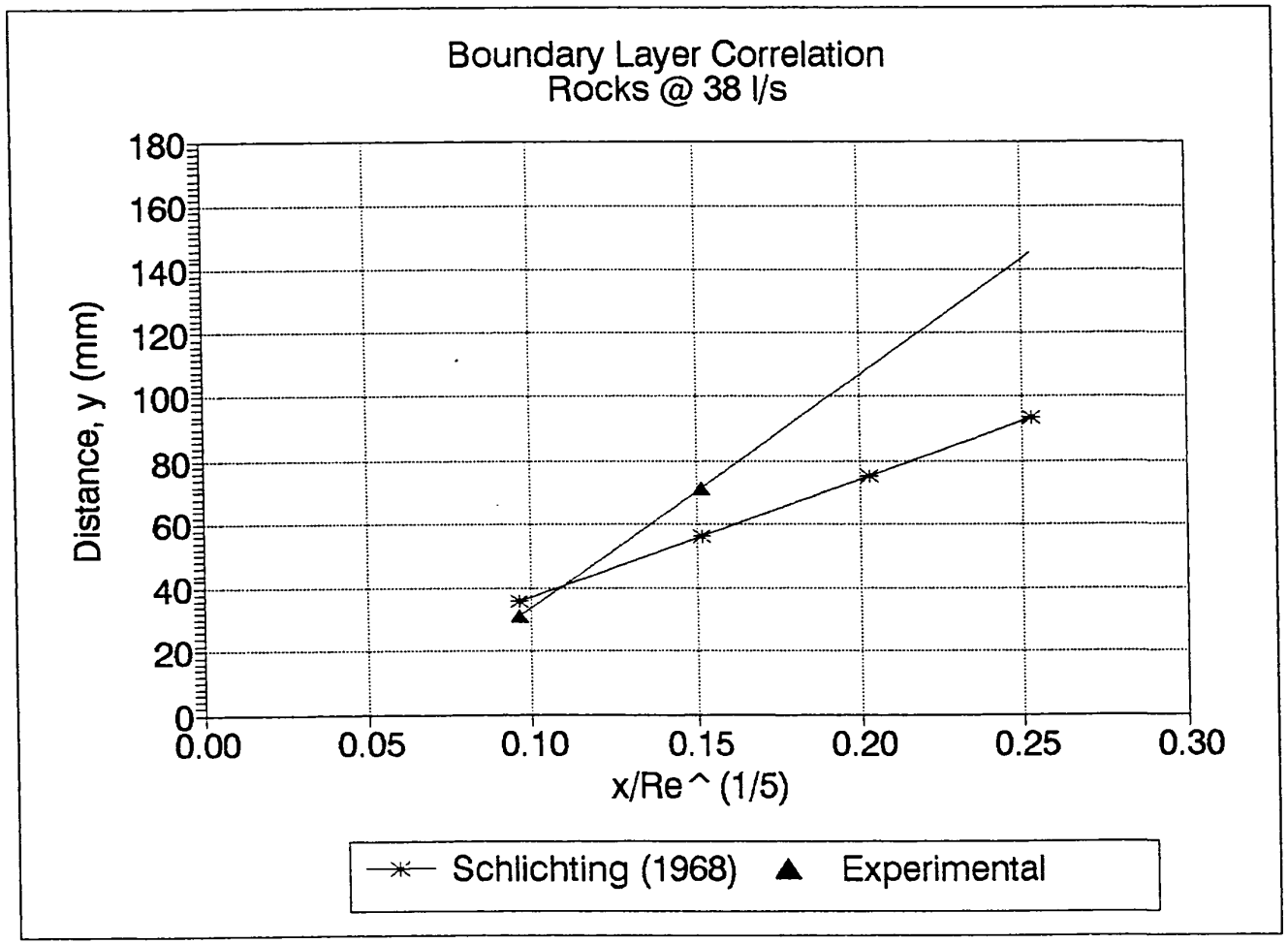

Figure 6.47 Boundary Layer Development: Rocks @ 38 l/s

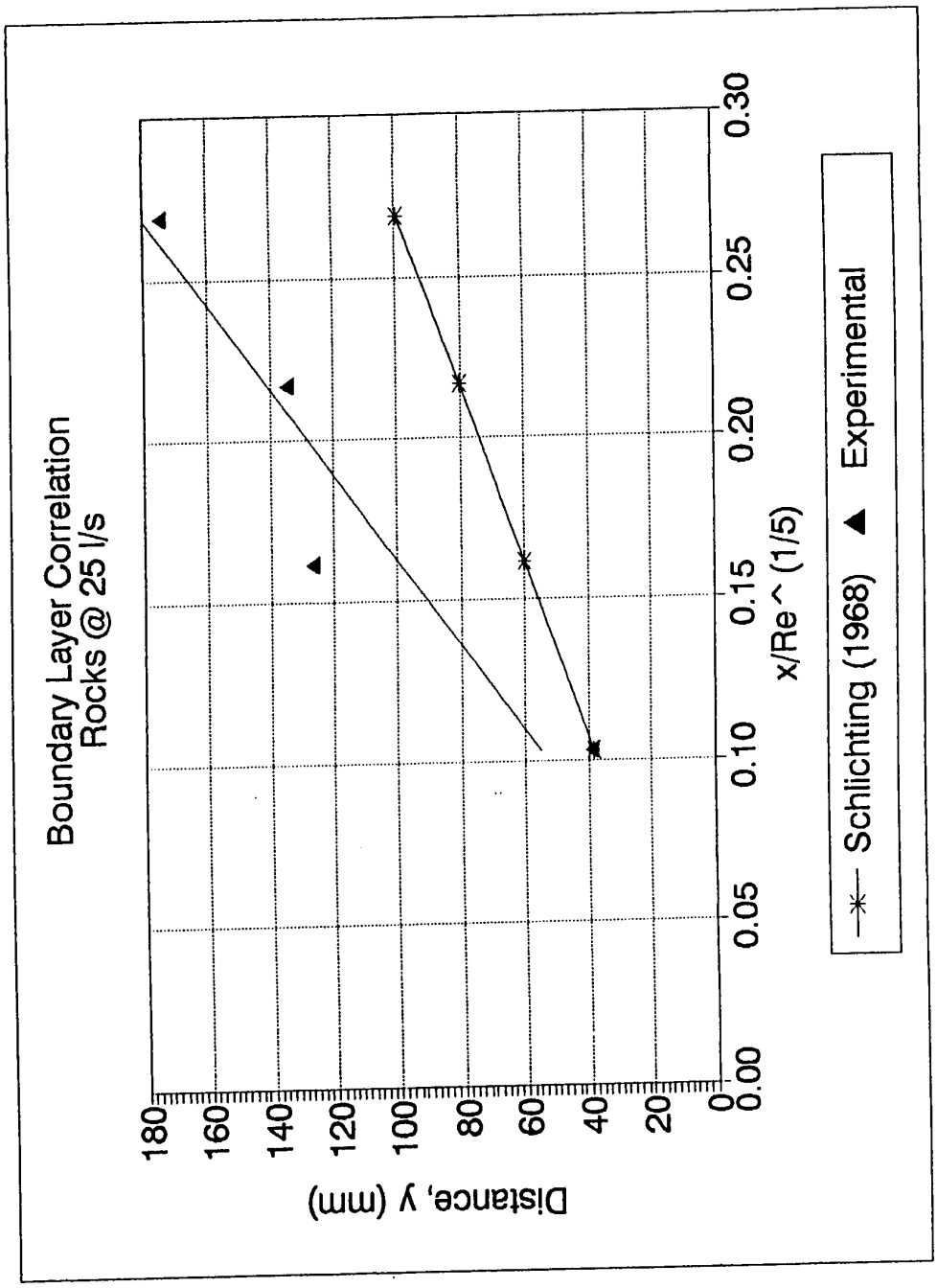

Figure 6.48 Boundary Layer Development: Rocks @ 25 l/s

Table 6.12 Local Power-law Exponents

Material Type	Flow rate l/s	Local Power-law Exponents, n								Average	
		Station 1		Station 2		Station 3		Station 4			
		Raw	Fit[1]	Raw	Fit[1]	Raw	Fit[1]	Raw	Fit[1]	Raw	Fit[1]
Water	25 l/s	7.5	7.5	8.5	8.5	8.5[2]	5.3	5.9[2]	5.1	7.6	6.6
	38 l/s	4.0	4.1	5.1	4.9	5.3	5.4	2.8	3.0	4.3	4.4
	63 l/s	7.9	7.5	6.5	6.8	5.7	5.7	6.8	6.7	6.7	6.7
Sand	25 l/s	5.3	8.2	4.6[2]	4.9	5.1[2]	4.6	3.3[2]	3.5	4.6	5.3
	38 l/s	9.2[3]	11.5	6.9	6.9	6.4	6.5	5.4	5.4	7.0	7.6
	63 l/s	11.7	11.7	5.9	5.8	6.7	6.8	6.1	6.0	7.6	7.6
Rocks	25 l/s	5.3	6.5	6.5	5.8	4.7	4.7	5.4	5.5	5.5	5.6
	38 l/s	8.5	8.5	5.5	5.5	3.4	3.4	8.1	8.1	6.4	6.4
	63 l/s	5.9	6.8	4.4	4.0	4.7	4.8	6.1	6.2	5.3	5.4

1 - Line of best fit (See Figure 6.49 to 6.57); 2 - Flow rates lower by approximately 3 l/s; 3 - Flow rate higher by approximately 3 l/s

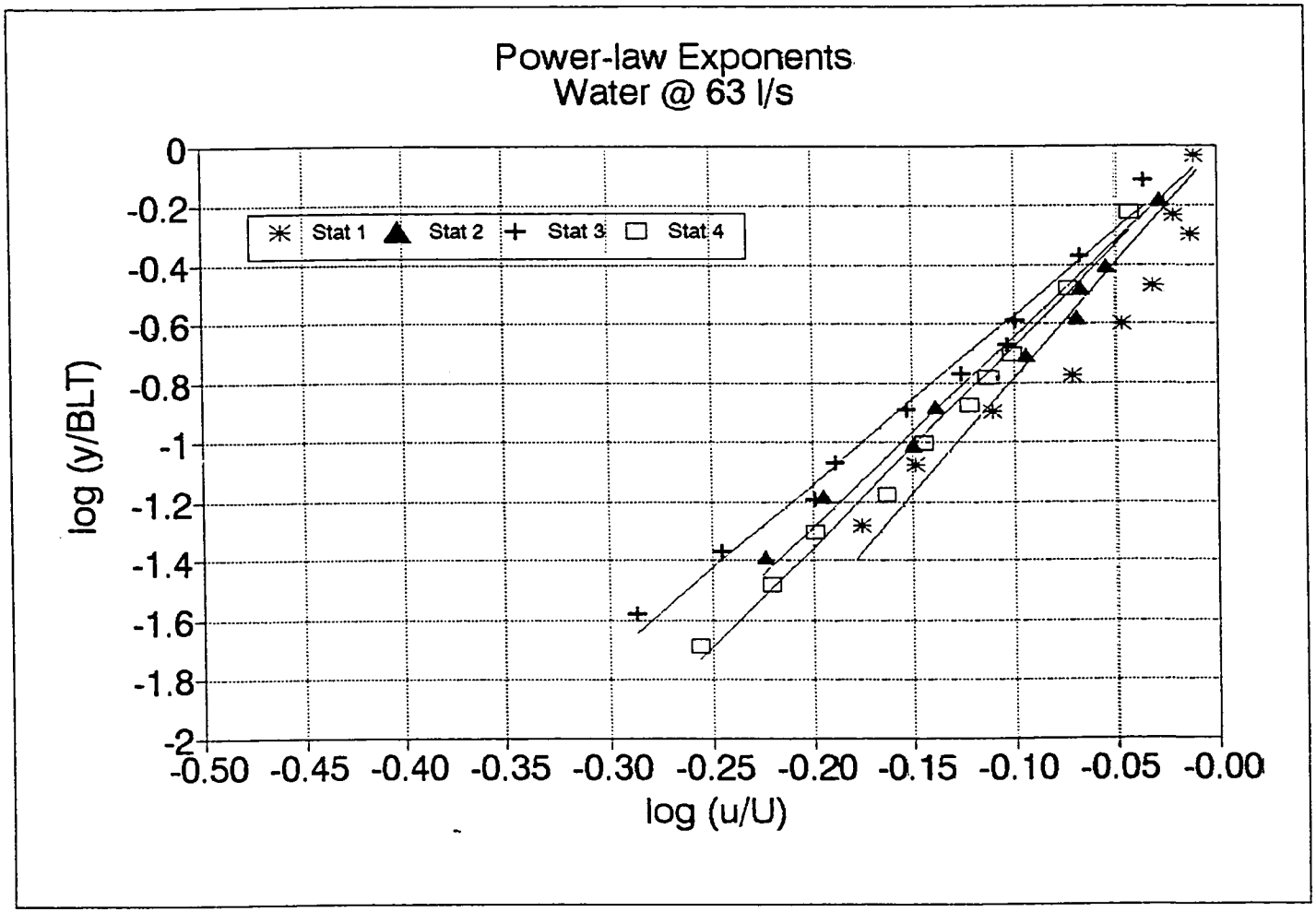

Figure 6.49 Power - law Exponents: Water @ 63 l/s

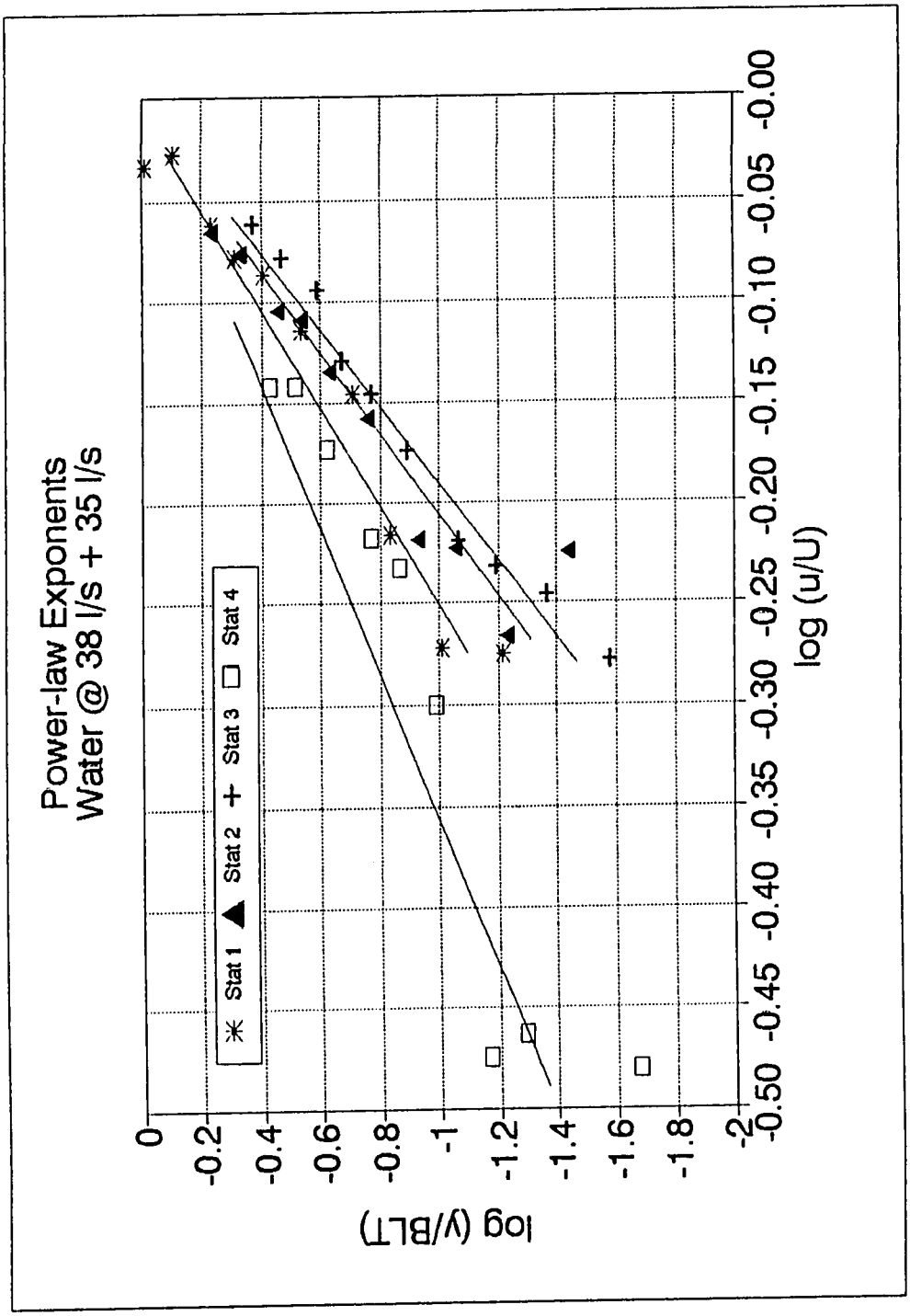

Figure 6.50 Power - law Exponents : Water @ 38 l/s & 35 l/s

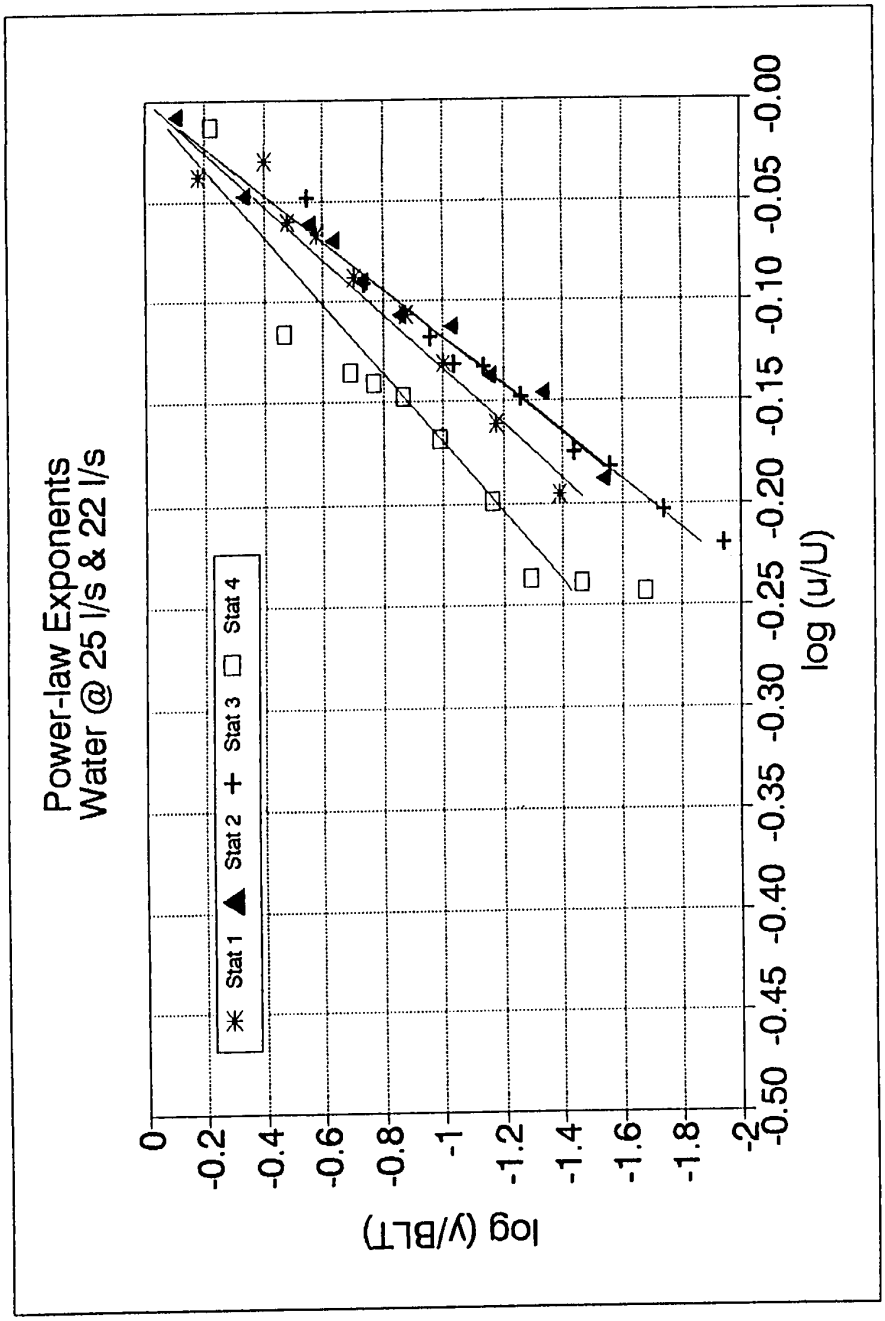

Figure 6.51 Power-law Exponents: Water @ 25 l/s & 22 l/s

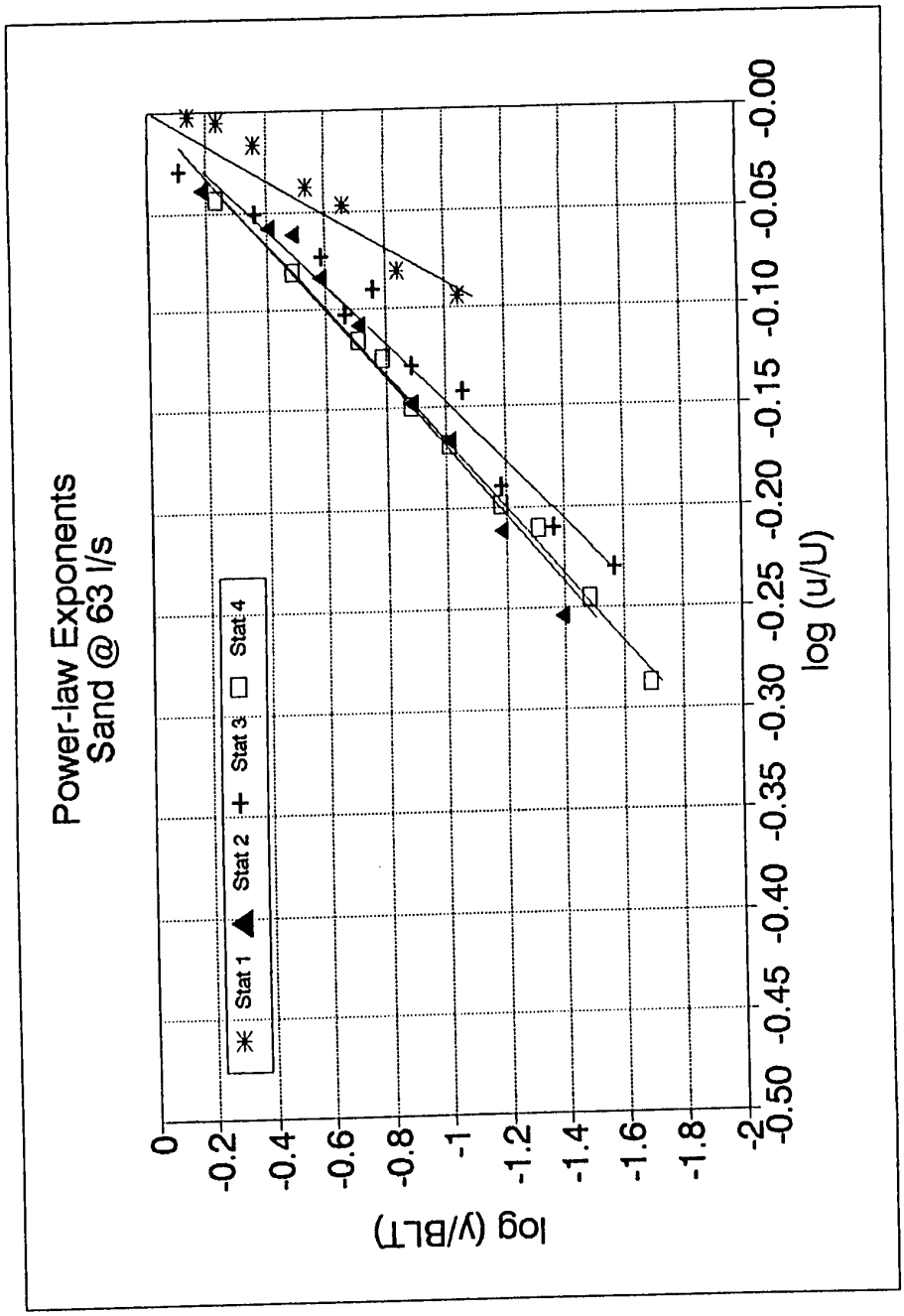

Figure 6.52 Power-law Exponents: Sand @ 63 l/s

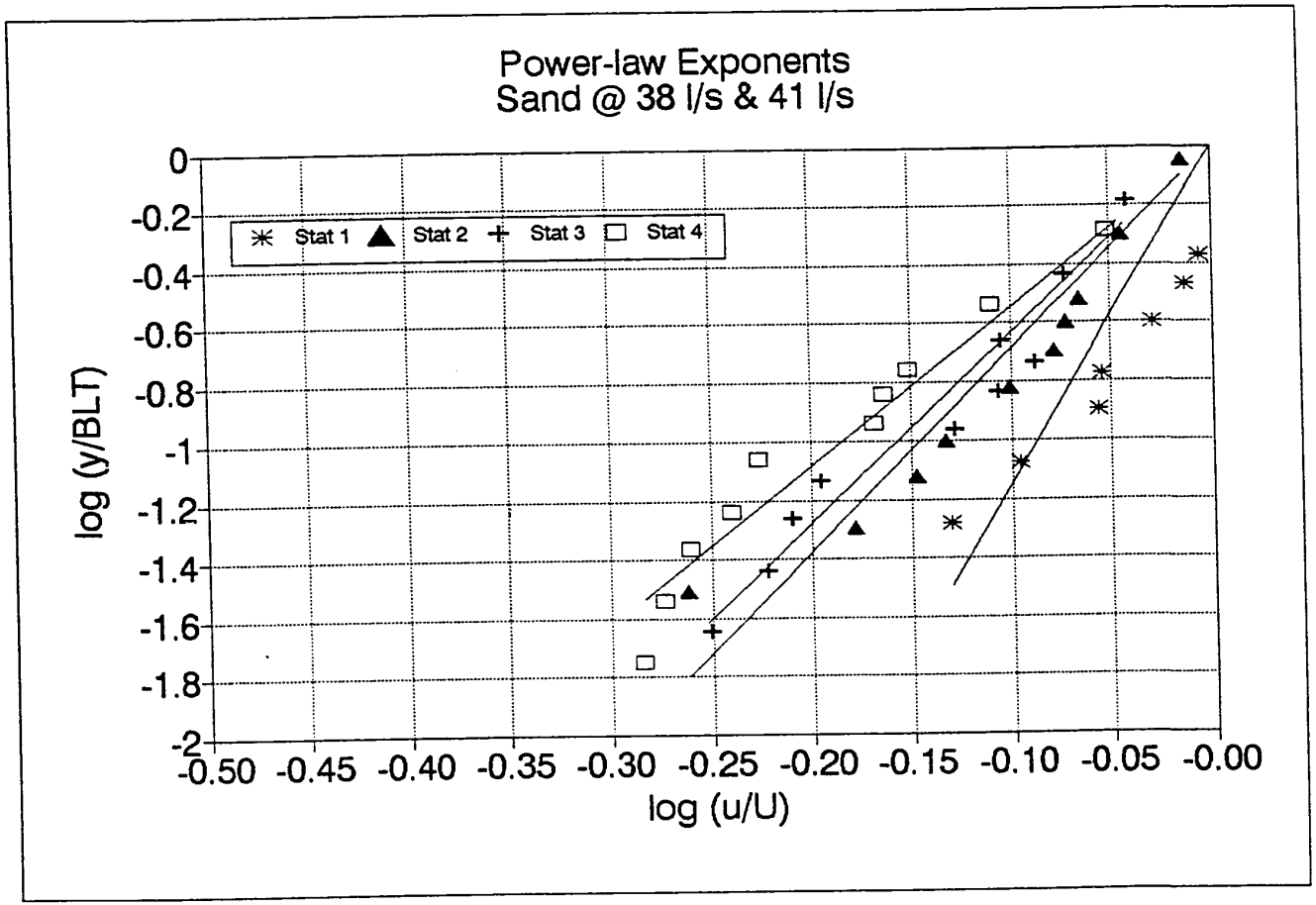

Figure 6.53 Power-law Exponents: Sand @ 38 l/s & 41 l/s

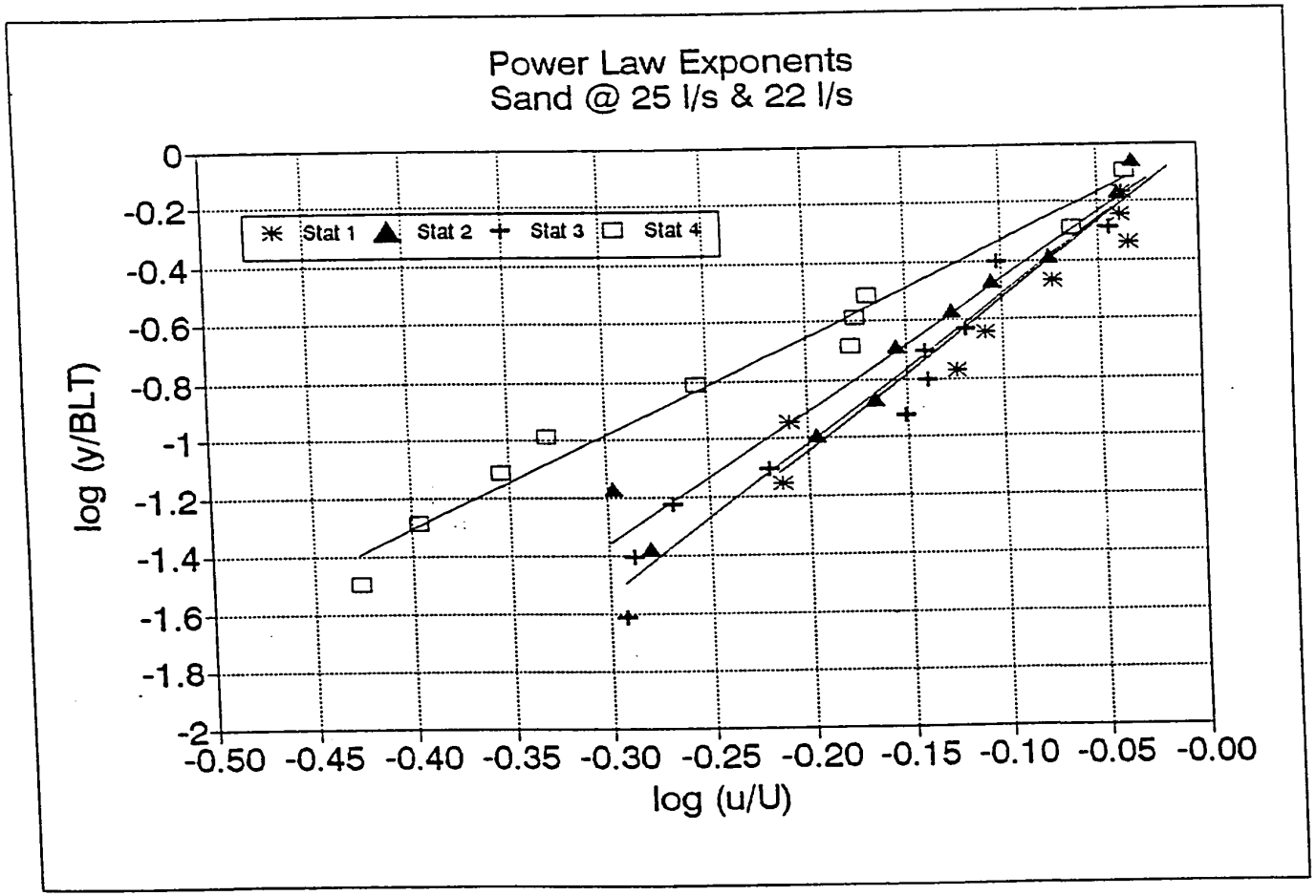

Figure 6.54 Power-law Exponents: Sand @ 25 l/s & 22 l/s

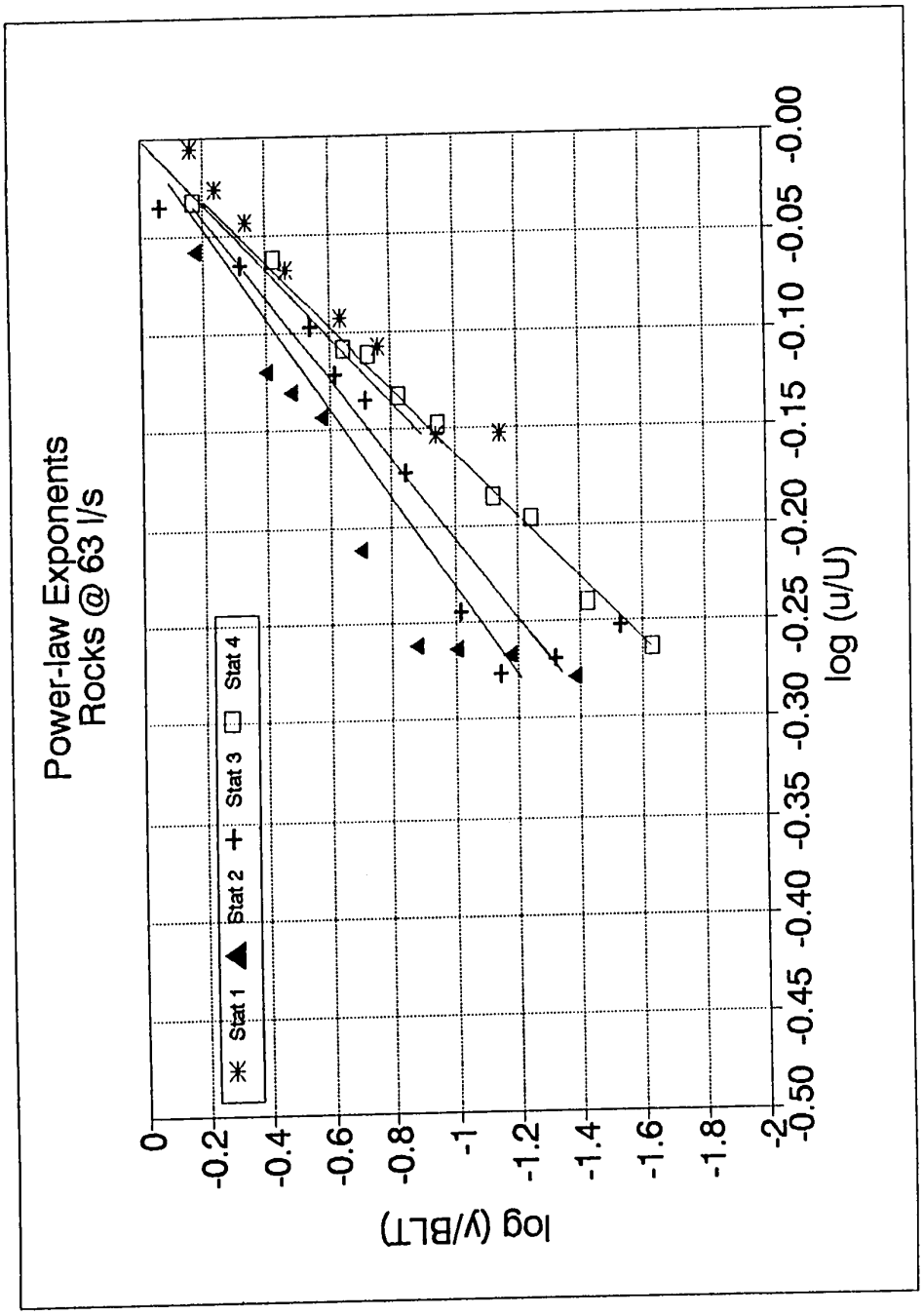

Figure 6.55 Power-law Exponents: Rocks @ 63 l/s

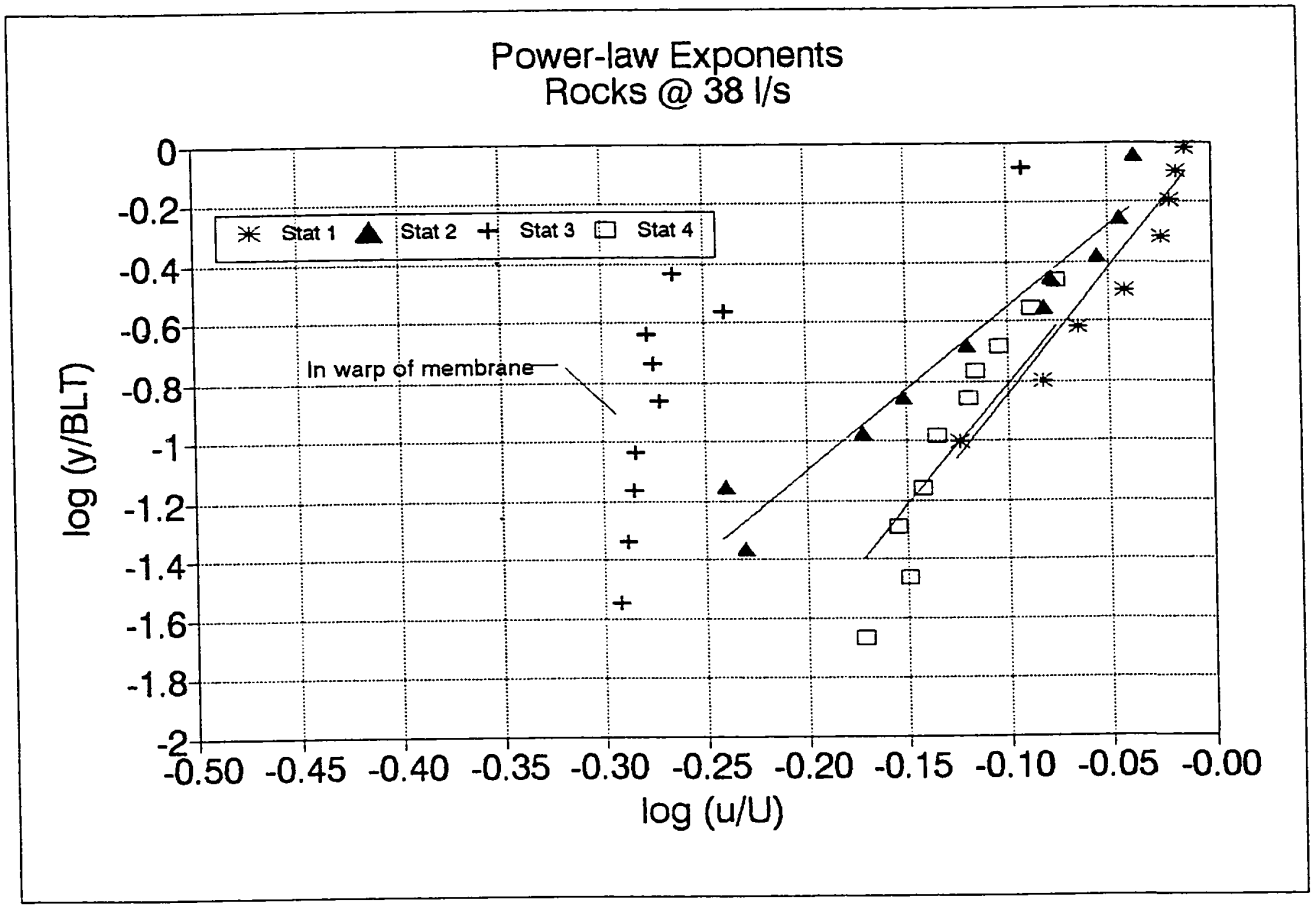

Figure 6.56 Power-law Exponents: Rocks @ 38 l/s

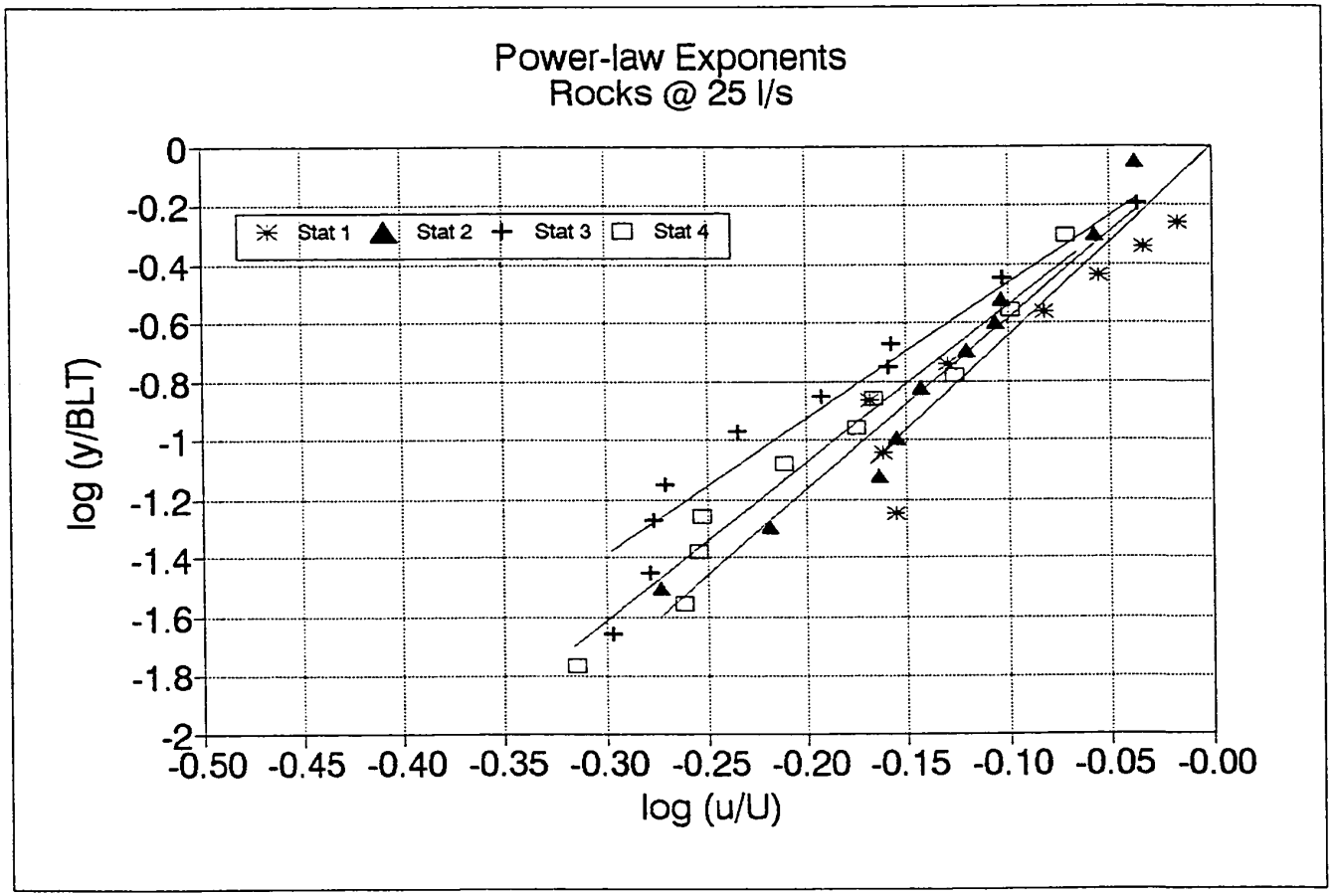

Figure 6.57 Power-law Exponents: Rocks @25 l/s

Table 6.13 Average Forces Recorded and Calculated @ Full Load (50 kg)

Material	Flow rate l/s	Recorded (N) Load cell	Bulkhead Force [1]	Total	Error [2]	Calculated (N) Momentum Flux	Pressure Force [1]	Total	Error [3]
Water	25 l/s	0.182	0.032	0.150	0.070	0.071	0.137	0.209	0.021
	38 l/s	0.220	-0.015	0.235	0.070	0.290	-0.010	0.280	0.087
	63 l/s	0.693	0.145	0.548	0.204	0.253	0.301	0.554	0.076
Sand	25 l/s	0.258	0.021	0.237	0.076	0.061	0.074	0.135	0.018
	38 l/s	0.289	0.021	0.268	0.091	0.238	0.088	0.326	0.071
	63 l/s	0.765	0.126	0.639	0.427	0.513	0.392	0.905	0.154
Rocks	25 l/s	0.303	0.019	0.284	0.070	0.094	0.193	0.287	0.028
	38 l/s	0.336	0.063	0.272	0.105	0.091	0.154	0.246	0.027
	63 l/s	0.767	0.189	0.578	0.356	0.298	0.341	0.639	0.089

1 - Differential Pressure Transducer; 2 - Level of uncertainty in results; 3 - Error in calculated force is approximately 30% of the momentum flux due to errors in "n", U and the growth of the boundary layer.

Table 6.14 Average Forces Recorded - Phase 1.0

Material Type	Flow rate l/s	No Load (0 kg)				Quarter Load (12.5 kg)				Half Load (25 kg)			
		Load cell	Bulkhead[1] Force	Total	Error[2]	Load cell	Bulkhead[1] Force	Total	Error[2]	Load cell	Bulkhead[1] Force	Total	Error[2]
Water	25 l/s	0.189	0.003	0.186	0.063	0.162	0.011	0.151	0.063	0.138	0.018	0.119	0.072
	38 l/s	NA	NA	NA	NA	0.218	-0.006	0.224	0.053	0.235	-0.008	0.243	0.087
	63 l/s	NA	NA	NA	NA	NA	NA	NA	NA	NA	NA	NA	NA
Sand	25 l/s	0.189	0.003	0.186	0.063	0.260	0.007	0.253	0.064	0.191	0.012	0.179	0.070
	38 l/s	NA	NA	NA	NA	0.259	0.007	0.251	0.079	0.239	0.012	0.227	0.095
	63 l/s	NA	NA	NA	NA	NA	NA	NA	NA	NA	NA	NA	NA
Rocks	25 l/s	0.189	0.003	0.186	0.063	0.166	0.009	0.156	0.065	0.177	0.012	0.165	0.066
	38 l/s	NA	NA	NA	NA	0.262	0.027	0.236	0.081	0.302	0.038	0.264	0.082
	63 l/s	NA	NA	NA	NA	NA	NA	NA	NA	NA	NA	NA	NA

1 - Differential Pressure Transducer; 2 - Level of uncertainty in results; NA - Not Applicable

Table 6.15 Calculated Local Drag Forces and Drag Coefficients @ Full Load (50 kg)

Material	Flow rate l/s	Station 1 - 2 Momentum Flux	Pressure Force[1]	Total	Cf	Station 2 - 3 Momentum Flux	Pressure Force[1]	Total	Cf	Station 3 - 4 Momentum Flux	Pressure Force[1]	Total	Cf
Water	25 l/s	0.003	0.031	0.034	0.0065	0.2236	0.0385	0.262	0.0468	0.09638	0.046	0.1422	0.024
	38 l/s	0.008	-0.002	0.006	0.0006	0.1483	-0.003	0.146	0.0139	1.464	-0.003	1.4607	0.130
	63 l/s	0.166	0.061	0.227	0.0104	0.6646	0.0814	0.746	0.0320	-0.03004	0.100	0.0704	0.003
Sand	25 l/s	0.038	0.020	0.058	0.0124	0.0297	0.0223	0.052	0.0103	0.2165	0.025	0.2411	0.044
	38 l/s	0.135	0.018	0.153	0.0142	0.2363	0.0239	0.260	0.0224	0.6478	0.029	0.6773	0.054
	63 l/s	0.347	0.069	0.416	0.0177	0.3472	0.1011	0.448	0.0178	1.204	0.131	1.3345	0.049
Rocks	25 l/s	0.060	0.037	0.097	0.0179	0.245	0.0512	0.296	0.0509	0.03869	0.064	0.103	0.016
	38 l/s	0.138	0.027	0.164	0.0153	0.7444	0.0395	0.784	0.0681	-1.102	0.051	-1.051	-0.085
	63 l/s	0.356	0.067	0.423	0.0179	0.279	0.0913	0.370	0.0147	-0.1879	0.114	-0.074	-0.003

1- Differential Pressure Transducer

Table 6.16 Average Recorded and Calulated Skin Friction Coefficients

Material Type	Flow rate l/s	Recorded				Calculated
		No Load (0 kg)	Quarter Load (12.5 kg)	Half Load (25 kg)	Full Load (50 kg)	Full Load (50 kg)
Water	25 l/s	0.0287	0.0151	0.0093	0.0082	0.0117
	38 l/s	NA	0.0108	0.0100	0.0067	0.0084
	63 l/s	NA	NA	NA	0.0075	0.0075
Sand	25 l/s	0.0287	0.0247	0.0134	0.0125	0.0084
	38 l/s	NA	0.0125	0.0089	0.0072	0.0088
	63 l/s	NA	NA	NA	0.0081	0.0113
Rocks	25 l/s	0.0287	0.0138	0.0130	0.0163	0.0155
	38 l/s	NA	0.0117	0.0110	0.0083	0.0067
	63 l/s	NA	NA	NA	0.0072	0.0080

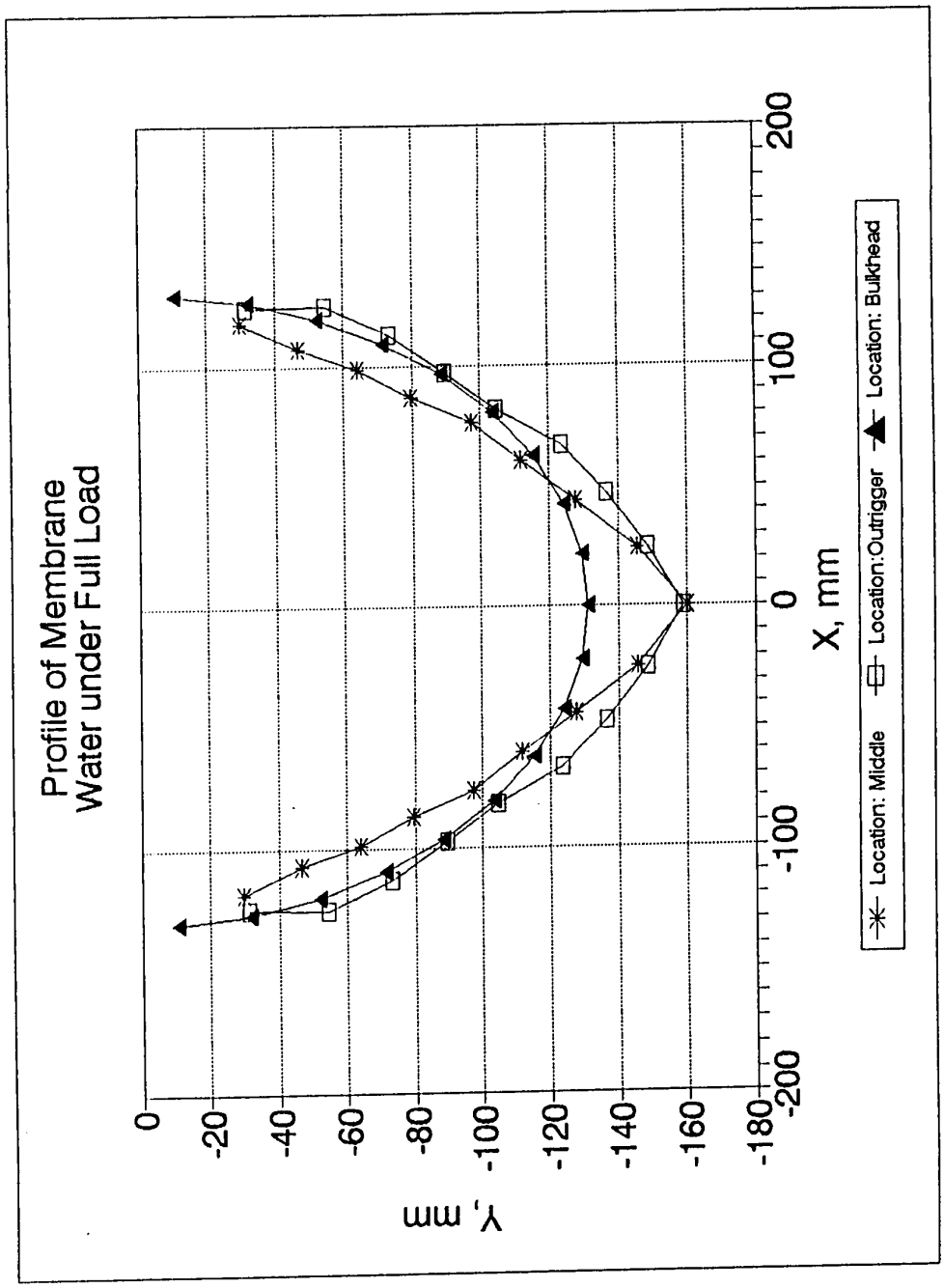

Figure 6.58 Profile of Membrane: Water

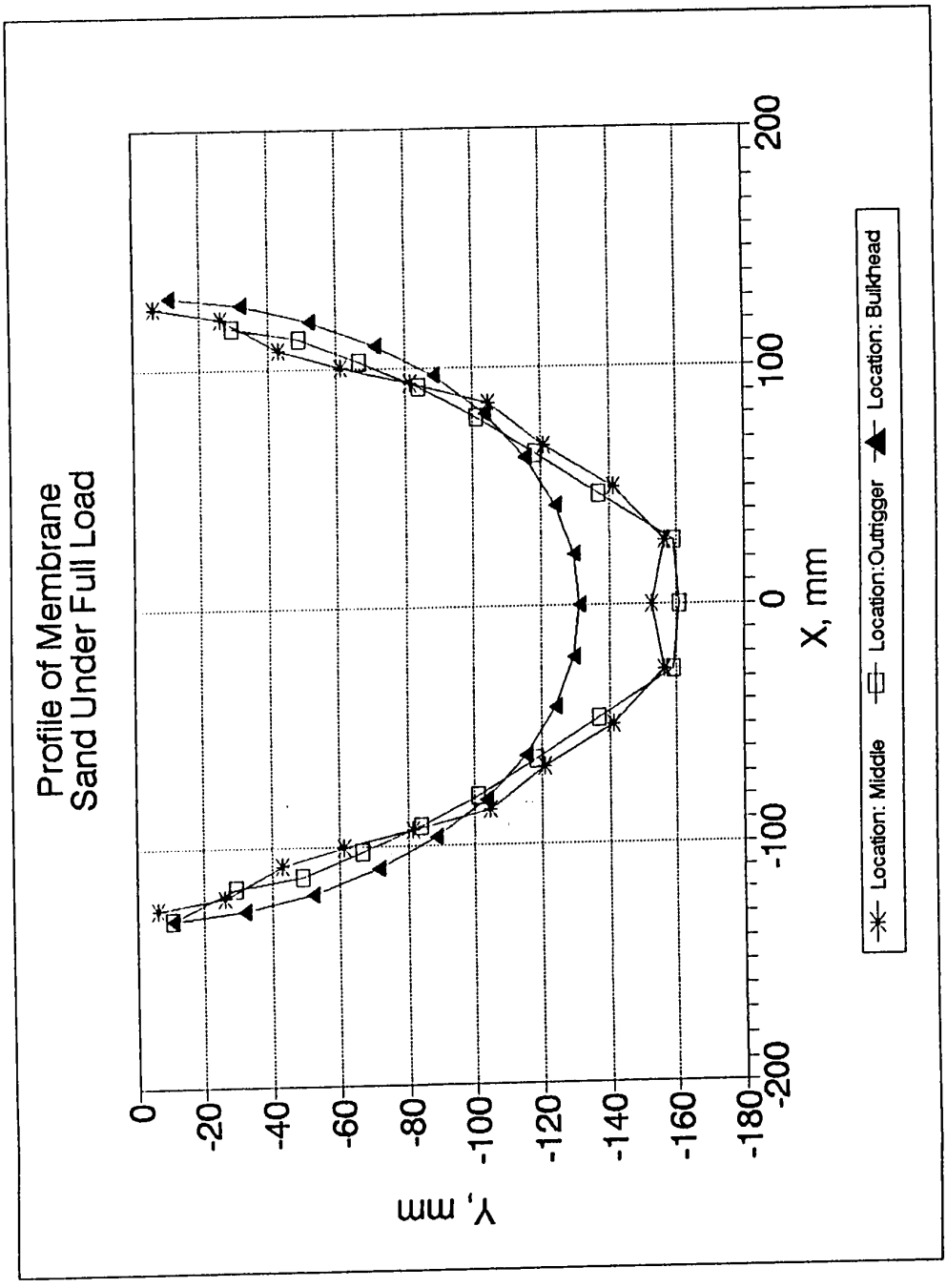

Figure 6.59 Profile of Membrane : Sand

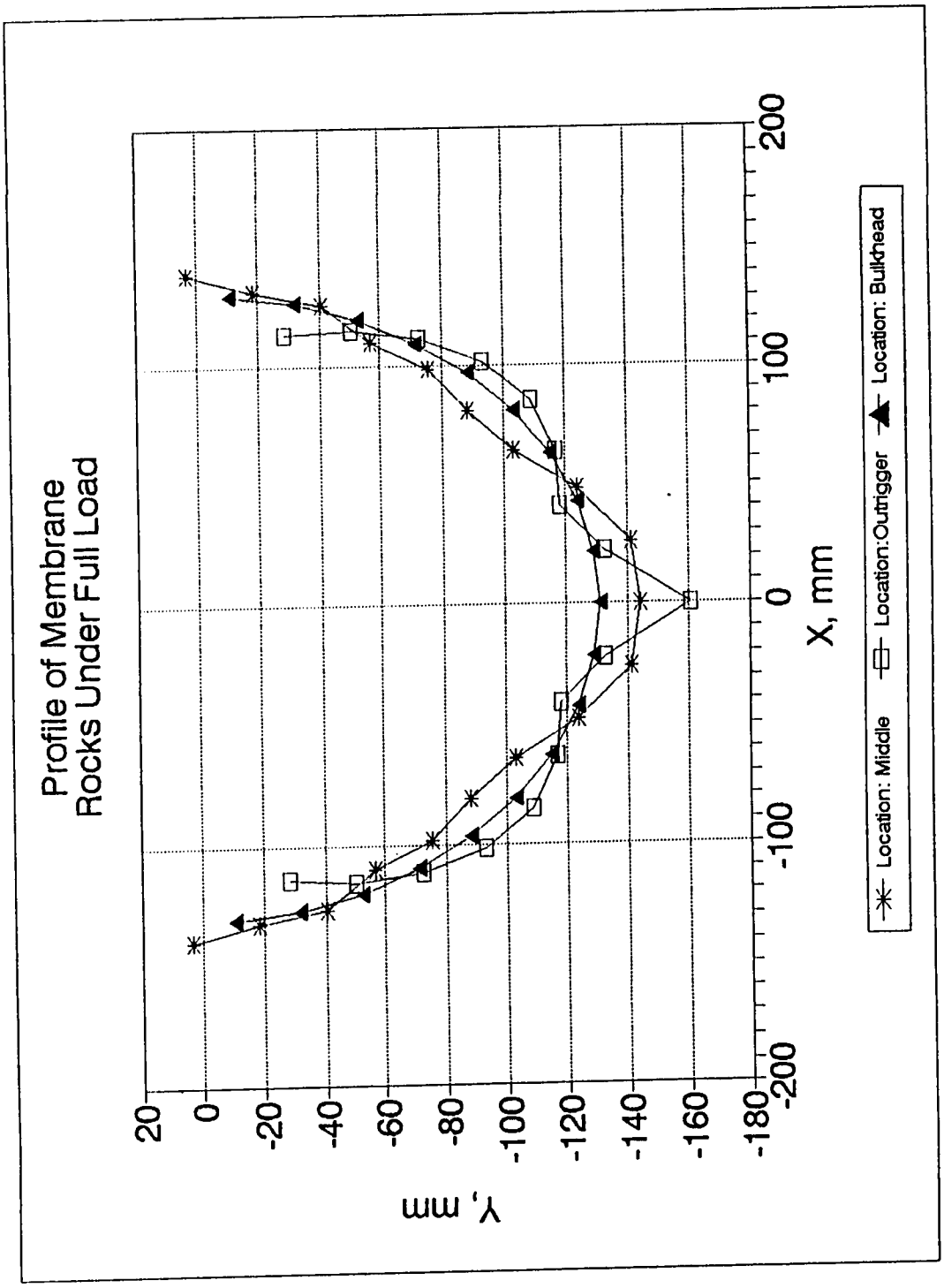

Figure 6.60 Profile of Membrane : Rocks

7.0 DISCUSSIONS

The determination of drag coefficients (C_f) of the Test Section, associated with various material type set-ups, was the primary objective of this research. The effects of certain dimensionless groups on C_f were investigated. The dimensional analysis performed in Chapter 3.0 led to the establishment of many dimensionless groups of which Reynolds Number and Froude Number were selected as a basis of comparison for the drag coefficients. The drag coefficients were a function of the drag force on the Test Section, which in turn was a function of the free stream velocity, boundary layer development and power-law exponents.

The raw data collected, and subsequently used for determining the drag coefficients, serves as a starting point for the discussion of the drag coefficients of the various material type set-ups. The effects of free stream velocity, boundary layer thickness and power-law exponents on the drag coefficients will then be discussed.

7.1 Raw Data

Force and pressure measurements collected by the data acquisition system, and profile measurements recorded manually are discussed in Sections 7.1, 7.2 and 7.3 respectively. Note, all raw data collected was used in the analysis, i.e., the

data was not pre-selected.

7.1.1 Force measurements

Samples of the load cell measurements collected are depicted in Figures 6.5 to 6.14. Upon comparison of the Bulkhead force data with the Inner Flume wall force data, the trends and range appear similar for water and rocks. In the case of sand the range was noticeably different. Maintaining the alignment and positioning of the Transition Sections with respect to the Test Section, during this test, proved to be difficult and may perhaps explain the differences in range.

The range or amplitude of the data was interpreted as an indication of the damping characteristics of the material type set-up. The ranges of the force data of water and rocks, at 63 l/s, appear to be similar, i.e., approximately 0.4 to 1.1 N. This implied that the damping characteristics of the two set-ups were similar. Sand displayed a higher range of approximately 0.3 to 1.18 N and was interpreted as behaving more as a rigid body than a flexible membrane.

7.1.2 Pressure measurements

Figures 6.15 to 6.26 are samples of the differential pressure recorded. The frequency and amplitude of the data may be affected by the two factors. The first factor is the attenuating capacity of the tubing linking the pitot-static

tube to the pressure transducer. The second factor is the geometry of the pitot-static tube which did not permit the recording of differences in phases associated with total and static pressure ports. Nevertheless, the data indicated that the levels of fluctuations increased as the distance from the boundary layer increased. The fluctuations were due to possible shedding vortices from the nose cone. Furthermore the level of fluctuations decreased in the downstream direction.

Figures 6.27 to 6.35 indicate that the velocity profiles were consistent with few exceptions. The exceptions are reflected in Figures 6.29, 6.32. The occasional inability (possible air entrainment from the pump intake) of the pump to maintain a constant flow rate throughout the test, resulted in an inconsistent velocity profiles with respect to the velocity profiles of the adjacent stations. This difference in flow rate characterised as a displaced velocity profile with an initial and final local mean velocity that was lower (or higher) than the corresponding stations.

The velocity gradient, in some instants (e.g. Figure 6.32) near the boundary is small. The reason for this was due to the distortion of the membrane under load, which resulted in difficulties at locating the pitot-static tube at the membrane. See Figure 6.58 to 6.60 for profile of membrane when under load.

7.2 Calculated Velocities

The velocities shown in Table 6.9 and 6.10 were calculated based on the assumption of a 1/7th power-law velocity distribution (see Equation 7.1 where n = 7) in the boundary layers of the Inner Flume walls and Test Section. This assumption, combined with velocities collected (using a current meter) at a point (300 mm) upstream of the Transition Section, provided a means for determining the theoretical boundary layer development along the surfaces in question. The theoretical boundary layer and displacement thickness was then calculated (Equations 7.2 and 7.3) using the boundary layer theory presented in Schlicting (1968).

$$u / U_{\infty} = (y / \delta)^{1/n} \quad \ldots 7.1$$

$$\delta(x) = 0.37\ x\ / Re^{-0.2} \quad \ldots 7.2$$

$$\delta(x)_1 = \delta(x) / (n + 1) \quad \ldots 7.3$$

Knowing the displacement thickness, the effective cross-sectional area at each station was calculated. This area was a function of the location of the Test Section in the Inner Flume, and the water depth. The location of the Test Section further depended on the load in the Test Section and the position of the outriggers. The water depth was dependent on the flow rate.

Table 6.10 summarises the average free stream velocities

for the material types. Fluctuations of less than 1% were calculated during Phases 1.0 and 2.0. However, when specifically comparing the high flow rate cases of water and rocks during Phase 1.0 tests, a decrease of approximately 2.4% in the average free stream velocities was calculated. The reason for this difference, and other differences listed in Tables 6.9 and 6.10, is specifically due to one or more of the following:

a) Spillage occurring during the manual transportation of up to 50 kg of the material resulted in less material been placed in the Test Section and consequently a lower draft,

b) Inconsistent distribution of material in the Test Section resulted in a difference in elevation of the upstream and down streams. Note differences of less than 2 mm over 3000 mm were ensured,

c) Inconsistent positioning of the outriggers, although monitored, further led to differences in the location of the Test Section,

d) Fluctuations in the flow rate of the order of +/- 0.5 l/s were practically impossible to avoid.

7.3 Boundary Layer Thickness:

The local mean free stream velocities calculated were used as the basis for determining the boundary layer thickness

at the respective stations. Figures 6.36 to 6.39 show the extrapolation of the velocity data to the local mean free stream velocity. In some instances, especially at station 1, the extreme data points collected appeared to lie within the main stream flow region.

The boundary layer thicknesses (Table 6.11) determined were plotted (Figure 6.40 to 6.48) and represent the boundary layer development under nonuniform flow and confined space conditions. For the sake of comparison, the boundary layer development along a flat plate under uniform flow and unconfined space conditions was plotted and is represented by the boundary layer theory presented in Schlicting (1968). Upon comparison of Schlicting curve and the experimental data, the slope of experimental data was calculated to be approximately double the slope of the Schlicting curve. A slope of 0.37 for the Schlicting curve is cited in Schlicting (1968). Extrapolation of the boundary layer growth line pertaining to the experimental data, indicates that the line does not pass through the origin. This implies that when $xRe^{-0.2}$ equals zero, the boundary layer thickness is not zero which is unlike the Schlicting curve. In the case of a flat plate, Prandtl suggested (according to Massey (1984)) that a zero intercept assumption agrees well with experimental data provided the onset of turbulence is assumed to occur at the leading edge of the flat plate. However, this assumption would

lead to a poor correlation between the data points and would lead to a false indication of boundary layer growth and was thus disregarded.

The boundary layer growth rates for all the materials at 63 l/s ($1.5 \times 10^6 < Re_x < 1.53 \times 10^6$) are very similar (Table 6.11), implying that the growth rate was independent of the material type at the selected membrane tension of 1.0 kN. At lower flow rates ($6.96 \times 10^5 < Re_x < 1.05 \times 10^6$) the boundary layer growth depended on the material type. This suggests that the damping characteristic of each material type affected the boundary layer growth. The Reynolds Number is based on x with x = 0 at the nose of the upstream Transition Section.

7.4 Power-Law Exponents:

The assumption of a power-law velocity distribution in a pipe was confirmed experimentally by Nikuradse (Schlicting 1968) for Reynolds Number (based on distance, x) between 4×10^3 and 3×10^6. The power-law velocity distribution over a flat plate was assumed by Prandtl, according to Schlicting (1968), to be identical to the velocity distribution in a pipe. Schlicting (1968) cited that Hansen and Burgers confirmed Prandtl's assumption for $Re_x < 10^6$.

The exponent, n, used in the power-law equation (Equation 7.1) was determined by plotting the dimensionless variables

log (u / U_∞) and log (y / δ) on a linear scale and linear regression to determine the slope (Figures 6.49 to 6.57). This slope corresponded to the exponent, n. The exponents are summarised in Table 6.12. The local values ranged from approximately 5 to 8.5 with the exception of a few cases in which the values were as high as 11.7 and as low as 3. The low extreme value can be attributed to the fact that a loss in flow rate occurred during this test. This resulted in perhaps an under or over calculation of the local free stream velocity, and thus an incorrect extrapolation.

In the 25 l/s flow rate case ($1.93 \times 10^5 < Re < 7.56 \times 10^5$), average exponent values of 6.6, 5.6, 5.3 were calculated for the water, rocks and sand set-ups respectively. In the 63 l/s flow rate case ($4.25 \times 10^6 < Re < 1.53 \times 10^6$), the values were very similar i.e., 6.7, 5.4, 7.6 for the water, sand and rocks set-ups respectively. Schlicting (1968) suggested that the exponent increases with increasing Reynolds Number. This was not observed due to the small range of Reynods Number ($1.93 \times 10^5 < Re < 1.53 \times 10^6$) used. When comparing the overall average exponents with material type, the exponents associated with rocks were consistently lower than sand. This was to be expected due to the higher damping characteristics of the rocks set-up. The nature of the rocks set-up resulted in pockets of air distributed throughout the mass in the Test Section. This air / water interface at the

pockets is believed to lead to an overall damping of the fluid fluctuations near the membrane boundary.

7.5 Drag Force

Tables 6.13 and 6.14 outline the recorded and calculated drag forces on the flexible membrane. The recorded and calculated drag forces are in good agreement as depicted by the standard deviation of the data. The magnitude of the forces increased with load carrying capacity of the Test Section. This was expected as the wetted area was a function of the live load. The total momentum flux in the x direction increased with flow rate; however, in the 25 l/s flow rate case the total drag force acting on the membrane was primarily due to the pressure gradient.

The methods utilised in determining the recorded and calculated drag forces are described below.

7.5.1 Recorded Drag Force

The force recorded by the load cell was in fact the profile drag acting on the Test Section. The friction drag, referred to as drag force from here on, was determined by deducting the Bulkhead pressure force from the load cell measurement. The pressure drag was calculated based on the recorded pressure drop between the upstream and downstream Bulkheads, and the submerged cross-sectional area of the

Bulkheads.

The recorded forces were analysed statistically using formulae for hypothesis testing (t - distribution) of two averages from independent populations. A significance level of 5% was used. The intent was to determine whether or not the averages of the forces recorded, under same flow rate with different material loads, were statistically different. The results are summarised in Table 7.1 and indicate that, with the exception of a few cases, the forces were statistically different and thus the magnitude of the forces were due to the material type, load or flow rate. An average of the Bulkhead and Inner Flume wall forces were used in the hypothesis testing. The standard deviations used were the square-root of the sum of the squares of the Bulkhead and Inner Flume wall standard deviations (see Table 6.5).

Further statistical analysis was performed separately on the Bulkhead force data and on the Inner Flume wall force data (see Appendix D: Statistical Data). This analysis indicated that under the 63 l/s and full load cases, the forces recorded were statistically the same, i.e, the recorded forces were independent of the material type and load.

7.5.2 Calculated Drag Force

The momentum equation was used to calculate the drag force acting on the membrane. The general momentum equation, with respect to the x direction, states that the summation of the external forces acting on a control must be balanced by

Table 7.1 Statistical Comparison of the Averages of the Recorded Forces

Material Type	Load (kg)	Sand						Rocks					
		25 l/s		38 l/s		63 l/s		25 l/s		38 l/s		63 l/s	
		Result[1]	Criterion[2]	Result[1]	Criterion[2]	Result[1]	Criterion[2]	Result[1]	Criterion[2]	Result[1]	Criterion	Result[1]	Criterion[2]
Water	12.5	-60.55	Reject	-9.98	Reject			-2.28	Reject	-10.62	Reject		
	25	-17.21	Reject	-0.68	Accept			-14.32	Reject	-11.52	Reject		
	50	-22.37	Reject	-12.54	Reject	-2.65	Reject	-40.85	Reject	-18.37	Reject	-3.15	Reject
Sand	12.5	Not Applicable						49.09	Reject	-0.65	Accept		
	25							5.27	Reject	-10.06	Reject		
	50							-13.33	Reject	-6.53	Reject	-0.07	Accept

1 - Result of hypothesis testing (t - distribution) for two means - Independent populations; 2 - Accept or Reject the hypothesis that forces are the same.

Note: $P(T \leq c1) = 2.5\%$ and $P(T \leq c2) = 97.5\%$ and with 299 degrees of freedom we obtain $c1 = -1.96$ and $c2 = 1.96$ from Kreyszig (1983).

Accept hypothesis if $c1 \leq t \leq c2$. Significance level of 5% was used.

the momentum flux in the x direction. The momentum flux consists of three components: momentum of the fluid entering at station 1, momentum of fluid exiting at station 4 and the momentum of the fluid between stations 1 and 4 that may be entering or leaving the control volume. A control volume was selected (Figure 7.1) with stations 1 and 4 providing the outer x limits, and the thickness of the boundary layer at station 4 the outer y limit. The three components will next be explained separately.

7.5.2a Station 1

The momentum of the fluid entering the control volume is given by Equation 7.4.

$$F_1 = -\rho \int_0^a u_1^2 \, dA \qquad \ldots 7.4$$

Where: $dA = r \, dr \, \theta$ ... 7.5

$$u_1 = U1_\infty \left(\frac{r_1 - r}{\delta 1}\right)^{1/n1} \qquad \ldots 7.6$$

At station 1, the integrand "a" depicted in Equation 7.4 consists of two regions. A region in which the velocity changes within the boundary layer and a region in which the

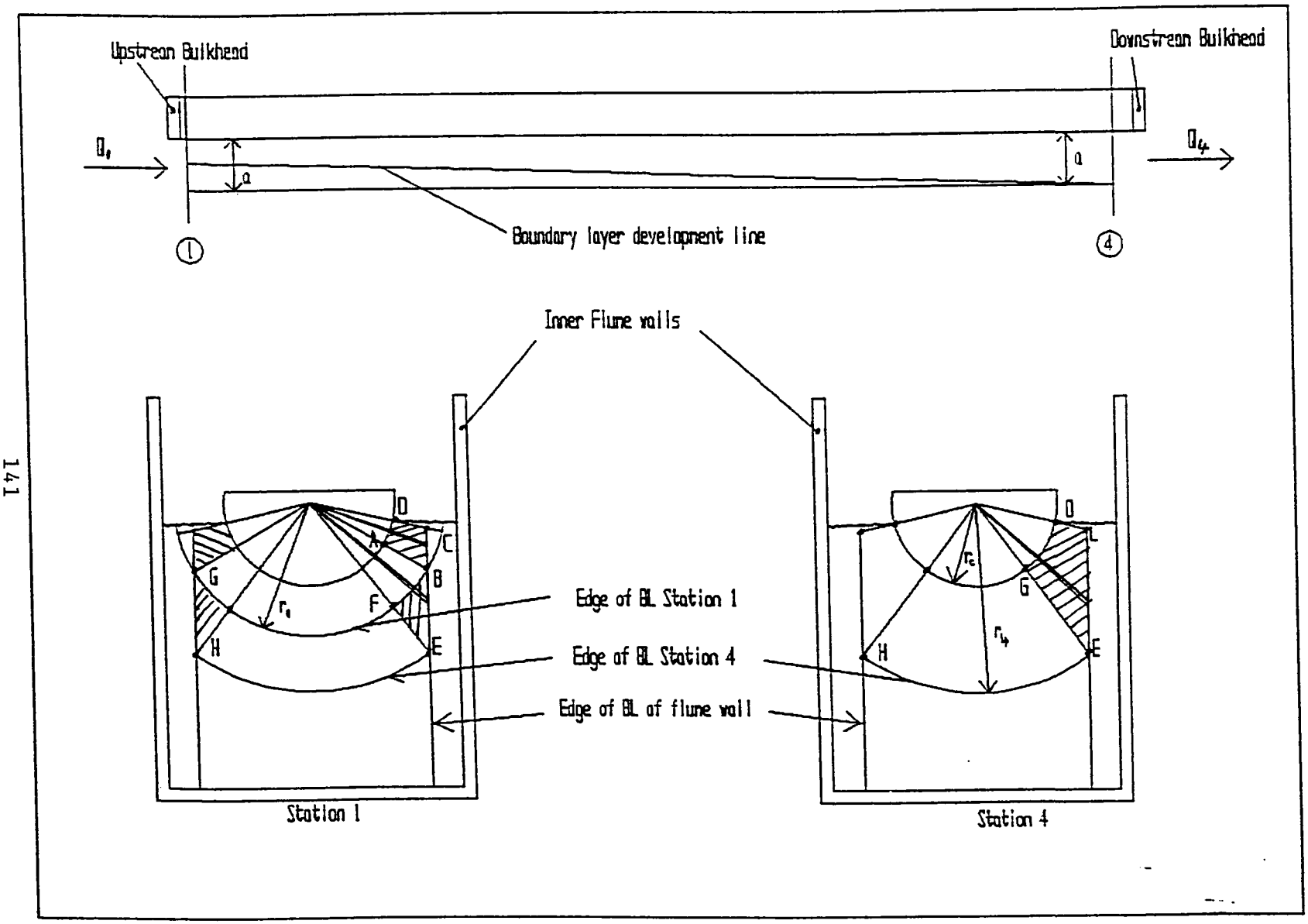

Figure 7.1 Sketches for Drag Force Calculations

velocity is constant. Equation 7.4 is further divided into Equation 7.7.

$$\rho \int_0^a u_1^2 \, dA = \rho(\pi/180)\theta_{BG} \int_{r_0}^{r_1} u_1^2 \, dr + \rho(\pi/180)\theta_{EH} \int_{r_1}^{r_4} U1_\infty^2 \, dr + 2F_{ABCD} + 2F_{BEF} \qquad \ldots 7.7$$

Where : $$F_{ABCD} = \rho(\pi/180) \; \Sigma_i \; (\theta_{1ai} \int_{r_0}^{r_{1ai}} u_1^2 \, dr) \qquad \ldots 7.8$$

$$F_{BEF} = \rho(\pi/180) \; \Sigma_i \; (\theta_{14ai} \int_{r_1}^{r_{14ai}} U1_\infty^2 \, dr) \qquad \ldots 7.9$$

The growth of the boundary layer along the Test Section was limited by the growth of the boundary layer along the Inner Flume walls. Equation 7.7 therefore includes two terms, F_{ABCD} and F_{BEF}, that reflect this influence of the Inner Flume wall boundary layer on the control volume. The integration limits of Equations 7.8 and 7.9 were based on the position at which the boundary layer of the Test Section intersected with the boundary layer of the Inner Flume walls. This is schematically indicated in Figure 7. The momentum of the shaded areas ABCD

and BEF are represented by Equation 7.8 and 7.9. The shaded areas were divided into small segments (angle of less than 1.3 degrees) and the momentum of each segment calculated. The total momentum of each area was the summation of the momentum of each segment.

7.5.2b Station 4

The momentum of the fluid entering the control volume is given by Equation 7.4.

$$F_4 = + \rho \int_0^a u_4^2 \, dA \qquad \ldots 7.10$$

Where: $dA = r \, dr \, \theta$

Where: $$u_4 = U4_\infty \left(\frac{r_4 - r}{\delta 4} \right)^{1/n4} \qquad \ldots . 7.11$$

The integrand "a" depicted in Equation 7.10 consists of one region; a region governed by the boundary layer thickness at station 4. Equation 7.10 is further divided into Equation 7.12.

$$\rho \int_0^a u_4^2 \, dA = \rho(\pi/180)\theta_{EH} \int_{r_0}^{r_4} u_4^2 \, dr + 2F_{DCGE} \qquad \ldots . \; 7.12$$

$$\text{Where: } F_{DCGE} = \rho\ (\pi/180)\ \Sigma_i\ (\theta_{4ai} \int_{r_0}^{r_{4ai}} U4_{\infty}^{2}\ dr) \qquad ....7.13$$

The momentum associated with the shaded area DCGE, depicted in Figure 7.1, is represented by Equation 7.13 and was explained in Section 7.52a.

7.5.2c Station 1 - 4

The momentum entering and exiting station 1 and 4 were calculated using Equations 7.4 to 7.13. However, the momentum of the fluid entering or exiting the boundary layer between these stations has yet to be determined and will be discussed next.

The flow rate entering stations 1 and exiting station 4 was calculated based on Equation 7.14 and 7.15.

$$Q_1 = (\pi/180)\ \theta_{BG} \int_{r_0}^{r_1} u_1\ dr + 2\ (Q_{ABCD} + Q_{BEF}) \qquad ... 7.14$$

$$Q_4 = (\pi/180)\ \theta_{EH} \int_{r_0}^{r_4} u_4\ dr + 2\ Q_{DCEG} \qquad ... 7.15$$

Where:

$$Q_{ABCD} = \rho\ (\pi/180)\ \Sigma_i\ (\theta_{1ai} \int_{r_0}^{r_{1ai}} u_1\ dr) \qquad \ldots\ 7.16$$

$$Q_{BEF} = \rho\ (\pi/180)\ \Sigma_i\ (\theta_{14ai} \int_{r_1}^{r_{14ai}} U1_\infty\ dr) \qquad \ldots\ 7.17$$

$$Q_{DCGE} = \rho\ (\pi/180)\ \Sigma_i\ (\theta_{4ai} \int_{r_0}^{r_{4ai}} U4_\infty\ dr) \qquad \ldots\ 7.18$$

The limits of integration associated with the flow rate equations are described in Section 7.5.2a. The momentum entering or exiting the boundary layer between the respective stations was calculated based on an average of the local free stream velocities at stations 1 and 4, and the net flow rate into or out of the boundary layer. This is represented by Equation 7.19.

$$FQ = \rho\ U14_\infty |(Q_4 - Q_1)| \qquad \ldots\ 7.19$$

Equation 7.20 represents a simplified version of the equations associated with the momentum flux in the x direction and the external forces acting on the control volume.

$$-F_D + \int_0^a \delta P \, dA = -\rho \int_0^a u_1^2 \, dA + \rho \int_0^a u_4^2 \, dA \pm FQ \quad \ldots 7.20$$

7.6 Skin Friction Coefficient

The average skin friction coefficient was calculated using Equation 7.21 and the results are summarised in Tables 7.2 and 7.3.

$$C_f = F_D / \rho u^2 L P \quad \ldots\ldots 7.21$$

Where: L - length of Test Section (3 m)

P - Wetted Perimeter

u - Average free stream velocity (Table 6.10)

The dependence of the average skin friction coefficient on Reynolds and Froude Numbers was investigated. The characteristic length used in Reynolds Number was the hydraulic radius of the Test Section, or the hydraulic depth of the Inner Flume. Figures 7.2 to 7.9 indicate the relationship between C_f and Reynolds Number. The data in these Figures appear to follow a curve that is characteristic of the Moody diagram. The C_f curve for the water set-up appears to fall below the smooth boundary while the sand and rock set-ups near the smooth boundary condition. The curves associated with

Table 7.2 Summary of Reynolds, Froude Numbers and Cf: Phase 1.0

Test No.	Material Type	Q l/s	Load kg	Re Rv/	Re HDu/	Fr u/(gD)	Fr u/(gHD)	Re xu/	Re xu/	Cf
1.1	na	25	0	2.27E+03	8.26E+04	0.301	0.063	1.65E+05	6.00E+05	0.0287
1.2	Water	25	12.5	4.46E+03	1.00E+05	0.219	0.059	1.70E+05	6.17E+05	0.0151
1.3	Water	25	25	6.22E+03	1.13E+05	0.189	0.058	1.75E+05	6.35E+05	0.0093
1.4	Water	25	50	9.07E+03	1.27E+05	0.163	0.059	1.85E+05	6.70E+05	0.0082
1.5	Water	38	12.5	7.09E+03	1.59E+05	0.293	0.080	2.42E+05	8.79E+05	0.0108
1.6	Water	38	25	8.77E+03	1.71E+05	0.267	0.079	2.47E+05	8.96E+05	0.0100
1.7	Water	38	50	1.30E+04	1.95E+05	0.228	0.081	2.60E+05	9.46E+05	0.0067
1.8	Water	63	50	1.86E+04	3.20E+05	0.339	0.112	3.82E+05	1.39E+06	0.0075
1.9	Sand	25	12.5	4.64E+03	1.02E+05	0.215	0.059	1.70E+05	6.19E+05	0.0247
1.10	Sand	25	25	6.52E+03	1.15E+05	0.185	0.058	1.76E+05	6.38E+05	0.0134
1.11	Sand	25	50	9.39E+03	1.28E+05	0.161	0.060	1.86E+05	6.75E+05	0.0125
1.12	Sand	38	12.5	6.86E+03	1.57E+05	0.296	0.080	2.41E+05	8.75E+05	0.0125
1.13	Sand	38	25	9.36E+03	1.75E+05	0.258	0.079	2.48E+05	8.99E+05	0.0089
1.14	Sand	38	50	1.36E+04	1.97E+05	0.223	0.081	2.62E+05	9.52E+05	0.0072
1.15	Sand	63	50	2.00E+04	3.26E+05	0.329	0.112	3.86E+05	1.40E+06	0.0081
1.16	Rocks	25	12.5	5.35E+03	1.07E+05	0.202	0.059	1.72E+05	6.25E+05	0.0138
1.17	Rocks	25	25	6.20E+03	1.12E+05	0.189	0.058	1.75E+05	6.34E+05	0.0130
1.18	Rocks	25	50	8.68E+03	1.26E+05	0.166	0.059	1.83E+05	6.65E+05	0.0163
1.19	Rocks	38	12.5	6.84E+03	1.57E+05	0.297	0.080	2.41E+05	8.75E+05	0.0117
1.20	Rocks	38	25	8.63E+03	1.70E+05	0.268	0.079	2.46E+05	8.92E+05	0.0110
1.21	Rocks	38	50	1.22E+04	1.91E+05	0.232	0.080	2.57E+05	9.33E+05	0.0083
1.22	Rocks	63	50	2.03E+04	3.27E+05	0.327	0.113	3.87E+05	1.40E+06	0.0072

1 - Reynols Number based on hydraulic radius; 2 - Reynolds Number based on hydraulic depth; 3 - Froude Number based on Draft; 4 - Froude Number based on hydraulic depth; Reynolds Number at x = 1.140 (start of Test Section) 6 - Reynolds Number at x = 4.140 (end of Test Section); 7 - Drag coefficient

Table 7.3 Summary of Reynolds, Froude Numbers and Cf: Phase 2.0

Test No.	Material Type	Q l/s	Load kg	Re Rv/	Re HDu/	Fr u/(gD)	Fr u/(gHD)	Re xu/	Re xu/	Cf
2.1	Water	25	50	8.83E+03	1.26E+05	0.165	0.059	1.84E+05	6.67E+05	0.0082
2.2	Water	38	50	1.23E+04	1.92E+05	0.233	0.080	2.58E+05	9.37E+05	0.0067
2.3	Water	63	50	1.88E+04	3.21E+05	0.337	0.112	3.82E+05	1.39E+06	0.0075
2.4	Sand	25	50	9.54E+03	1.29E+05	0.160	0.060	1.87E+05	6.77E+05	0.0125
2.5	Sand	38	50	1.35E+04	1.96E+05	0.225	0.081	2.63E+05	9.53E+05	0.0072
2.6	Sand	63	50	2.02E+04	3.26E+05	0.328	0.113	3.87E+05	1.41E+06	0.0081
2.7	Rocks	25	50	9.15E+03	1.28E+05	0.163	0.060	1.85E+05	6.72E+05	0.0163
2.8	Rocks	38	50	1.34E+04	1.96E+05	0.225	0.081	2.62E+05	9.52E+05	0.0083
2.9	Rocks	63	50	2.02E+04	3.26E+05	0.328	0.113	3.87E+05	1.41E+06	0.0072

1 - Reynols Number based on hydraulic radius; 2 - Reynolds Number based on hydraulic depth; 3 - Froude Number based on draft; 4 - Froude Number based on hydraulic depth; 6 - Reynolds Number at x = 1.140 (start of Test Section)

6 - Reynolds Number at x = 4.140 (end of Test Section); 7 - Drag coefficient

rocks and sand set-ups were surprisingly similar. Sand was expected to exhibit a higher (than rocks) C_f for a given Reynolds Number, since the set-up of sand in the Test Section, is similar to a flow across a rigid body with no damping effects. The C_f values for the water set-ups were lower than for the other materials type set-ups. This is believed to be due to the damping characteristic of the water set-up. However, in the rock set-up, C_f values lower than water were expected, since with the rock set-up the membrane/air interface in the voids should have a greater damping effect than water. This was not observed as a net effect. It is believed that the irregular form of the Test Section, when loaded with rocks, offsets the damping qualities of this type of set-up, See Figures 6.58 to 6.60.

The C_f values were investigated to determine whether the differences observed were of a statistical nature rather than of a physical nature. Section 7.5.1 outlines the statistical analysis performed on the recorded forces. The conclusion drawn from this analysis apply also to the C_f values since, by Equation 7.21, C_f is proportional to F_D with free stream velocity and wetted perimeter similar for each set-up.

The dependency of C_f on Reynolds Number and material type was observed to be more pronounced in the region $Re_{HR} < 1 \times 10^4$ or $Re_{HD} < 2 \times 10^5$. In the region $Re_{HR} > 1 \times 10^4$ or $Re_{HD} < 2 \times 10^5$, C_f was independent of Reynolds Number and material type and

was found to be approximately 0.0175.

The range of Re_x associated with the Test Section length is between 1.65×10^5 and 9.52×10^5. Schlicting (1968) suggests that the transition to turbulence takes place between $3.5 \times 10^5 < Re < 1 \times 10^6$, with Reynolds Number based on distance x.

Although the effects of Reynolds Number and Froude Number cannot be separated, the trends associated with Froude Number and C_f were investigated and are shown in Figures 7.10 to 7.17. Conclusions regarding the effects on Fr_D on C_f were difficult to reach due to the scatter of the results. The effects of Fr_{HD} on C_f were not evident in Figure 7.14 to 7.17, and a Reynolds Number effect is more likely evident in these plots.

The local average skin friction coefficients between station (1 and 2), (2 and 3), (3 and 4) were calculated using principles to those described in Section 7.5. The pressure gradient along the Test Section, used in the calculations in Section 7.5, was divided according to the section lengths. Equation 7.21 was then used to calculate the friction coefficients. Averages of the local free stream velocities, i.e., an average between for example station 2 and 3, were used in the local skin friction calculation.

7.7 Uncertainty Analysis

The uncertainty in the force data collected is shown in Tables 6.13 and 6.14. This was calculated using the standard deviations listed in Table 6.5 and the error band associated with the Loop System.

The mean pressures and standard deviations associated with the boundary layer measurements of the 63 l/s case are shown in Tables 6.6 to 6.8.

7.8 Applications

The design of a WBC system requires an understanding of the mecanisms effecting the drag force of the system. The mechanisms can be described in terms of the velocity profile, free body diagram and a control volume of a section of the belt (Figures 7.18, 7.19 and 7.20 respectively). The equilibrium equations indicate that the weight of the material is balanced by the buoyancy force (Equation 7.22) and the drag force on the belt balanced by the shear force on the channel, pressure force and momentum flux (Equation 7.23).

$$F_W = F_B \qquad \ldots 7.22$$

$$-\frac{dP}{dx} L_b A_{ch} + \rho (C_f)_b V_a^2 P_b L_b - \rho (C_f)_{ch} V_a^2 P_{ch} L_b = \rho Q^2 \beta \frac{(A_1 - A_2)}{A_1 A_2} \qquad \ldots . 7.23$$

To simplify the analysis of Equations 7.23, the following assumptions were made :

a) $V_a = V_{belt} / 2$

b) $(C_f)_b = (C_f)_{ch}$

c) For uniform steady state flow: $A_1 = A_2$

7.8.1 Comparison of Traditional and WBC systems

The traditional conveyor system referred to in Table 3.1 was designed for 1000 t/h. This system was used as basis for comparison against a water bed conveyor (WBC) system designed for the same mass flow rate. The comparison was limited to the following variables: primary resistance (top run), velocity of belt and power required to overcome primary resistance. These variables were selected based on the assumption that the carry side (top run) of the WBC system was supported by water and the return side (bottom run) supported in the same manner as the traditional conveyor system. The results are shown in Table 7.4 and show that the WBC system uses approximately 142% less power than the traditional conveyor system. Alternatively, the WBC system may convey approximately 35 % more material than the traditional conveyor.

The method used to calculate the drag force consists of the following steps:

a) Calculate hydraulic radius of the WBC system. Note,

Equation 7.22 may be simplified to $A_{disp} = A_{load}\ SG_{load}$

b) Calculate Reynolds Number based on hydraulic radius and $V_a = V_{belt} / 2$,

c) Determine $(C_f)_b$: if $Re_{HR} > 10000$ use $(C_f)_b = 0.0175$, if $Re_{HR} < 10000$ use Figure 7.4,

d) Calculate F_D, $F_D = \rho(C_f)_b V_a^2 P_b L_b$.

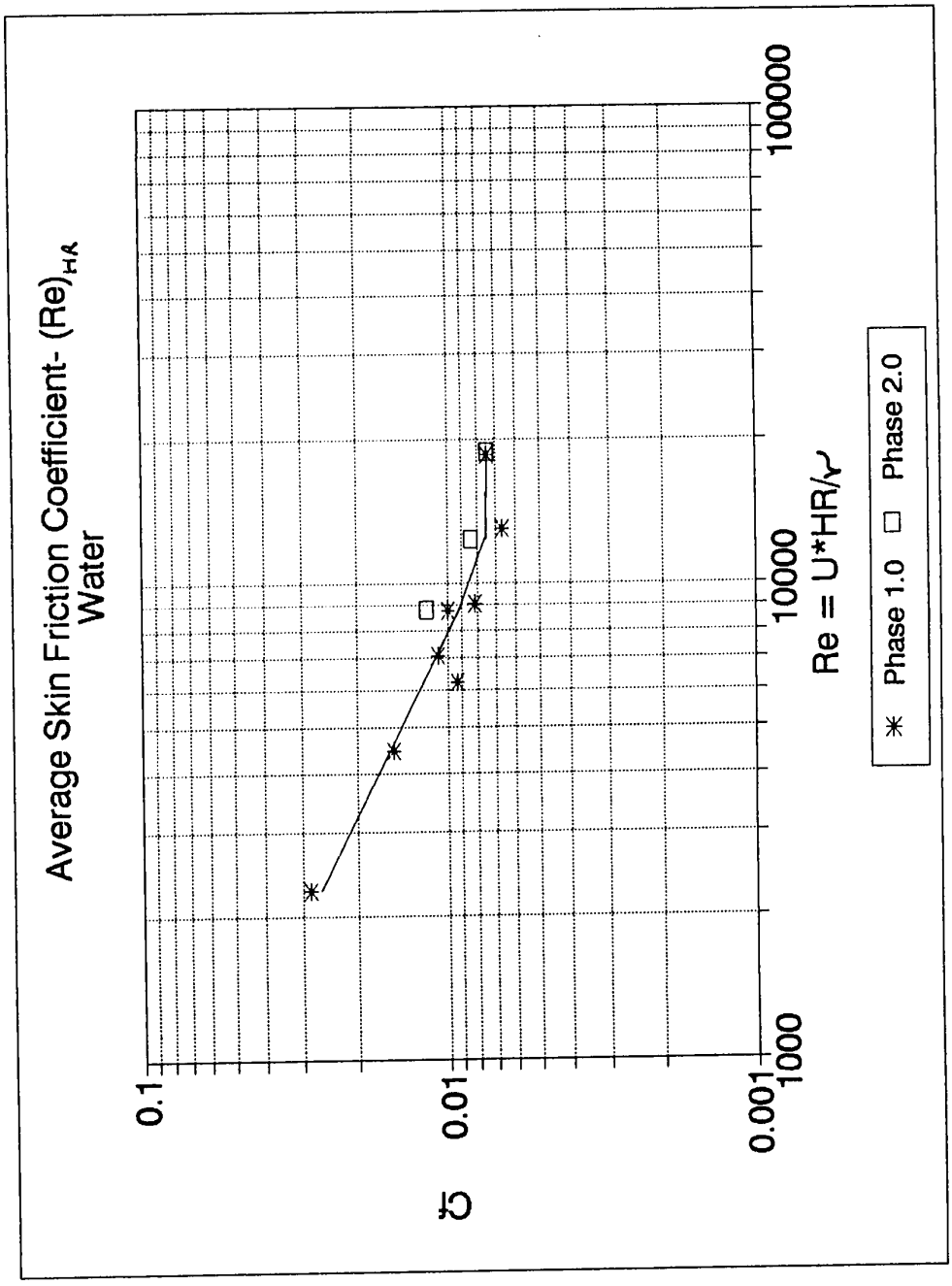

Figure 7.2 Variation of Skin Friction Coefficient with $(Re)_{HR}$: Water

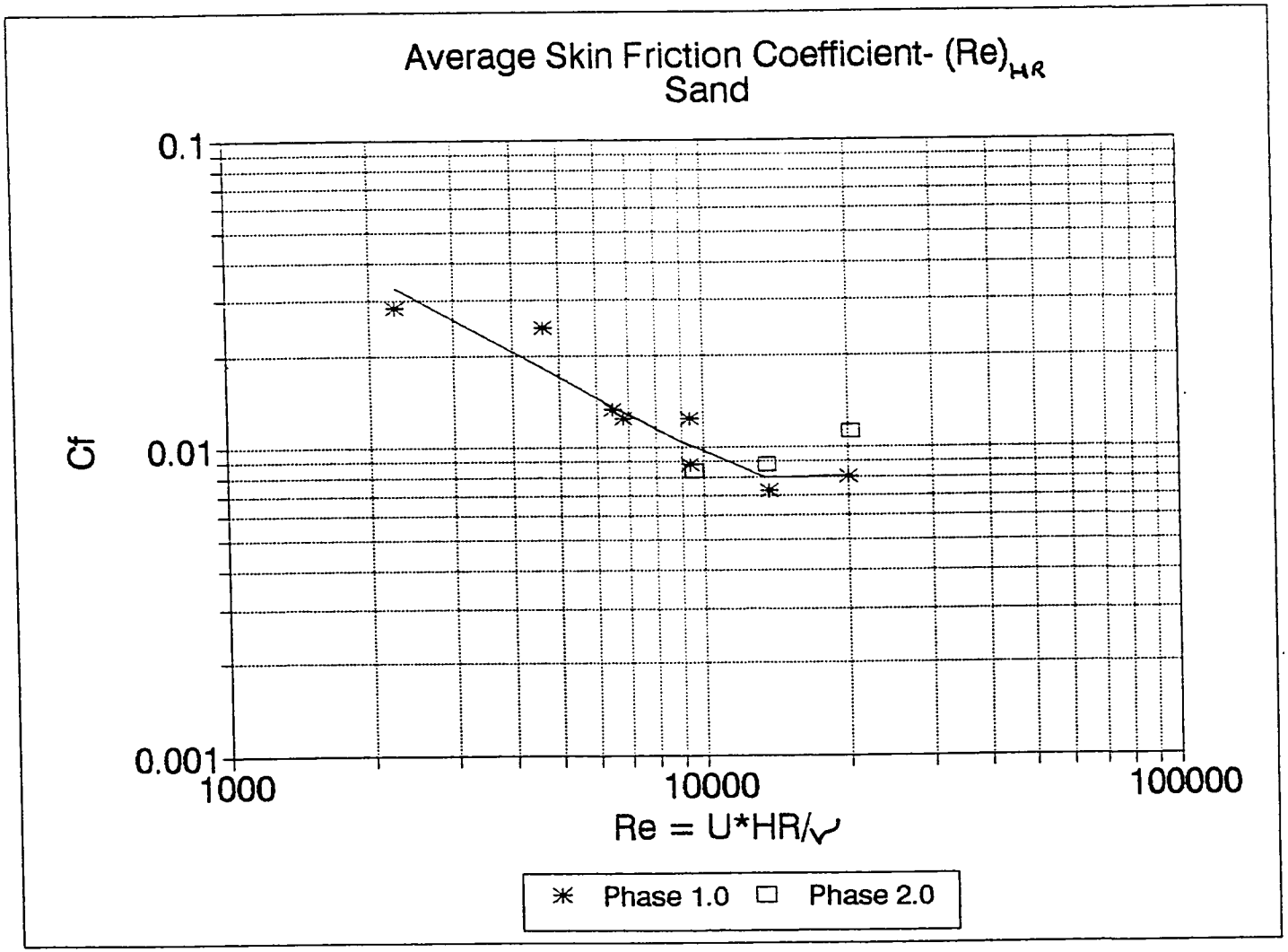

Figure 7.3 Variation of Average Skin Friction Coefficient with $(Re)_{HR}$: Sand

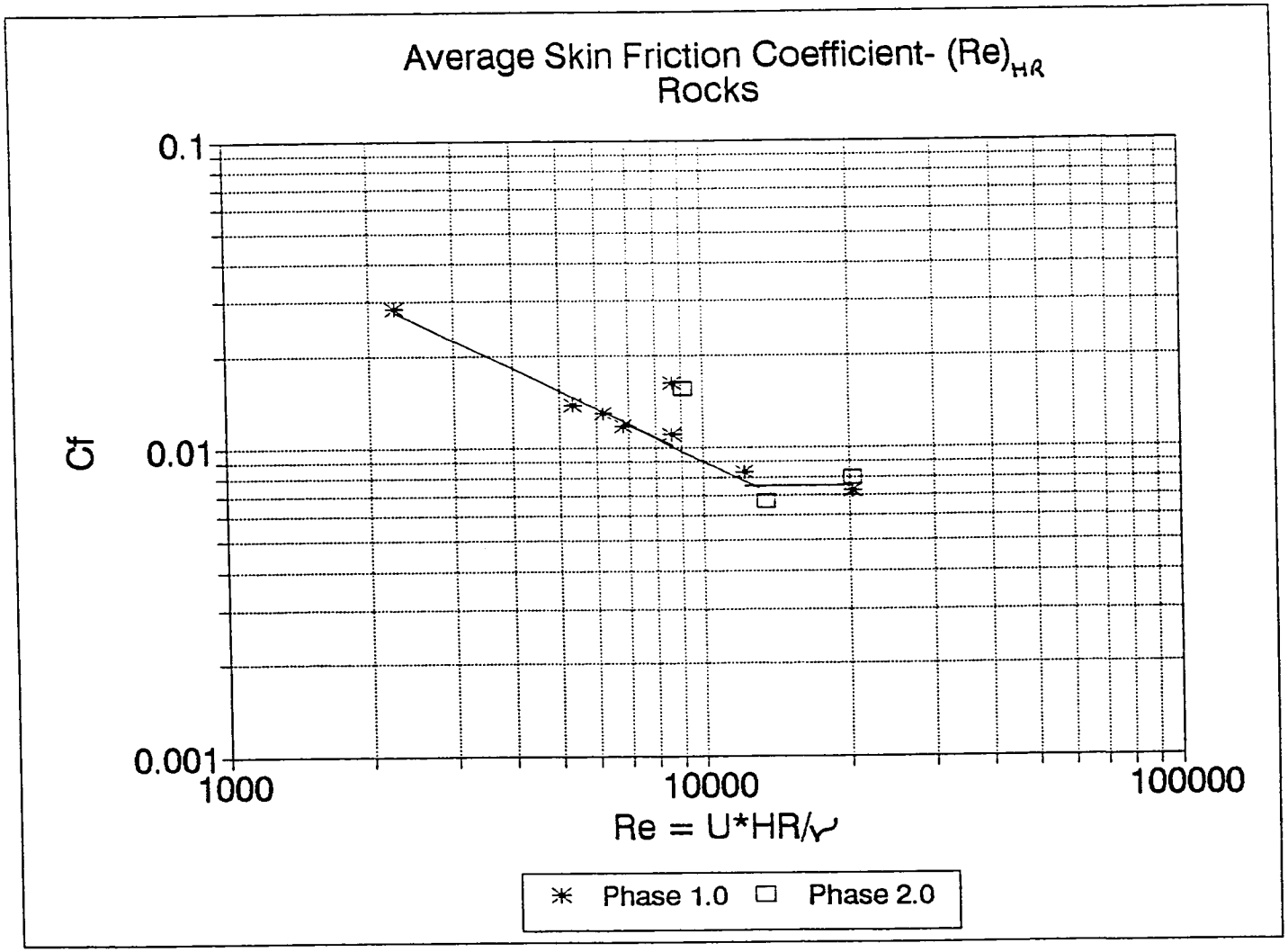

Figure 7.4 Variation of Average Skin Friction Coefficient with $(Re)_{HR}$: Rocks

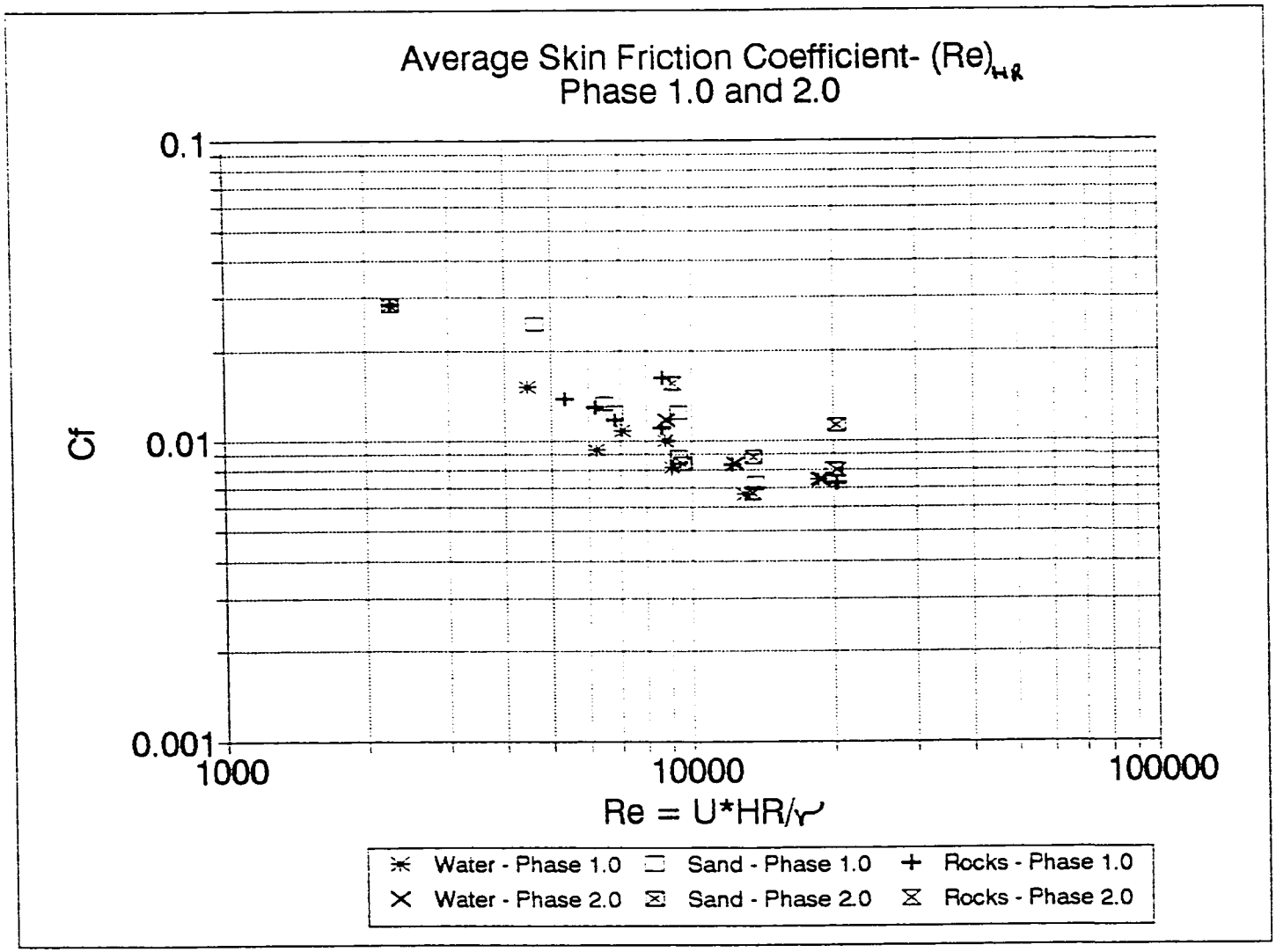

Figure 7.5 Variation of Average Skin Friction Coefficient with $(Re)_{HR}$ Phase 1.0 and 2.0

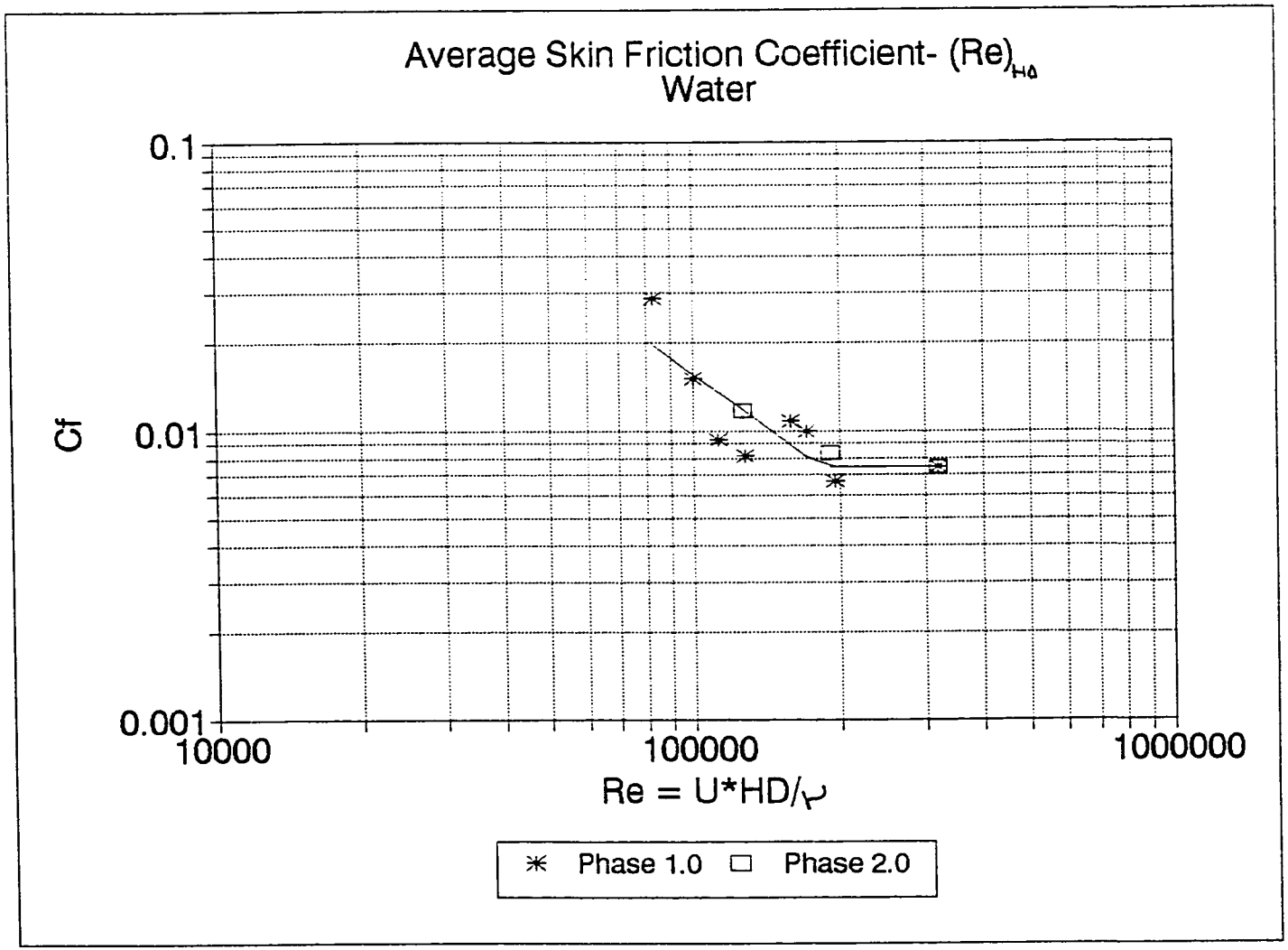

Figure 7.6 Variation of Average Skin Friction Coefficient with $(Re)_{H\Delta}$: Water

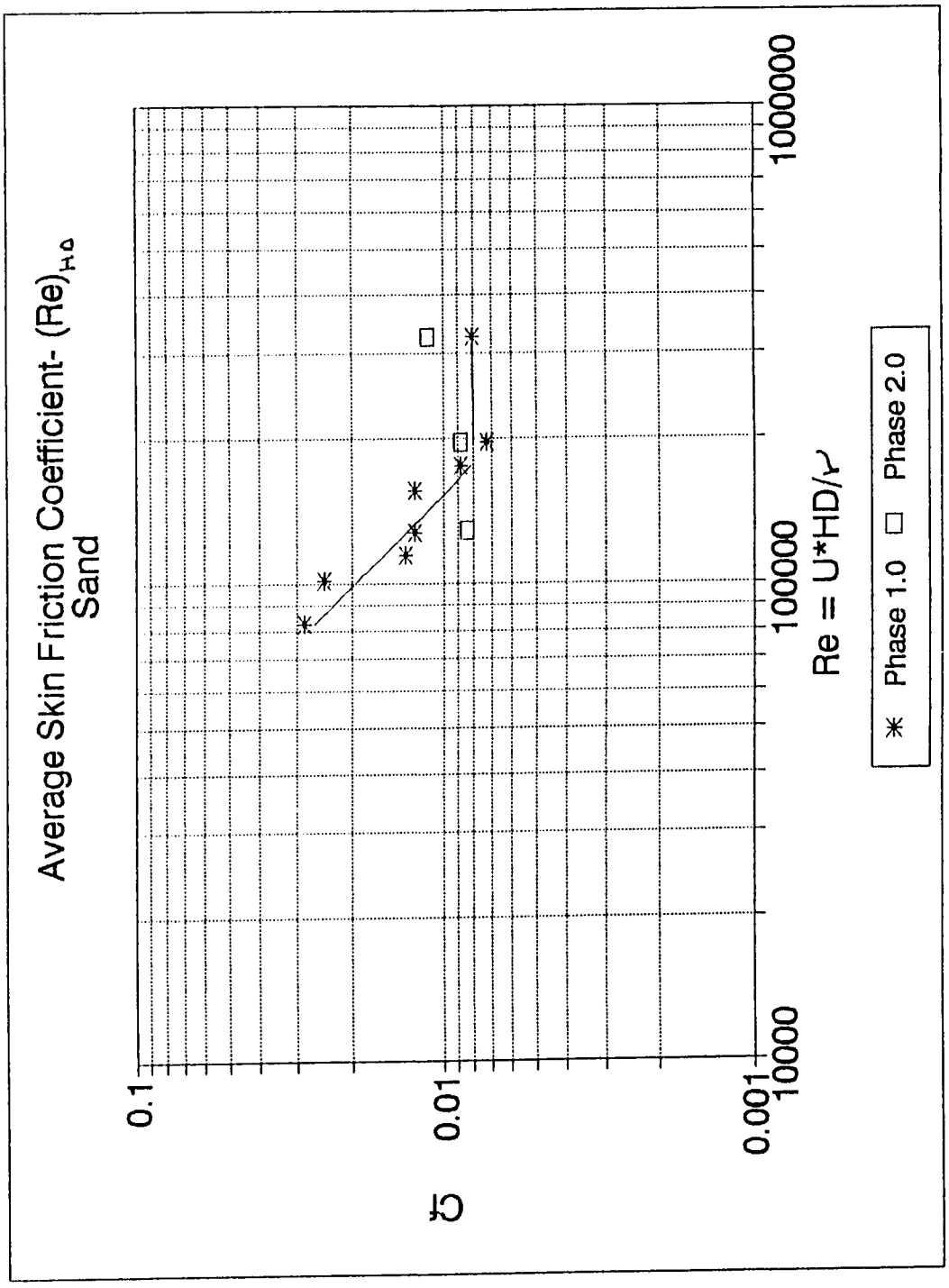

Figure 7.7 Variation of Average Skin Friction Coefficient with $(Re)_{HD}$: Sand

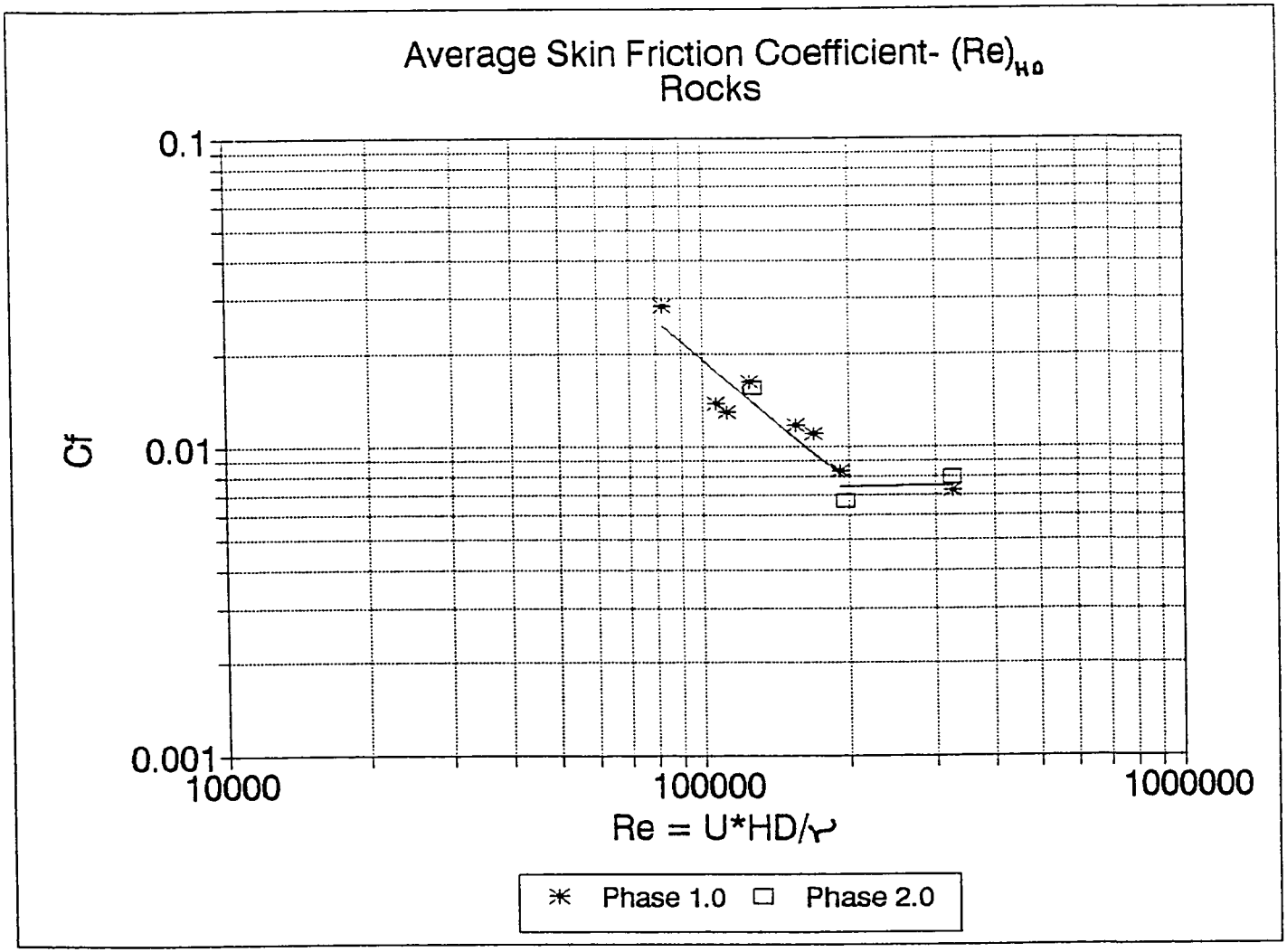

Figure 7.8 Variation of Average Skin Friction Coefficient with $(Re)_{HD}$: Rocks

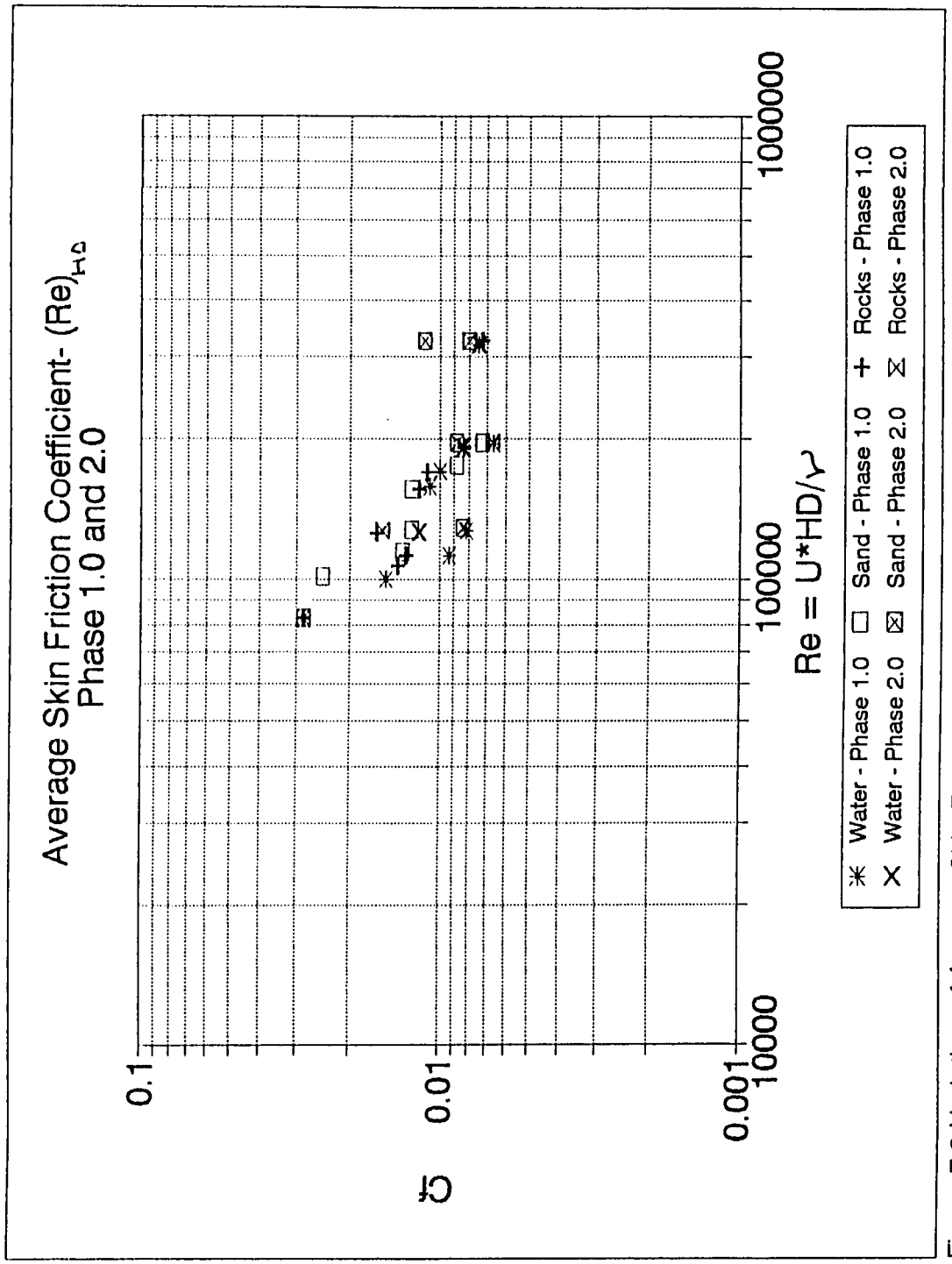

Figure 7.9 Variation of Average Skin Friction Coefficient with (Re)$_{H\delta}$ Phase 1.0 and 2.0

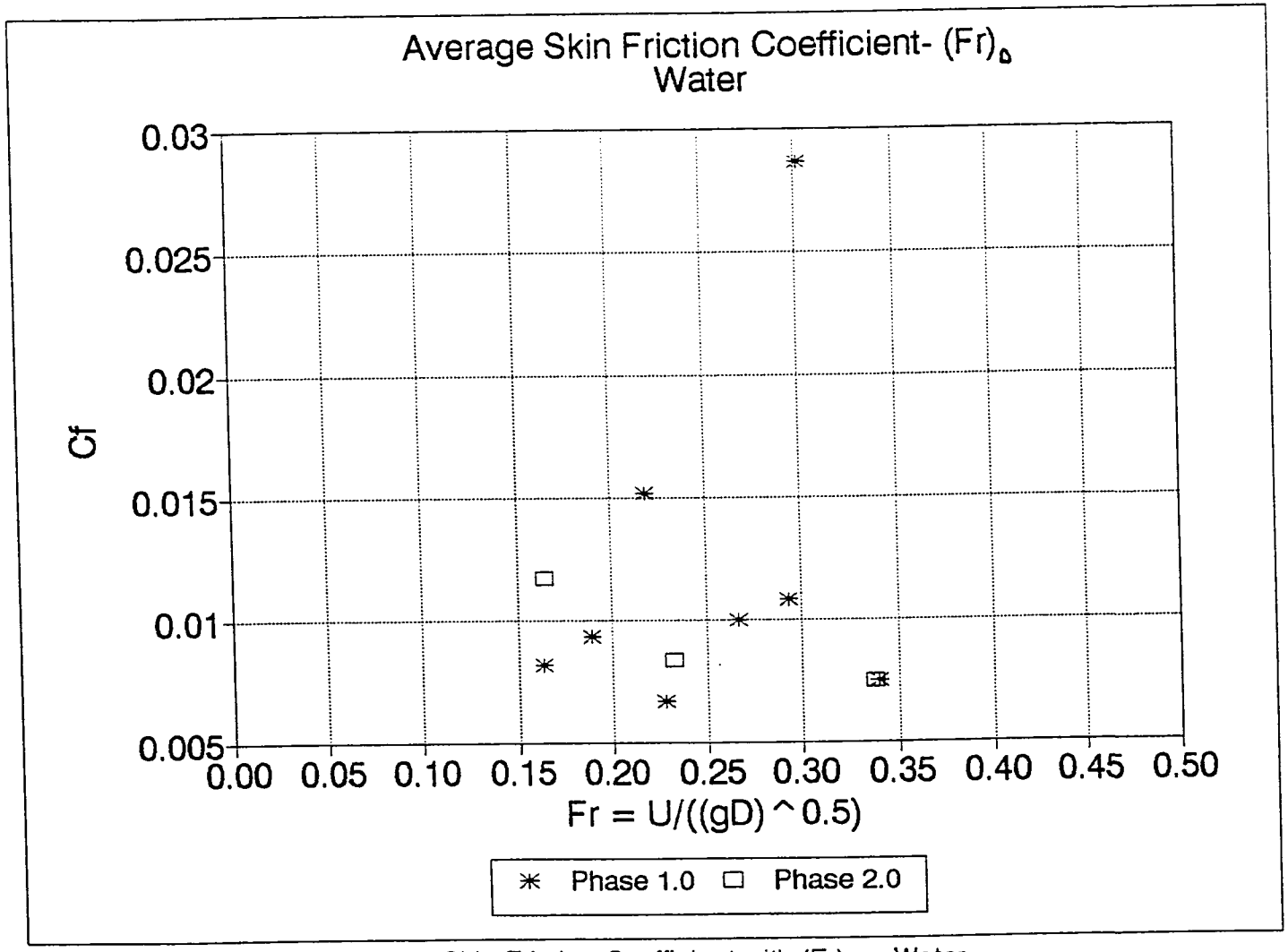

Figure 7.10 Variation of Average Skin Friction Coefficient with $(Fr)_D$: Water

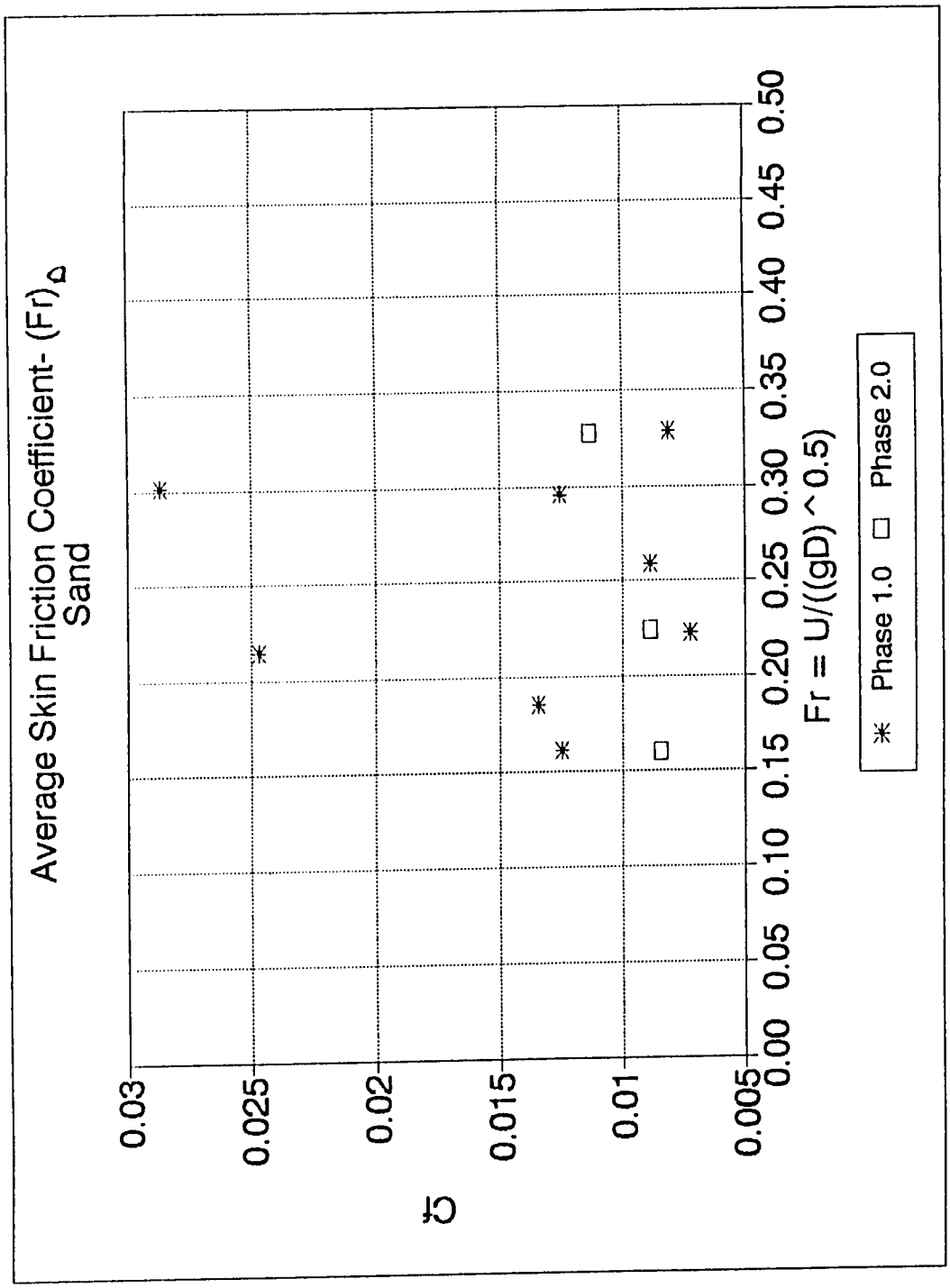

Figure 7.11 Variation of Average Skin Friction Coefficient with $(Fr)_\Delta$: Sand

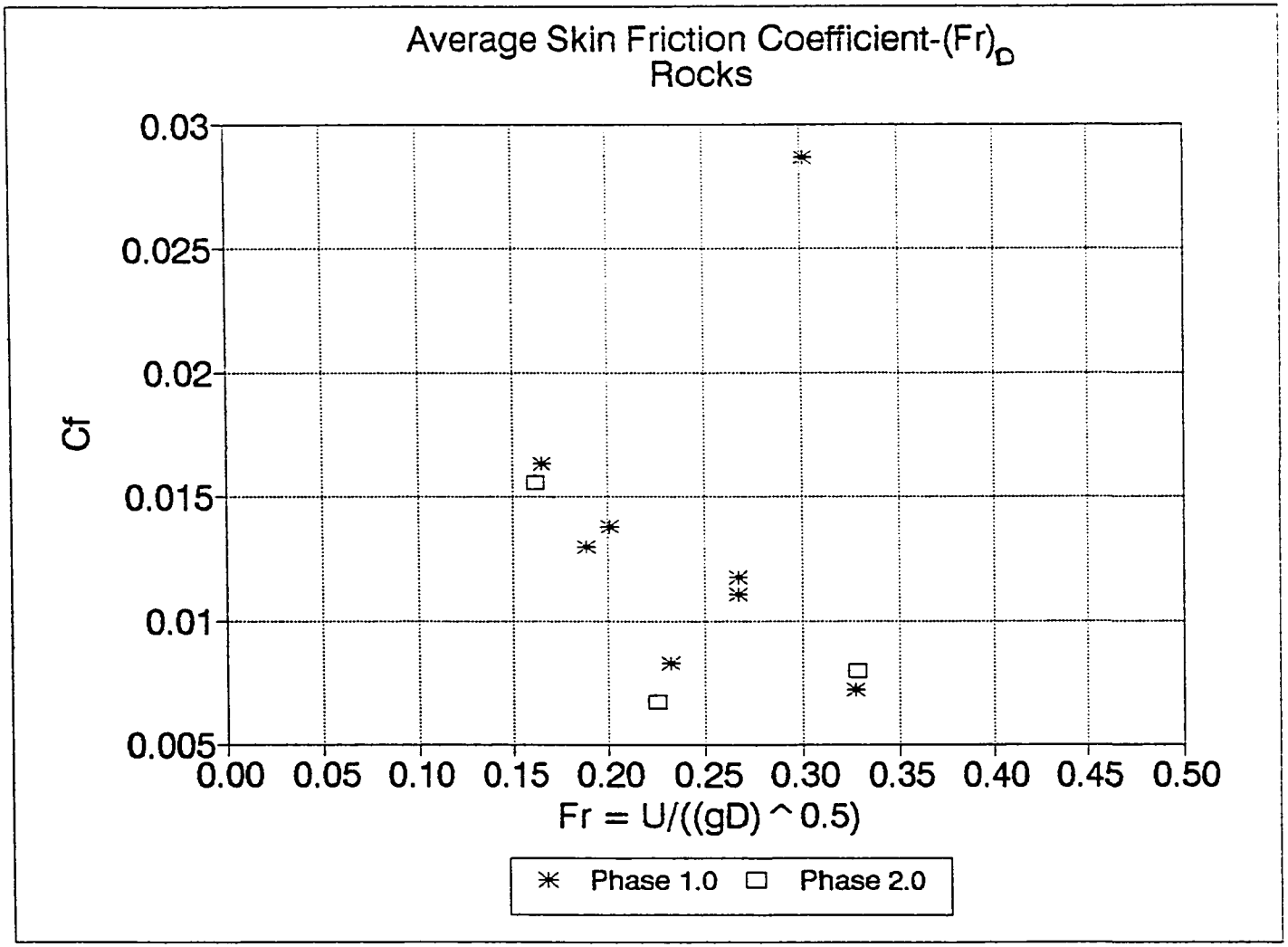

Figure 7.12 Variation of Average Skin Friction Coefficient with $(Fr)_D$: Rocks

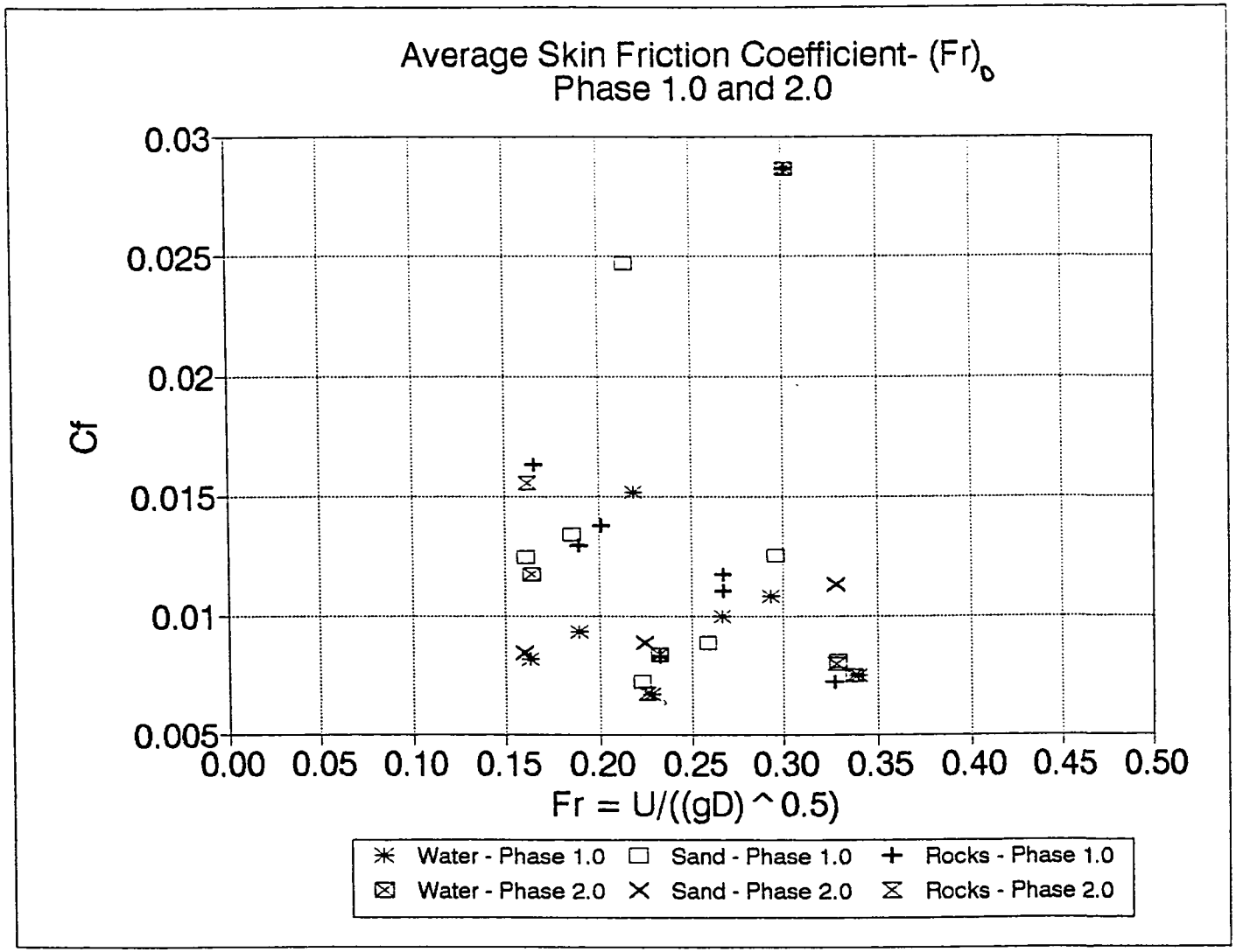

Figure 7.13 Variation of Average Skin Friction Coefficient with $(Fr)_D$: Phase 1.0 and 2.0

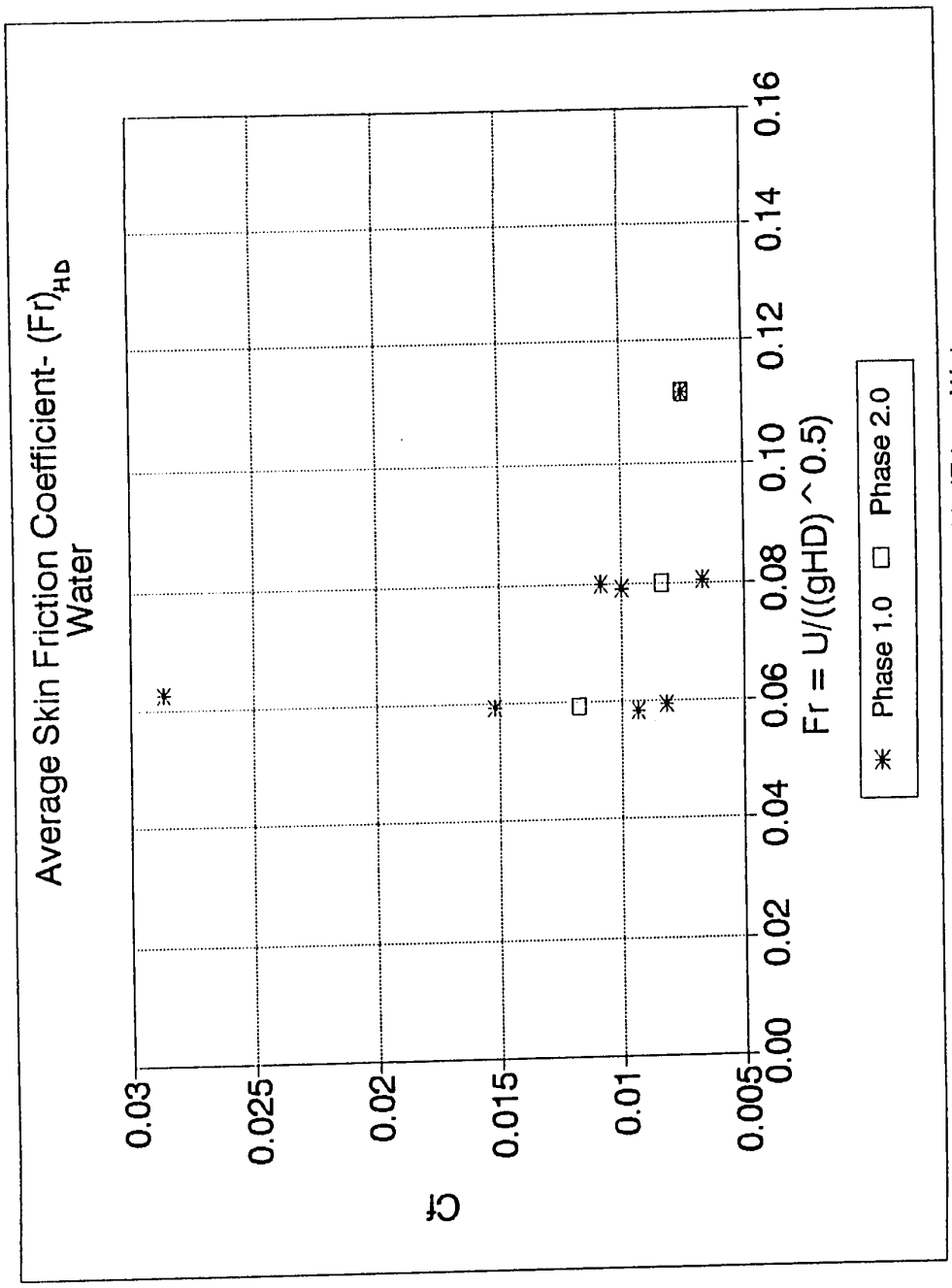

Figure 7.14 Variation of Average Skin Friction Coefficient with $(Fr)_{HD}$: Water

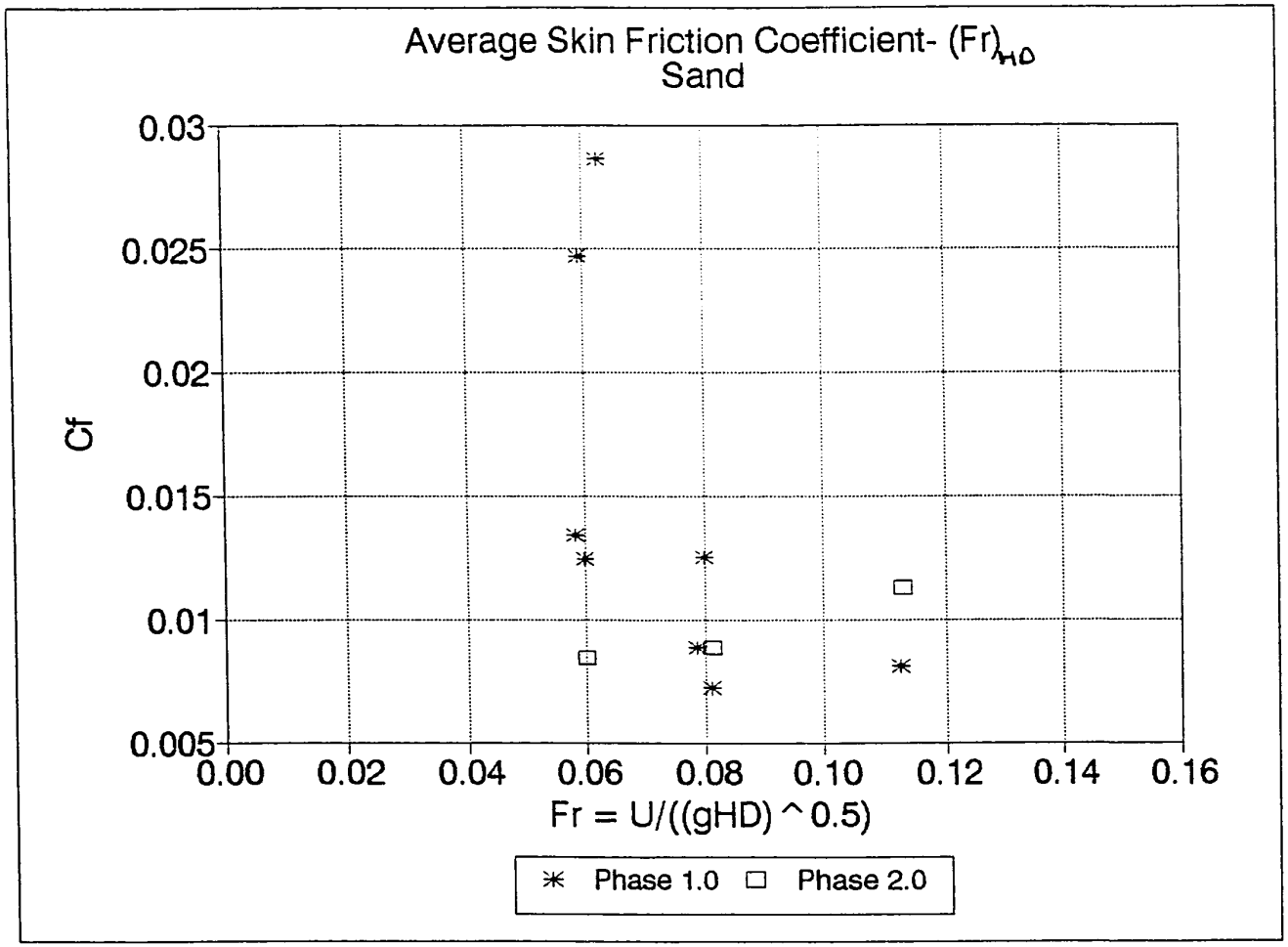

Figure 7.15 Variation of Average Skin Friction Coefficient with $(Fr)_{HD}$: Sand

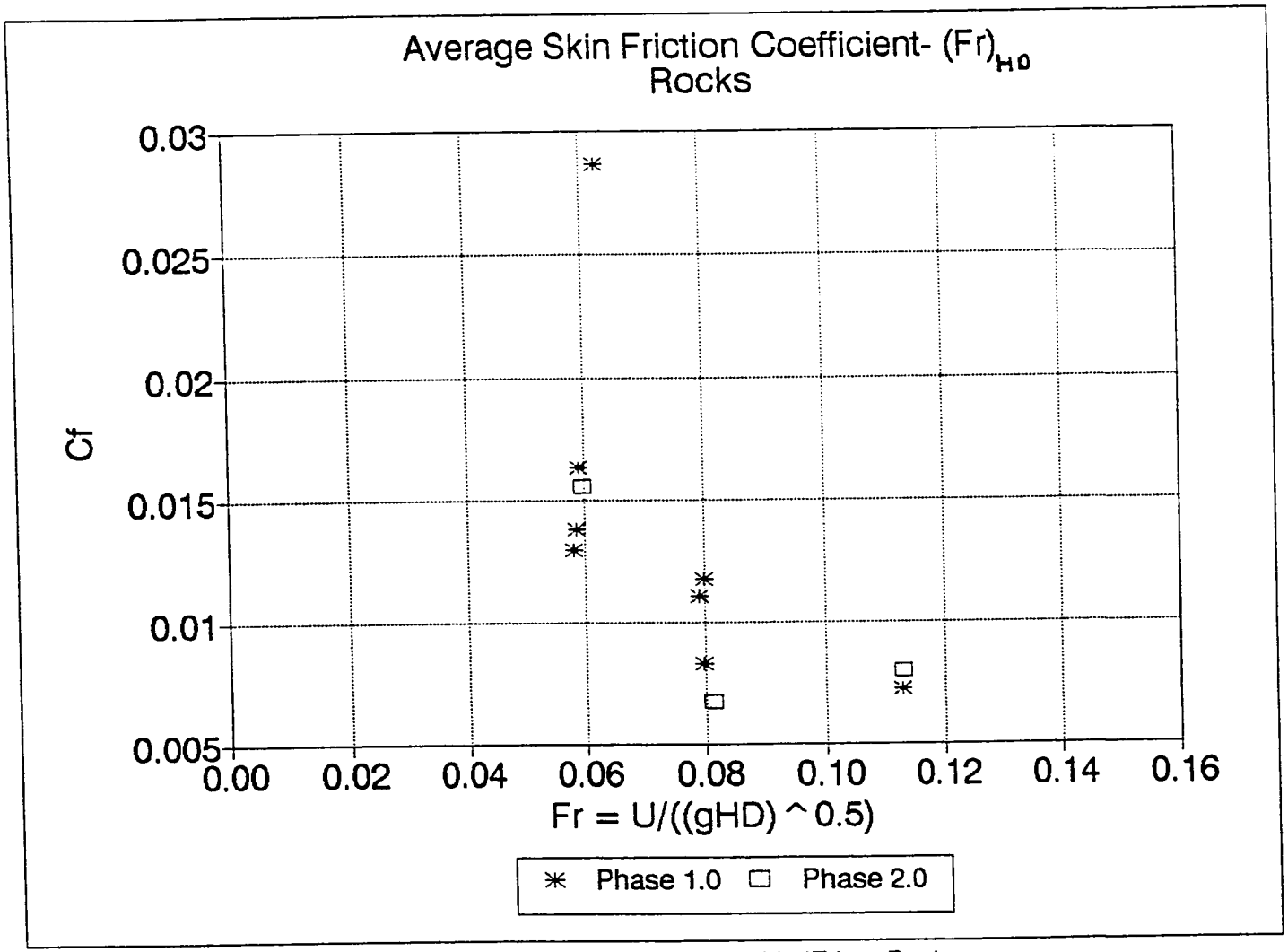

Figure 7.16 Variation of Average Skin Friction Coefficient with $(Fr)_{HO}$: Rocks

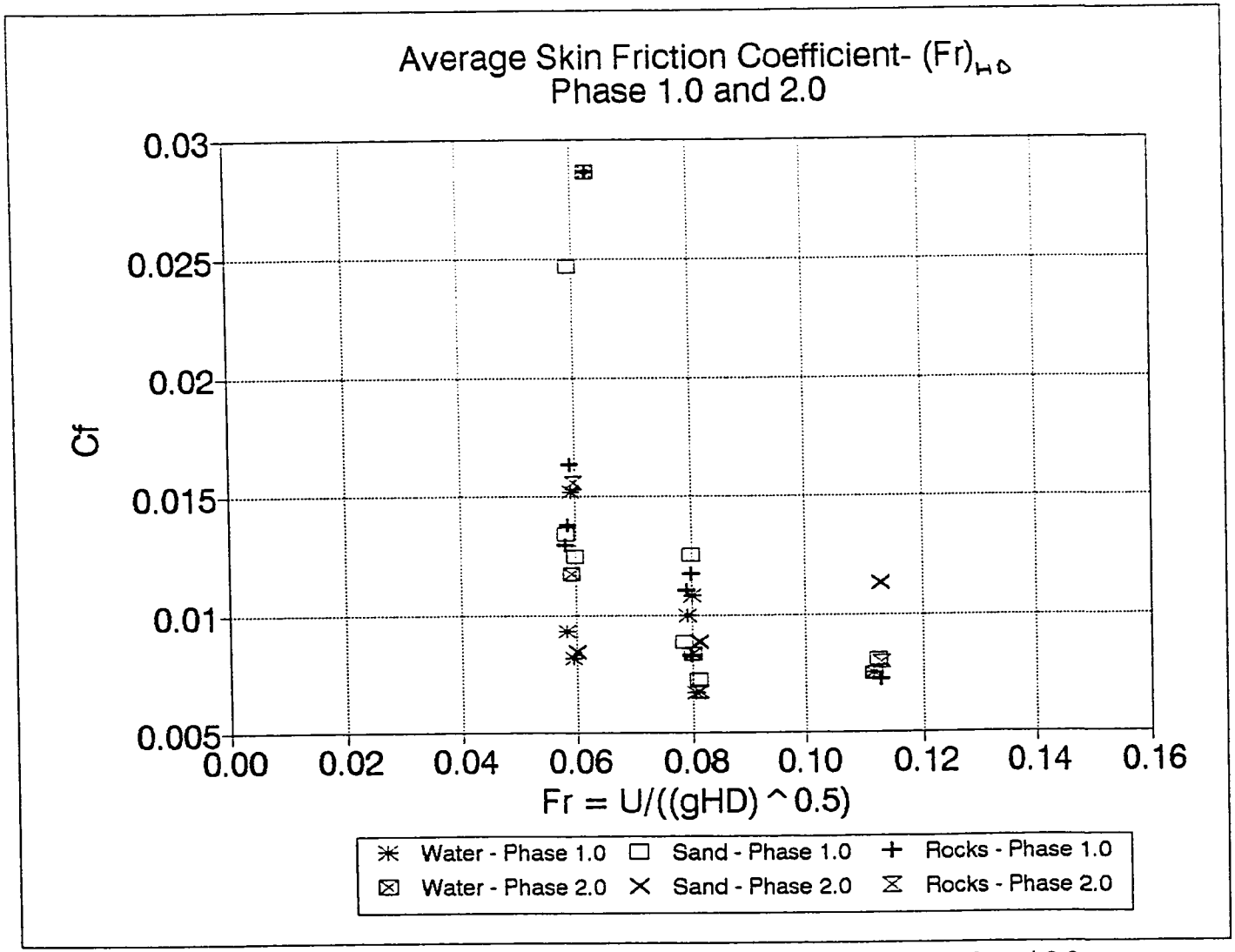

Figure 7.17 Variation of Average Skin Friction Coefficient with $(Fr)_{HD}$: Phase 1.0 and 2.0

Table 7.4 Comparison of Traditional Conveyor and WBC Systems

Traditional Conveyor System	Water Bed Conveyor Case A	Water Bed Conveyor Case B
Mass Flow rate: 1000 t/h	Mass Flow rate: 1000 t/h	Mass Flow rate: 1350 t/h
Belt velocity: 0.6 m/s	Belt velocity: 1.5 m/s	Belt velocity: 2.01 m/s
Primary Resistance: 32.81 kN	Drag force: 5.41 kN	Drag force: 9.867 kN
Required Power : 19.7 kW	Required Power: 8.12 kW	Required Power: 19.9 kW
	Hydraulic Radius : 0.1751	Hydraulic Radius : 0.1751
	Reynolds Number: 128,728	Reynolds Number: 172,495
	Drag Coefficient, Cf: 0.0175	Drag Coefficient, Cf: 0.0175

1 - Top run (See Table 3.1); 2 - Based on hydraulic radius of WBC; 3 - See Figure 7.2.

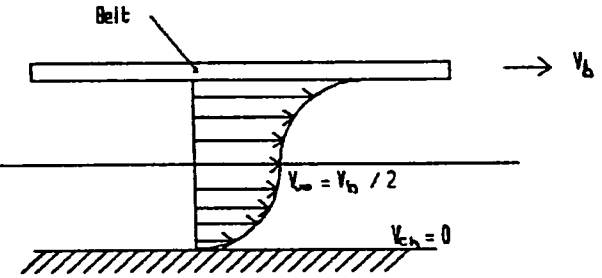

Figure 7.18 Velocity Profile

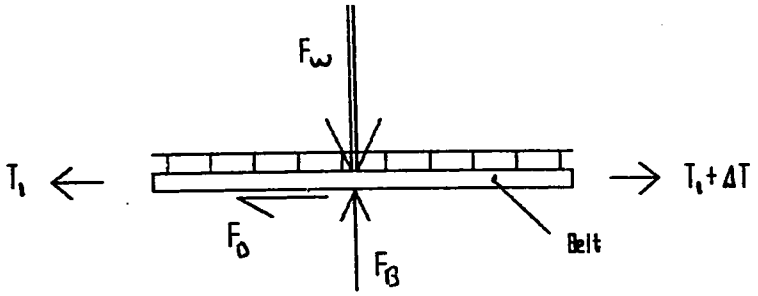

Figure 7.19 Free Body Diagram of Belt

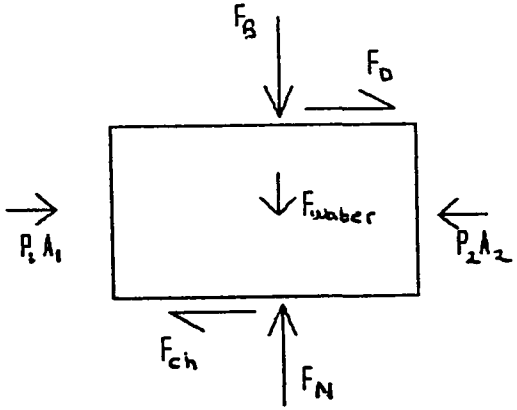

Figure 7.20 Control Volume for Water

8.0 CONCLUSIONS AND RECOMMENDATIONS

8.1 Conclusions

The primary objective of this research was to record the drag force and subsequently calculate the drag coefficient on a tensioned flexible membrane subjected to various loads. This required an investigation into the boundary layer development along the Test Section and the power law exponents associated with the velocity distribution in the boundary layer.

8.1.1 Boundary Layer Development

The boundary layer growth rates of all material type set-ups were consistently higher than the calculated boundary layer growth rate along a rigid body.

The boundary layer growth equation (Equation 7.2), developed from the momentum integral equation (uniform flow) and Blasius formula for hydraulically smooth pipes, should be modified to account for the material type set-up and flow rate.

8.1.2 Power-Law Exponents

The 1/7th power-law exponent is a good approximation to determine the velocity distribution within the boundary layer of a tensioned (2.5 N / mm width of belt) flexible membrane.

8.1.3 Drag Force

The recorded and calculated drag forces were in good agreement. This confirmed that the application of momentum principle is a suitable technique for determining the drag force on a tensioned flexible membrane subjected to steady nonuniform flow.

8.1.4 Drag Coefficient

The drag coefficient is a function of the material type and flow rate. Reynolds Number, based on the hydraulic radius (HR) of the Test Section may be used to determining the drag coefficient of a different belt and material configurations. The drag coefficient was found to be independent of Reynolds Number and material type for Re_{HR} greater than 10000. For Re_{HR} less that 10000, the drag coefficient of the water set-up was found to be consistently lower than for the sand and rock set-ups. The drag coefficients of the sand set-up was found to be marginally higher than for the rock set-up.

The effects of Froude number on the drag coefficient were found to be small under the test conditions selected.

8.2 Recommendations

A brief overview of the parameters used in this research will facilitate an understanding of other possible parameters worth investigating. The smooth membrane was subjected to a 1000 N tension. Water, sand and rocks were the materials used.

Four load types were used, namely no load (0 kg), quarter load (12.5 kg), half load (25 kg) and full load (50 kg). Three flow rates were selected: 25 l/s; 38 l/s and 63 l/s. A weir height of 285 mm was selected (see Figure. 4.1).

The effects of tension on the load carrying capacity of the Test Section is important and should be investigated as this will provide insight into the stability of the load on the belt. Knowledge of this will help in deciding the location of the support idlers (Figure 1.2). Dimensionless group, $\pi_7 = m_m v^2/T$ can be useful for determining this relationship.

The effects of tension on the drag coefficient is worth investigating. The damping characteristics, which are a function of the tension in the membrane, may provide further insight into the effects of tension on the drag coefficient.

The effect of roughness on the development of the boundary layer along the membrane, and consequently the drag coefficient should be investigated; furthermore, establish whether the membrane surface may be considered as hydraulically smooth.

The impact of different material types on the form of the belt should be investigated. Materials of a lower density than water, such as grain (used in agriculture industry) or coal as well as high density materials such as iron ore should be considered. Dimensionless groups, $\pi_9 = \rho_m v^2/G_c$ may be useful in establishing this relationship.

The height of the Test Section above the Inner Flume

floor was dependent on the weir height. Changing the weir height will effect the boundary layer development and consequently the drag force and drag coefficient. To minimise the drag force and to facilitate the selection of the optimum volumetric flow rate and flume dimensions, the height of the weir should be investigated.

NOMENCLATURE

Dimensions are given in terms of mass (M), length (L), time (T).

a	-	Integrand	L
A	-	Flow area	L^2
A_w	-	Wetted area of plate	L^2
C_δ	-	Constant of integration for Equation 2.5	Dimensionless
$C_{\delta 2}$	-	Constant of integration for Equation 2.8	Dimensionless
C_f	-	Skin friction coefficient	Dimensionless
F	-	Force for Equation 2.2 or rate of change of momentum	ML/T^2
F_D	-	Drag force	ML/T^2
FQ	-	rate of change of momentum between station 1 and station 4	ML/T^2
Fr	-	Froude Number	Dimensionless
L	-	Length	L
m	-	Mass for Equation 2.2	M
n	-	Power-law exponent	Dimensionless
n1	-	Power-law exponent at station 1	Dimensionless
n4	-	Power-law exponent at station 4	Dimensionless
P	-	Wetted perimeter	L
Q	-	Flow rate	L^3/T
Re	-	Reynolds Number	Dimensionless
r_0	-	Radius of Bulkhead	L
r	-	Radius of boundary layer relative to Bulkhead, see Figure 7.1	L
U_∞	-	Local free stream velocity	L/T

$U1_\infty$	-	Local free stream velocity at station 1	L/T
$U4_\infty$	-	Local free stream velocity at station 4	L/T
$U14_\infty$	-	Average of free stream velocity at station 4 and station 1	L/T
u	-	Local velocity in boundary layer	L/T
V_∞	-	Average free stream velocity over length of belt, for Equation 7.22	L/T
v	-	Velocity for Equation 2.2	L/T
x	-	Distance along physical model with x=0 at start of upstream Transition Section	L

Greek Symbols

β	-	Momentum correction factor	Dimensionless
δ	-	Boundary layer thickness	L
δ_1	-	Displacement thickness	L
δ_2	-	Momentum thickness	L
$\delta 1$	-	Boundary layer thickness at station 1	L
$\delta 4$	-	Boundary layer thickness at station 4	L
θ	-	Angle between the points of intersection of the boundary layers of the Test Section and the Inner Flume walls. See Figure 7.1	
τ_0	-	Shear stress on membrane or flat plate	M/T^2L
ρ	-	Density	M/L^3
	-	Kinematic viscosity	L^2/T
δP	-	Differential pressure between station 1 and station 4	M/T^2L

Subscripts

1	-	Station 1
1ai	-	Incremental angle or radius of small element in area enclosed by points A, B, C and D.
14ai	-	Incremental angle or radius of small element in area enclosed by points B, E and F.
4	-	Station 4
4ai	-	Incremental angle or radius of small element in area enclosed by points D, C, G and E.
B	-	Buoyancy
b	-	belt
D	-	Draft
w	-	Weight of material on WBC system
BG	-	Points B and G in Figure 7.1
ch	-	Channel
EH	-	Points E and H in Figure 7.1
HD	-	Hydraulic depth of Inner Flume
HR	-	Hydraulic radius of Test Section
BEF	-	Points B, E and F in Figure 7.1
ABCD	-	Points A, B, C and D in Figure 7.1
DCGE	-	Points D, C, G and E in Figure 7.1

APPENDIX A: Bench Top Model Test

Table A.1 Effect of Mass on Width of Membrane: Radius 75 mm

	T1			T2			T3		
Reading No.	Mass (exl cont'nr) (g)	Mass (cummul.) (g)	Width (mm)	Mass (exl cont'nr) (g)	Mass (cummul) (g)	Width (mm)	Mass (exl cont'nr) (g)	Mass (cummul) (g)	Width (mm)
1'st	420	420	163	440	440	163	420	420	159
2'nd	400	820	160	440	880	160	450	870	159
3'rd	420	1240	159	420	1300	159	440	1310	158
4'th	420	1660	153	410	1710	153	420	1730	155
5'th	150	1810	150	240	1950	150	320	2050	149
6'th	NA	NA	NA	220	2170	146	NA	NA	NA
Total (incl model):		2250			2610			2490	
Direct from scales:		2340			2640			2520	

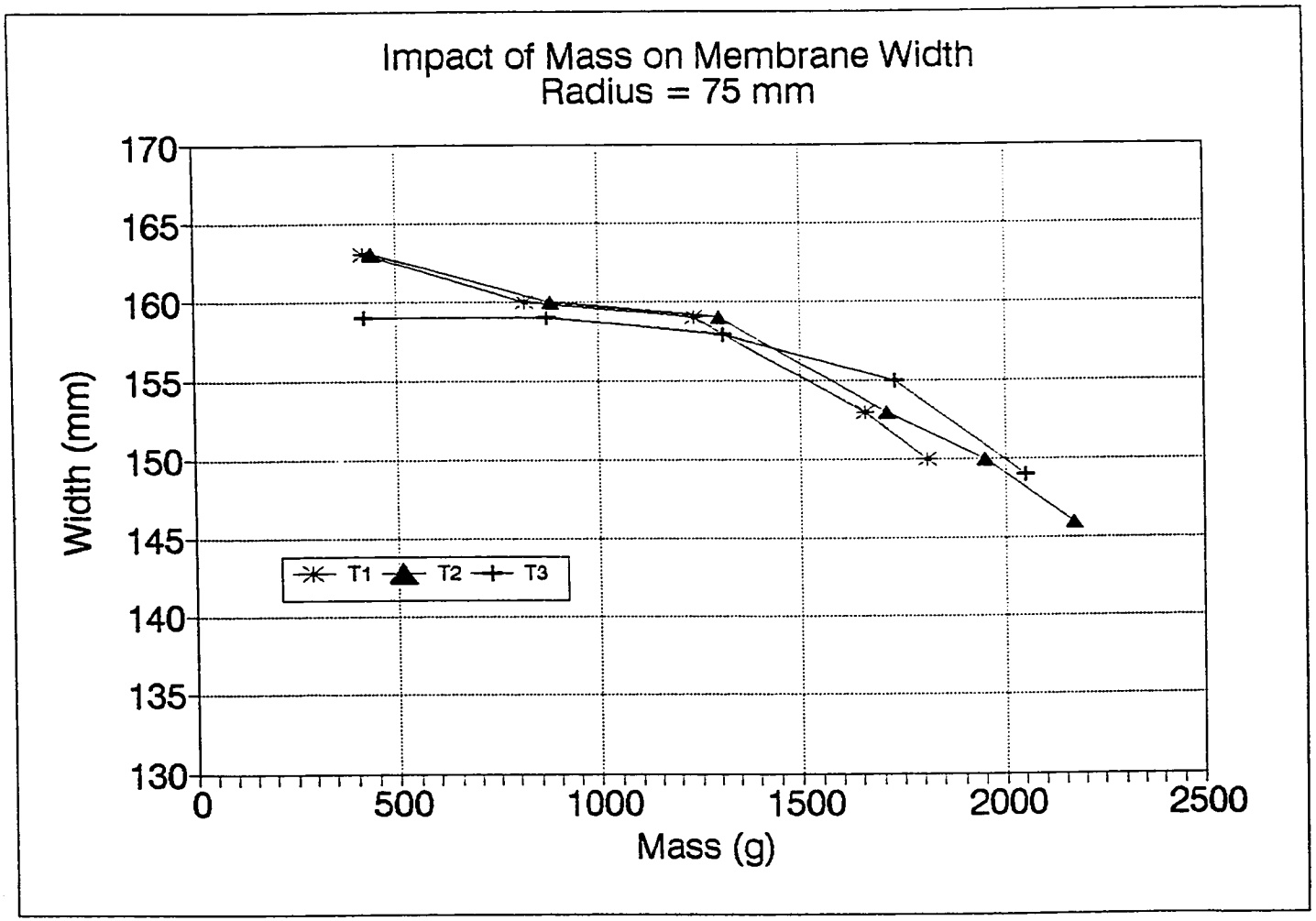

Figure A.1 Impact of Mass on Membrane Width: Radius = 75 mm

Table A.2 Effect of Mass on Width of Membrane: Radius 118 mm

	T1			T2			T3		
Reading No.	Mass (exl cont'nr) (g)	Mass (cummul.) (g)	Width (mm)	Mass (exl cont'nr) (g)	Mass (cummul) (g)	Width (mm)	Mass (exl cont'nr) (g)	Mass (cummul) (g)	Width (mm)
1'st	420	420	212	420	420	196	420	420	192
2'nd	420	840	197	420	840	194	430	850	191
3'rd	420	1260	189	460	1300	191	400	1250	190
4'th	430	1690	178	400	1700	184	420	1670	185
5'th	230	1920	168	NA	NA	NA	NA	NA	NA
6'th	NA	NA	NA	NA	NA	NA	NA	NA	NA
Total (incl model):		2400			2180			2150	
Direct from scales:		2420			2210			NA	

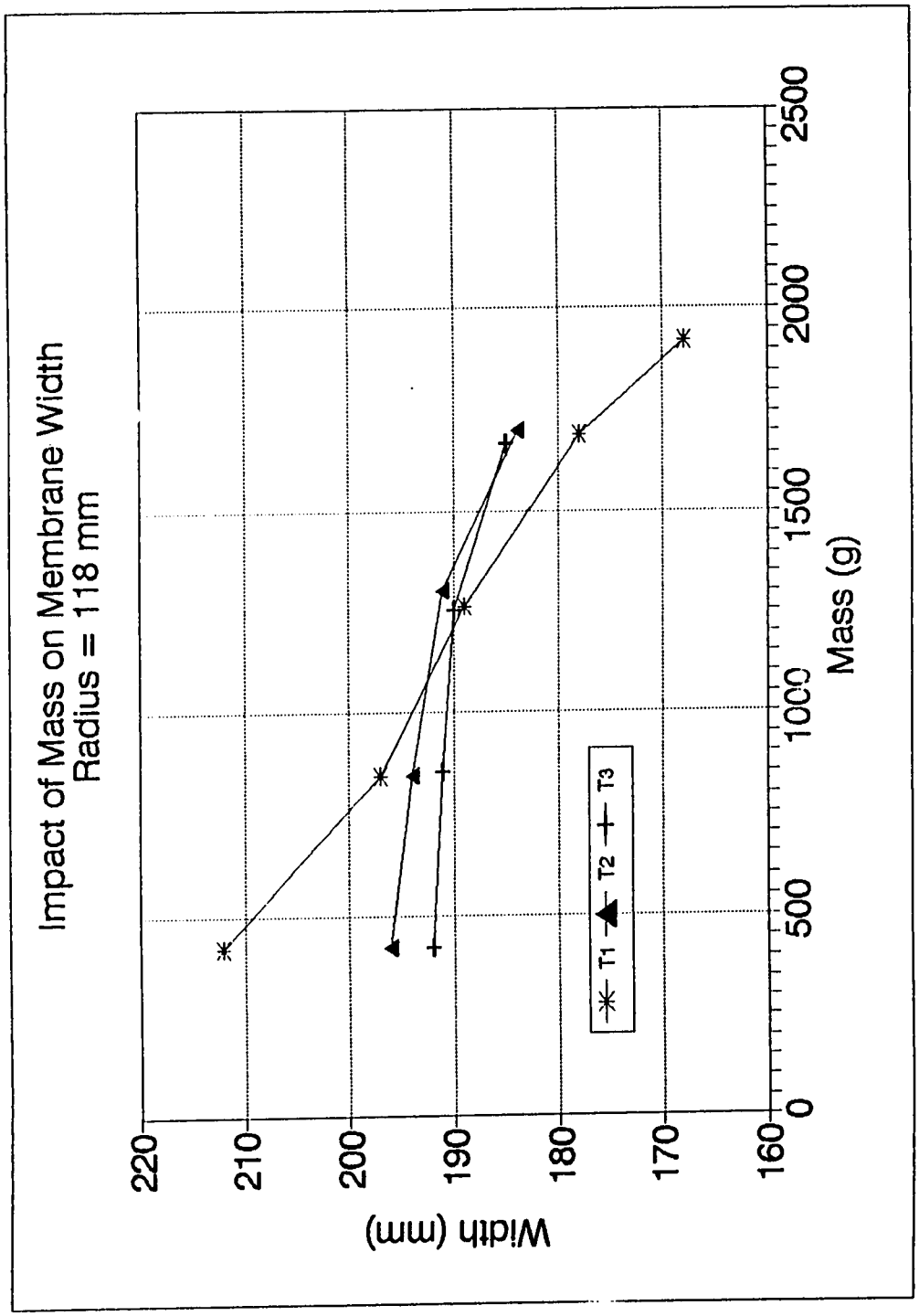

Figure A.2 Impact of Mass on Membrane Width: Radius = 118 mm

APPENDIX B: Materials

C.T. SOIL & MATERIALS ENGINEERING INC.

GEOTECHNICAL ENGINEERING & CONSTRUCTION MATERIALS INSPECTION & TESTING
1960 Provincial Road o R.R. #1 Windsor o Windsor, Ontario o N9A 6J3
Phone (519) 966-8863 Fax (519) 966-8870

REPORT ON SIEVE ANALYSIS TEST RESULTS

Sieve Size		Percent of Sample Passing Sieve	Specification
½ in.	13.2 mm		
3/8 in	9.5 mm		
No. 4	4.75 mm	100	100
No. 8	2.36 mm	99.4	95 - 100
No. 16	1.18 mm	93.7	60 - 100
No. 30	600 µm	78.9	35 - 80
No. 50	300 µm	38.7	15 - 50
No. 100	150 µm	5.0	2 - 15
No. 200	75 µm	2.0	0 - 5

Comments:

Job No.:	95Q04N	Lab No.:	112
Client:	Erie Sand and Gravel		
Project:	Quality Control		
Material:	Masonry Sand		
Reference Standard:	OPSS 1004-2		
Sample Location:			
Sample Obtained By:	Client	Sample Tested By:	D. Schincariol
Date Sampled:	January 30, 1995	Test Date:	January 31, 1995

Report Distribution: Erie Sand and Gravel

Results Reviewed By:
C. Palmer, C.E.T.,
Field & Laboratory Manager

Group 1

STONE #	W (GR)	V (ML)	SPEC.GR
78	934	380	2.46
99	500	200	2.50
109	608	240	2.53
127	573	220	2.60
154	475	190	2.50
173	505	220	2.30
288	625	285	2.19
303	516	210	2.46
343	549	205	2.68
348	513	220	2.33
352	538	220	2.45
368	510	225	2.27
388	570	250	2.28
415	400	170	2.35
443	522	200	2.61
450	650	250	2.60
573	700	310	2.26
581	705	243	2.90
588	465	205	2.27
599	515	215	2.40
625	895	340	2.63
627	810	310	2.61
Total Mass, kg	13.078		
Ave Mass, kg	0.594		
Ave Volume, ml		0.241	

Group 2

STONE #	W (GR)	V (ML)	SPEC.GR
67	614	250	2.46
95	412	180	2.29
219	470	200	2.35
224	369	160	2.31
284	426	185	2.30
304	544	230	2.37
326	445	190	2.34
336	530	205	2.59
339	578	240	2.41
371	523	205	2.55
382	461	200	2.31
421	518	200	2.59
428	511	200	2.56
470	367	150	2.45
509	455	190	2.39
510	385	150	2.57
514	870	385	2.26
534	540	245	2.20
561	380	140	2.71
568	395	140	2.82
595	435	170	2.56
645	470	185	2.54
658	420	160	2.63
661	310	135	2.30
677	885	305	2.90
692	330	140	2.36
697	395	150	2.63
700	395	160	2.47
Total Mass, kg	13.433		
Ave Mass, kg	0.480		
Ave Volume, ml		0.195	

Group 3

STONE #	W (GR)	V (ML)	SPEC.GR
46	504	180	2.80
52	446	185	2.41
100	288	115	2.50
106	858	350	2.45
128	739	290	2.55
145	416	200	2.08
151	637	250	2.55
209	329	115	2.86
234	719	300	2.40
250	414	150	2.76
271	600	245	2.45
273	402	155	2.59
318	466	185	2.52
319	490	205	2.39
345	474	195	2.43
362	342	140	2.44
396	614	250	2.46
503	480	210	2.29
513	380	160	2.38
565	525	205	2.56
575	665	280	2.38
584	515	215	2.40
633	380	150	2.53
642	350	155	2.26
688	345	145	2.38
Total Mass, kg	12.378		
Ave Mass, kg	0.495		
Ave Volume, ml		0.201	

Group 4

STONE #	W (GR)	V (ML)	SPEC.GR
23	675	250	2.70
42	835	325	2.57
49	575	250	2.30
69	745	310	2.40
193	512	225	2.28
297	621	250	2.48
356	709	290	2.44
385	665	295	2.25
400	884	365	2.42
433	672	270	2.49
473	740	285	2.60
515	860	350	2.46
518	845	335	2.52
521	905	470	1.93
576	800	360	2.22
589	610	275	2.22
593	445	205	2.17
616	610	230	2.65
Total Mass, kg	12.708		
Ave Mass, kg	0.706		
Ave Volume, ml		0.297	

APPENDIX C: Tensile Test

Table C.1 Instron and Specimen Set-up

	Specimen			Specimen
	1a	1b	2a	2b
X, mV/mm	0.5	0.5	0.5	0.5
Y, mV/mm	0.5	0.5	0.5	0.5
pen speed, mm/sec	50	50	50	50
Speed - load, mm/min	100	100	100	100
Max Tension, N	261	208	205	148
Elong - recorded, inches	0.109	0.062	0.064	0.054
Elong - recorded, mm	2.77	1.57	1.63	1.37
Gauge length, mm	41		46	
Dist between jaws, mm	79.375		82.55	
Width of specimen - at guage, mm	24		23.5	
- at jaws, mm	30		30	
Thickness, mm	1.62		1.66	

Table C.2 Summary of Results of Tensile Test

Specimen No.	Tension (from chart) N	Stress MPa	Strain %	Modulus of elasticity GPa
1a	48.26	1.24	3.25	0.04
	144.79	3.72	5.28	0.07
	222.68	5.73	7.32	0.08
	270.32	6.95	8.94	0.08
Average				0.07
1b	39.50	1.02	3.17	0.03
	113.54	2.92	4.07	0.07
	162.86	4.19	4.88	0.09
	219.69	5.65	6.50	0.09
Average				0.07
2a	70.12	1.80	3.19	0.06
	143.83	3.69	4.06	0.09
	196.34	5.03	4.78	0.11
	230.00	5.90	5.80	0.10
Average				0.09
2b	32.70	0.84	2.54	0.03
	87.10	2.23	3.26	0.07
	128.40	3.29	3.99	0.08
	148.00	3.79	5.07	0.07
Average				0.06

APPENDIX D: MISCELLANEOUS DATA

Table D.1 Statistical Comparison of the Average of Recorded Forces: Bulkheads

Material	Load	Sand			Rocks		
		25 l/s	38 l/s	63 l/s	25 l/s	38 l/s	63 l/s
Water	12.5	-85.17 Reject	14.15 Reject		-0.50 Accept	-13.66 Reject	
	25	-12.26 Reject	-0.75 Accept		-8.88 Reject	-15.50 Reject	
	50	-29.31 Reject	-18.03 Reject	-6.15 Reject	-41.79 Reject	-17.99 Reject	-6.85 Reject
Sand	12.5				69.94 Reject	-21.48 Reject	
	25				5.62 Reject	-16.34 Reject	
	50				-6.29 Reject	-1.94 Accept	-0.35 Accept

Table D.2 Statistical Comparison of the Average of Recorded Forces: Flume wall

		Sand			Rocks		
		25 l/s	38 l/s	63 l/s	25 l/s	38 l/s	63 l/s
Water	12.5	-86.14 Reject	-37.77 Reject		-5.99 Reject	-16.62 Reject	
	25	-35.79 Reject	-1.28 Accept		-29.34 Reject	-18.35 Reject	
	50	-34.94 Reject	-17.44 Reject	-1.55 Accept	-76.01 Reject	-34.41 Reject	-1.76 Accept
Sand	12.5				68.91 Reject	18.62 Reject	
	25				9.69 Reject	-12.15 Reject	
	50				-32.18 Reject	-17.46 Reject	0.16 Accept

REFERENCES

Nagy, S., Water Bed Type Conveyors. International Conference on Mines Transport, United Kingdom (1983).

Greune, A., Hager, M., The Energy - Saving Design of Belt Conveyors. Bulk Solids Handling, 10, No. 3 (August 1990).

Jonkers, C., The Indentation Rolling Resistance of Belt Conveyors. Forden und Heben, 30, No. 4 (1980).

Spaans, C., The Calculation of the Main Resistance of Belt Conveyors. Bulk Solids Handling, 11, No. 4 (November 1990).

Joseph, M.C., McCorquodale, J.A., Sridhar, K., Power Law for Turbulent Cylindrical Boundary Layers. The Aeronautical Journal of the Royal Aeronautical Society, 75, (January 1971).

Schlicting, H., Boundary Layer Theory, 6th Ed., McGraw-Hill Book Co., New York (1968).

Sharekh, A., Pathak, S.K., Asawa, G.L., Porey, P.D., Turbulent Boundary Layer over Flat Plate with Rigid and Flexible Surfaces. Journal of Engineering Mechanics, 120, No. 8 (August 1994).

Carpenter, P.W., Garrad, A.D., The Hydrodynamic Stability of Flow over a Kramer-type Compliant Surface. Part 1 Tollmien - Schlicting instabilities. Journal of Fluid Mechanics, 155, No. 10 (1985).

Bushnell, D.M., Hefner, J.N., Ash, R.L., Effect of Compliant wall Motion on Turbulent Boundary Layers. Physics of Fluids, 20, No. 10, pg s31-s48 (October 1977).

Contitech, Conveyor Belt System Design, 4th Ed., Continental Aktiengesellscht, Hanover, Germany (1990).

Bridgestone, Conveyor Belt Design Manual.

Brouwers, S., New Frontiers in Hi-Tech Belting Research - Computer Design an Testing Programs. Bulk Solids Handling 6, No. 3 (June 1986).

Pramano, W., Personal Communication, (June 1995).

Massey, B.S., Mechanics of Fluids, 5th Ed., Van Nostrstrand Reinhold Co. Ltd, United Kingdom (1984).

Kreyszig, E., Advanced Engineering Mathematics, 5th Ed., John Wiley & Sons Inc., United States of America (1983), pg 956.

VITA AUCTORIS

NAME:	Rick Anema
PLACE OF BIRTH:	Sydney, Australia
YEAR OF BIRTH:	1966
EDUCATION:	Northcliff High School, Northcliff, South Africa 1980 - 1982
	Scoresby High School, Scoresby, Victoria, Australia 1983 - 1984
	Monash University - Caulfield Campus, Melbourne, Victoria, Australia 1985 - 1989, B.Eng (Mechanical and Computing)
	University of Windsor, Widsor, Ontario, Canada 1993 - 1996, M.A.Sc (Environmental Engineering)